Fluorescent substituted maleimides: From small molecule fluorophore to polymeric barcoding

Yujie Xie

Submitted for the degree of Doctor of Philosophy

Department of Chemistry

To Peilan Cheng and Delan Guo

Table of Contents

List of Figures

List of Tables

Acknowledgements

Firstly, I would like to thank my supervisor Prof. Rachel O'Reilly for bringing me here for the first place and give me the opportunity to work in her group. I am truly grateful for her time, mentorship, and invaluable advice in the past four years. Without her constant encouragement and continued optimism, it is impossible for me to finish this Ph.D.

I would like to thank the University of Warwick and Chancellor's International Scholarship for providing funding for me to carry out my study here. A special thanks goes to Dr. Miquel Torrent-Sucarrat from the University of the Basque Country for providing invaluable computational support and scientific advice during my whole Ph.D. I would also like to thank Professor Feihe Huang for providing the opportunity to visit and learn new skills in his group and I am grateful for the hospitality of the whole group during my time at Zhejiang University.

A huge thanks to the O'Reilly group members, both past and present, for providing all the helps, advices and laughs that make my Ph.D. time more colorful. A special thanks to Dr Jonathan Husband for providing patient help and discussion at the beginning of my PhD and helped me countless times during the past four years. I would also like to thank Dr Turgay Yildirim for the advice and support in my postdoc application. The massive thanks go to Dr. Stefan Lawrenson, Dr. Jonathan Husband, Dr. Jennifer Frommer, and Dr. Tom Wilks for proofreading my thesis and contributing the invaluable suggestions. A special thank you goes to the "Chinese Mafia": Dr. Zan Hua, Dr. Jin Huang, Bo Li, Tianlai Xia, and Dr. Zaizai Tong for making the past four years more enjoyable.

Finally, I need to thank my wonderful parents Xiaohong Guo and Faxiang Xie for years of endless love and support. I would particularly thank my grandparents Peilan Cheng and Delan Guo for their constant encouragement and caring from thousand of miles away. I would also like to thank my best friends Huan Yang for years of sharing the joys and laughs. None of this would be possible without the love and support from my family and friends. A special thank you goes to my partner and best friend Dr. Wei Yu for years of company, caring, and giving me the courage to pursue my dream.

Declaration of Authorship

This thesis is submitted to the University of Warwick in support for the degree of Doctor of Philosophy. It has been composed by myself and has not been submitted in any previous application for any degree.

The work presented (including data generated and data analysis) was carried out by the author except in the cases which are outlined below, and clearly labeled in the corresponding text.

Chapter 2,3,4: Computational studies in support of fluorescence hypotheses were conducted by Dr. Miquel Torrent-Sucarrat (University of the Basque Country).

Chapter 3: Absolute quantum yields and fluorescent lifetimes of the aminothiol maleimides (ATM) were conducted by Dr. Huan Yang (Lanzhou University)

Chapter 4: Cell viability and living cell incubations of the nanogels were conducted by Dr. Maria C Arno (University of Birmingham)

Parts of this thesis have been published by the author (see list of publications).

List of Publications

1. Rational design of substituted maleimide dyes with tunable fluorescence and solvafluorochromism (Chapter 2, 3).

   Y. Xie, J. T. Husband, M. T.-Sucarrat, H. Yang, W. Liu, and R. K. O'Reilly, *Chem. Commun.*, 2018, **54**, 3339-3342

2. Manipulating the fluorescence lifetime at the sub-cellular scale via photo-switchable barcoding (Chapter 4).

   Y. Xie, M. C. Arno, J. T. Husband, M. T.-Sucarrat, and R. K. O'Reilly, *Nat. Commun.*, 2020, **11**, 2460

3. Polymerization-Induced Polymersome Fusion.

   S. Varlas, R. Keogh, **Y. Xie,** S. L. Horswell, J. C. Foster,and R. K. O'Reilly, *J. Am. Chem. Soc.* 2019, **141**, 20234−20248

4. Nickel-Catalyzed Coordination Polymerization-Induced Self-Assembly of Helical Poly(aryl isocyanide)s.

   S. Jimaja, S. Varlas, **Y. Xie**, J. C. Foster, D. Taton, A. P. Dove, and R. K. O'Reilly, *ACS Macro Lett.* 2020, **9**, 226−232

5. Functional nanostructures by NiCCo-PISA of helical poly(aryl isocyanide) copolymers.

   S. Jimaja, **Y. Xie**, J. Foster, D. Taton, A. P. Dove, and R. K. O'Reilly, *Polym. Chem*. 2020, accepted

6. Environment-independent solidification-induced fluorescence in an aminomaleimide fluorophore.

   J. T. Husband, **Y. Xie**, L. Male, M. Torrent-Sucarrat, T. R. Wilks, V. G. Stavros, and R. K. O'Reilly, under submission

Thesis Summary

This thesis explored the synthesis and the fluorescence properties of the substituted maleimides and investigated their applications in polymer and bio related applications.

Chapter 1: A general introduction is given in terms of the basic mechanism in the fluorescent involved photo-physical process. The design strategies of fluorescent materials were described and exampled. The polymer-based fluorescent materials were further highlighted with diverse applications in imaging, labeling, information storage, and many other areas.

Chapter 2: Substituted maleimides as the new class of small molecule fluorophores have been introduced with ideal functional capacity in polymer modification areas. In this chapter, several mono-substituted maleimides have been designed and synthesized through mono-substitution reactions to explore the effect on fluorescent properties. By systematically tailoring the substituents on the C=C double bond (halogen and electron-donating groups), remarkable fluorescent properties such as tunable emission, high fluorescence quantum yields (up to 64%), and solvafluorochromic properties were achieved. Supported by the computational results, the variation of substitution groups allowed us to explore the fluorescence mechanism related to the electron localization. In this regard, the fluorescent properties of substituted maleimide structures could potentially be predicted and tuned for various applications.

Chapter 3: Building upon chapter 2, further exploring the relationship between the structure of maleimides and their optical properties is essential for a full understanding of the fluorescence mechanism. In this chapter, a series of unsymmetrical di-substituted

maleimides bearing multiple groups have been designed and synthesized to explore the effect on fluorescent properties and achieve higher degree of modification within one molecule. Significantly, the optical properties were investigated with remarkable red-shifted emissions (~50 nm) expanded from blue to yellow region and achieved large stocks shifts around 160 nm. More importantly, the different electron localization caused by the two substituents were rationalized based on the DFT simulation results. The unexpected aggregation-induced emission effect in amino thiol maleimides bearing thiophenol groups was discovered for the first time, which lead to an interest in the investigation of the maleimides fluorophores in response to the aggregation states.

Chapter 4: A substituted maleimides based polymeric nanogel system has been developed which exhibited robust lifetime-switching behavior *via* fluorescence resonance energy transfer to a spiropyran photoswitch. In this nanogel system, the manipulating of the fluorescent lifetime by means of UV/Vis light could be applied in the information encrypting and encoding. The ability to reversibly code using fluorescent lifetime enables us to solve the problems of spectra overlap and difficulty in resolving the signal in previous fluorescence barcoding. Furthermore, we showcase the biological applications in living cell barcoding and achieved subcellular coding by fluorescence lifetime imaging technique.

Abbreviations

A	Amplitude
Abs	Absorption
ABM	Aminobromomaleimide
ACM	Aminochloromaleimide
AIM	Aminoiodomaleimide
ACQ	Aggregation Caused Quenching
AFM	Atomic Force Microscopy
AIBN	2,2′-Azobis(2-methylpropionitrile)
AIE	Aggregation Induced Emission
ATM	Aminothiomaleimide
ATRP	Atom Transfer Radical Polymerization
BCP	Block Copolymer
BODIPY	Boron-dipyrromethene
Bz	Benzyl
c	Concentration
CDSA	Crystallization Driven Self-Assembly

CLSM	Confocal Laser Scanning Microscopy
CLD	Cross-Linking Density
CMC	Critical Micelle Concentration
CTA	Chain Transfer Agent
CuAAC	Copper-Catalysed Azide-Alkyne Cycloaddition
d	Binomial Doublet in ^{1}H NMR Spectrum
DBM	Dibromomaleimide
DCM	Dichloromaleimide
DIM	Dichloromaleimide
DE	Diethyl Ether
Dh	Hydrodynamic Diameters
DLS	Dynamic Light Scattering
DMF	N,N-Dimethylformamide
DMSO	Dimethylsulfoxide
DNA	Deoxyribonucleic Acid
DoF	Degree of Functionalisation
DOX	Doxorubicin
DP	Degree of Polymerization

DTM	Dithiomaleimide
DTMMA	Dithiomaleimide Methacrylate
DSE	Dual-State Emission
EDPT	Electron Driven Proton Transfer
em	Emission
eq.	Equation
EGDMA	Ethyleneglycol Dimethacrylate
Equiv.	Equivalents
ex	Excitation
ESI-MS	Electrospray Ionization Mass Spectrometry
Et	Ethyl
EtOAc	Ethyl Acetate
ex	Excitation
F	Integral Photon Flux (emission integral)
f	Absorption Factor
FBS	Fetal Bovine Serum
FLIM	Fluorescence-Lifetime Imaging Microscopy
FRET	Förster Resonance Energy Transfer

FTIR	Fourier Transform Infra-Red
FWHM	Full Width Half Maximum
GSH	Glutathione
h	Planck’s Constant
HOMO	Highest Occupied Molecular Orbital
HPLC	High-Performance Liquid Chromatography
HRMS	High-Resolution Mass Spectrometry
HeLa	Immortal Cervical Cancer Cell Line Derived from Henrietta Lacks
IC	Internal Conversion
ISC	Intersystem Crossing
IONP	Iron Oxide Nanoparticle
IRF	Instrument Response Function
J	NMR Coupling Constant
k_r	Radiative Rate Constant
k_{nr}	Nonradiative Rate Constant
k_{IC}	Internal Conversion Rate Constant
k_{SIC}	Intersystem Crossing Rate Constant

KPS	Potassium Persulfate
NMR	Spectroscopy Coupling Constant
LCST	Lower Critical Solution Temperature
LUMO	Lowest Unoccupied Molecular Orbital
M	Monomer
m	Multiplet Peak in ^{1}H NMR Spectrum
m/z	Mass to Charge Ratio
MA	Methyl Acrylate
MAM	Monoaminomaleimide
MBM	Monobromomaleimide
Me	Methyl
MeOH	Methanol
MMA	Methyl Methacrylate
Mn	Number Average Molecular Weight
MRI	Magnetic Resonance Imaging
Mw	Mass Average Molecular Weight
MS	Mass Spectroscopy
n	Refractive Index

N	Number of Excited Molecules
NA	Avogadro’s Number
NAI	Naphthalimide
NBO	Natural Bond Orbital
NIR	Near Infra-red
NMR	Nuclear Magnetic Resonance
NMM	N-Methylmorpholine
NPA	Natural Population Analysis
OCM	Alkoxychloromaleimide
OLED	Organic Light-Emitting Diode
PCM	Polarization Continuum Model
PEG	Polyethylene Glycol
PD	Polydispersity
Ph	Phenyl
PISA	Polymerization-Induced Self-Assembly
ppm	Parts per Million
R	Radius
RAFT	Reversible Addition Fragmentation Chain Transfer

ref	Reference
ROS	Reactive Oxygen
RNS	Reactive Nitrogen
PCC	Pearson Correlation Coefficient
PLGA	Poly(lactic-co-glycolic acid)
PVA	Polyvinyl Acetate
ROMP	Ring-Opening Metathesis Polymerization
ROP	Ring-Opening Polymerisation
ROI	Region of Interests
rt	Room Temperature
s	Singlet in NMR Spectrum
S	Singlet State
SDS	Sodium Dodecylsulfate
SEC	Size Exclusion Chromatography
SRM	Super-Resolved Fluorescence Microscopy
SP	Spyropyran
SPMA	2-(3',3'-Dimethyl-6-nitrospiro[chromene-2,2'-indolin]-1'-yl)ethyl Methacrylate

SPT	Single-Photon Timing Technique
T	Temperature
T	Triplet State
t	Binomial Triplet in ^{1}H NMR Spectrum
t	Time
TCSPC	Time-Correlated Single Photon Counting
TD-DFT	Time-Dependent Density Functional Theory
TEA	Triethylamine
TEM	Transition Electron Microscopy
TFA	Trifluoroacetic Acid
THF	Tetrahydrofuran
TICT	Twisted Intramolecular Charge Transfer
TLC	Thin Layer Chromatography
TMS	Trimethylsilane Group or Tetramethylsilane NMR Standard
TPE	Tetraphenylehtlyene
TPP	Triphenylphosphonium
UV	Ultraviolet

UA	Uranyl Acetate
MWCO	Molecular Weight Cut-Off
v	volume
vis	Visible
w	Weight Percentage
ε	molar absorption coefficient
δ	Chemical Shift in NMR Spectroscopy
λ	Wavelength
Φ_f	Quantum Yield
ν	Frequency
τ	Fluorescence Lifetime
$\tau_{Av,A}$	Amplitude Average Fluorescence Lifetime
$\tau_{Av,I}$	Intensity Average Fluorescence Lifetime

Chapter 1 Introduction

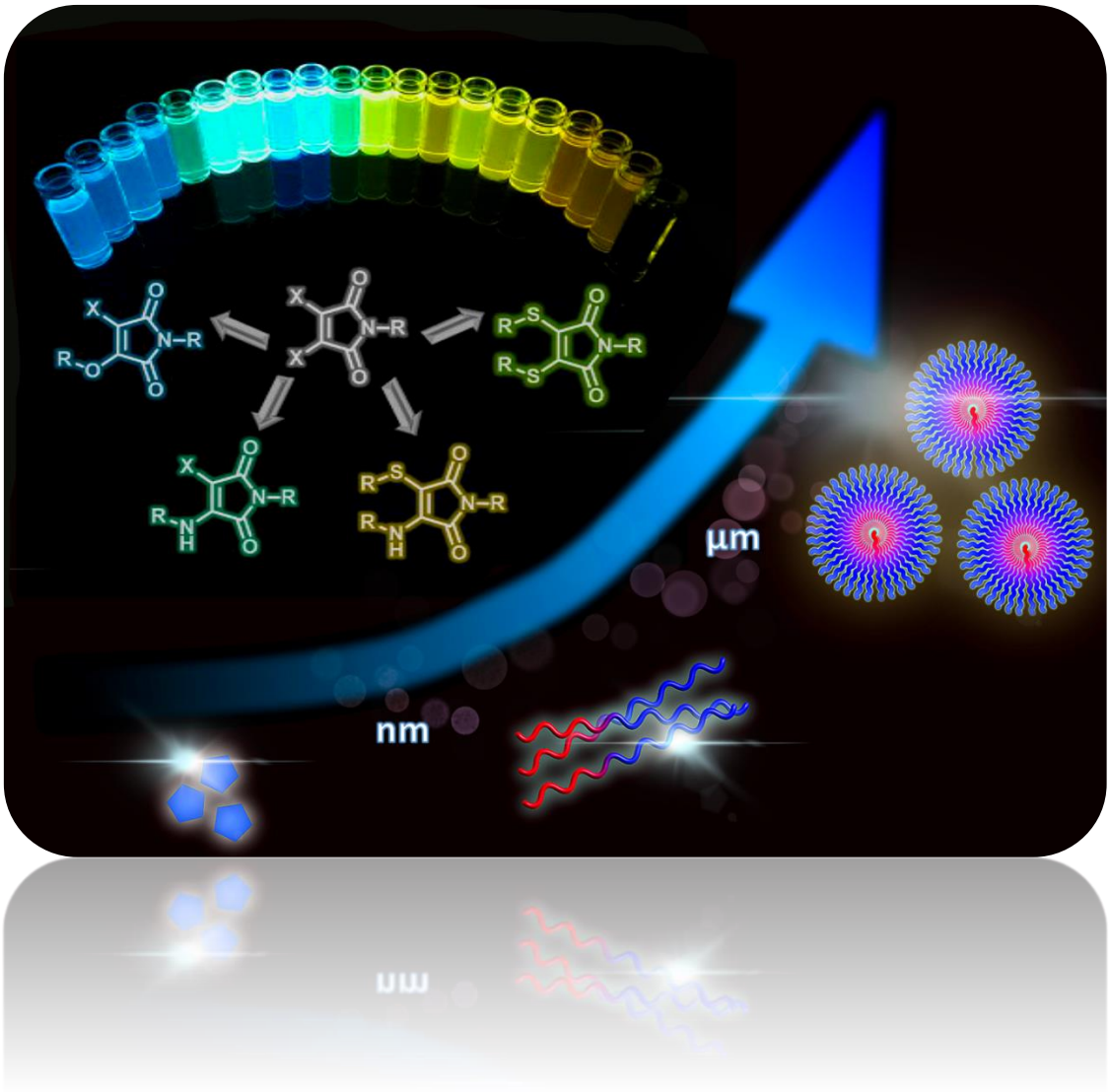

Owing to the fast signaling, non-invasive nature, and high temporal resolution, fluorescence has become an extremely popular technique to quantify and visualize complex systems in various fields across science and medicine.[1] Therefore, interest in fluorescence has continued to grow at a rapid pace, particularly in the search for novel fluorescent materials based on organic molecules,[2] inorganic complexes[3] and more recently nanomaterials.[4, 5] Among these, organic fluorophores are one of the most studied and commercialized, taking advantage of their relatively small size, tunable functionality, and flexible molecular design. The molecular structure of small molecule fluorophores is detrimental to their fluorescent properties.[6] Functionalized small-molecule fluorophores, exhibiting emissions across the visible to infrared regions, like rhodamines, fluoresceins, cyanines, and BODIPY, *etc*., are now well-established for specifically visualizing cellular and sub-cellular structures, as well as tracking important biology processes.[7] More recently, studies on these small-molecule fluorophores have not only aimed to optimize the fluorescent properties, such as increasing the fluorescence quantum yield or expanding the emission wavelength but more frequently aim to develop responsive properties and multi-functionalization.

The incorporation of small molecule fluorophores with polymer materials has generated great interests owing to the enormous molecular structural versatility of polymer materials which could offer various responsiveness in fluorescent applications. Therefore, the rational design of the fluorescent polymer provided unheralded interest in bio-diagnosis, cell imaging, energy transition, display technology and many other areas. In this introduction, we summarize the different design strategies for polymeric fluorescent materials and their applications in the areas of monitoring the chemical/physical behaviors of polymers, imaging the biology structures, analyzing/diagnosing the small molecules, and storing the information.

1.1 Photoluminescence

The investigation of light and its related photophysical processes has attracted great interest throughout modern history, particularly in the last few centuries. The in-depth understanding of the behavior of light, from the electromagnetic wave predicted by Maxwell, to the duality of waves and particles determined by Einstein and Plank, provides the opportunity for scientists in the 21st century to utilize these photophysical processes for exploring the microscopic world.[8] The utilization of these photophysical processes has been especially important for scientists engaged in investigating the intricacies of molecular structures and their associated interactions.[9] In general, the interaction of electromagnetic radiation with molecules can be explored by spectroscopy, given different structures and photophysical information among the distinct energy or wavelength of the light range (Figure 1.1a). For example, nuclear magnetic resonance

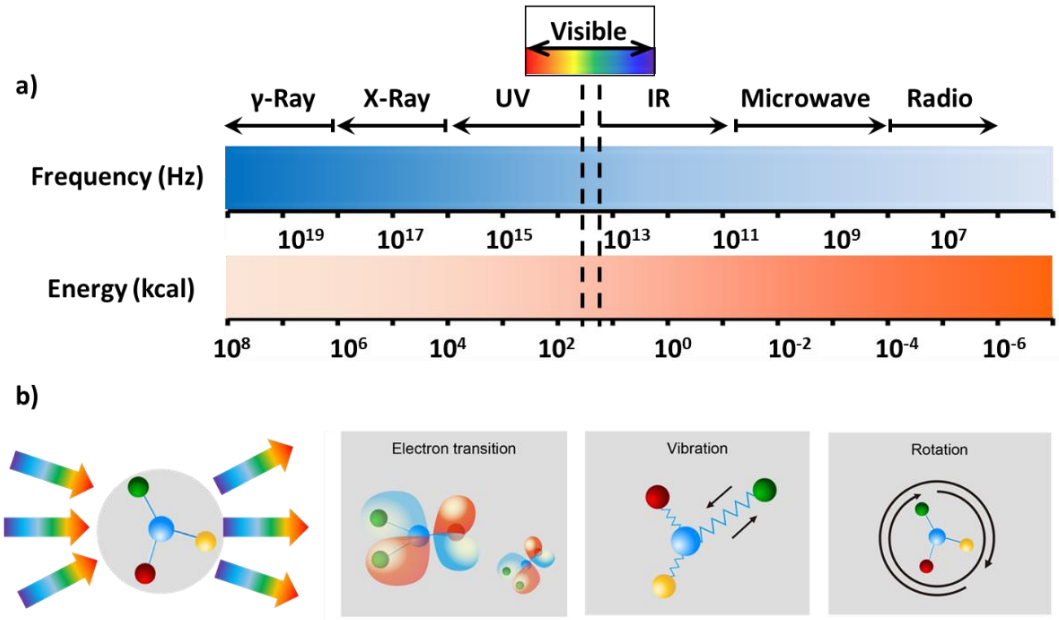

Figure 1.1 a) The illustration of the electromagnetic spectrum regarding the different wavelengths and energies of light.[8] b) The electron transition, vibration, rotation, and other molecular information can be acquired by different spectroscopic techniques.

(NMR) spectroscopy is the commonly used technique to identify the structures of the organic compounds, by recording the changes in the spin of atomic nucleus at radio frequency about 10^8 Hz.[10] With the increase of radiation frequency (10^{11}–10^{13} Hz), the information of the intramolecular rotations and vibrations could be detected by vibrational spectroscopy (IR and Raman) (Figure 1.1b).

Photoluminescence, as one of these key photophysical phenomena, is caused by a molecule absorbing energy of a specific wavelength and then re-remiting energy at a different wavelength. Luminescence behavior mainly occurs in the UV–visible/near-infrared region of the electromagnetic spectrum. It is precisely defined as the "spontaneous emission of radiation from an electronically excited species or from a vibrationally excited species not in thermal equilibrium with its environment".[8] Luminescence has long been utilized as an indispensable analytical tool in modern research, finding widespread applications in areas such as biological labels and probes,[11] chemosensors,[12] medical diagnostics[13], and photoactive materials in light-emitting devices.[14]

1.1.1 Competing Processes of luminescence

The luminescence photophysical events happened in organic compounds, which include fluorescence and phosphorescence, can be clearly illustrated by the Jablonski diagram (Figure 1.2).[15] Here, following excitation by a photon of light, two distinct electronic states can be generated, depending on whether the electron spins are paired (singlet state, S) or unpaired (triplet state, T). Firstly, the excitation process triggers the rapid transition to a higher-order singlet state, which is indicated by the absorption step shown in Figure 1.2. The electrons in this higher electronic state (S_n) will then relax to the lowest excited state (S_1) through a non-radiative transition, which is known as internal conversion (IC).

Following this transition to the lowest excited state (S_1), the molecule will then either undergo a relaxation, from the excited state to ground state (S_0) by emitting a photon (fluorescence) or undergo a non-radiative internal conversion process. Besides the internal conversion between the same spin multiplicity, the electron transition between two isoenergetic vibrational levels belonging to electronic states of different multiplicities can also occur, which is known as intersystem crossing (ISC). In this case, electrons that have transitioned to the first excited triplet state (T_1) will then cross to the electronic singlet ground state through radiative de-excitation, known as phosphorescence. Due to this transition being spin forbidden, due to the required change in spin states, the lifetime of the triplet (up to 100 s) is normally much longer than the lifetime of an excited singlet state (10-100 ns).[8]

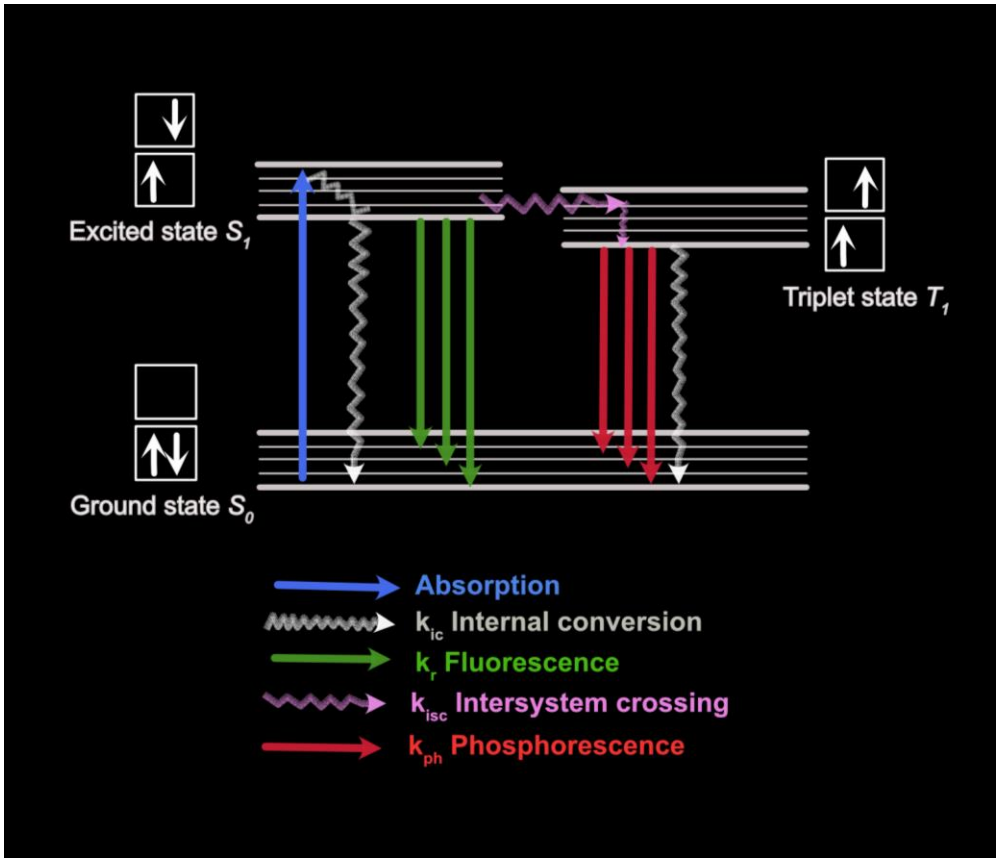

Figure 1.2 Simplified Jablonski diagram explaining the photophysical processes between the absorption and emission of light.

1.1.2 Fluorescence Emission

A rather interesting observation regarding the mechanism of fluorescence is that the emission normally occurs at different wavelengths than absorption. The wavelength difference between the maximum emission and absorption is defined as the Stokes shift (Figure 1.3a). As a multiparametric technique, steady-state fluorescence spectroscopy is utilized to monitor and analyze the fluorescence excitation, emission, spectral shifts, and anisotropy of fluorophores *via* a 90-degree angle light path from the incident light source and the detector (Figure 1.3b). For most fluorophores, the emission spectra are independent of the excitation wavelength and can be superimposable on its excitation spectrum. The intensity value of the fluorescence from the fluorometer (Fluorescence intensity, FI) is closely related to the concentration of the fluorophore, the measurement set up, light source, and could be possibly influenced by the solvent, pH, and other microenvironmental factors. Therefore, very little quantitative information can be obtained from the intensity measurement

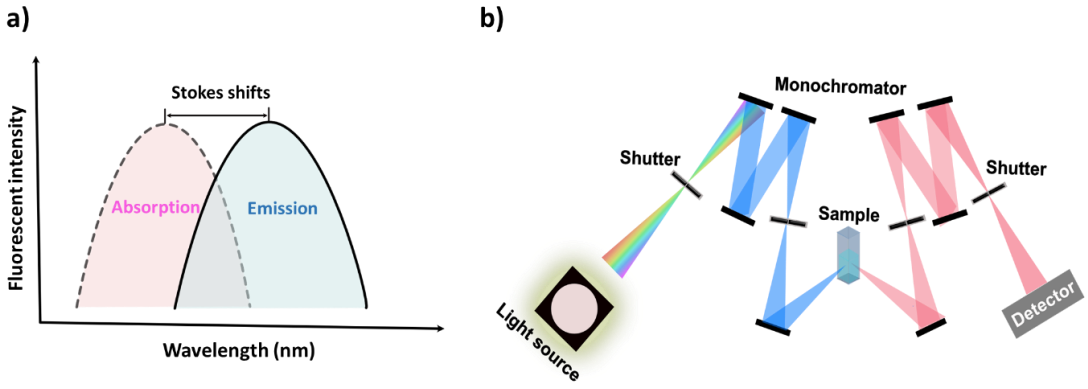

Figure 1.3 a) Illustration of the absorption and fluorescence spectrum; b) Simplified instrument set-up of the fluorescence spectroscopy.

1.1.3 Brightness and Fluorescence Quantum Yield

As mentioned above, the fluorescent intensity is generally influenced by environmental factors, such as solvent, concentration, and the light source, which can generate inaccuracy when measuring and comparing the fluorescent behaviors between fluorophores. To quantify the analytical sensitivity of fluorophores and efficiency of the fluorescent emission, the concepts of fluorescence brightness and quantum yield are often used. The fluorophore's brightness (B) is determined by both fluorescence quantum yield (φ_f) and the molar absorption coefficient at the excitation wavelength ($\varepsilon_{(\lambda ex)}$):[7]

$$B = \varphi_f \times \varepsilon_{(\lambda ex)} \quad (1.1)$$

Where the fluorescence quantum yield (φ_f) is defined as the efficiency of the conversion of absorbed photons into emitted photons, which can be generally described by two rate constants:

$$\varphi_f = \frac{k_r}{k_r + k_{nr}} \quad (1.2)$$

k_r is the radiative rate constant and k_{nr} is the nonradiative rate constant including all possible competing deactivation pathways, such as internal conversion, intersystem crossing, or other intra- and intermolecular quenching mechanisms.[8] However, the uncertainty of the nonradiative rate constant (k_{nr}) leads to the theoretical inability to predict the fluorescence quantum yield of a certain fluorophore.[8] In contrast to the fluorescence emission intensity, which is closely related to the concentration of the fluorophore, the measured fluorescence quantum yield is independent to the concentration when using highly dilute solutions. However, temperature may influence the quantum yield due to the non-radiative processes related to thermal agitation.[8] Furthermore, other factors such as pH, hydrogen bonding, polarity may also influence the quantum yield in various ways depending on the fluorescent material.

Although several photothermal methods have been established to measure the φ_f of novel fluorophores in a relatively accurate way, these techniques generally require specialized equipment.[16] The more commonly used techniques use optical methods, such as relative methods, by comparing to a standard of known fluorescence quantum yield, or absolute methods by directly measuring the conversion of photons using an integrating sphere setup. The relative method for calculating the fluorescence quantum yield involves comparing the integrated emission and absorbance spectra of the sample and the standard at a specific excitation wavelength:

$$\frac{\Phi_{f,x}}{\Phi_{f,st}} = \frac{n_x^2}{n_{st}^2}\frac{\int_0^\infty F(\lambda_F)\, d\lambda_F}{\int_0^\infty F_{st}(\lambda_F)\, \lambda_F} \quad (1.3)$$

The equation can be simplified as:

$$\Phi_{f,x} = \Phi_{f,st} \cdot \frac{F_x}{F_{st}} \cdot \frac{f_{st}}{f_x} \cdot \frac{n_x^2(\lambda_{em})}{n_{st}^2(\lambda_{em})} \quad (1.4)$$

In this case, F represents the integral photon flux (emission integral), f is the absorption factor, n is the refractive index of the solvent. The index x represents the sample, and the index st represents the standard. When the absorbance for the standard and sample match ($f_{st}/f_x=1$) can be neglected.

The selection of the standard fluorophores requires that the optical properties closely match that of sample being investigated and is crucial to ensure an accurate measurement. Several well-established fluorophores, such as quinine sulfate, rhodamine, and fluorescein, etc. have been reported as suitable quantum yield standards for measuring the relative quantum yield of novel fluorophores (Table 1.1).[7, 16, 17] Although, it is important that the measuring environment is identical between the sample and the standard, to diminish any uncertainty occurring due to differences in the solvent, temperature, the monochromators, polarization effects, amongst other factors. Although the relative method is straightforward in terms of operation, not requiring the use of

Table 1.1 Fluorescence emission ranges and quantum yields of some commercial available dyes as the standards for measuring the relative quantum yield.[7]

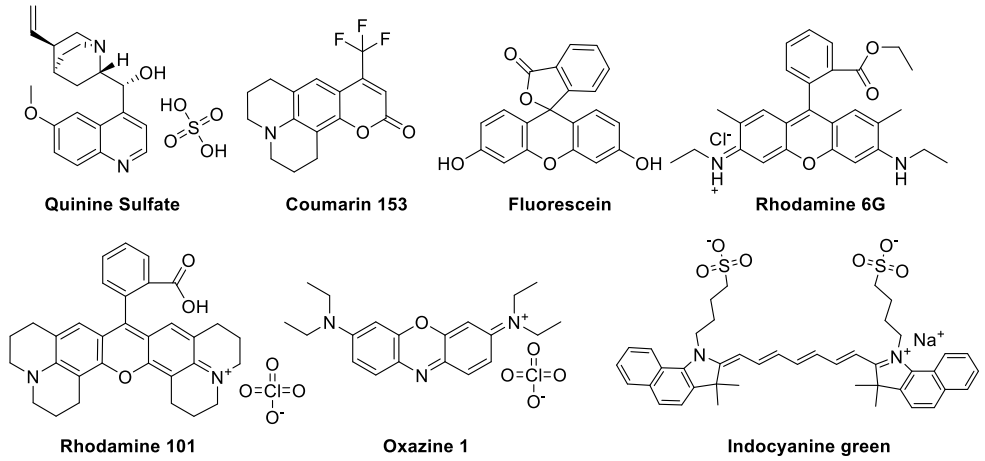

	QS	C153	F	R6G	R101	OX1	HITCI	IR125
Solvent	0.105M $HClO_4$	Ethanol	0.1 M NaOH	Ethanol	Ethanol	Ethanol	Ethanol	DMSO
Abs (nm)	270-400	350-500	400-500	425-575	475-620	500-710	535-825	550-875
λ_{Em} (nm)	385-700	465-750	490-690	505-750	540-75-	615-95-	700-950	750-1000
φ_f	0.59	0.53	0.89	0.91	0.91	0.15	0.3	0.23

specialized systems or equipment, it should be noted that the accuracy of this relative quantum yields methods cannot be better than 5-10% due to errors from the light source, detection environment, and standards.

The preferred approach for determining absolute quantum yield would be the method of directly measuring the conversion of the photons with an integrating sphere setup. In the conventional fluorescence spectrometer set up with the high reflectance inside the integrating sphere allows for collecting the full reflection of the emitted light (Figure 1.4).[18] The calculation for the absolute quantum yield can be summarized as the ratio of the number of emitted photons to the number of absorbed photons:

$$\Phi = \frac{N_{em}}{N_{abs}} \quad (1.5)$$

$$\Phi = \frac{E_{smaple} - E_{reference}}{S_{reference} - S_{sample}} \quad (1.6)$$

E refers to the integral of the scan in the emission region, whereas, the S refers to the integral of the scan in the scattering region. The solvent can be used as the reference when calculating the absolute quantum yield of the solution to simplify the measurement. Meanwhile, due to being less affected by the orientation and reflection of the sample, the absolute method is more commonly used to determine the quantum yield in films and solids.

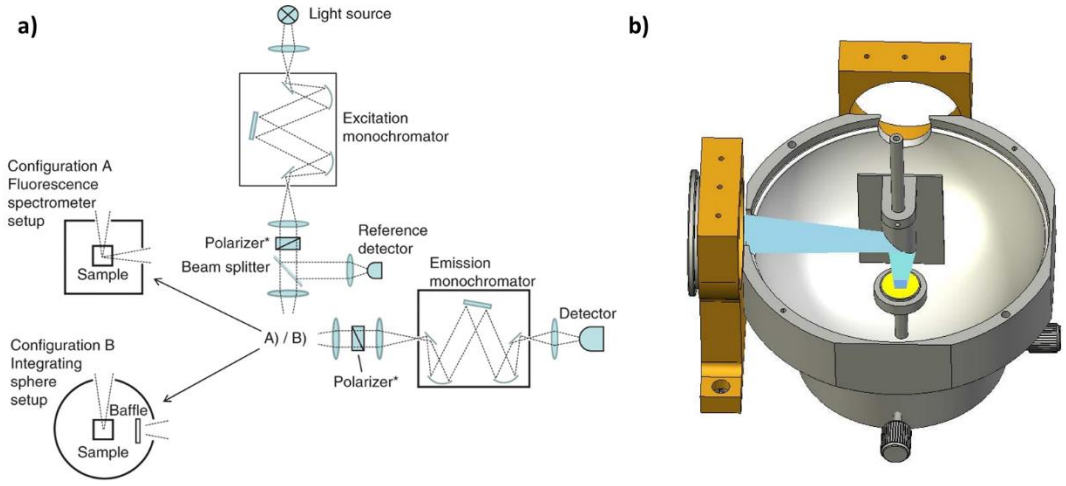

Figure 1.4 a) Comparison of a fluorescence spectrometer (configuration A) and an integrating sphere setup (configuration B).[7] b) Schematic illustration of the integrating sphere from Edinburgh instruments.

1.1.4 Fluorescence Lifetime

Another key characteristic of a fluorophore is fluorescence lifetime. The fluorescence lifetime is defined as the average time the fluorophore spends in its excited singlet state ($S_1 \rightarrow S_0$). As demonstrated in the Jablonski diagram shown earlier (Figure 1.2), the excited state of the fluorophore can decay by emitting a photon through the radiative

pathway (k_r) or by other non-radiative pathways (k_{nr}), such as internal conversion (k_{IC}) or intersystem crossing (k_{SIC}). This kinetic process, in which the excited fluorophores (F*) return to the ground state (F), can be simplified by the following equation:

$$-\frac{d[F^*]}{dt} = (k_r + k_{nr})[F^*] \quad (1.7)$$

The integration of this equation leads to:

$$[F^*] = [F^*]_0 \exp\left(-\frac{t}{\tau}\right) \quad (1.8)$$

Where the fluorescence lifetime (τ) is described as

$$\tau = \frac{1}{k_r + k_{nr}} \quad (1.9)$$

Although the uncertainties of the non-radiative process hinder the prediction of the fluorescence lifetime, the time-resolved fluorescence intensity, which exhibits an exponential decay, can be applied in detecting the fluorescence lifetime experimentally. The development of time-resolved fluorescence techniques, such as time-correlated single-photon counting (TCSPC) or single-photon timing (SPT), allows for detecting a single photon at time t after an excitation pulse, which is proportional to the fluorescence intensity at that time.[19] The time-resolved fluorescence decay can, therefore, be fitted to a multiple exponential models:

$$F(t) = A_1 \exp\left(-\frac{t}{\tau_1}\right) + A_2 \exp\left(-\frac{t}{\tau_2}\right) + A_3 \exp\left(-\frac{t}{\tau_3}\right) + \cdots \quad (1.10)$$

While the average fluorescent lifetime can then be calculated as intensity averaged ($\tau_{Av,I}$) or amplitude averaged ($\tau_{Av,A}$):

$$\tau_{Av,I} = \frac{\sum A_i \tau_i^2}{\sum A_i \tau_i} \quad (1.11)$$

$$\tau_{Av,A} = \frac{\sum A_i \tau_i}{\sum A_i} \quad (1.12)$$

As an intrinsic property of the fluorophore, the fluorescence lifetime is associated with the molecule configuration, microenvironment, and several external factors, such as temperature, polarity, and any fluorescence quenching effects.[20] Compared with the fluorescence emission, the fluorescence lifetime is less affected by experimental setups, such as the excitation light source or the measurement techniques, and can provide more quantitative results. More importantly, the fluorescence lifetime is independent of fluorophore concentration and is not influenced by the photobleaching effect, meaning it serves as the prominent tool for investigating the interactions of the fluorophore within the microenvironment.

The fluorescence lifetime will vary in different fluorescent materials, ranging from nanoseconds to microseconds. The fluorescence lifetimes of some commonly used fluorophores are summarized in Table 1.2.[20] With the development of fluorescence lifetime imaging microscopy (FLIM), the fluorescence lifetime signal can be visualized providing quantifiable and reliable information from higher dimensions.

Table 1.2 Fluorescence lifetime of some commonly used fluorophores[20]

Class of fluorophores	fluorescence lifetime range
endogenous fluorophores	0.1-7 ns
organic dyes	0.1-20 ns, up to 90 ns (pyrenes)
fluorescent proteins	0.1-4 ns
quantum dots average	average, 10-30 ns, up to 500 ns
organometallic complexes	10-700 ns
lanthanides	from μs (Yb, Nd) to ms (Eu, Tb)
fullerenes	<1.2 ns
single wall nanotubes	10-100 ns, up to 10 μs for short nanotubes

1.2 Fluorescence Studies of Polymer Containing Systems

Polymer materials have a broad diversity of applications in daily life, as well as scientific research, largely on account of their enormous molecular structural versatility.[21] The introduction of fluorescent properties into polymeric systems has allowed for real-time monitoring of the polymerization process with quantitative output. More importantly, these polymeric fluorescent materials benefit from the versatility provided by the polymer matrix, facilitating variable properties, including stimuli-responsive behavior,[22-24] degradability,[25] biocompatibility, *etc.* and therefore have seen use in an array of applications, such as information storage,[26] drug delivery,[27] cellular activity imaging[28], and therapeutics monitoring.[29] In addition, the development of these polymerization methods has led to different strategies that can be utilized to create an impressive range of fluorescent polymeric systems in which the fluorescent components are modified on the backbone or the side chain of the polymers.

1.2.1 Design of the Fluorescent Polymers

In terms of the design of fluorescent polymers, it is pivotal to consider the compatibility when incorporating the fluorescence motifs onto the polymer chain. Specifically, the fluorescence properties need to be maintained or selectively controlled without influencing the chemical environment. Additionally, the incorporation of the fluorophore should not dramatically affect the chemical or physical properties of the polymer. Considering these criteria, one of the general and adaptable strategies to obtain a fluorescent polymer is through a direct polymerization method, in which a fluorescence monomer or initiator are directly polymerized onto the polymer chain (Figure 1.5). [30-34] Depending on the different polymerization methods, the resulting polymer can bear the fluorophore at the chain end,[35, 36] on the side chain[37-39] or backbone of the polymer.[40]

Another commonly used strategy for fluorescent polymer formation is through post-modification methods, in which the fluorophores containing suitable functional groups could be covalently incorporated into the polymer through a variety of reactions (Figure 1.5).[41] These approaches, combined with different polymerization methods, present many pros and cons, which are detailed in the following sections.

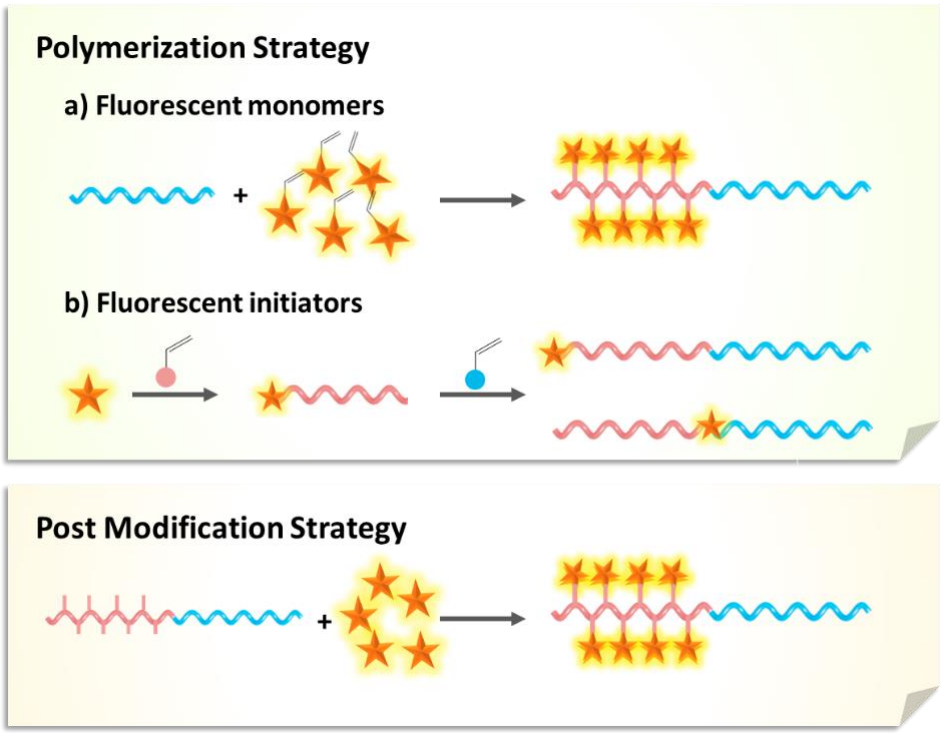

Figure 1.5 Schematic illustration of the design strategies of the fluorescent polymers.

1.2.2 Fluorescent Monomers

As one of the most straightforward strategies, the direct polymerization of fluorescent monomers leads to the random or controlled length of the fluorescence blocks depending on the different polymer systems. These design strategies for fluorescent monomers are varied and the locations on the polymer chain are also diverse, due to the different polymerization methods. The fluorescent conjugated polymer is the class of fluorescent polymers in which the fluorescent or pre-fluorescent monomers can be conjugated to the

backbone of the polymer. Such pathways involve the extended π conjugated backbone which generated the band edge for charge transport and also exhibiting emission with high quantum efficiency.[42] In another strategy, fluorescent monomers bearing two or more functional groups have been polymerized on the polymer backbone utilizing step-growth polymerization. Various aggregation-induced emission (AIE) luminogens containing building blocks like alkyne/azide, thiol/alkyne as the fluorescent monomers have been used extensively by Tang's group to prepare the functional polymers by "click reaction" involved step-growth polymerization (Figure 1.6).[43] Compared with the well-exploited olefin polymers with carbon-carbon backbones, such "clicked" polymer backbones constructed by an optically active monomer offers the sensitive signals in response to a change of polarizability, hydrophilicity and morphology etc.[44, 45 46] Despite these enticing prospects, the high density of fluorophores on the backbone of the polymer is not ideal for aggregation caused quenching (ACQ) fluorophores, as the fluorescence can be partially influenced or even quenched by the increased chance of intermolecular interactions.

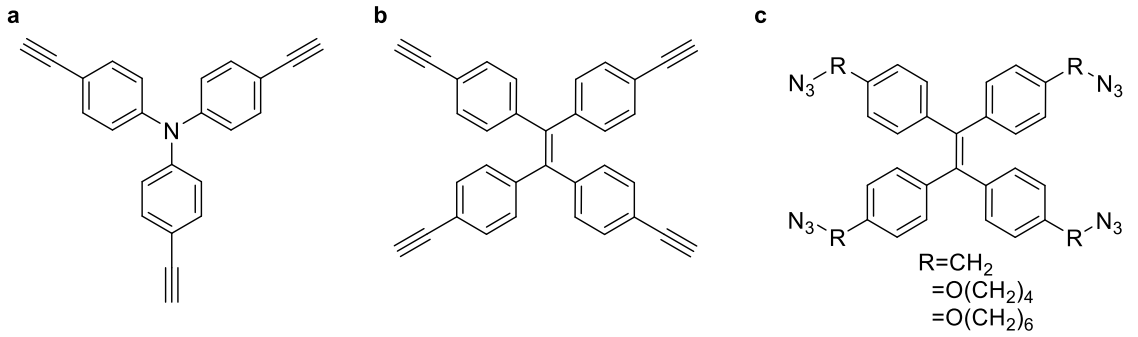

Figure 1.6 Reported AIE monomers for "click" polymerization; a. Triazide functionalized fluorescent monomer for Cu(I)-catalyzed alkyne/azide click polymerization [44] b. Alkyne modified TPE-monomer for thiol−yne click polymerization; c. Azide functionalized TPE-monomer for metal-free alkyne/azide click polymerization.[47]

Free radical polymerization techniques have long been a useful way of creating very diverse block copolymers, taking advantage of the control offered over the polymerization process. Various commercially available fluorophores have been tailored to copolymerize on the polymer chain through free radical polymerization.[30, 31, 48] The modification of the vinyl group is the most employed strategy for the formation of fluorescent monomers, enabling the copolymerization of the fluorophores onto the side chain of the polymer. Such fluorescent monomers possess advantageous properties, such as ease of design and controlled functionalization. Meanwhile, the ACQ fluorophores on the polymer chain can be separated by a spacer or other monomers allowing the fluorescence properties to be maintained as the chance of intermolecular interactions is reduced.[49] For example, two acrylate functionalized naphthalimide (NAI) and triarylamine have been designed by the Hudson group as the fluorescent monomers for Cu(0)-reversible deactivation radical polymerization (Cu(0)-RDRP).[30] Both linear and star polymers were formed by copolymerizing these fluorescent monomers. Interestingly, a thermo-responsive fluorescent material was achieved by combining both two monomers in an N-isopropylacrylamide (NIPAM)-based copolymer, given emission from blue to red with ratiometric changes in both color and emission lifetime.

Substituted maleimides derivatives are a class of novel fluorophores distinguished by their small size and bright fluorescence emissions.[50-54] The major advantage of these fluorescent maleimide derivatives, in comparison to commercially available fluorophores, is their small size, which allows for ready incorporation into architectures without affecting or disrupting the scaffold.[55] Therefore, these fluorophores provided unheralded interest in polymer and material functionalization which have been extensively investigated by our group (compounds **a**-**d**, Figure 1.7). [53, 56, 57] A series of acrylate or methacrylate modified dithiol maleimides (DTM) have been copolymerized on the side

chain of polymers *via* RAFT polymerization. Meanwhile, such DTM monomers can be polymerized *in situ* by emulsion polymerization, leading to the highly emissive nanogel structure with tunable responsive properties. Substituted maleimide monomers for other polymerization techniques such as ROMP polymerization and click polymerizations have also been investigated.[58] The applications of the substituted maleimides in polymer applications are introduced in chapter 2 and chapter 3.

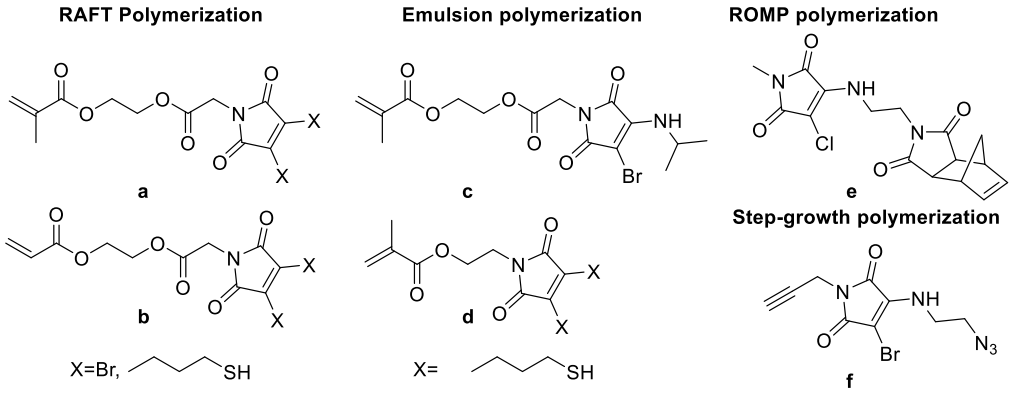

Figure 1.7 Several substituted maleimides based fluorescent monomers for different polymerization techniques: RAFT polymerization,[52, 59] emulsion polymerization,[51, 54] ROMP polymerization[58], and step-growth polymerization.

1.2.3 Fluorophore Initiated Polymerization

Another strategy for introducing fluorescent motifs onto the polymer chain involves the design of fluorescent initiators. The fluorophore can be used to initiate the polymerization process by incorporating specific functional groups.[60] Such a strategy provides the possibility to introduce a single fluorophore per polymer chain which largely decreases the intermolecular interactions which lead to the quenching effect.[50] For example, three commercially available fluorophores bearing primary or secondary amino functionalities have been reported by the Alexander group to initialize ring-opening polymerization (Figure 1.8).[35] The developed PLGA copolymers constructed with the fluorophore at the

polymer chain end could be further self-assembled into well-defined nanoparticles, which maintained the optical properties for tracking drug delivery into subcellular locations. AIEgens,[61] pyrene[60], and other fluorophores were also modified as the initiator to fabricate fluorescent polymers with fluorophores at the chain end.

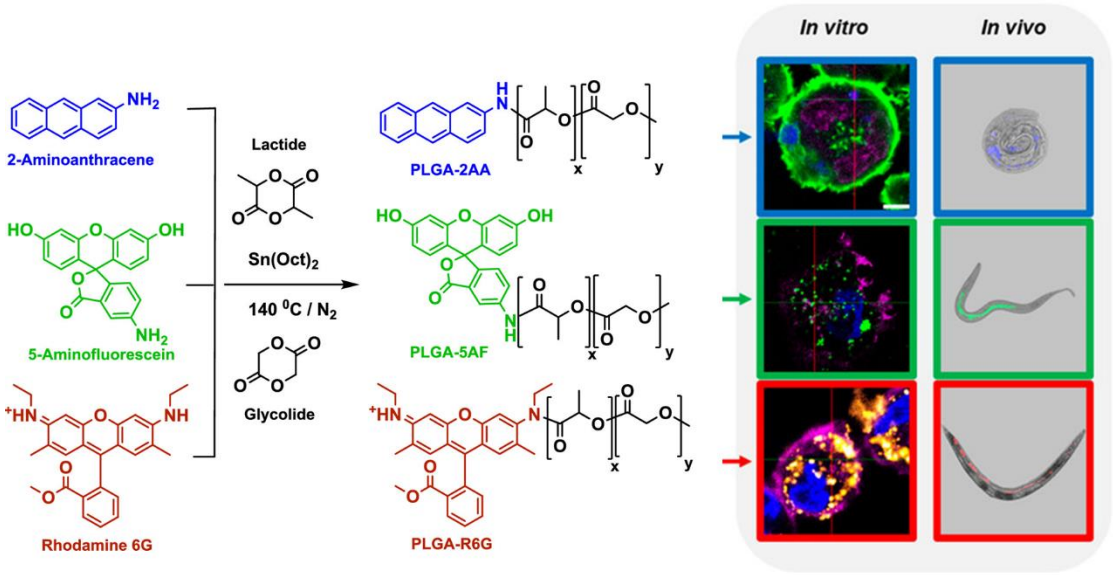

Figure 1.8 Three commercially available dyes used as initiators for the ring-opening polymerization and cellular imaging applications (blue: aminoanthracene, green: 5-aminofluorescein ; red: rhodamine-6G). Figure adapted from ref 35.

The fluorophore initialized polymerization not only allows the fluorophores to be incorporated on the chain end of the developed polymers, but it has also been tailored for further functionalization on the fluorophores sides. Our group has reported dithiol maleimide fluorophores bearing the hydroxide group functionality, which could effectively initialize the ring-opening polymerization of lactide (Figure 1.9).[50] Meanwhile, the maleimide fluorophore was selectively modified with a chain-transfer agent (CTA) group on the imide side, allowing for the further chain extension *via* RAFT polymerization. Therefore, a diblock copolymer can be constructed bearing two building blocks with the multi functionalized maleimide fluorophores in the middle as both the

fluorophore and functional linker. Additionally, the further assembly of this fluorescent polymer in water led to the formation of interface-labeled micelles with high emission by preventing the self-quenching between dyes.

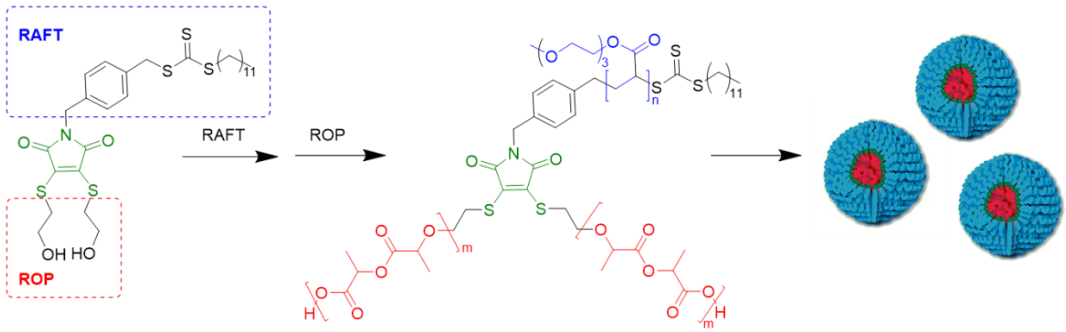

Figure 1.9 Substituted maleimides bridged block copolymer system for the assembly of interface-labeled micelles with highly emissive properties. Figure adapted from refs 50.

1.2.4 Post-grafted Fluorescent Polymers

Despite being a straightforward functionalization method, the direct polymerization of fluorescent monomers is not always generally adaptable to many polymer systems, due to the relatively sophisticated structures of the fluorophores which may influence the polymerization process. Apart from the direct polymerization methods, post-modification strategies have also been utilized to create an impressive range of fluorescent polymers.[62-67] Generally, monomers with suitable functional handles can be polymerized, followed by selectively reacting with fluorophores to introduce fluorescent behavior. The development of highly efficient and controllable reactions is crucial for the post-modification of the polymers, as such, various functional groups and reactions ranging from dehydration condensations to “click” reactions have been utilized for this approach (Figure 1.10).[68] For example, polymers featuring active ester groups have been utilized as the functional handle for post-modification of the naphthalimide dyes bearing the primary amine group.[41] This strategy results in a water-soluble fluorescent polymer,

which could potentially be applied for *in vitro* diagnostics and cell imaging. "Click" chemistry has also emerged as prominent reaction methodology since 2001 and has been extensively applied in various polymeric systems, due to their high modularity, orthogonality, and versatility.[69] Fluorophores bearing azide or alkyne groups have been designed for post-modifying the polymer through the copper-catalyzed azide-alkyne cycloaddition (CuAAC), which has been employed by several groups.[67, 70, 71] Similarly, thiol–ene reactions for post-modification of fluorescent polymers has been explored by the Bowman group, resulting in a polymer with tunable backbone and intrinsic functionalization.[66]

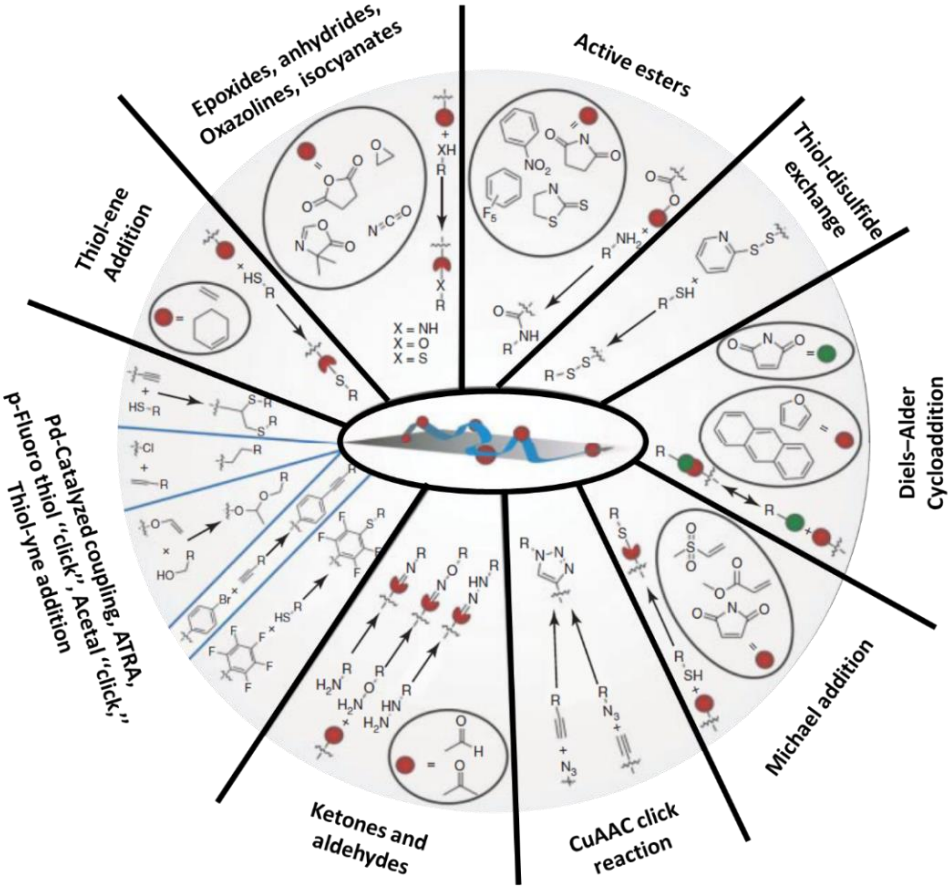

Figure 1.10 Reported methods for constructing functional polymers *via* post-polymerization modification.[68] Figure adapted from refs 68.

1.3 Application of Fluorescent Polymeric Materials

To date, fluorescent materials have been widely applied in fields such as analytical sensing, optical imaging, and information storage.[1] Through their rational design, fluorescent materials have been developed ranging from micro-level small-molecular fluorophores or fluorescent nanoparticles to macro-level fluorescent films (Figure 1.11). As one of the most wildly used fluorescent materials, fluorescent polymers inherit their flexibility and tunability from the polymeric materials and the responsive output signals from the fluorescent motifs. Therefore, polymers containing fluorescent materials have made tremendous progress covering both the polymeric assembles at the nanoscale and fluorescent hydrogels at macro level, which has led to unheralded interest in the fluorescent material community.

The aim to design the polymeric materials bearing fluorescent outputs is to provide the quantitative estimation over the conformational and dynamic behavior of polymer chains, like monitoring the polymerization and assembly process.[72-75] Additionally, the tuneablity and responsive output of fluorescent polymers has been a powerful tool for the sensing biomolecules, bioimaging, and diagnosis. [76-79] Meanwhile, the fast signaling and *in situ* fluorescent readout in such polymeric systems has lead to great potential in the area of information storage and encryption at either the micro or the macro-scale.[80]

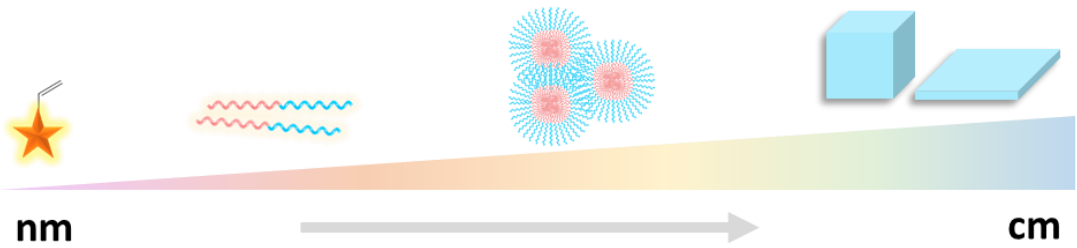

Figure 1.11 Schematic illustrating soft fluorescent materials, ranging from small molecules with nanometre scales to bulk materials with centimeter scales.

1.3.1 *In situ* Monitoring of Physical Processes

At the molecular level, the chemical properties of polymers, such as their composition, structure, molecular weight, and topology *etc.* determine their properties.[21] Furthermore, the polymers' physical properties, such as self-assembly behavior, crystallization, phase separation, degradation, and other polymer-based physical processes are also dramatically influenced by these chemical factors. The understanding of these processes at the micro-level, with accuracy and sensitivity, is therefore a topic of major interest for polymer chemists. To date, numerous characterization techniques, such as Nuclear magnetic resonance (NMR), Size-exclusion chromatography (SEC), mass spectrometry (MS), multiangle light scattering (MALS), dynamic light scattering (DLS) and more have been applied in the characterization of these chemical and physical properties of polymers.

As mentioned previously, the uniqueness of fluorescent techniques, such as fast signaling, being non-invasive, and highly sensitive, enables this technique to provide key chemical and physical information as well as allow the monitoring of changes in the polymer system *in-situ* when rationally designed. Fluorophores which respond to changes in the environment or the packing state have been incorporated into the polymer systems and applied to monitor the polymerization and other key processes. Recently, Tang's group designed a fluorescent AIE initiator for the *in situ* visualization of the polymerization process by tracking the viscosity change during polymerization (Figure 1.12a).[81] The *in situ* monitoring of the conversion *via* fluorescence techniques lies in the fact that the increase of the viscosity during the polymerization process restricts the intramolecular motion of the non-fluorescent AIE initiator, which further exhibited strong photoluminescence as the output signal. The design of the fluorescent systems to monitor other polymer properties, such as critical solution temperatures,[72] crystallization,[73-75] phase separation,[82], and gelation process[83] have also been extensively investigated.

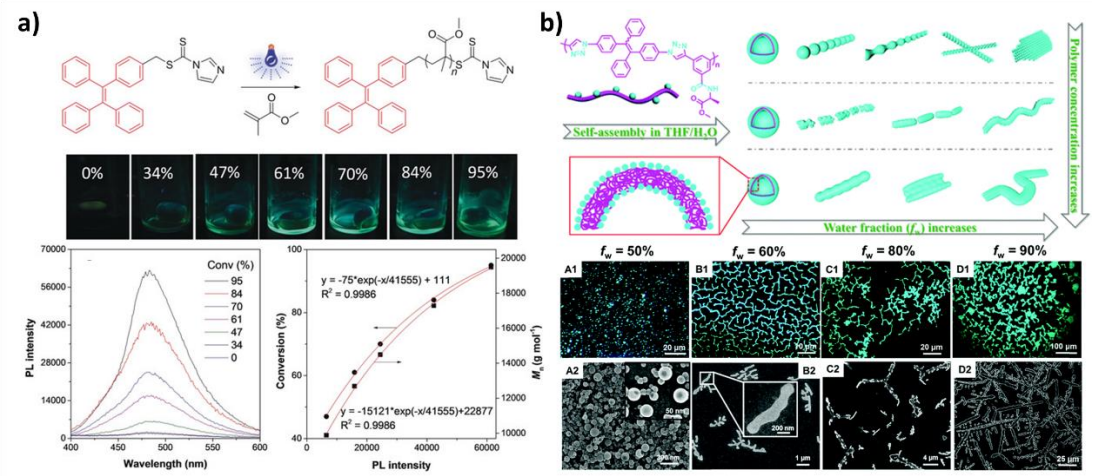

Figure 1.12 a) AIE fluorophore functionalized RAFT CTA for in situ visualization of the polymerization process;[81] b) Investigation of the morphological transitions of the polymeric assemblies *via in-situ* fluorescence imaging technique.[84] Figure adapted from refs 81, 84.

The assembly behavior of polymers plays an important role in constructing nanomaterials for different applications and has become important in polymer research.[85] To date, a large number of research groups working with fluorescent polymer systems have paid particular attention to tracking and monitoring such assembly processes through fluorescent techniques. [84-87] In 2018, Tang *et. al.* investigated the morphological transitions of polymeric assemblies *via* fluorescence imaging (Figure 1.12b).[84] In this case, the fluorescent properties of the polymeric system are not only beneficial in monitoring the polymer assembly process but also the disassembly and degree of the polymerization are also able to be tracked by fluorescence outputs.[52]

Apart from the single fluorophore system, the interaction of two fluorophores can provide useful information on the distance between them through the energy transfer, which has been utilized in monitoring complicated polymer processes. Our group has reported a system formed *via* photo-polymerization induced self-assembly (photo-PISA) which showed interesting fusion properties in different morphologies (Figure 1.13).[58] To investigate such a fusion process, fluorescent monomers incorporating rhodamine and a

substituted maleimide were designed and polymerized. By monitoring the change in fluorescence lifetime, the fusion process was well studied, and such behavior visualized by confocal microscopy.

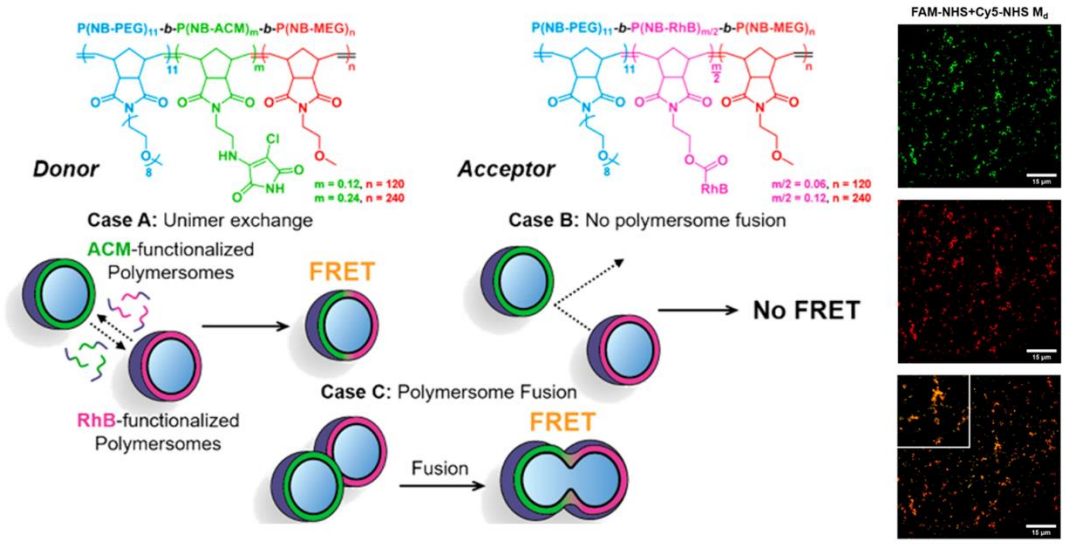

Figure 1.13 Design strategy for the FRET system for direct monitoring of membrane fusion during the polymersome mixing.[58] Figure adapted from refs 58.

1.3.2 Imaging in Biological Systems

The investigation of biomolecular interactions and behaviors at the intracellular level play a vital role in understanding many complex biological and biomedical processes. With the development of diverse commercialized fluorophores, fluorescence microscopy is quickly becoming a key technique for studying various micro-structures from cell cultures and tissues, to bacterial and mammalian cells.[88] Owing to the high flexibility of polymeric materials, fluorescent polymers bearing different functional groups have been extensively investigated in visualizing these specific cellular structures and biomolecular

interactions. Meanwhile, the biomimetic design of polymeric materials could also achieve better compatibility within biological environments.

To date, many fluorescent polymeric systems have been utilized to provide 2D and 3D information on intracellular systems *via* confocal laser scanning microscopic (CLSM) techniques. Fluorescent polymers with different emissions have been applied in visualizing the various cell structures including stem cells,[76] cancer cells[77], and many others.[78, 79] Additionally, the modification of tracking groups on the polymer structure allows for selectively monitoring specific cellular structures like plasma membranes,[89] microtubules[90] and mitochondria.[91] The imaging of advanced biological structures like tissues and organs are not only crucial in scientific research, it is of particular importance in medical operations such as visualization of the diseased or nondiseased tissues and further directing the surgery by increasing the contrast (Figure 1.14a).[92, 93] Xiong's Group has established fluorescent polymer dots that were successfully used in visualizing the structure of the valves, capillaries, and vessels in *vivo* at a high temporal and spatial resolution.[94] Besides imaging at the cellular level, the groups of Yury Gogotsi and Peter I. Lelkes have designed a fluorescent composite based on the poly(l-lactic acid) which uses a fluorescent nanodiamond as the bone scaffold, allowing for fluorescent monitoring of the bone re-growth *in vivo*.[95]

Despite these interesting results, one obstacle conventional fluorescence microscopy (FLM) and CLSM suffer from is the limited resolution for objects smaller than 200 nm, due to the diffraction limit of light. The researchers that require exquisite spatial and temporal resolution are hampered before the investigation of the super-resolved fluorescence microscopy (SRM), which has recently emerged as a prominent technique for imaging at the nanoscale.[96] Using this technique, Sun and Wu *et.al.* have constructed several fluorescence polymer dots for dual-color imaging of different subcellular

structures, like microtubule filaments and clathrin-coated vesicles (Figure 1.14b).[97] Liu's group has reported a photo-switchable spiropyran-terminated poly(ε-caprolactone) for localization-based super-resolution microscopy, which was able to visualize nanostructures with sub-50 nm resolution in the live cell.[98]

Fluorescence polarization,[99] multiphoton fluorescence,[100] and other fluorescence techniques have also been investigated to increase resolution, diminish background influence, and provide a greater level of information across multiple dimensions. FLIM is a pioneering technique that allows for visualizing the fluorescence lifetime changes at the intracellular level.[101, 102] Different to the fluorescence intensity, the fluorescence lifetime is a property that is less affected by the concentration, light source, and measurement methods. Our group has reported a fluorescent polymeric system in which the lifetime of the fluorophore is only dependent on the morphology of the assemblies (Figure 1.14c).[50] Utilizing the FLIM technique, the different morphologies of the polymeric assembles in the cellular environment were mapped by the different fluorescence lifetime signals.

In addition to using the single technique, the combination of multiple imaging techniques allows for synergic visualization of the biosystem, providing varying levels of information. Tian's group designed a poly(*N*-(2-hydroxypropyl)methacrylamide) system bearing a gadolinium complex for magnetic resonance imaging (MRI) imaging and a naphthalimide fluorophore for fluorescence imaging.[38] Combining two techniques, such multimodality (MRI/fluorescence) system achieved both optical and MRI-based pH sensing at cellular scale. A similar polymeric system has been designed by Yi *et.al* for FL/MR dual-modal imaging (Figure 1.14d).[103] The excellent biocompatibility and FL/MR dual-modal imaging capability of this polymer system has been proved in both HeLa cells and mice as models.

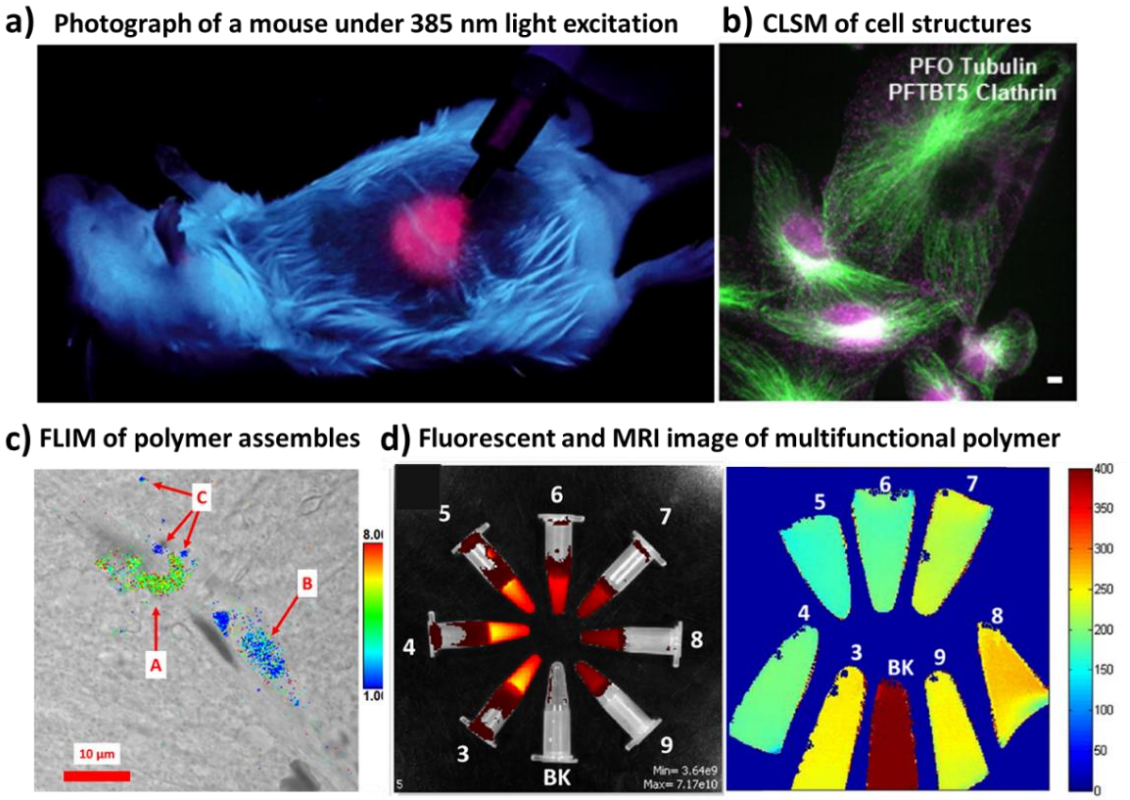

Figure 1.14 a) Photograph of a mouse injected with fluorescent polymer dot−GOx under 385 nm light excitation. [93] b) Dual-colour imaging of microtubule filaments and clathrin-coated vesicles labeled using polymer dots.[97] c) FLIM of polymer assemblies constructed by the Dithiomaleimide functionalized polymer in cellular environment.[50] d) MRI relaxation (T_2) maps (left) and fluorescence imaging (right) of the fluorescent polymer solution at different pH.[38] Figures adapted from refs 38, 50, 93 and 97.

To summarize, the development of fluorescent microscopy techniques and the investigation of polymeric fluorescent materials has led to the understanding of biological behavior with high precision and accuracy, providing unparalleled levels of detail. The tremendous progress in fabricating stable, highly functional, biocompatible polymeric fluorescent materials for imaging applications has shown great potential, encouraging investigation into future applications across both academia and industry.

1.3.3 Sensing and Detection

Besides applications within imaging, the fast signaling and high sensitivity of fluorescence have also been widely applied in analytic and diagnostic chemistries. Fluorescent chemosensors, defined as "compounds incorporating a binding site, a fluorophore, and a mechanism for communication between the two sites", are particularly important to monitor species in intracellular environments.[104] After the first development of a fluorescent chemosensor by F. Goppelsröder in 1867, many fluorescent chemosensors have been designed based on the small molecule fluorophores and inorganic complexes.[105] By selective design of the molecular structures and binding site over the fluorophores, the fluorescent signal could respond to certain targets in a fast and sensitive manner. Furthermore, with the development of polymeric stimuli-responsive systems, the incorporation of fluorophores allows for further development of fluorescent chemosensors, by controlling the interaction behavior of polymer matrix. To date, a large number of fluorescent polymeric sensors have been developed in response to diverse species, ranging from metal ions, small molecules to biomolecules (Table 1.3).

Table 1.3 The summary of some reported fluorescent polymeric sensors.

Sensing targets	Published researches on fluorescent polymeric sensors
metal ions	Cations: H^+,[106-109] Al^{3+},[110, 111] Cu^{2+},[112, 113] Zn^{2+},[114] Hg^{2+},[48, 115] Pb^{2+},[116] Co^{2+},[117] K^+.[118] Anions: F^-,[119, 120] ClO^-,[121] reactive oxygen (ROS) and nitrogen (RNS).[39, 122]
Small molecules	H_2O,[123] sugars,[124, 125] amino acids,[126, 127] neutral ROS/RNS,[128-132] explosives,[133-136] chiral compounds[137-139] organic vapours,[140] gases including O_2,[106, 141] H_2S,[138, 142, 143] CO_2,[54, 144]
Biomolecules	ATP,[145] DNA,[146, 147] RNA,[148-150] peptidase,[151, 152] protein,[153] enzyme,[154] disease biomarkers.[155]

The fluorescent polymeric sensors could be designed by directly incorporating fluorescent chemosensors with specific binding sites onto the polymers (Figure 1.15).[115, 132, 142] Utilising the polymer as the matrix or scaffold may also be an option, which could potentially solve some problems that are observed with the small molecule chemosensors, like solubility, stability, and some biological behaviors, such as accumulation times and capacities.[156] By directly polymerizing naphthalic chemosensors, Chen *et. al.* have developed an endogenous HClO sensing system with good water dispersibility, fast response (< 40 s), and high sensitivity, which achieved the visualization of endogenous HClO with lipopolysaccharides induced acute liver injury in zebrafish.[122]

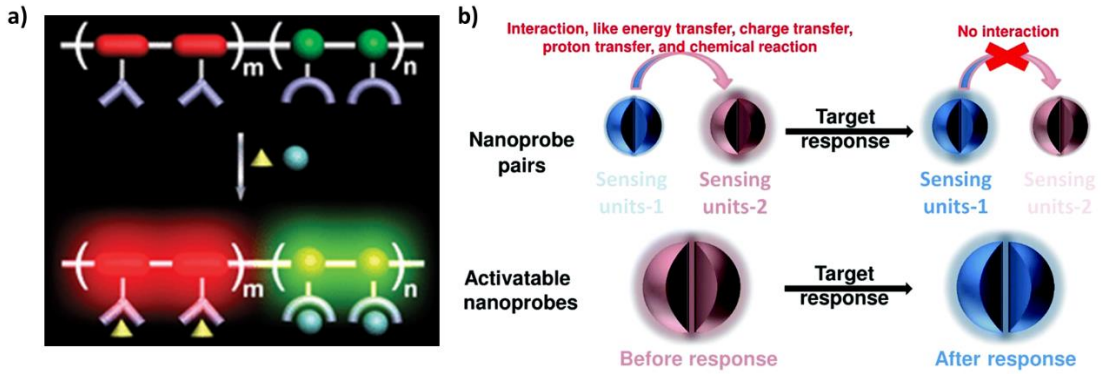

Figure 1.15 a) Schematic illustration of the polymeric fluorescent sensor by direct incorporation of the small molecule fluorophores;[146] b) Design of the responsive polymers based fluorescent sensing systems.[157] Figure adapted from refs. 146 and 157.

Another design strategy for fluorescent polymeric sensors is achieved by incorporating the fluorophores onto the polymeric structures which have selective interacting sites or responsive behaviors.[153, 158, 159] The selective swelling, degrading, assembly/disassembly, and many other responsive properties, allows for selectively changing the microenvironment and interactions of the incorporated fluorophores, which will further influence their photophysical behaviors. For example, the Inada group has reported a series of fluorescent polymeric thermometers for monitoring the temperature inside live

cells based on thermo-responsive polymers and environmental-sensitive fluorophores.[160, 161] The phase transition of the thermo-responsive poly(*N*-isopropylacrylamide) could effectively influence the microenvironment of the conjugated fluorophores which resulted in the thermo-responsive fluorescence. Interestingly, through a similar design, temperature-dependent changes in the fluorescence lifetime were also achieved to minimize the influence of the excitation source and the concentration.[162, 163]

Molecular imprinting is another strategy to design the polymeric sensing system by spatially controlling the binding site to the target agent. Using the target analyte as the template molecule the target agent was initially involved in the construction of the polymeric structures through a covalent or noncovalent bond (Figure 1.16). After removal of the template molecule, the binding ability is achieved with the spatial binding sites which are complementary to the template.[164] Zhao's group has prepared a polymeric fluorescence sensing system for detecting folate receptors by a molecular imprinting strategy. The folate receptors were used as the temperate molecule, where binding in the

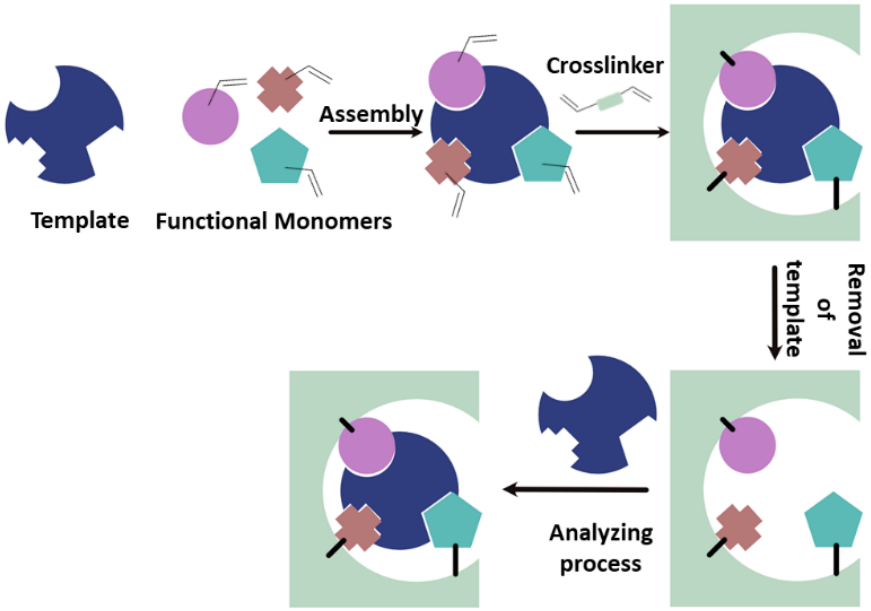

Figure 1.16 Design of a fluorescence sensing system based on the molecular imprinting strategy.

doubly cross-linkable micelles resulted in the polymeric imprinted nanoparticles.[165] With the ability to introduce spatial binding sites *via* the template molecule such molecular imprinting strategy has been wildly applied in sensing into complex biomolecular structures.[139, 164-167]

In addition to monitoring micro-level interactions, the design of bulk fluorescent sensors based on polymeric materials, like fluorescent films and hydrogels, is particularly interesting for the real-time analysis and *in situ* detection with visible outputs. For example, Jun Zhang *et.al.* designed cellulose-based fluorescent materials with superior amine-response, which allow for fast and accurate detection of biogenic amines by eye in real-time (Figure 1.17a).[168] Except for small molecule detection, the MacLachlan group has designed a stretchable elastomer encapsulating cellulose nanocrystals to provide the real-time information on mechanical stress (Figure 1.17b).[169]

Interestingly, the construction of bulk fluorescent materials allows for spatial localization of the fluorescence outputs within three dimensions. Tang's group have constructed a fluorescent macroscopic adhered hydrogel with manipulatable macroscopic structure (Figure 1.17c).[170] A Rubik's Cube-like structure was constructed by seven AIE dyes encapsulated within hydrogels which provide the possibility to construct fluorescent patterns with dynamic structures. In 2019, Chen's group have designed a fluorescent color-switchable hydrogel actuator based on supramolecular dynamic metal-ligand coordination (Figure 1.17d).[171] Both the 3D shape deformation and switchable emission have been achieved in the single hydrogel system which provided the fluorescence information in multiple dimensions. In summary, the construction of such bulk polymeric materials with the fluorescent readout provides real-time and readable information which allows for further application in fluorescent displays, biomimetic soft robotics, and portable biological sensors.

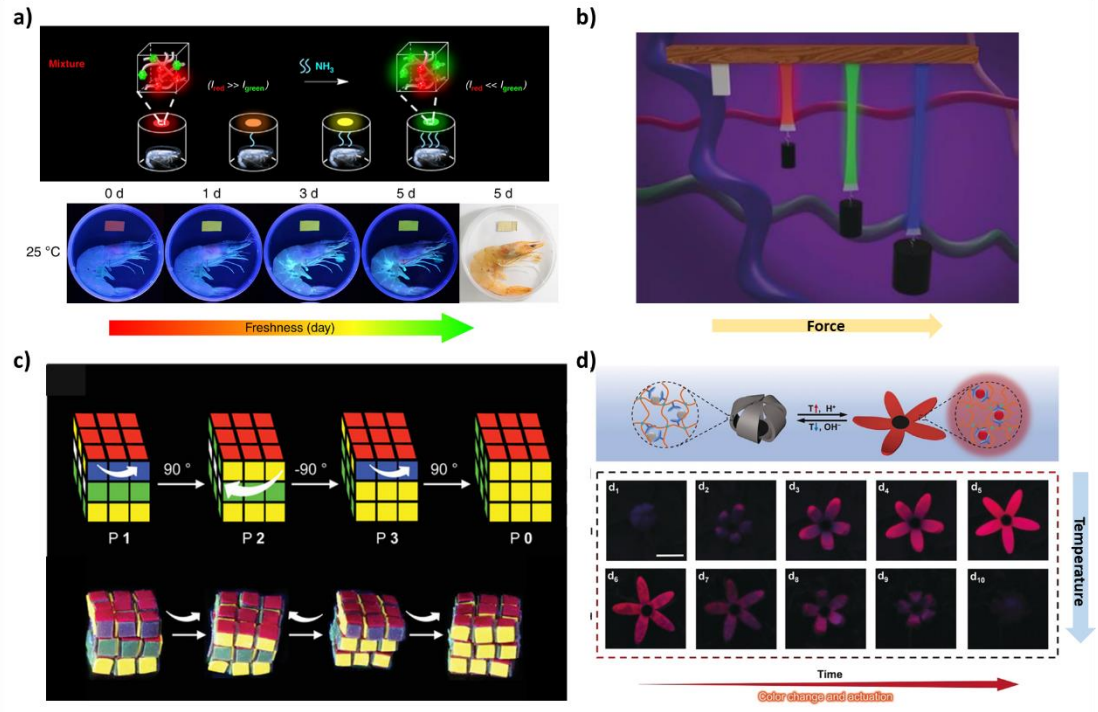

Figure 1.17 a) Biopolymer-based ratiometric fluorescent materials for real-time detecting the biogenic amines;[168] b) Stretchable elastomer system with the responsive output under different mechanical stress;[169] c) Pattern transformable fluorescent Rubik's cube fabricated by the fluorescent hydrogels.[170] d) The fluorescent actuator-based artificial apricot flowers bearing with the switchable emission and shape-deformation capabilities. [171] Figure adapted from refs.

1.3.4 Information Storage

The high specificity of the fluorescent readout has long been applied to our daily life as an information storage technique, with an interesting example being in anti-counterfeiting applications for goods and currency. The versatile fluorescent coding techniques are particularly beneficial in coding and identifying multiplex and high-throughput information across the fields of biological, medicinal, and material sciences.[172, 173] Fluorescence emission,[174, 175] lifetimes,[176, 177] polarities,[178], and other related parameters[179] have been employed as the readout signals for medical diagnosis,[180] drugs screening[174] and information storage (Figure 1.18).[80] In recent decades, fluorescent

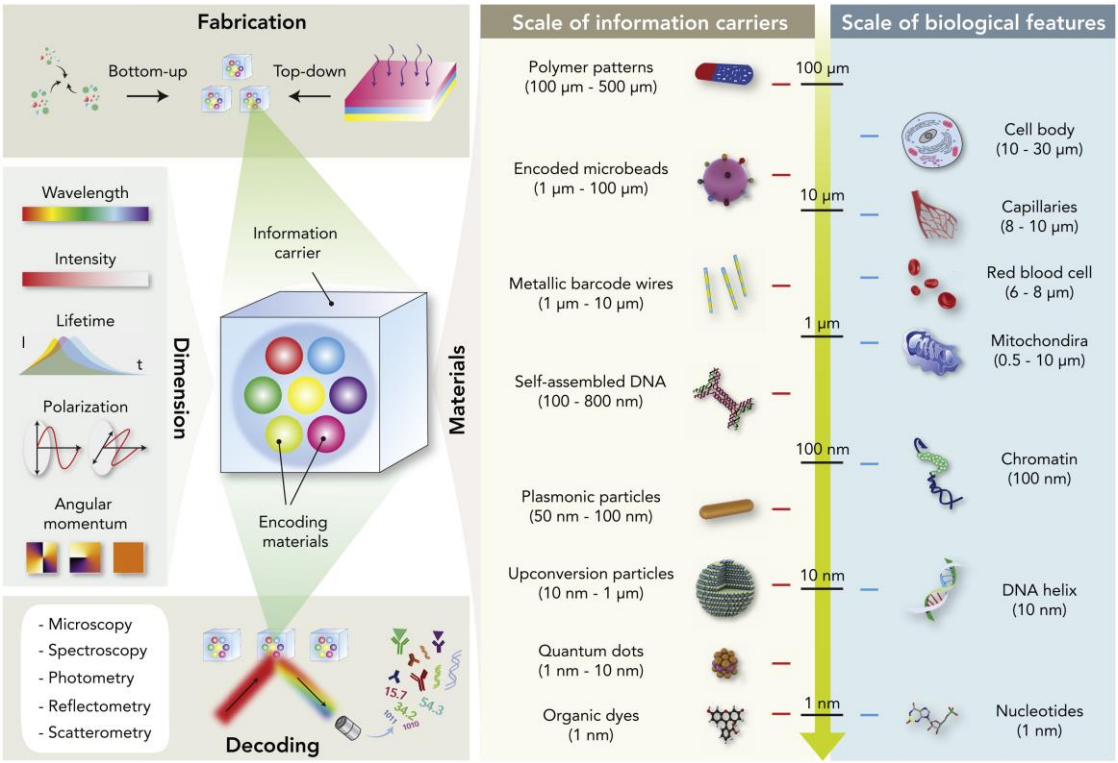

Figure 1.18 The illustration of the fluorescent materials as the information carriers from microscopic to nanoscale, comparable with various intracellular biological features (right) and utilizing the different decoding techniques (left).[181] Figure adapted from refs.

materials at different scales have been tailored as information carriers for the storage and selective extraction of various biological features from the molecular level, like nucleotides, to the macro and even bulk level, such as cell and tissues. Owing to their flexibility, polymers have provided unheralded interest in constructing the different assemblies ranging from macroscopic (e.g. hydrogel) to nanoscale (e.g. polymer dots). For example, nano-assembles fabricated by conjugate polymers have been achieved by Qin and Wu's group in which the multiple fluorescent emissions as information outputs have been applied for full-color patterning.[182] The extraordinary stability fluorescence of such materials under UV lamp illumination allows for fabricating different readable images based on the inkjet printing method (Figure 1.19).

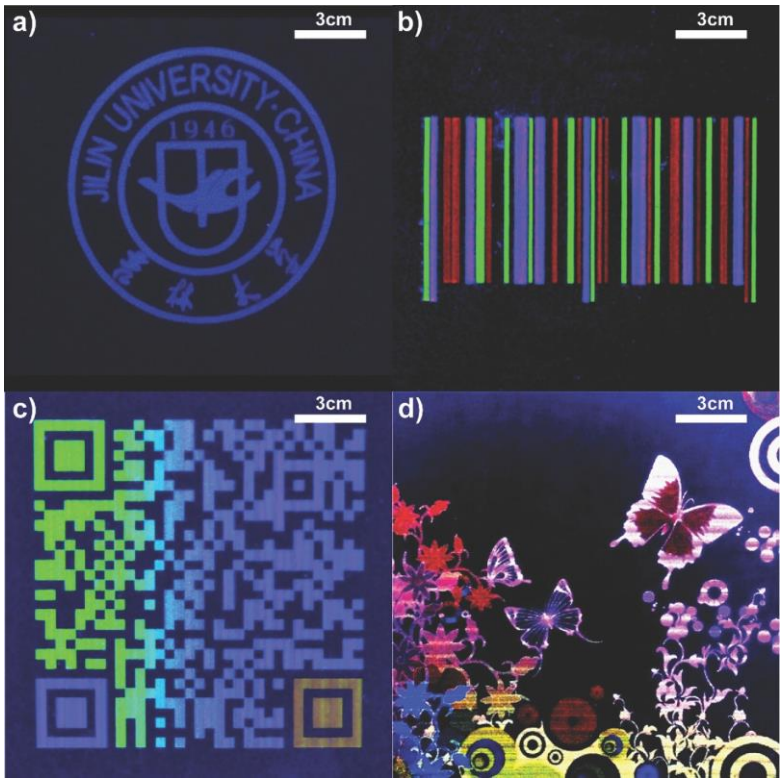

Figure 1.19 The fluorescence photograph of the inkjet printing of full - color fluorescence patterning using the polymer dots inks. a) printed university logo; (b) and c) 1D and 2D barcodes; d) sophisticated pattern. [182] Figure adapted from refs 182.

Besides nanoparticles, the storage of information at higher dimensional degrees has attracted great attention for more complex systems. Crystallization-driven self-assembly (CDSA) is a novel polymer assembly methodology in which block copolymers with crystallizable core-forming blocks can be manipulated to create a range of structures with exquisite control.[183] In addition to spherical structures, 1D cylindrical assembles and 2D platelet structures can be accessed by different core-corona chemistries and ratios. Particularly, the epitaxial growth of such crystallized structures offers an unambiguous way to attach multiple functionalities at specific locations. Taking advantage of this, the Winnik group has fabricated nanoscale fluorescent barcodes with cylindrical structure *via* CDSA (Figure 1.20a).[184] By selective epitaxial growth of a nonfluorescent polymer, barcode information by combing fluorescent segments separated by nonemissive

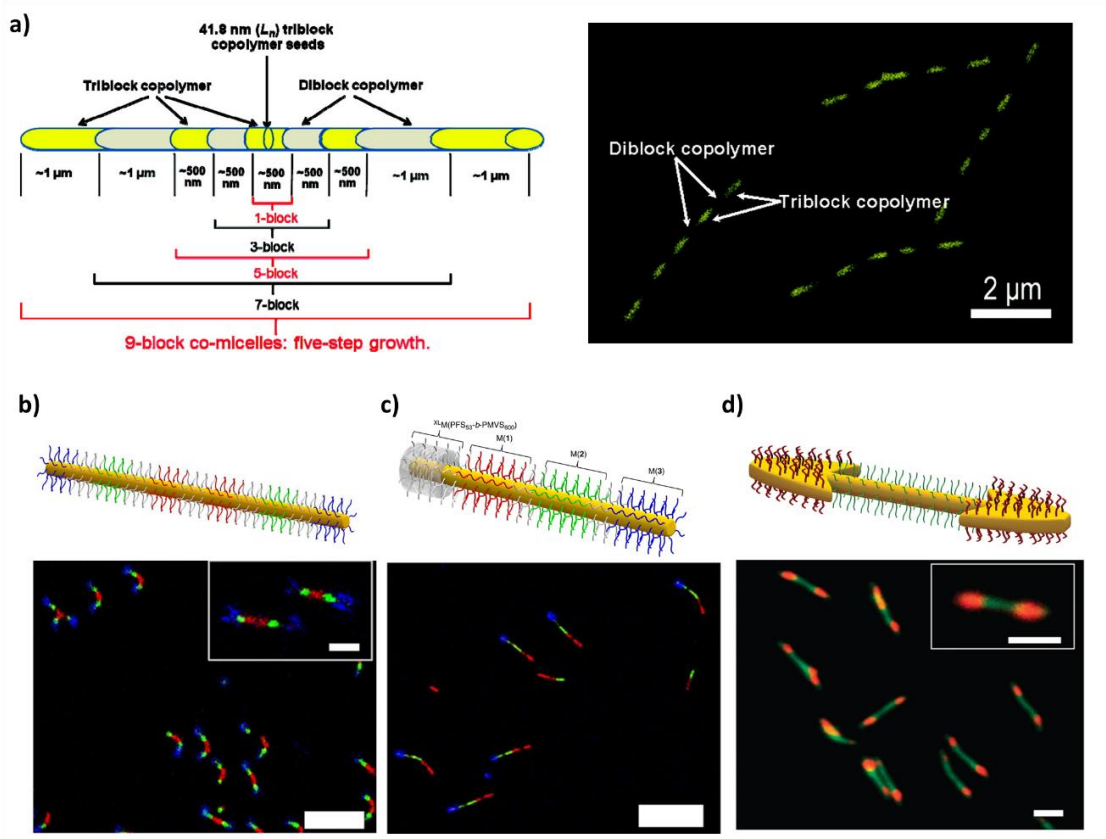

Figure 1.20 a) Design of the 9-block cylindrical assembles with the controlled length of the fluorescence blocks (gray, non-fluorescent copolymer; yellow, fluorescent copolymer) [184] b-c) Centrosymmetric and non-centrosymmetric triblock comicelles encoded with different fluorescent information.[185] d) Double-headed spear-like micelle architectures with encoded fluorescent information.[186] Figure adapted from refs 184,185 and 186.

segments was realized with the controlled length extracted by confocal microscopy. Different from the single fluorescence of the information output, multiple emission has been achieved by the Manners group which leads to higher level of information coding and more precisely decoding.[185, 186] Controlled growth of cylindrical assemblies led to the precise localization of the fluorophores at the nanoscale, generating pixels with fully tunable color (Figure 1.20 b-d). Such controllable assembles with distinct domains allow for storing multiple fluorescence information on a single structure which offers a potential fluorescent material for high-throughput imaging and diagnostics.

1.4 Summary

As an important photophysical process, fluorescence has long been an indispensable tool in chemical, biological, and materials research. The first section of this introduction has comprised of some basic fluorescence concepts and characterizing methods for quantifying or visualizing the fluorescent signals. This was followed by a brief introduction on the different types of fluorescent materials, with fluorescent polymers being the primary focus, due to their robust properties, combining both good flexibilities from the polymer matrix and the opportunity to produce responsive output signals with the fluorescent components. Several design strategies for fluorescent polymer systems were summarized in this chapter, including the polymerization of fluorescent monomers *in situ*, fluorophore-initiated polymerization, and post modifications to generate fluorescent polymers. Various polymer systems bearing different fluorescent components have been exampled which are compatible with different polymerization techniques or functional methodologies. Substituted maleimides derivatives are a class of novel fluorophores distinguished by their small size and bright fluorescence emissions, which have been identified as the ideal fluorescent components for the polymer functionalization. The detailed fluorescent mechanism of the substituted maleimides and its applications in polymer materials are discussed in Chapters 2 and 3.

Finally, combined with pioneering work in fluorescent spectroscopy and microscopy, fluorescent polymeric materials constructed at different length scales can be tailored for various applications, such as monitoring the chemical/physical behaviors of polymers, imaging the biology structures, analyzing/diagnosing the small molecules, and storing the information. In chapter 4, the substituted maleimides based polymeric nanogel system has been designed for the information coding and fluorescent lifetime imaging in the live cell environment.

1.5 References

1. Vendrell, M.; Zhai, D.; Er, J. C.; Chang, Y. T., Combinatorial strategies in fluorescent probe development. *Chem. Rev.* **2012,** *112* (8), 4391.

2. Klymchenko, A. S., Solvatochromic and Fluorogenic Dyes as Environment-Sensitive Probes: Design and Biological Applications. *Acc. Chem. Res.* **2017,** *50* (2), 366.

3. Weng, G.; Thanneeru, S.; He, J., Dynamic Coordination of Eu-Iminodiacetate to Control Fluorochromic Response of Polymer Hydrogels to Multistimuli. *Adv. Mater.* **2018,** *40* (11), 1706526.

4. Ren, H.; Long, Z.; Cui, M.; Shao, K.; Zhou, K.; Ouyang, J.; Na, N., Dual-Functional Nanoparticles for In Situ Sequential Detection and Imaging of ATP and H2 O2. *Small* **2016,** *12* (29), 3920.

5. Zhang, Z.; Shikha, S.; Liu, J.; Zhang, J.; Mei, Q.; Zhang, Y., Upconversion Nanoprobes: Recent Advances in Sensing Applications. *Anal. Chem.* **2018,** *91* (1), 548.

6. Bernard, V.; Mário N. B. S.; Molecular Fluorescence, Wiley‐VCH Verlag GmbH & Co, 2012.

7. Würth, C.; Grabolle, M.; Pauli, J.; Spieles, M.; Resch-Genger, U., Relative and absolute determination of fluorescence quantum yields of transparent samples. *Nat. Protoc.* **2013,** *8* (8), 1535.

8. Markus S.; Johan H.; Jörg E.; Handbook of Fluorescence Spectroscopy and Imaging, Wiley‐VCH Verlag GmbH & Co, 2011.

9. Quack, M.; Kutzelnigg, W., Molecular-Spectroscopy and Molecular-Dynamics - Theory and Experiment. *Berichte Der Bunsen-Gesellschaft-Physical Chemistry Chemical Physics* **1995,** *99* (3), 231.

10. Król, A. K., Molecular Spectroscopy—Experiment and Theory. Springer, Cham: 2019.

11. Xiong, H.; Zuo, H.; Yan, Y.; Occhialini, G.; Zhou, K.; Wan, Y.; Siegwart, D. J., High-Contrast Fluorescence Detection of Metastatic Breast Cancer Including Bone and Liver Micrometastases via Size-Controlled pH-Activatable Water-Soluble Probes. *Adv. Mater.* **2017**, 1700131.

12. Bruemmer, K. J.; Walvoord, R. R.; Brewer, T. F.; Burgos-Barragan, G.; Wit, N.; Pontel, L. B.; Patel, K. J.; Chang, C. J., Development of a General Aza-Cope Reaction Trigger Applied to Fluorescence Imaging of Formaldehyde in Living Cells. *J. Am. Chem. Soc.* **2017,** *139* (15), 5338.

13. Heo, C. H.; Cho, M. K.; Shin, S.; Yoo, T. H.; Kim, H. M., Real-time monitoring of vesicle pH in an endocytic pathway using an EGF-conjugated two-photon probe. *Chem. Commun.* **2016,** *52* (97), 14007.

14. Lavis, L. D.; Raines, R. T., Bright Ideas for Chemical Biology. *ACS Chemical Biology* **2008,** *3* (3), 142.

15. Lakowicz, J. R., Principles of Fluorescence Spectroscopy. **2006**.

16. Tomasini, E. P.; San Román, E.; Braslavsky, S. E., Validation of Fluorescence Quantum Yields for Light-Scattering Powdered Samples by Laser-Induced Optoacoustic Spectroscopy. *Langmuir* **2009,** *25* (10), 5861.

17. Resch-Genger, U.; Bremser, W.; Pfeifer, D.; Spieles, M.; Hoffmann, A.; DeRose, P. C.; Zwinkels, J. C.; Gauthier, F.; Ebert, B.; Taubert, R. D.; Monte, C.; Voigt, J.; Hollandt, J.; Macdonald, R., State-of-the art comparability of corrected emission spectra. 1. Spectral correction with physical transfer standards and spectral fluorescence standards by expert laboratories. *Anal. Chem.* **2012,** *84* (9), 3889.

18. Porres, L.; Holland, A.; Palsson, L. O.; Monkman, A. P.; Kemp, C.; Beeby, A., Absolute measurements of photoluminescence quantum yields of solutions using an integrating sphere. *J. Fluoresc.* **2006,** *16* (2), 267.

19. Time-Resolved Fluorescence Techniques. In *Molecular Fluorescence*, pp 285.

20. Berezin, M. Y.; Achilefu, S., Fluorescence lifetime measurements and biological imaging. *Chem. Rev.* **2010,** *110* (5), 2641.

21. Zhang, Z. P.; Rong, M. Z.; Zhang, M. Q., Polymer engineering based on reversible covalent chemistry: A promising innovative pathway towards new materials and new functionalities. *Prog. Polym. Sci.* **2018,** *80*, 39.

22. Herbert, K. M.; Schrettl, S.; Rowan, S. J.; Weder, C., 50th Anniversary Perspective: Solid-State Multistimuli, Multiresponsive Polymeric Materials. *Macromolecules* **2017,** *50* (22), 8845.

23. Meng, F.; Hennink, W. E.; Zhong, Z., Reduction-sensitive polymers and bioconjugates for biomedical applications. *Biomaterials* **2009,** *30* (12), 2180.

24. Che, H.; van Hest, J. C. M., Stimuli-responsive polymersomes and nanoreactors. *J. Mater. Chem. B* **2016,** *4* (27), 4632.

25. Nair, L. S.; Laurencin, C. T., Biodegradable polymers as biomaterials. *Prog. Polym. Sci.* **2007,** *32* (8-9), 762.

26. Cheng, S.; Jin, Y.; Wang, N.; Cao, F.; Zhang, W.; Bai, W.; Zheng, W.; Jiang, X., Self-Adjusting, Polymeric Multilayered Roll that can Keep the Shapes of the Blood Vessel Scaffolds during Biodegradation. *Adv. Mater.* **2017,** *29* (28), 1700171.

27. Kamaly, N.; Yameen, B.; Wu, J.; Farokhzad, O. C., Degradable Controlled-Release Polymers and Polymeric Nanoparticles: Mechanisms of Controlling Drug Release. *Chem. Rev.* **2016,** *116* (4), 2602.

28. Canfarotta, F.; Whitcombe, M. J.; Piletsky, S. A., Polymeric nanoparticles for optical sensing. *Biotechnol. Adv.* **2013,** *31* (8), 1585.

29. Ganugula, R.; Arora, M.; Saini, P.; Guada, M.; Kumar, M., Next Generation Precision-Polyesters Enabling Optimization of Ligand-Receptor Stoichiometry for

Modular Drug Delivery. *J. Am. Chem. Soc.* **2017,** *139* (21), 7203.

30. Christopherson, C. J.; Mayder, D. M.; Poisson, J.; Paisley, N. R.; Tonge, C. M.; Hudson, Z. M., 1,8-Naphthalimide-Based Polymers Exhibiting Deep-Red Thermally Activated Delayed Fluorescence and Their Application in Ratiometric Temperature Sensing. *ACS Appl. Mater. Interfaces.* **2020**, 20000.

31. Grazon, C.; Rieger, J.; Méallet-Renault, R.; Charleux, B.; Clavier, G., Ultrabright Fluorescent Polymeric Nanoparticles Made from a New Family of BODIPY Monomers. *Macromolecules* **2013,** *46* (13), 5167.

32. Hu, J.; Li, Q.; Wang, X.; Shao, S.; Wang, L.; Jing, X.; Wang, F., Developing Through-Space Charge Transfer Polymers as a General Approach to Realize Full-Color and White Emission with Thermally Activated Delayed Fluorescence. *Angew. Chem., Int. Ed.* **2019,** *58* (25), 8405.

33. Hu, Y.; Han, T.; Yan, N.; Liu, J.; Liu, X.; Wang, W. X.; Lam, J. W. Y.; Tang, B. Z., Visualization of Biogenic Amines and In Vivo Ratiometric Mapping of Intestinal pH by AIE-Active Polyheterocycles Synthesized by Metal-Free Multicomponent Polymerizations. *Adv. Funct. Mater.* **2019,** *29* (31), 1902240

34. Sauve, E. R.; Tonge, C. M.; Hudson, Z. M., Aggregation-Induced Energy Transfer in Color-Tunable Multiblock Bottlebrush Nanofibers. *J. Am. Chem. Soc.* **2019,** *141* (41), 16422.

35. Al-Natour, M. A.; Yousif, M. D.; Cavanagh, R.; Abouselo, A.; Apebende, E. A.; Ghaemmaghami, A.; Kim, D.-H.; Aylott, J. W.; Taresco, V.; Chauhan, V. M.; Alexander, C., Facile Dye-Initiated Polymerization of Lactide–Glycolide Generates Highly Fluorescent Poly(lactic-co-glycolic Acid) for Enhanced Characterization of Cellular Delivery. *ACS Macro Lett.* **2020,** *9* (3), 431.

36. Wu, G.; Wang, Z.-S.; Bai, Q.-Y., Simultaneous Dual Thermoresponsiveness and

Fluorescence of Degradable Amphiphilic Diblock Copolymers in Water: Synergy of Supramolecular Interactions and Crystallization. *Macromolecules* **2019,** *52* (15), 5907.

37. Li, X.; Sun, Y.; Chen, J.; Wu, Z.; Cheng, P.; Li, Q.; Fang, J.; Chen, D., Enhanced fluorescence quantum yield of syndiotactic side-chain TPE polymers via Rh-catalyzed carbene polymerization: influence of the substitution density and spacer length. *Polym. Chem.* **2019,** *10* (13), 1575.

38. Su, F.; Agarwal, S.; Pan, T.; Qiao, Y.; Zhang, L.; Shi, Z.; Kong, X.; Day, K.; Chen, M.; Meldrum, D.; Kodibagkar, V. D.; Tian, Y., Multifunctional PHPMA-Derived Polymer for Ratiometric pH Sensing, Fluorescence Imaging, and Magnetic Resonance Imaging. *ACS Appl. Mater. Interfaces.* **2018,** *10* (2), 1556.

39. Zhang, M.; Song, C. C.; Su, S.; Du, F. S.; Li, Z. C., ROS-Activated Ratiometric Fluorescent Polymeric Nanoparticles for Self-Reporting Drug Delivery. *ACS Appl. Mater. Interfaces.* **2018,** *10* (9), 7798.

40. Repenko, T.; Rix, A.; Ludwanowski, S.; Go, D.; Kiessling, F.; Lederle, W.; Kuehne, A. J. C., Bio-degradable highly fluorescent conjugated polymer nanoparticles for bio-medical imaging applications. *Nat. Commun.* **2017,** *8* (1), 470.

41. Relogio, P.; Bathfield, M.; Haftek-Terreau, Z.; Beija, M.; Favier, A.; Giraud-Panis, M.-J.; D'Agosto, F.; Mandrand, B.; Farinha, J. P. S.; Charreyre, M.-T.; Martinho, J. M. G., Biotin-end-functionalized highly fluorescent water-soluble polymers. *Polym. Chem.* **2013,** *4* (10), 2968.

42. McQuade, D. T.; Pullen, A. E.; Swager, T. M., Conjugated Polymer-Based Chemical Sensors. *Chem. Rev.* **2000,** *100* (7), 2537.

43. Qin, A.; Lam, J. W.; Tang, B. Z., Click polymerization. *Chem. Soc. Rev.* **2010,** *39* (7), 2522.

44. Qin, A.; Lam, J. W. Y.; Jim, C. K. W.; Zhang, L.; Yan, J.; Häussler, M.; Liu, J.;

Dong, Y.; Liang, D.; Chen, E.; Jia, G.; Tang, B. Z., Hyperbranched Polytriazoles: Click Polymerization, Regioisomeric Structure, Light Emission, and Fluorescent Patterning. *Macromolecules* **2008,** *41* (11), 3808.

45. Yao, B.; Hu, T.; Zhang, H.; Li, J.; Sun, J. Z.; Qin, A.; Tang, B. Z., Multi-Functional Hyperbranched Poly(vinylene sulfide)s Constructed via Spontaneous Thiol–Yne Click Polymerization. *Macromolecules* **2015,** *48* (21), 7782.

46. Yuan, W. Z.; Yu, Z.-Q.; Tang, Y.; Lam, J. W. Y.; Xie, N.; Lu, P.; Chen, E.-Q.; Tang, B. Z., High Solid-State Efficiency Fluorescent Main Chain Liquid Crystalline Polytriazoles with Aggregation-Induced Emission Characteristics. *Macromolecules* **2011,** *44* (24), 9618.

47. Qin, A. Tang, L.; Lam, J. W. Y.; Jim, C. K. W.; Yu, Y.; Zhao, H.; Sun, J.; Tang, B. Z., Metal-Free Click Polymerization: Synthesis and Photonic Properties of Poly(aroyltriazole)s. *Adv. Funct. Mater.* **2009,** *19* (12), 1891.

48. Zhang, D.; Yao, Y.; Wu, J.; Protsak, I.; Lu, W.; He, X.; Xiao, S.; Zhong, M.; Chen, T.; Yang, J., Super Hydrophilic Semi-IPN Fluorescent Poly(N-(2-hydroxyethyl)acrylamide) Hydrogel for Ultrafast, Selective, and Long-Term Effective Mercury(II) Detection in a Bacteria-Laden System. *ACS Appl. Bio. Materials.* **2019,** *2* (2), 906.

49. Zhang, T.; Ma, X.; Tian, H., A facile way to obtain near-infrared room-temperature phosphorescent soft materials based on Bodipy dyes. *Chem. Sci.* **2020,** *11* (2), 482.

50. Robin, M. P.; Mabire, A. B.; Damborsky, J. C.; Thom, E. S.; Winzer-Serhan, U. H.; Raymond, J. E.; O'Reilly, R. K., New Functional Handle for Use as a Self-Reporting Contrast and Delivery Agent in Nanomedicine. *J. Am. Chem. Soc.* **2013,** *135* (25), 9518.

51. Robin, M. P.; Raymond, J. E.; O'Reilly, R. K., One-pot synthesis of super-bright fluorescent nanogel contrast agents containing a dithiomaleimide fluorophore. *Mater.*

Horiz. **2015,** *2* (1), 54.

52. Robin, M. P.; Osborne, S. A. M.; Pikramenou, Z.; Raymond, J. E.; O'Reilly, R. K., Fluorescent Block Copolymer Micelles That Can Self-Report on Their Assembly and Small Molecule Encapsulation. *Macromolecules* **2016,** *49* (2), 653.

53. Mabire, A. B.; Robin, M. P.; Quan, W. D.; Willcock, H.; Stavros, V. G.; O'Reilly, R. K., Aminomaleimide fluorophores: a simple functional group with bright, solvent dependent emission. *Chem. Commun.* **2015,** *51* (47), 9733.

54. Mabire, A. B.; Brouard, Q.; Pitto-Barry, A.; Williams, R. J.; Willcock, H.; Kirby, N.; Chapman, E.; O'Reilly, R. K., CO2/pH-responsive particles with built-in fluorescence read-out. *Polym. Chem.* **2016,** *7* (38), 5943.

55. Wang, H.; Xu, M.; Xiong, M.; Cheng, J., Reduction-responsive dithiomaleimide-based nanomedicine with high drug loading and FRET-indicated drug release. *Chem. Commun.* **2015,** *51* (23), 4807.

56. Xie, Y.; Husband, J. T.; Torrent-Sucarrat, M.; Yang, H.; Liu, W.; O'Reilly, R. K., Rational design of substituted maleimide dyes with tunable fluorescence and solvafluorochromism. *Chem. Commun.* **2018,** *54* (27), 3339.

57. Robin, M. P.; Wilson, P.; Mabire, A. B.; Kiviaho, J. K.; Raymond, J. E.; Haddleton, D. M.; O'Reilly, R. K., Conjugation-Induced Fluorescent Labeling of Proteins and Polymers Using Dithiomaleimides. *J. Am. Chem. Soc.* **2013,** *135* (8), 2875.

58. Varlas, S.; Keogh, R.; Xie, Y.; Horswell, S. L.; Foster, J. C.; O'Reilly, R. K., Polymerization-Induced Polymersome Fusion. *J. Am. Chem. Soc.* **2019,** *141* (51), 20234.

59. Robin, M. P.; O'Reilly, R. K., Fluorescent and chemico-fluorescent responsive polymers from dithiomaleimide and dibromomaleimide functional monomers. *Chem. Sci.* **2014,** *5* (7), 2717.

60. Su, C. H.; Wu, Z.; Lin, C. K.; Han, H. A.; Chen, Y. A.; Chou, P. T.; Fu, X.; Peng,

C. H., Polystyrene with Persistently Enhanced Fluorescence: Photo-Induced Atom Transfer Radical Polymerization Using a Pyrene-Based Initiator. *ChemPhotoChem* **2019,** *3* (11), 1153.

61. Jiang, R.; Liu, M.; Huang, Q. Huang, H.; Wan, Q.; Wen, Y.; Tian, J.; Cao, Q.-y.; Zhang, X.; Wei, Y., Fabrication of multifunctional fluorescent organic nanoparticles with AIE feature through photo-initiated RAFT polymerization. *Polym. Chem.* **2017,** *8* (47), 7390.

62. Melnychuk, N.; Egloff, S.; Runser, A.; Reisch, A.; Klymchenko, A. S., Light-Harvesting Nanoparticle Probes for FRET-Based Detection of Oligonucleotides with Single-Molecule Sensitivity. *Angew. Chem., Int. Ed.* **2020,** *59* (17), 6811.

63. Grazon, C.; Si, Y.; Placial, J. P.; Rieger, J.; Meallet-Renault, R.; Clavier, G., Core-shell polymeric nanoparticles comprising BODIPY and fluorescein as ultra-bright ratiometric fluorescent pH sensors. *Photochem. Photobiol. Sci.* **2019,** *18* (5), 1156.

64. Kumar, S.; Maiti, B.; De, P., Carbohydrate-Conjugated Amino Acid-Based Fluorescent Block Copolymers: Their Self-Assembly, pH Responsiveness, and/or Lectin Recognition. *Langmuir* **2015,** *31* (34), 9422.

65. Chen, F.; Cheng, Z.; Zhu, J.; Zhang, W.; Zhu, X., Synthesis of poly(vinyl acetate) with fluorescence via a combination of RAFT/MADIX and “click” chemistry. *Eur. Polym. J.* **2008,** *44* (6), 1789.

66. Wang, C.; Podgórski, M.; Bowman, C. N., Monodisperse functional microspheres from step-growth “click” polymerizations: preparation, functionalization and implementation. *Mater. Horiz.* **2014,** *1* (5), 535.

67. Ouadahi, K.; Sbargoud, K.; Allard, E.; Larpent, C., FRET-mediated pH-responsive dual fluorescent nanoparticles prepared via click chemistry. *Nanoscale* **2012,** *4* (3), 727.

68. Kemal Arda Gunay, P. T., and Harm-Anton Klok, History of Post-Polymerization Modification. In *Functional Polymers by Post-Polymerization Modification*, Patrick Theato, H. A. K., Ed. 2013; p 1.

69. Espeel, P.; Du Prez, F. E., "Click"-Inspired Chemistry in Macromolecular Science: Matching Recent Progress and User Expectations. *Macromolecules* **2015,** *48* (1), 2.

70. Baczko, K.; Fensterbank, H.; Berini, B.; Bordage, N.; Clavier, G.; Méallet-Renault, R.; Larpent, C.; Allard, E., Azide-functionalized nanoparticles as quantized building block for the design of soft-soft fluorescent polystyrene core-PAMAM shell nanostructures. *J. Polym. Sci., Part A: Polym. Chem.* **2016,** *54* (1), 115.

71. Rousseau, G.; Fensterbank, H.; Baczko, K.; Cano, M.; Allard, E.; Larpent, C., Azido-Coated Nanoparticles: A Versatile Clickable Platform for the Preparation of Fluorescent Polystyrene Core–PAMAM Shell Nanoparticles. *Macromolecules* **2012,** *45* (8), 3513.

72. Inal, S.; Kölsch, J. D.; Chiappisi, L.; Janietz, D.; Gradzielski, M.; Laschewsky, A.; Neher, D., Structure-related differences in the temperature-regulated fluorescence response of LCST type polymers. *J. Mater. Chem. C* **2013,** *1* (40), 6603.

73. Ye, X.; Liu, Y.; Lv, Y.; Liu, G.; Zheng, X.; Han, Q.; Jackson, K. A.; Tao, X., In Situ Microscopic Observation of the Crystallization Process of Molecular Microparticles by Fluorescence Switching. *Angew. Chem., Int. Ed.* **2015,** *54* (27), 7976.

74. Khorloo, M.; Cheng, Y.; Zhang, H.; Chen, M.; Sung, H. H. Y.; Williams, I. D.; Lam, J. W. Y.; Tang, B. Z., Polymorph selectivity of an AIE luminogen under nano-confinement to visualize polymer microstructures. *Chem. Sci.* **2020,** *11* (4), 997.

75. Liang, G.; Weng, L.-T.; Lam, J. W. Y.; Qin, W.; Tang, B. Z., Crystallization-Induced Hybrid Nano-Sheets of Fluorescent Polymers with Aggregation-Induced Emission Characteristics for Sensitive Explosive Detection. *ACS Macro Lett.* **2013,** *3* (1),

21.

76. Lorenz, M. R.; Holzapfel, V.; Musyanovych, A.; Nothelfer, K.; Walther, P.; Frank, H.; Landfester, K.; Schrezenmeier, H.; Mailander, V., Uptake of functionalized, fluorescent-labeled polymeric particles in different cell lines and stem cells. *Biomaterials* **2006,** *27* (14), 2820.

77. Zhang, X.; Zhang, X.; Yang, B.; Liu, M.; Liu, W.; Chen, Y.; Wei, Y., Polymerizable aggregation-induced emission dye-based fluorescent nanoparticles for cell imaging applications. *Polym. Chem.* **2014,** *5* (2), 356.

78. Thapaliya, E. R.; Zhang, Y.; Dhakal, P.; Brown, A. S.; Wilson, J. N.; Collins, K. M.; Raymo, F. M., Bioimaging with Macromolecular Probes Incorporating Multiple BODIPY Fluorophores. *Bioconjug. Chem.* **2017,** *28* (5), 1519.

79. Huang, Z.; Chen, Q.; Wan, Q.; Wang, K.; Yuan, J.; Zhang, X.; Tao, L.; Wei, Y., Synthesis of amphiphilic fluorescent polymers via a one-pot combination of multicomponent Hantzsch reaction and RAFT polymerization and their cell imaging applications. *Polym. Chem.* **2017,** *8* (33), 4805.

80. Yang, J. C.; Ho, Y. C.; Chan, Y. H., Ultrabright Fluorescent Polymer Dots with Thermochromic Characteristics for Full-Color Security Marking. *ACS Appl. Mater. Interfaces.* **2019,** *11* (32), 29341.

81. Liu, S.; Cheng, Y.; Zhang, H.; Qiu, Z.; Kwok, R. T. K.; Lam, J. W. Y.; Tang, B. Z., In Situ Monitoring of RAFT Polymerization by Tetraphenylethylene-Containing Agents with Aggregation-Induced Emission Characteristics. *Angew. Chem., Int. Ed.* **2018,** *57* (21), 6274.

82. Han, T.; Gui, C.; Lam, J. W. Y.; Jiang, M.; Xie, N.; Kwok, R. T. K.; Tang, B. Z., High-Contrast Visualization and Differentiation of Microphase Separation in Polymer Blends by Fluorescent AIE Probes. *Macromolecules* **2017,** *50* (15), 5807.

83. Wang, Z.; Nie, J.; Qin, W.; Hu, Q.; Tang, B. Z., Gelation process visualized by aggregation-induced emission fluorogens. *Nat. Commun.* **2016,** *7*, 12033.

84. Liu, Q.; Xia, Q.; Wang, S.; Li, B. S.; Tang, B. Z., In situ visualizable self-assembly, aggregation-induced emission and circularly polarized luminescence of tetraphenylethene and alanine-based chiral polytriazole. *J. Mater. Chem. C* **2018,** *6* (17), 4807.

85. Chen, C.; Wylie, R. A. L.; Klinger, D.; Connal, L. A., Shape Control of Soft Nanoparticles and Their Assemblies. *Chem. Mater.* **2017,** *29* (5), 1918.

86. Wang, G.; Zhou, L.; Zhang, P.; Zhao, E.; Zhou, L.; Chen, D.; Sun, J.; Gu, X.; Yang, W.; Tang, B. Z., Fluorescence Self-Reporting Precipitation Polymerization Based on Aggregation-Induced Emission for Constructing Optical Nanoagents. *Angew. Chem., Int. Ed.* **2019**, 2.

87. Zhang, N.; Chen, H.; Fan, Y.; Zhou, L.; Trepout, S.; Guo, J.; Li, M. H., Fluorescent Polymersomes with Aggregation-Induced Emission. *ACS Nano* **2018,** *12* (4), 4025.

88. Oomen, P. E.; Aref, M. A.; Kaya, I.; Phan, N. T. N.; Ewing, A. G., Chemical Analysis of Single Cells. *Anal. Chem.* **2019,** *91* (1), 588.

89. Chen, X.; Zhang, X.; Wang, H. Y.; Chen, Z.; Wu, F. G., Subcellular Fate of a Fluorescent Cholesterol-Poly(ethylene glycol) Conjugate: An Excellent Plasma Membrane Imaging Reagent. *Langmuir* **2016,** *32* (39), 10126.

90. Ye, F.; Wu, C.; Jin, Y.; Wang, M.; Chan, Y. H.; Yu, J.; Sun, W.; Hayden, S.; Chiu, D. T., A compact and highly fluorescent orange-emitting polymer dot for specific subcellular imaging. *Chem. Commun.* **2012,** *48* (12), 1778.

91. Kulkarni, P. S.; Haldar, M. K.; Confeld, M. I.; Langaas, C. J.; Yang, X.; Qian, S. Y.; Mallik, S., Mitochondria-targeted fluorescent polymersomes for drug delivery to cancer cells. *Polym. Chem.* **2016,** *7* (25), 4151.

92. Orosco, R. K.; Tsien, R. Y.; Nguyen, Q. T., Fluorescence imaging in surgery. *IEEE T BIO-MED ENG* **2013,** *6*, 178.

93. Sun, K.; Tang, Y.; Li, Q.; Yin, S.; Qin, W.; Yu, J.; Chiu, D. T.; Liu, Y.; Yuan, Z.; Zhang, X.; Wu, C., In Vivo Dynamic Monitoring of Small Molecules with Implantable Polymer-Dot Transducer. *ACS Nano* **2016,** *10* (7), 6769.

94. Li, Y.; Yang, Y.; Tang, S.; Zhang, Y.; Li, X.; Guan, W.; Ma, F.; Zhang, C.; Xiong, L., High-Resolution Imaging of the Lymphatic Vascular System in Living Mice/Rats Using Dual-Modal Polymer Dots. *ACS Appl. Bio. Materials.* **2019,** *2* (9), 3877.

95. Zhang, Q.; Mochalin, V. N.; Neitzel, I.; Knoke, I. Y.; Han, J.; Klug, C. A.; Zhou, J. G.; Lelkes, P. I.; Gogotsi, Y., Fluorescent PLLA-nanodiamond composites for bone tissue engineering. *Biomaterials* **2011,** *32* (1), 87.

96. Hansel, C. S.; Holme, M. N.; Gopal, S.; Stevens, M. M., Advances in high-resolution microscopy for the study of intracellular interactions with biomaterials. *Biomaterials* **2020,** *226*, 119406.

97. Chen, X.; Liu, Z.; Li, R.; Shan, C.; Zeng, Z.; Xue, B.; Yuan, W.; Mo, C.; Xi, P.; Wu, C.; Sun, Y., Multicolor Super-resolution Fluorescence Microscopy with Blue and Carmine Small Photoblinking Polymer Dots. *ACS Nano* **2017,** *11* (8), 8084.

98. Zhu, M.-Q.; Zhang, G.-F.; Hu, Z.; Aldred, M. P.; Li, C.; Gong, W.-L.; Chen, T.; Huang, Z.-L.; Liu, S., Reversible Fluorescence Switching of Spiropyran-Conjugated Biodegradable Nanoparticles for Super-Resolution Fluorescence Imaging. *Macromolecules* **2014,** *47* (5), 1543.

99. Jia, T.; Fu, C.; Huang, C.; Yang, H.; Jia, N., Highly sensitive naphthalimide-based fluorescence polarization probe for detecting cancer cells. *ACS Appl. Mater. Interfaces.* **2015,** *7* (18), 10013.

100. Wu, C.; Szymanski, C.; Cain, Z.; McNeill, J., Conjugated Polymer Dots for

Multiphoton Fluorescence Imaging. *J. Am. Chem. Soc.* **2007,** *129* (43), 12904.

101. Dougherty, C. A.; Vaidyanathan, S.; Orr, B. G.; Banaszak Holl, M. M., Fluorophore:dendrimer ratio impacts cellular uptake and intracellular fluorescence lifetime. *Bioconjug. Chem.* **2015,** *26* (2), 304.

102. Zhao, Q.; Zhou, X.; Cao, T.; Zhang, K. Y.; Yang, L.; Liu, S.; Liang, H.; Yang, H.; Li, F.; Huang, W., Fluorescent/phosphorescent dual-emissive conjugated polymer dots for hypoxia bioimaging. *Chem. Sci.* **2015,** *6* (3), 1825.

103. Pan, Y.; Chen, W.; Yang, J.; Zheng, J.; Yang, M.; Yi, C., Facile Synthesis of Gadolinium Chelate-Conjugated Polymer Nanoparticles for Fluorescence/Magnetic Resonance Dual-Modal Imaging. *Anal. Chem.* **2018,** *90* (3), 1992.

104. Czarnik, A. W., Chemical Communication in Water Using Fluorescent Chemosensors. *Acc. Chem. Res.* **1994,** *27* (10), 302.

105. Orellana, G. In *FLUORESCENCE-BASED SENSORS*, Dordrecht, Springer Netherlands: Dordrecht, 2006; p 99.

106. Xu, W.; Lu, S.; Xu, M.; Jiang, Y.; Wang, Y.; Chen, X., Simultaneous imaging of intracellular pH and O2 using functionalized semiconducting polymer dots. *J. Mater. Chem. B* **2016,** *4* (2), 292.

107. Fu, L.; Yuan, P.; Ruan, Z.; Liu, L.; Li, T.; Yan, L., Ultra-pH-sensitive polypeptide micelles with large fluorescence off/on ratio in near infrared range. *Polym. Chem.* **2017,** *8* (6), 1028.

108. Kim, H. J.; Lee, H. I., Polymeric Micelles Based on Light-Responsive Block Copolymers for the Phototunable Detection of Mercury(II) Ions Modulated by Morphological Changes. *ACS Appl. Mater. Interfaces.* **2018,** *10* (40), 34634.

109. Tao, W.; Wang, J.; Parak, W. J.; Farokhzad, O. C.; Shi, J., Nanobuffering of pH-Responsive Polymers: A Known but Sometimes Overlooked Phenomenon and Its

Biological Applications. *ACS Nano* **2019,** *13* (5), 4876.

110. Dong, W.; Wu, H.; Chen, M.; Shi, Y.; Sun, J.; Qin, A.; Tang, B. Z., Anionic conjugated polytriazole: direct preparation, aggregation-enhanced emission, and highly efficient Al3+sensing. *Polym. Chem.* **2016,** *7* (37), 5835.

111. Zhang, M.; Yang, Y.; Liu, L.; Chang, W.; Li, J., Pseudo-Cryptand-Containing Copolymers: Cyclopolymerization and Biocompatible Water-Soluble Al3+Fluorescent Sensorin Vitro. *Macromolecules* **2016,** *49* (3), 844.

112. Lou, X.; Zhang, Y.; Li, S.; Ou, D.; Wan, Z.; Qin, J.; Li, Z., A new polyfluorene bearing pyridine moieties: a sensitive fluorescent chemosensor for metal ions and cyanide. *Polym. Chem.* **2012,** *3* (6), 1446.

113. Bak, J. M.; Lee, H. I., Use of Core-Cross-Linked Polymeric Micelles Induced by the Selective Detection of Cu(II) Ions for the Sustained Release of a Model Drug. *ACS Appl. Mater. Interfaces.* **2019,** *11* (15), 14368.

114. Liu, T.; Liu, S., Responsive polymers-based dual fluorescent chemosensors for Zn2+ ions and temperatures working in purely aqueous media. *Anal. Chem.* **2011,** *83* (7), 2775.

115. Balamurugan, A.; Lee, H.-i., Water-Soluble Polymeric Probes for the Selective Sensing of Mercury Ion: pH-Driven Controllable Detection Sensitivity and Time. *Macromolecules* **2015,** *48* (4), 1048.

116. Cai, X.; Li, J.; Zhang, Z.; Yang, F.; Dong, R.; Chen, L., Novel Pb2+ ion imprinted polymers based on ionic interaction via synergy of dual functional monomers for selective solid-phase extraction of Pb2+ in water samples. *ACS Appl. Mater. Interfaces.* **2014,** *6* (1), 305.

117. Happ, B.; Pavlov, G. M.; Perevyazko, I.; Hager, M. D.; Winter, A.; Schubert, U. S., Induced Charge Effect by Co(II) Complexation on the Conformation of a Copolymer

Containing a Bidentate 2-(1,2,3-Triazol-4-yl)pyridine Chelating Unit. *Macromol. Chem. Phys.* **2012,** *213* (13), 1339.

118. Hu, J.; Liu, S., Responsive Polymers for Detection and Sensing Applications: Current Status and Future Developments. *Macromolecules* **2010,** *43* (20), 8315.

119. Hu, J.; Whittaker, M. R.; Davis, T. P.; Quinn, J. F., Application of Heterocyclic Polymers in the Ratiometric Spectrophotometric Determination of Fluoride. *ACS Macro Lett.* **2015,** *4* (2), 236.

120. Jiang, Y.; Hu, X.; Hu, J.; Liu, H.; Zhong, H.; Liu, S., Reactive Fluorescence Turn-On Probes for Fluoride Ions in Purely Aqueous Media Fabricated from Functionalized Responsive Block Copolymers. *Macromolecules* **2011,** *44* (22), 8780.

121. Balamurugan, A.; Lee, H.-i., Aldoxime-Derived Water-Soluble Polymer for the Multiple Analyte Sensing: Consecutive and Selective Detection of Hg2+, Ag+, ClO–, and Cysteine in Aqueous Media. *Macromolecules* **2015,** *48* (12), 3934.

122. Zhang, P.; Wang, H.; Hong, Y.; Yu, M.; Zeng, R.; Long, Y.; Chen, J., Selective visualization of endogenous hypochlorous acid in zebrafish during lipopolysaccharide-induced acute liver injury using a polymer micelles-based ratiometric fluorescent probe. *Biosens. Bioelectron.* **2018,** *99*, 318.

123. Deng, Q.; Li, Y.; Wu, J.; Liu, Y.; Fang, G.; Wang, S.; Zhang, Y., Highly sensitive fluorescent sensing for water based on poly(m-aminobenzoic acid). *Chem. Commun.* **2012,** *48* (24), 3009.

124. Ye, T.; Bai, X.; Jiang, X.; Wu, Q.; Chen, S.; Qu, A.; Huang, J.; Shen, J.; Wu, W., Glucose-responsive microgels based on apo-enzyme recognition. *Polym. Chem.* **2016,** *7* (16), 2847.

125. Wu, Q.; Du, X.; Chang, A.; Jiang, X.; Yan, X.; Cao, X.; Farooqi, Z. H.; Wu, W., Bioinspired synthesis of poly(phenylboronic acid) microgels with high glucose selectivity

at physiological pH. *Polym. Chem.* **2016,** *7* (42), 6500.

126. Awino, J. K.; Gunasekara, R. W.; Zhao, Y., Sequence-Selective Binding of Oligopeptides in Water through Hydrophobic Coding. *J. Am. Chem. Soc.* **2017,** *139* (6), 2188.

127. Feng, X.; Ashley, J.; Zhou, T.; Halder, A.; Sun, Y., A facile molecularly imprinted polymer-based fluorometric assay for detection of histamine. *RSC Adv.* **2018,** *8* (5), 2365.

128. Liu, L.; Rui, L.; Gao, Y.; Zhang, W., Self-assembly and disassembly of a redox-responsive ferrocene-containing amphiphilic block copolymer for controlled release. *Polym. Chem.* **2015,** *6* (10), 1817.

129. Wei, H.; Zeng, R.; Wang, S.; Zhang, C.-H.; Chen, S.; Zhang, P.; Chen, J., Engineering of a zero cross-talk fluorescent polymer nanoprobe for self-referenced ratiometric imaging of lysosomal hypochlorous acid in living cells. *Mater. Chem. Front.* **2020,** *4* (3), 862.

130. Li, P.; Zhang, D.; Zhang, Y.; Lu, W.; Wang, W.; Chen, T., Ultrafast and Efficient Detection of Formaldehyde in Aqueous Solutions Using Chitosan-based Fluorescent Polymers. *ACS Sens.* **2018,** *3* (11), 2394.

131. Liu, G.; Zhang, G.; Hu, J.; Wang, X.; Zhu, M.; Liu, S., Hyperbranched Self-Immolative Polymers (hSIPs) for Programmed Payload Delivery and Ultrasensitive Detection. *J. Am. Chem. Soc.* **2015,** *137* (36), 11645.

132. Wang, C. H.; Nesterov, E. E., Amplifying fluorescent conjugated polymer sensor for singlet oxygen detection. *Chem. Commun.* **2019,** *55* (61), 8955.

133. Xu, S.; Lu, H.; Li, J.; Song, X.; Wang, A.; Chen, L.; Han, S., Dummy molecularly imprinted polymers-capped CdTe quantum dots for the fluorescent sensing of 2,4,6-trinitrotoluene. *ACS Appl. Mater. Interfaces.* **2013,** *5* (16), 8146.

134. Hassanzadeh, J.; Khataee, A.; Mosaei Oskoei, Y.; Fattahi, H.; Bagheri, N.,

Selective chemiluminescence method for the determination of trinitrotoluene based on molecularly imprinted polymer-capped ZnO quantum dots. *New J. Chem.* **2017,** *41* (19), 10659.

135. Li, H.; Wang, J.; Sun, J. Z.; Hu, R.; Qin, A.; Tang, B. Z., Metal-free click polymerization of propiolates and azides: facile synthesis of functional poly(aroxycarbonyltriazole)s. *Polym. Chem.* **2012,** *3* (4), 1075.

136. Kumar, V.; Maiti, B.; Chini, M. K.; De, P.; Satapathi, S., Multimodal Fluorescent Polymer Sensor for Highly Sensitive Detection of Nitroaromatics. *Sci. Rep.* **2019,** *9* (1), 7269.

137. Song, F.; Wei, G.; Wang, L.; Jiao, J.; Cheng, Y.; Zhu, C., Salen-Based Chiral Fluorescence Polymer Sensor for Enantioselective Recognition of α-Hydroxyl Carboxylic Acids. *J. Org. Chem.* **2012,** *77* (10), 4759.

138. Wei, G.; Zhang, S.; Dai, C.; Quan, Y.; Cheng, Y.; Zhu, C., A new chiral binaphthalene-based fluorescence polymer sensor for the highly enantioselective recognition of phenylalaninol. *Chemistry* **2013,** *19* (47), 16066.

139. Awino, J. K.; Zhao, Y., Imprinted micelles for chiral recognition in water: shape, depth, and number of recognition sites. *Org. Biomol. Chem.* **2017,** *15* (22), 4851.

140. Jiang, X.; Gao, H.; Zhang, X.; Pang, J.; Li, Y.; Li, K.; Wu, Y.; Li, S.; Zhu, J.; Wei, Y.; Jiang, L., Highly-sensitive optical organic vapor sensor through polymeric swelling induced variation of fluorescent intensity. *Nat. Commun.* **2018,** *9* (1), 3799.

141. Shi, H.; Ma, X.; Zhao, Q.; Liu, B.; Qu, Q.; An, Z.; Zhao, Y.; Huang, W., Ultrasmall Phosphorescent Polymer Dots for Ratiometric Oxygen Sensing and Photodynamic Cancer Therapy. *Adv. Funct. Mater.* **2014,** *24* (30), 4823.

142. Sun, K.; Liu, X.; Wang, Y.; Wu, Z., A polymer-based turn-on fluorescent sensor for specific detection of hydrogen sulfide. *RSC Adv.* **2013,** *3* (34), 14543.

143. Wang, P.; Zhang, C.; Liu, H. W.; Xiong, M.; Yin, S. Y.; Yang, Y.; Hu, X. X.; Yin, X.; Zhang, X. B.; Tan, W., Supramolecular assembly affording a ratiometric two-photon fluorescent nanoprobe for quantitative detection and bioimaging. *Chem. Sci.* **2017,** *8* (12), 8214.

144. Zhang, D.; Fan, Y.; Chen, H.; Trepout, S.; Li, M. H., CO2 -Activated Reversible Transition between Polymersomes and Micelles with AIE Fluorescence. *Angew. Chem., Int. Ed.* **2019,** *58* (30), 10260.

145. Qiao, J.; Chen, C.; Shangguan, D.; Mu, X.; Wang, S.; Jiang, L.; Qi, L., Simultaneous Monitoring of Mitochondrial Temperature and ATP Fluctuation Using Fluorescent Probes in Living Cells. *Anal. Chem.* **2018,** *90* (21), 12553.

146. Wu, W.; Bazan, G. C.; Liu, B., Conjugated-Polymer-Amplified Sensing, Imaging, and Therapy. *Chem* **2017,** *2* (6), 760.

147. Chen, J.; Wang, Y.; Li, W.; Zhou, H.; Li, Y.; Yu, C., Nucleic acid-induced tetraphenylethene probe noncovalent self-assembly and the superquenching of aggregation-induced emission. *Anal. Chem.* **2014,** *86* (19), 9866.

148. Yuan, Z.; Zhou, Y.; Gao, S.; Cheng, Y.; Li, Z., Homogeneous and sensitive detection of microRNA with ligase chain reaction and lambda exonuclease-assisted cationic conjugated polymer biosensing. *ACS Appl. Mater. Interfaces.* **2014,** *6* (9), 6181.

149. Zhou, Y.; Zhang, J.; Zhao, L.; Li, Y.; Chen, H.; Li, S.; Cheng, Y., Visual Detection of Multiplex MicroRNAs Using Cationic Conjugated Polymer Materials. *ACS Appl. Mater. Interfaces.* **2016,** *8* (2), 1520.

150. Chen, J.; Liu, Q.; Xiao, J.; Du, J., EpCAM-Antibody-Labeled Noncytotoxic Polymer Vesicles for Cancer Stem Cells-Targeted Delivery of Anticancer Drug and siRNA. *Biomacromolecules* **2015,** *16* (6), 1695.

151. Malik, A. H.; Hussain, S.; Iyer, P. K., Aggregation-Induced FRET via Polymer-

Surfactant Complexation: A New Strategy for the Detection of Spermine. *Anal. Chem.* **2016,** *88* (14), 7358.

152. An, L.; Tang, Y.; Feng, F.; He, F.; Wang, S., Water-soluble conjugated polymers for continuous and sensitive fluorescence assays for phosphatase and peptidase. *J. Mater. Chem.* **2007,** *17* (39), 4147.

153. You, C. C.; Miranda, O. R.; Gider, B.; Ghosh, P. S.; Kim, I. B.; Erdogan, B.; Krovi, S. A.; Bunz, U. H.; Rotello, V. M., Detection and identification of proteins using nanoparticle-fluorescent polymer 'chemical nose' sensors. *Nat. Nanotechnol.* **2007,** *2* (5), 318.

154. Pitzler, C.; Wirtz, G.; Vojcic, L.; Hiltl, S.; Boker, A.; Martinez, R.; Schwaneberg, U., A fluorescent hydrogel-based flow cytometry high-throughput screening platform for hydrolytic enzymes. *Chem. Biol.* **2014,** *21* (12), 1733.

155. Kumaraswamy, S.; Bergstedt, T.; Shi, X.; Rininsland, F.; Kushon, S.; Xia, W.; Ley, K.; Achyuthan, K.; McBranch, D.; Whitten, D., Fluorescent-conjugated polymer superquenching facilitates highly sensitive detection of proteases. *Proc. Natl. Acad. Sci. U. S. A.* **2004,** *101* (20), 7511.

156. Sanjuán, A. M.; Reglero Ruiz, J. A.; García, F. C.; García, J. M., Recent developments in sensing devices based on polymeric systems. *React. Funct. Polym.* **2018,** *133*, 103.

157. Huang, X.; Song, J.; Yung, B. C.; Huang, X.; Xiong, Y.; Chen, X., Ratiometric optical nanoprobes enable accurate molecular detection and imaging. *Chem. Soc. Rev.* **2018,** *47* (8), 2873.

158. Guo, B.; Yao, Z.; Liu, L.; Wu, H. C., Revealing different aggregational states of a conjugated polymer in solution by a nanopore sensor. *Chem. Sci.* **2016,** *7* (8), 5287.

159. Zhong, H.; Liu, C.; Ge, W.; Sun, R.; Huang, F.; Wang, X., Self-Assembled

Conjugated Polymer/Chitosan-graft-Oleic Acid Micelles for Fast Visible Detection of Aliphatic Biogenic Amines by "Turn-On" FRET. *ACS Appl. Mater. Interfaces.* **2017,** *9* (27), 22875.

160. Uchiyama, S.; Gota, C.; Tsuji, T.; Inada, N., Intracellular temperature measurements with fluorescent polymeric thermometers. *Chem. Commun.* **2017,** *53* (80), 10976.

161. Uchiyama, S.; Matsumura, Y.; de Silva, A. P.; Iwai, K., Fluorescent Molecular Thermometers Based on Polymers Showing Temperature-Induced Phase Transitions and Labeled with Polarity-Responsive Benzofurazans. *Anal. Chem.* **2003,** *75* (21), 5926.

162. Inada, N.; Fukuda, N.; Hayashi, T.; Uchiyama, S., Temperature imaging using a cationic linear fluorescent polymeric thermometer and fluorescence lifetime imaging microscopy. *Nat. Protoc.* **2019,** *14* (4), 1293.

163. Okabe, K.; Inada, N.; Gota, C.; Harada, Y.; Funatsu, T.; Uchiyama, S., Intracellular temperature mapping with a fluorescent polymeric thermometer and fluorescence lifetime imaging microscopy. *Nat. Commun.* **2012,** *3*, 705.

164. Zhang, H., Molecularly Imprinted Nanoparticles for Biomedical Applications. *Adv. Mater.* **2019**, 1806328.

165. Duan, L.; Zhao, Y., Selective Binding of Folic Acid and Derivatives by Imprinted Nanoparticle Receptors in Water. *Bioconjug. Chem.* **2018,** *29* (4), 1438.

166. Yang, K.; Berg, M. M.; Zhao, C.; Ye, L., One-Pot Synthesis of Hydrophilic Molecularly Imprinted Nanoparticles. *Macromolecules* **2009,** *42* (22), 8739.

167. Wylie, R. G.; Ahsan, S.; Aizawa, Y.; Maxwell, K. L.; Morshead, C. M.; Shoichet, M. S., Spatially controlled simultaneous patterning of multiple growth factors in three-dimensional hydrogels. *Nat. Mater.* **2011,** *10* (10), 799.

168. Jia, R.; Tian, W.; Bai, H.; Zhang, J.; Wang, S.; Zhang, J., Amine-responsive

cellulose-based ratiometric fluorescent materials for real-time and visual detection of shrimp and crab freshness. *Nat. Commun.* **2019,** *10* (1), 795.

169. Boott, C. E.; Tran, A.; Hamad, W. Y.; MacLachlan, M. J., Cellulose Nanocrystal Elastomers with Reversible Visible Color. *Angew. Chem., Int. Ed.* **2020,** *59* (1), 226.

170. Ji, X.; Li, Z.; Liu, X.; Peng, H. Q.; Song, F.; Qi, J.; Lam, J. W. Y.; Long, L.; Sessler, J. L.; Tang, B. Z., A Functioning Macroscopic "Rubik's Cube" Assembled via Controllable Dynamic Covalent Interactions. *Adv. Mater.* **2019,** *31* (40), 1902365.

171. Wei, S.; Lu, W.; Le, X.; Ma, C.; Lin, H.; Wu, B.; Zhang, J.; Theato, P.; Chen, T., Bioinspired Synergistic Fluorescence-Color-Switchable Polymeric Hydrogel Actuators. *Angew. Chem., Int. Ed.* **2019,** *58* (45), 16243.

172. Shikha, S.; Salafi, T.; Cheng, J.; Zhang, Y., Versatile design and synthesis of nano-barcodes. *Chem. Soc. Rev.* **2017,** *46* (22), 7054.

173. Yang, M.; Liu, Y.; Jiang, X., Barcoded point-of-care bioassays. *Chem. Soc. Rev.* **2019,** *48* (3), 850.

174. Fu, F.; Shang, L.; Zheng, F.; Chen, Z.; Wang, H.; Wang, J.; Gu, Z.; Zhao, Y., Cells Cultured on Core-Shell Photonic Crystal Barcodes for Drug Screening. *ACS Appl. Mater. Interfaces.* **2016,** *8* (22), 13840.

175. Hu, F.; Zeng, C.; Long, R.; Miao, Y.; Wei, L.; Xu, Q.; Min, W., Supermultiplexed optical imaging and barcoding with engineered polyynes. *Nat. Methods* **2018,** *15* (3), 194.

176. Lu, Y.; Lu, J.; Zhao, J.; Cusido, J.; Raymo, F. M.; Yuan, J.; Yang, S.; Leif, R. C.; Huo, Y.; Piper, J. A.; Paul Robinson, J.; Goldys, E. M.; Jin, D., On-the-fly decoding luminescence lifetimes in the microsecond region for lanthanide-encoded suspension arrays. *Nat. Commun.* **2014,** *5*, 3741.

177. Chen, C.; Corry, B.; Huang, L.; Hildebrandt, N., FRET-Modulated Multihybrid Nanoparticles for Brightness-Equalized Single-Wavelength Barcoding. *J. Am. Chem. Soc.*

2019, *141* (28), 11123.

178. Ye, S.; Teng, Y.; Juan, A.; Wei, J.; Wang, L.; Guo, J., Modulated Visible Light Upconversion for Luminescence Patterns in Liquid Crystal Polymer Networks Loaded with Upconverting Nanoparticles. *Adv. Opt. Mater.* **2017,** *5* (4), 1600956.

179. Tang, S.; Zhang, Y.; Dhakal, P.; Ravelo, L.; Anderson, C. L.; Collins, K. M.; Raymo, F. M., Photochemical Barcodes. *J. Am. Chem. Soc.* **2018,** *140* (13), 4485.

180. Fang, X.; Zheng, Y.; Duan, Y.; Liu, Y.; Zhong, W., Recent Advances in Design of Fluorescence-Based Assays for High-Throughput Screening. *Anal. Chem.* **2019,** *91* (1), 482.

181. Lin, G.; Baker, M. A. B.; Hong, M.; Jin, D., The Quest for Optical Multiplexing in Bio-discoveries. *Chem* **2018,** *4* (5), 997.

182. Chang, K.; Liu, Z.; Chen, H.; Sheng, L.; Zhang, S. X.; Chiu, D. T.; Yin, S.; Wu, C.; Qin, W., Conjugated polymer dots for ultra-stable full-color fluorescence patterning. *Small* **2014,** *10* (21), 4270.

183. Ganda, S.; Stenzel, M. H., Concepts, fabrication methods and applications of living crystallization-driven self-assembly of block copolymers. *Prog. Polym. Sci.* **2020,** *101*, 101195.

184. He, F.; Gadt, T.; Manners, I.; Winnik, M. A., Fluorescent "barcode" multiblock co-micelles via the living self-assembly of di- and triblock copolymers with a crystalline core-forming metalloblock. *J. Am. Chem. Soc.* **2011,** *133* (23), 9095.

185. Hudson, Z. M.; Lunn, D. J.; Winnik, M. A.; Manners, I., Colour-tunable fluorescent multiblock micelles. *Nat. Commun.* **2014,** *5* (1), 3372.

186. Hudson, Z. M.; Boott, C. E.; Robinson, M. E.; Rupar, P. A.; Winnik, M. A.; Manners, I., Tailored hierarchical micelle architectures using living crystallization-driven self-assembly in two dimensions. *Nat. Chem.* **2014,** *6* (10), 893.

Chapter 2 Rational Design of Mono-Substituted Maleimides Towards Novel Fluorescent Properties

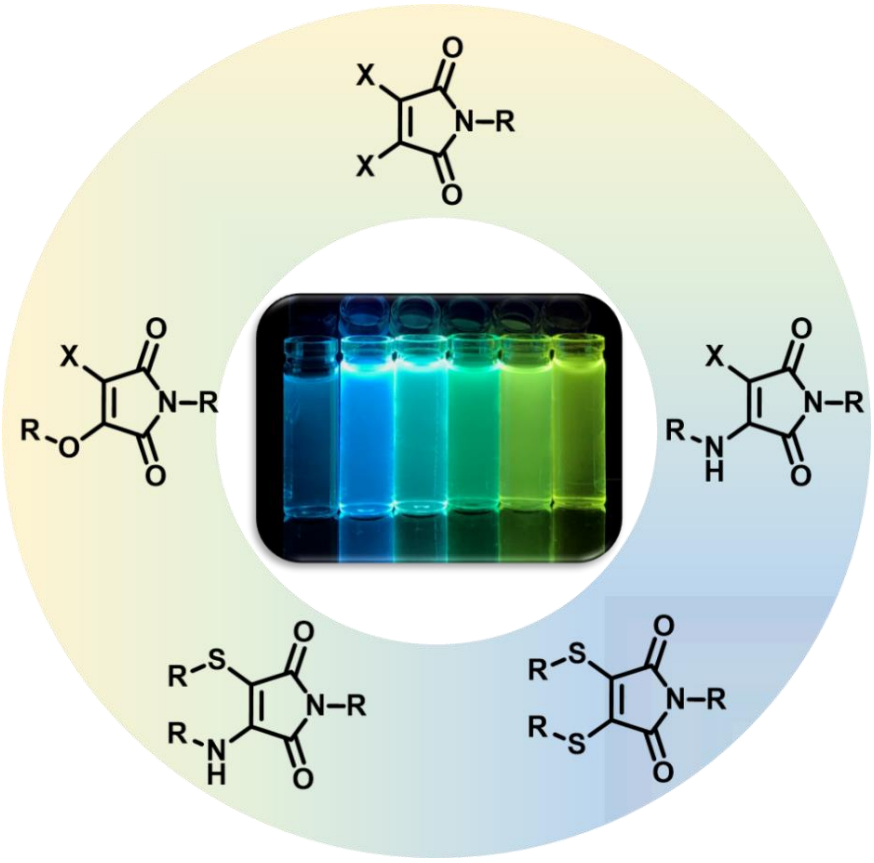

2.1 Abstract

Organic fluorophores have received a significant amount of attention across a range of fields of science and medicine. Owing to their simplicity of attachment, good optical properties, and relatively flexible molecular structures, such fluorophores have become indispensable tools for binding to or reacting with targets of interest. However, many currently used fluorophores suffer from complex syntheses, large size, and poor solubility, limiting their applications in fluorescence labeling and functionalization. Substituted maleimide is one of the novel classes of small molecule fluorophores, benefiting from its small size and promising fluorescent profiles. Therefore, the investigation of their fluorescence mechanism in relation to the substitution structures is pivotal in this area, which allows for rationalizing and predicting the fluorescence properties for various applications.

In this work, we designed and synthesized several types of maleimide derived fluorophores through mono-substitution reactions. By systematically tailoring the substituents on the C=C double bond (halogen and substituted groups like amines and alcohols), remarkable fluorescent properties such as tunable emission, high fluorescence quantum yields (up to 64%), and large Stokes shift and solvafluorochromic properties were achieved. Meanwhile, the variation of substitution groups allowed us to explore the fluorescence mechanism related to the electron localization, which was supported by the computational results. In this regard, the fluorescent properties of substituted maleimide structures could be predicted and tuned for various applications, especially in polymer functionalization.

2.2 Introduction

2.2.1 Small-molecule Fluorophores

In recent decades, a variety of fluorescent dyes, proteins, and nanoparticles have been extensively studied because of their promising potentials in various applications such as biological labels and probes,[1] chemosensors,[2] medical diagnostics[3], and photoactive materials.[4, 5] Among them, small fluorescent organic molecules are particularly important as they are small in size, can be easily modified, have the ability to amplify signals and give a combination of outputs.[6]

Indeed, the rational design of organic fluorophores has provided a straightforward method for generating various fluorescent functional materials.[7-9] Numerous efforts have been made to design water-soluble and biocompatible fluorescent molecules with excellent optical properties, such as high quantum yields and narrow emission bands. Some of the small molecule fluorophores have already been commercialized (Figure 2.1). The flexible modifications and tunable structures allow these fluorophores to be applied in many areas like imaging the specific cell structures[10], biomolecule labelings[11], and ions detectings.[12]

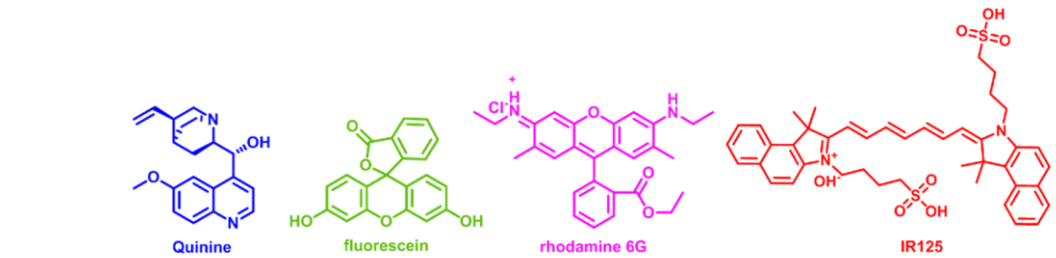

Figure 2.1 Fluorescence quantum yield (Φ_f) and emission range of some commercial dyes. Measured in 0.105M $HClO_4$ (Quinine), 0.1 M NaOH (Fluorescein), ethanol (R6G) and DMSO (IR125).[13]

One of the major advantages of these small molecule fluorophores is their capacity in combining with other materials to achieve the fluorescent functions. In this regard, the design of novel fluorophores not only requires the notable fluorescent properties and the versatile reactivity, ideal compatibilities are also essential for material modifications. However, many commercialized fluorophores with bulky planar structures suffer from complex syntheses, large size, and poor solubility, limiting their applications in functionalizing other materials. Therefore, the search for new fluorophores' structures bearing both ideal fluorescent properties and versatile functional methods is crucial in this field.

2.2.2 Substituted Maleimides Derived Fluorophores

Unsubstituted maleimides have been extensively reported as effective fluorescence quenchers through direct conjugation to fluorophores.[12, 14, 15] The low lying n-π* transition of the maleimide ring can provide a nonradiative pathway for excited state decay and significantly reduce the emission of fluorophores.[16-18] In 2009, Stephen Caddick and James R. Baker reported that bromomaleimides could undergo a rapid and selective addition–elimination reaction with cysteine.[19] Since this report, attentions have been focused on the bromomaleimides and their derivatives as modifying agents for thiol or disulfide containing antibodies and peptides.[19-26] Meanwhile, the versatile and facile chemistry of maleimide derivatives allows for easy modification with thiol groups towards specific applications such as drug deliveries,[27] reversible linking[23], and polymer functionalizations.[28] Recently, our group discovered the unexpected fluorescence behavior of two maleimide derivatives: dithiomaleimides (DTM) and aminobromomaleimides (ABM), which inherited the versatile modification

chemistries from the maleimide structures. More importantly, the fluorescence properties of these substituted maleimides were observed which can be tuned by carefully modifying the substituents and are dependent upon the molecules' microenvironment.[29-31] The small size, multiplex modification chemistries, and remarkable fluorescent properties of such substituted maleimides provided unheralded interest in fluorescent labeling and imaging applications.

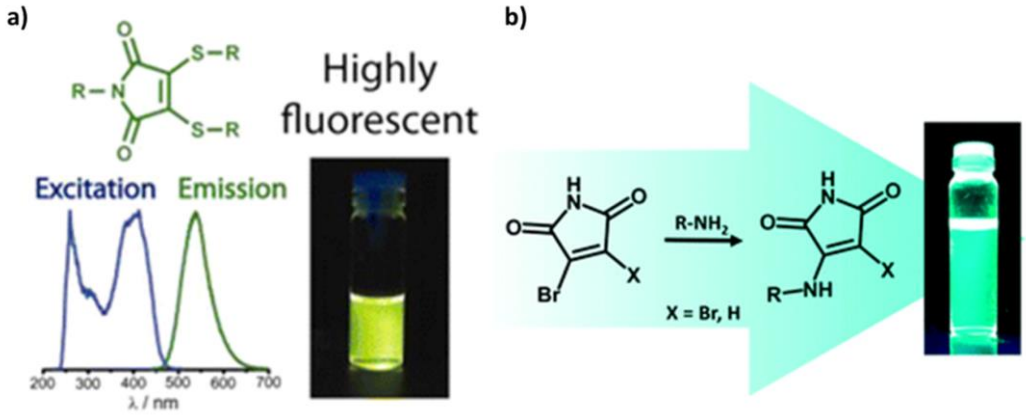

Figure 2.2 The generic structure and solution fluorescence of dithiomaleimides (a)[32] and aminomaleimides (b).[33] Figures reproduced from references 32, 33.

2.2.3 Substituted Maleimides for Polymer Functionalization

The main advantage of these fluorescent maleimide derivatives is their small size, which allows for ready incorporation into architectures without affecting or disrupting the scaffold.[27] Therefore, such maleimide fluorophores have subsequently been used as ideal fluorescent linkers in polymer functionalization and protein labeling.[31, 32, 34-37] Our group first utilized substituted maleimides in radical polymerizations as a labeling technique that did not require protection of the C=C double bond.[38] Methacrylate modified DTM could be polymerized on the sidechain of the block copolymer and subsequently assembled into the nanostructures with maintained fluorescence properties which were dependent on the polymer assemblies (Figure 2.3a).[38, 39] In another strategy, a substituted

maleimide functionalized chain transfer agent (CTA) was synthesized which could facilitate RAFT polymerization at one end and ring-opening polymerization on the other. Such a design allowed the fluorescent functional unit to be located in the interface of amphiphilic block copolymers where the fluorescence output was dependent on polymer assembly.[40] Furthermore, DTM and ABM monomers were also able to be incorporated inside the crosslinked nanogel through the emulsion polymerization (Figure 2.3c).[41, 42]

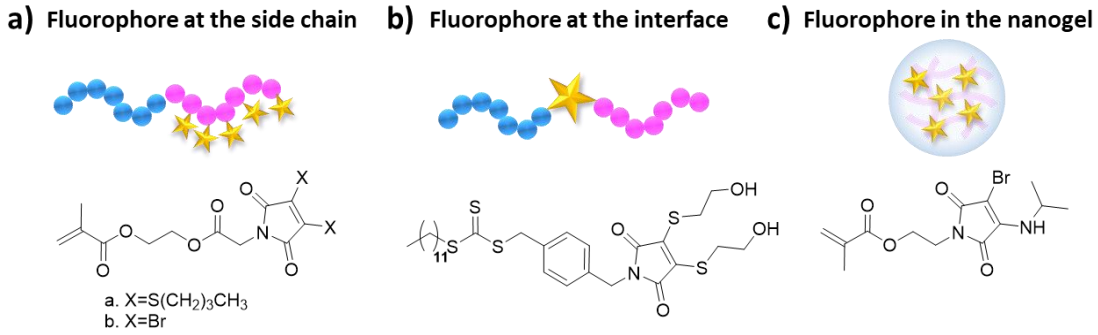

Figure 2.3 a) Substituted maleimides as the functionalized side chain of the polymer[38, 39]; b) Incorporation of substituted maleimides at the interface of an amphiphilic polymer;[40] c) Substituted maleimides at the core of a cross-linked nanogel.[41, 42]

Despite the recent advances, there has been little work on varying the maleimide structure and studying subsequent impacts on their fluorescence.[30, 43-50] The search for a versatile maleimide fluorophore is pivotal in this area, where structures with well-defined reactivities and varying fluorescent profiles are needed. In this chapter, we systemically expand the scope of substitution patterns, through mono-substitution reactions from various halogen precursors. Moreover, we explore the relationship between the substituents and the dyes' optical properties. In this regard, the rational design of maleimide fluorophores provides a straightforward method for generating diverse fluorescent functionalized materials as the potential tool for sensing and imaging applications.

2.3 Results and Discussion

2.3.1 Design Strategy for Mono-substituted Maleimides

Aminobromomaleimdies (ABM) have been previously investigated by our group as a new class of small-molecule fluorophore. It has been shown that the fluorescent properties of ABMs are closely related to two factors: the ring functionality and the dye's micro-environment.[30] For example, the fluorescence quantum yields of ABMs have been demonstrated as largely dependent on the structure of the amino groups. Owing to the perturbation of the electronic structure, the direct conjugation of aromatic rings to ABM molecules quenched the fluorescence (Figure 2.4).[30] Meanwhile, the fluorescent properties in ABMs are largely correlated to the surrounding solvation shell. This early study has deduced that the fluorescence of ABMs relies upon photoinduced intermolecular charge transfer between the electron-donating group (the substituents on the C=C moiety) and the electron-withdrawing group (the C=O groups), in which the fluorescence emission and quantum yields were affected by the changing of amino substituents. Therefore, these interesting optical properties prompted us to further

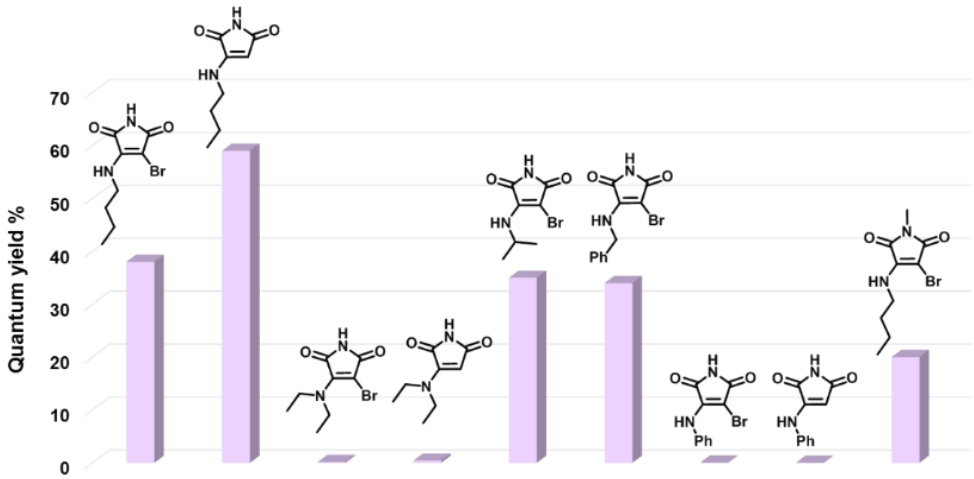

Figure 2.4 Diagram of substituted maleimides and associated fluorescence quantum yields, showing how amino substitution affects emission, reported by Mabire *et al*. Figures reproduced from reference. [33]

research the potential photoinduced intermolecular charge transfer mechanism and the relationship between the substitution patterns and their optical properties in this study.

In this chapter, we aimed to expand the variety of structures of mono-substituted maleimides and explored the effect of substitution on the fluorescent properties. Once a better understanding of substituent effects upon fluorescence is realized, we could determine rules which could be used to predict and adjust fluorescence properties for further applications. As a result of the photoinduced intermolecular charge transfer mechanism of the dye, the fluorescence of mono-substituted maleimides is largely affected by the electron structure of the dye.

Our initial strategy began with selectively changing the electron density of the C=C double bond by tailoring the halogen substituents - from Br to Cl and I (Figure 2.5). Another straightforward strategy to investigate the photoinduced intramolecular charge transfer within these molecules is to compare how the fluorescence properties vary with different electron-donating groups (the substituents on the C=C moiety). As a relatively weaker electron-donating group, alcohol substituted maleimides were designed to investigate the effect on the fluorescent properties, which could allow us to rationalize the relationship between the fluorescence properties and substitution structure.

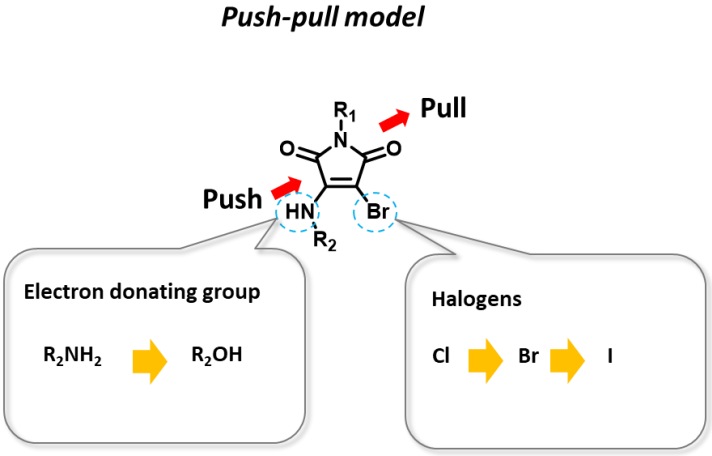

Figure 2.5 Design strategy of the substituted maleimides structures *via* varying the substitution groups.

2.3.2 Design and Synthesis of Halogenated Aminomaleimide Derivatives

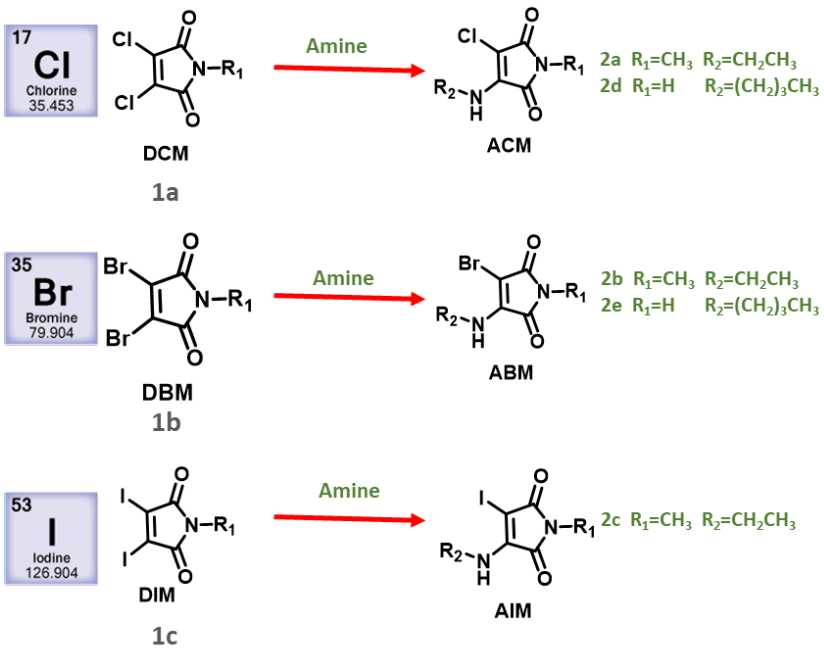

Figure 2.6 Designed synthetic strategy of different aminomaleimides for investigating the effect of halogen group on fluorescence properties.

Previously our group has reported that dibromomaleimide is able to undergo an efficient addition–elimination reaction with amines.[33] This reaction has proved to be effective for synthesizing a range of aminobromomaleimide derivatives with impressive fluorescent properties. To expand beyond this chemistry, we aimed to synthesize several aminomaleimide derivatives with different halogens on C=C bonds: 3-amino-4-chloro-maleimide (ACM), 3-amino-4-bromo-maleimide (ABM) and 3-amino-4-iodo-maleimide (AIM).

The di-halogenated precursors - 2,3-dichloromethylmaleimide (**1a**) and 2,3-diiodo methylmaleimide (**1c**) have been synthesized according to methods by previously reported procedures (detailed in Experimental section).[51, 52] 2,3-

dichloromethylmaleimide (**1a**) was synthesized by refluxing the 2,3-dichloromaleic anhydride in the presence of methylamine (Figure 2.7a).[52] 2,3-diiodomethylmaleimide (**1c**) was prepared from the commercially available2,3-dibromomethylmaleimide (M-**DBM**) and NaI *via* the halogen exchange reaction (Figure 2.7b).

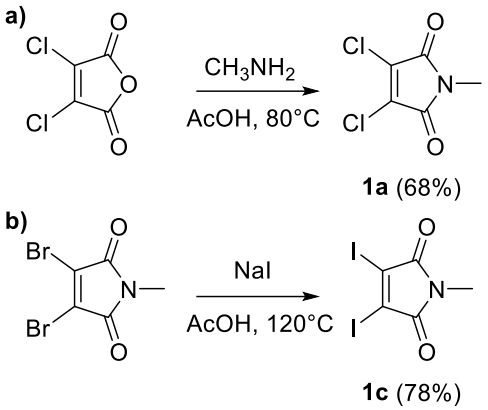

Figure 2.7 Synthesis of 2,3-diiodo/dichloro methylmaleimide precursors.

Both **1a** and **1c** were successfully isolated evidenced by their ^{1}H NMR spectra with only the singlet peak of the methyl group being present (see experimental section). Comparing the ^{13}C NMR spectra of dibromo, dichloro, and diiodomethylmaleimide, a clear shift of the halogen bonded carbon peak from 133.0 to 116.8 ppm was observed, which confirmed the successful halogen exchange (Figure 2.8).

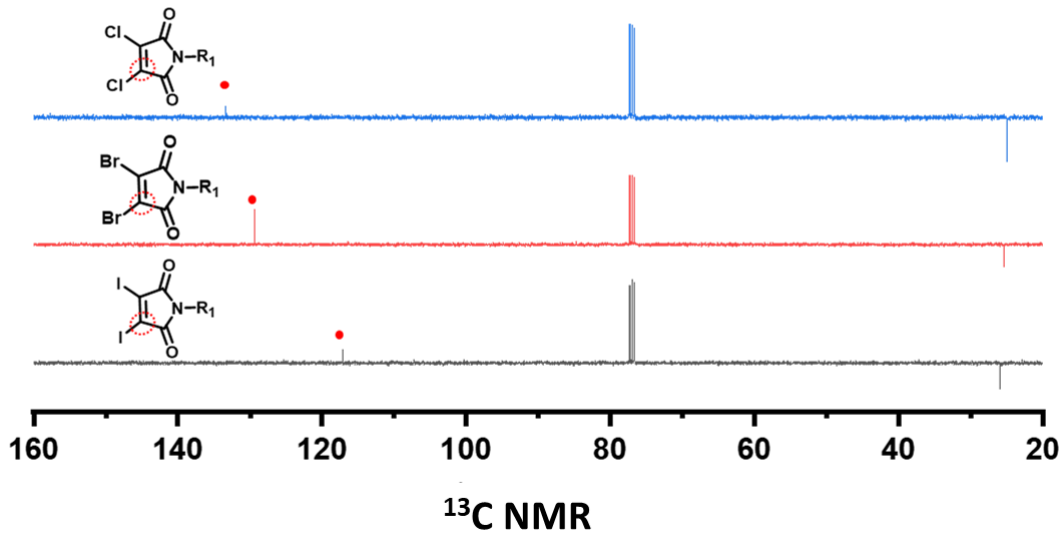

Figure 2.8 ^{13}C NMR spectra of 2,3-dichloromaleimide (blue), 2,3-dibromomaleimide (red) and 2,3-diiodomaleimide (black) ($CDCl_3$, 400 MHz).

Followed by these precursors, we targeted the synthesis of their ethylaminomaleimide derivatives: 2,3-ethylaminochloromaleimide (**2a**), 2,3-ethylaminobromomaleimide (**2b**) and 2,3-ethylaminoiodomaleimide (**2c**) (Figure 2.9). The substitution reaction of the 2,3-dibromomaleimdies with amines has been investigated in the previous report with the formation of aminobromomaleimides (ABM) as the major product.[33] Based on this method, the reaction resulted in the formation of mono-substituted products for all precursors.

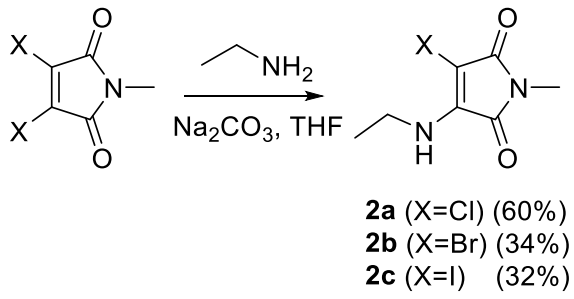

Figure 2.9 Synthesis of various halogen-aminomaleimide derivatives.

In general, the reaction of 2,3-dibromomaleimide/ 2,3-dibromomethylmaleimide was undertaken in THF at room temperature in the presence of sodium carbonate and a small excess of amine. The reactions were monitored by TLC followed by purification (wash and column chromatography). Both 2,3-aminochloromaleimide (**2a**) and 2,3-aminoiodomaleimide (**2c**) have been generated through analogous reactions and the major products confirmed by NMR spectroscopy and HR-MS (Experimental section). All compounds exhibited good solubility in common organic solvents.

Although the reactions proceeded for all compounds, different reactivities of the di-halogenated precursors were encountered evidencing by the reaction yield and rate. The reaction of the chloro compound (**1a)** with ethylamine was complete (evidenced by TLC), within half-hour with an isolated yield of around 60%, while the iodo variant (**1c)** was isolated in 32 % yield after a 4-hour reaction. The mechanism of these reactions is proposed in Figure 2.10 involving a two-step addition–elimination mechanism, in which the addition of the amine to the vinyl halide is followed by the elimination of the halide leaving group. Owing to the large steric effect, **1c** is more hindered within the addition-step which controls the formation of the intermediate and results in the low reaction yield of **2c.** Although the iodo is a better leaving group, the reaction time (**1a**>**1b**>**1c**) further proved that the nucleophilic addition step is the rate-determining step, due to the steric trend (I> Br > Cl). This mechanism is similar to nucleophilic aromatic substitution in which the addition-step is the rate-determining step.[53]

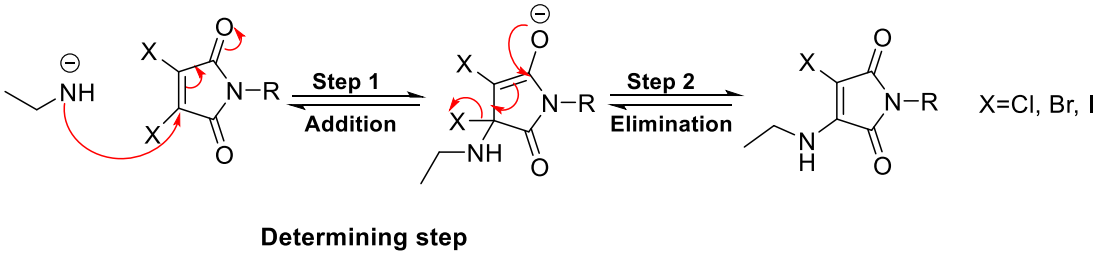

Figure 2.10 Proposed mechanism for the two-step formation of amino-substituted maleimides.

2.3.3 Alternating Fluorescence Properties by Variation of Halogens in Aminomaleimide Derivatives

To gain further insight into the halogen's influence on the fluorescence, the emission properties of acquired aminomaleimide derivatives were evaluated. No fluorescence was observed in the di-halogenated maleimides precursors (1**a**-**c**) due to the lack of electron-donating groups, in which no photo-driven electron transfer was happening. After reacting with the amine, the mono-substitution products (**2a**-**e**) exhibited blue fluorescence in diethyl ether (Figure 2.11a). The normalized emission spectra of **2a**-**c** were compared at the same concentration (10 μM) in diethyl ether (Figure 2.11b). Interestingly, both aminochloromaleimide (**2a**) and aminobromomaleimide (**2b**) showed similar green emission with λ_{max} around 475 nm, while the aminoiodomaleimide (**2c**) produced a slightly red-shifted emission with the λ_{max} around 487 nm. When changing the amine and imide structures (**2d**-**e**), a clear shift of the emission was identified with maximum wavelength blue-shifted to 461 nm. Whereas in both varieties, variation of the halogen had no impact upon the emission wavelength. Although the emission wavelength i s

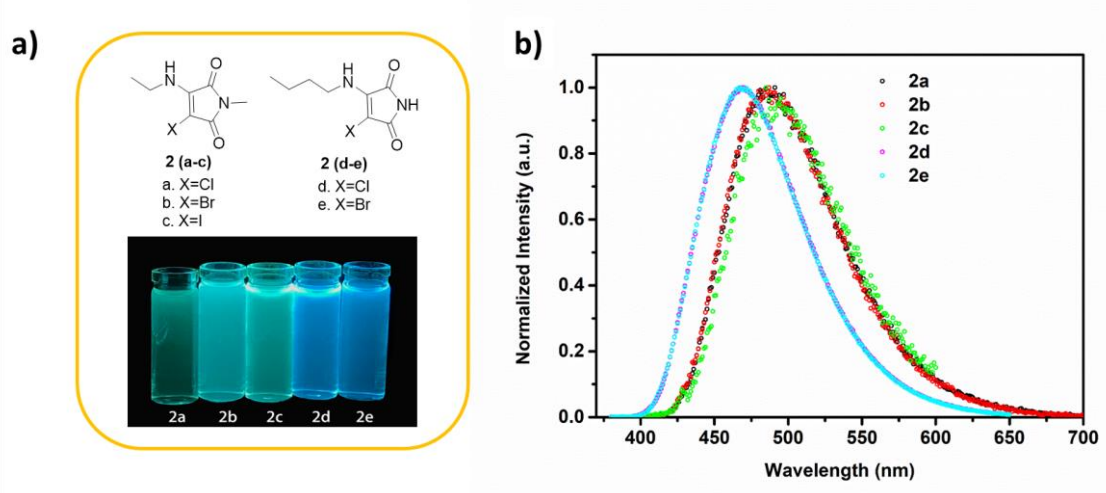

Figure 2.11(a) Structures of analyzed dyes and solution fluorescence of different amino-substituted maleimides under UV light (365 nm) in dioxane; (b) Fluorescence emission spectra of the studied aminomaleimide (**2a-e**) in diethyl ether (10 μM; λ_{ex} 385 nm; Slit: 2.5 nm, 2.5 nm).

similar in **2a-c**, a dramatic decrease in the fluorescence intensity from **2a** to **2c** was observed as size of the halogen increased (Figure 2.11a). 2D excitation-emission spectra of **2a-d** were carried out in diethyl ether with a 5 nm step for both excitation and emission. The emission of **2a-d** exhibited two excitation bands ranging from 230 to 290 nm and 320-430 nm, resulting in the same emission peak ranging from 430 nm to 650 nm (Figure 2.12), which presumably is due to the same amine as the electron donor. These results coincide with the corresponding absorption spectra, where two absorption peaks around 238 nm and 370 nm were observed (Table 2.1, Figure 2.14).[54]

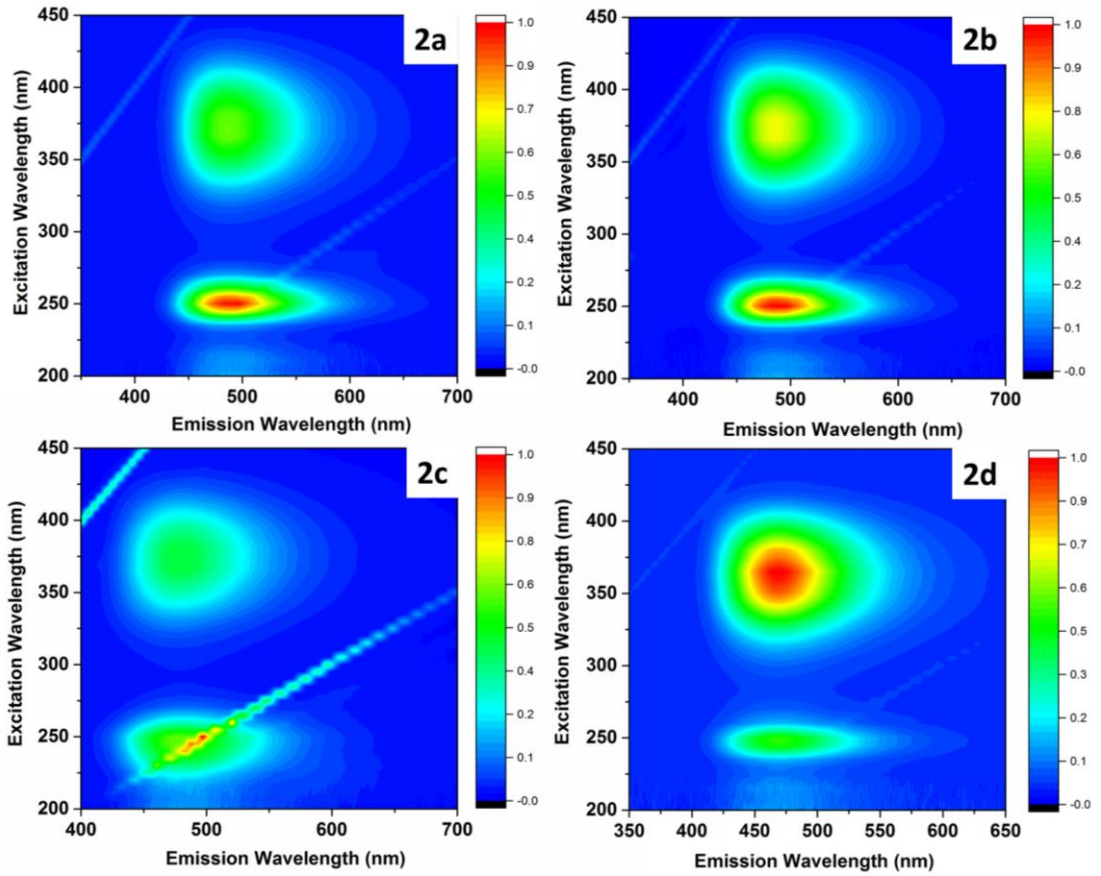

Figure 2.12 2D excitation-emission spectra (with a 5 nm step) of **2a-d** in diethyl ether at 10 μM. Peaks at $\lambda_{ex} = \lambda_{em}$ are due to Rayleigh scattering from the solution and harmonic generation at $2*\lambda_{ex} = \lambda_{em}$.

When the fluorophore is dissolved in a solvent, the ground state, and the excited states are stabilized by solute-solvent interactions, which infers solvatofluorochromic properties. Herein, the fluorescence properties of 2**a-c** were further investigated in eight solvents across a wide polarity range (H_2O, MeOH, DMF, dioxane, THF, Et_2O, CH_2Cl_2, and cyclohexane). All compounds (**2a-c**) exhibited quenched fluorescence in protic solvents like methanol and water (Figure 2.13). This is consistent with our previous work which showed that the hydrogen bonding between protic solvents and the C=O group in maleimides causes quenching through electron driven proton transfer from the solvent to the fluorophore.[55] Meanwhile, the absorption and emission maxima of the fluorophores 2**a-c** are highly sensitive toward the polarity of the solvent. For example, the emission of

2a exhibits hypsochromic (blue) shifts in non-polar solvents like diethyl ether (λ_{em} 475 nm) and cyclohexane (λ_{em} 482 nm) while exhibiting bathochromic (red) shifts in protic solvents like methanol (λ_{em} 550 nm) and water (Figure 2.14).

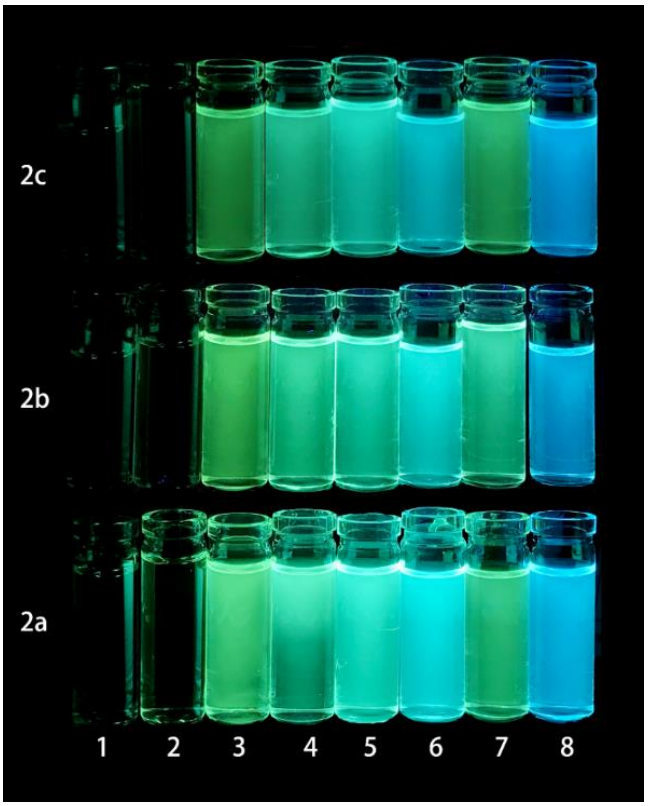

Figure 2.13 Photographs illustrating fluorescence of aminomaleimides (**2a**–**c**) in eight solvents (1–8: H_2O, MeOH, DMF, Dioxane, THF, Et_2O, CH_2Cl_2, and Cyclohexane) under UV light (365 nm).

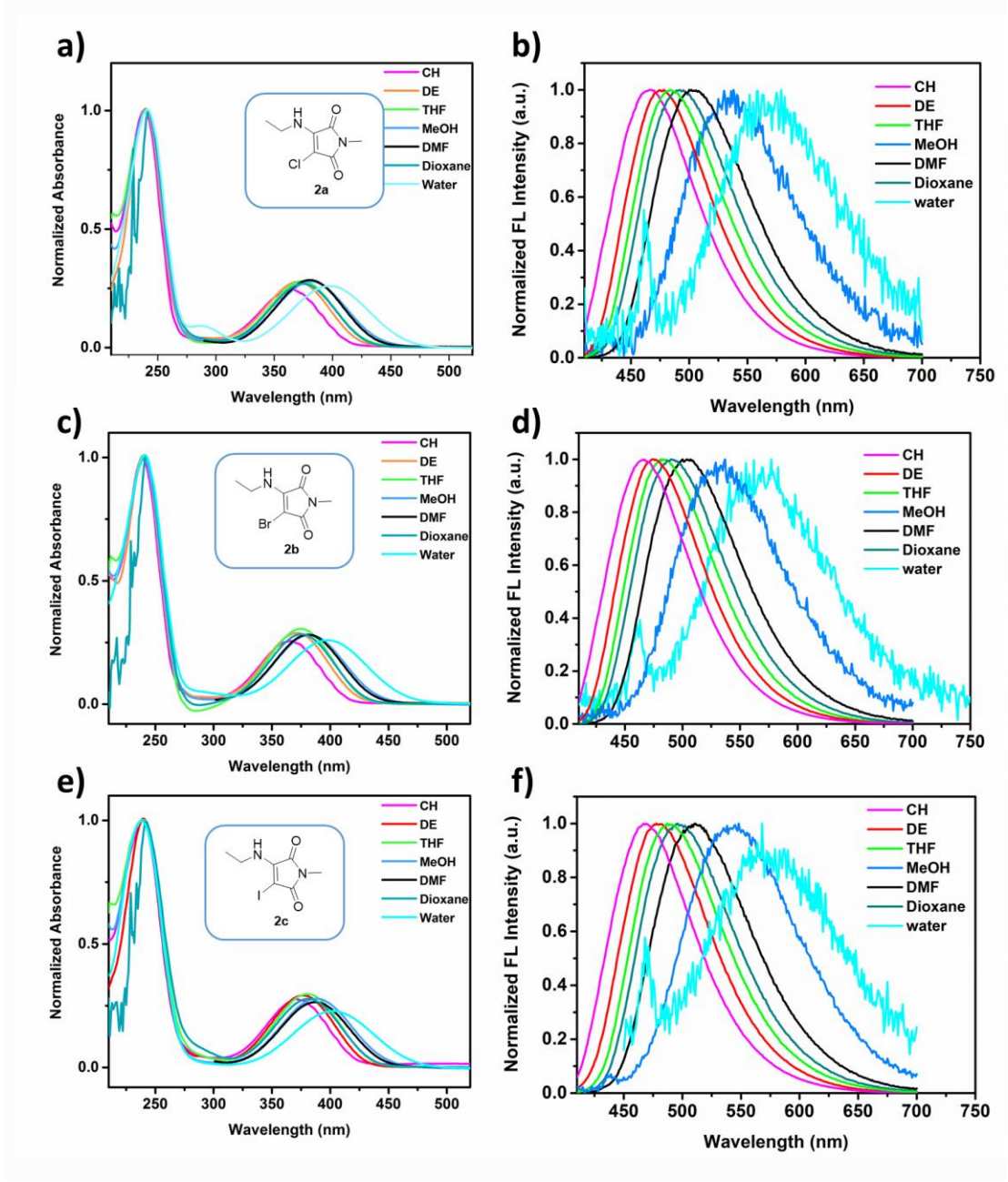

Figure 2.14 Normalized absorption (left) and emission (right) spectra of ACM, ABM, and AIM in different solvents: H_2O, MeOH, DMF, Dioxane, THF, Et_2O (DE), and Cyclohexane (CH) (10 μM; λ_{ex} 385 nm; Slit: 2.5 nm, 2.5 nm).

As mentioned above, the solvatofluorochromic properties are normally caused by solute-solvent interactions, which results from the migration of electric charges during an electronic transition. The theory to rationalize such solvatofluorochromic shifts has been summarized as the Lippert – Mataga equation [56]:

$$\Delta v = -\frac{2}{hc}\frac{\Delta\mu^2}{a^3}\Delta f + const$$

where Δv is the observed Stokes shift in a given solvent, h is Planck's constant, c is the velocity of light, $\Delta\mu$ is the change in dipole upon excitation, a is the radius of the solvent sphere surrounding the molecule, Δf is the solvent orientation polarizability, a value derived from both the solvent's dielectric constant (ε) and refractive index (n):

$$\Delta f = \frac{\varepsilon - 1}{2\varepsilon + 1} - \frac{n^2 - 1}{2n^2 + 1}$$

Based on the above equations, the emission Stokes shifts (Δv) of 2**a**-**d** are plotted as the function of solvent orientation polarizability (Δf). In non-protic solvents, all compounds (2**a**-**d**) showed the linear correlation between the Stokes shift and solvent orientation polarizability (Δf) (Figure 2.15). Similar slopes of the fitting line were observed in 2**a**-**c**, indicating that the change of halogen did not affect the stabilization of the excited state. However, when comparing the Δv and Δf in all six solvents including the protic solvents (water and MeOH), larger deviations from the fitting line were identified. One possible reason is that the hydrogen bonding is not considered in the theories of solvatochromic shifts *via* the Lippert – Mataga equation.[57] The Stavros and O'Reilly groups have investigated the quenching effect of amino-maleimides in protic solvents.[55] The interaction between the protic solvent (MeOH) and the aminomaleimide has been described by an electron driven proton transfer (EDPT) process, in which a proton transfer

from MeOH to the maleimide occurs, facilitated by a transfer of electron. (Figure 2.16).

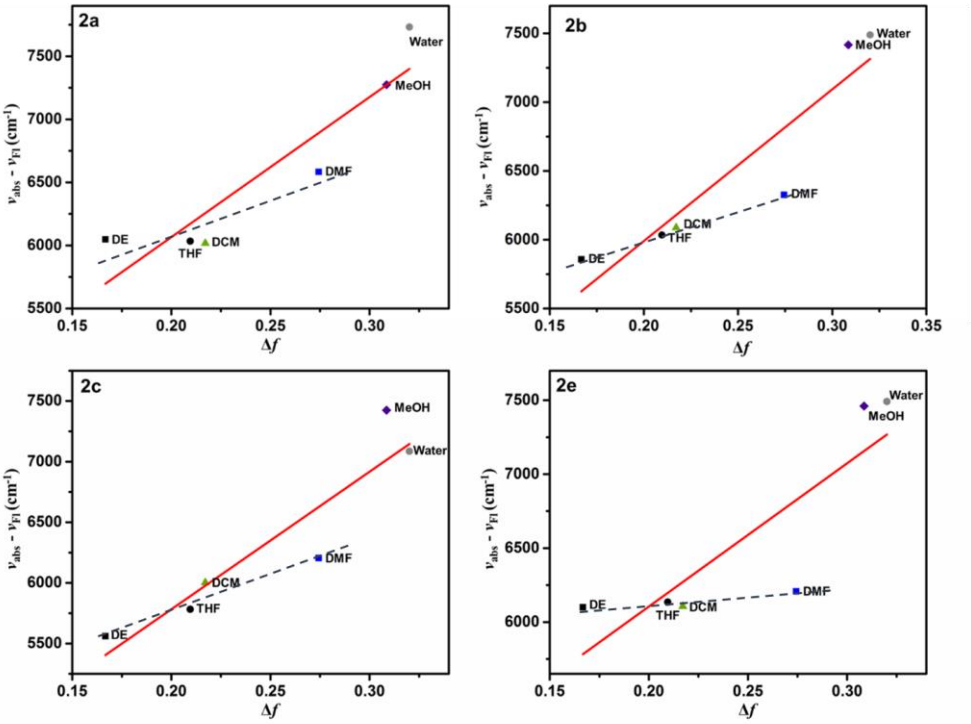

Figure 2.15 The Lippert-Mataga plot of 2**a-d** where the Stokes shift ($\Delta\nu$) from emission spectra is plotted as a function of solvent orientation polarizability (Δf). Redline: linear fitting in six solvents (DE, THF, DCM, DMF, MeOH, and water); Grey dash line: linear fitting in non-protic solvents (DE, THF, DCM, DMF).

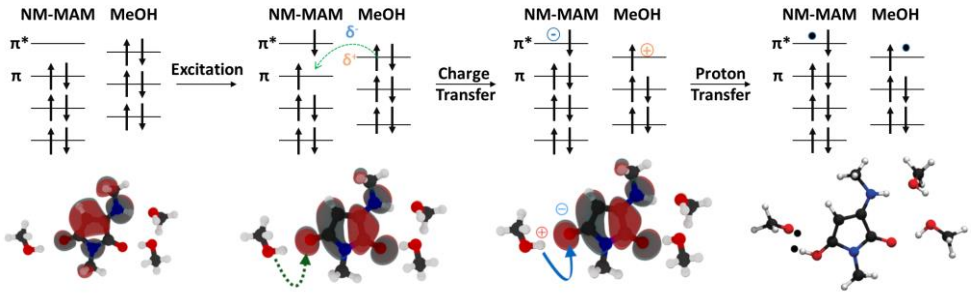

Figure 2.16 The EDPT mechanism for the quenching effect of amino-maleimides in protic solvent (MeOH), reported by the Stavros and O'Reilly groups.[55]

The fluorescence quantum yield (Φ_f), as one of the most important characteristics of a fluorophore, represents the efficiency measured as the ratio between emitted photons to the absorbed photons. The Φ_f of the aminomaleimides with different halogens (2**a**-**e**) were further measured, using a relative method (59% quinine sulfate as the reference, in 0.105 M $HClO_4$), [13] to establish the effect of the halogen (Figure 2.17). The details of the methodology used to measure the Φ_f are based on the method of relative method in experimental section. The Φ_f of all compounds (**2a-c**) exhibited trends in which the Φ_f was reduced in protic solvents (methanol, water) due to EDPT. In non-polar solvents such as cyclohexane, bright emission with the highest Φ_f was observed owing to the minimal charge transfer with the solvent.[43]

We then compare the Φ_f changes between the different compounds in the same solvent (diethyl ether). The Φ_f decreased from Cl (**2a**, 37%) through Br (**2b**, 30%) to I (**2c**, 8%) (Figure 2.17, Table 2.1), matching the trend in decreasing electronegativity. This suggests that a more electron-withdrawing halogen results in an increase in the fluorescence intensity and Φ_f as a consequence of lower electron density on the donor nitrogen atom. To confirm this hypothesis, we compared the previously reported highly emissive **ABM** (**2e**) to the analogous chloro derivative (**2d**).[30] The Φ_f of **2d** was higher (42% in diethyl ether and 65% in cyclohexane) which is the highest Φ_f of all reported amino halogen maleimides.

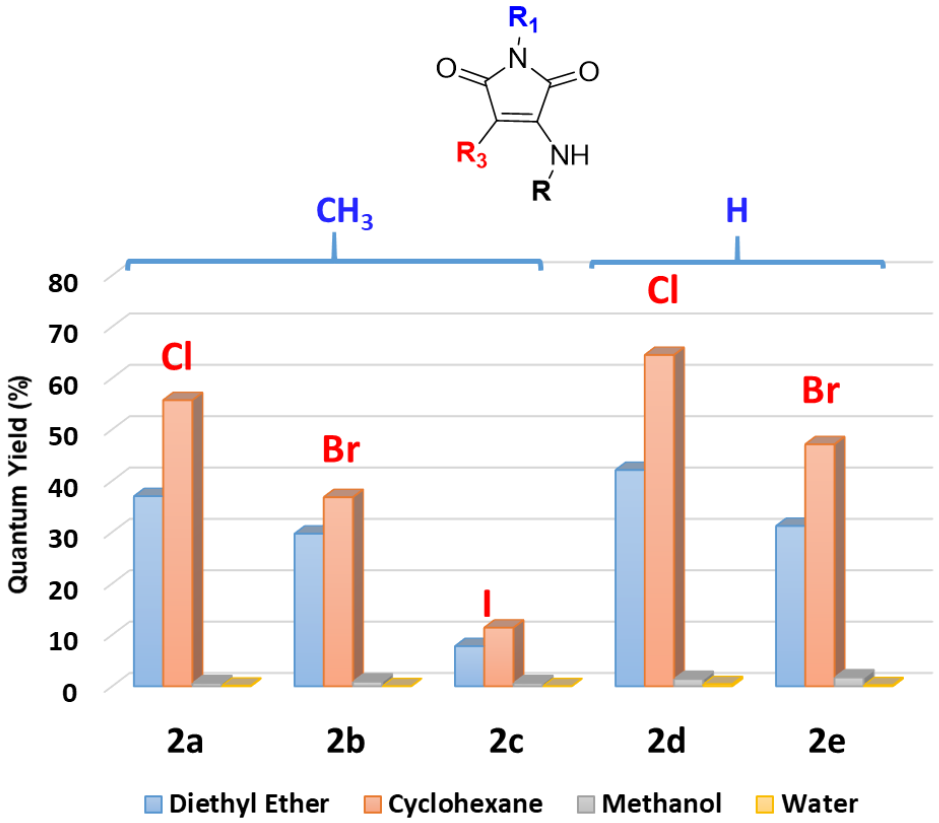

Figure 2.17 Fluorescence quantum yield of the **2a-e** in different solvents (diethyl ether, cyclohexane, methanol, and water) using quinine sulfate (Φ_f = 59% in 0.105 M $HClO_4$) as the reference.

Table 2.1 Fluorescent properties of studied compounds in different solvents.

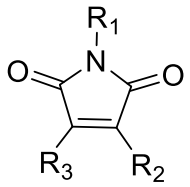

No.	R_1	R_2	R_3	Solvent	Φ_f %	ε_{max} $M^{-1}cm^{-1}$	λ_{abs} nm	λ_{ex} nm	λ_{em} nm	$\Delta\lambda$ nm
2a	CH_3	$NHCH_2CH_3$	Cl	Diethyl Ether	37.0	3669	239,369	365	475	106
				Cyclohexane	55.7	3198	238, 365	364	482	117
				Methanol	0.6	3355	239, 379	380	550	171
				Water	0.1	2442	241, 398	397	580	182
2b	CH_3	$NHCH_2CH_3$	Br	Diethyl Ether	29.7	3733	239, 370	371	474	104
				Cyclohexane	36.8	3496	239, 366	364	472	106
				Methanol	0.9	4811	241, 384	379	548	164
				Water	<0.1	3645	241, 400	397	583	183
2c	CH_3	$NHCH_2CH_3$	I	Diethyl Ether	7.8	4419	237, 370	368	487	117
				Cyclohexane	11.4	3483	239, 372	363	472	100
				Methanol	0.6	3405	238, 388	383	560	172
				Water	<0.1	2925	238, 404	396	580	176
2d	H	$NH(CH_2)_3CH_3$	Cl	Diethyl Ether	42.1	5073	226, 359	355	461	102
				Cyclohexane	64.5	4220	226, 356	352	442	72
				Methanol	1.4	4313	229, 374	370	512	142
				Water	0.4	2867	228, 387	387	550	180
2e	H	$NH(CH_2)_3CH_3$	Br	Diethyl Ether	31.2	5531	226, 358	458	461	103
				Cyclohexane	47.1	4489	226, 355	351	441	86
				Methanol	1.7	4451	229, 374	367	513	139
				Water	0.2	2768	228, 387	387	547	160

2.3.4 Simulation of the Electron Density in Substituted Maleimides Derivatives*

To rationalize the possible relationship between the electronic structure and fluorescence quantum yields derived from results, the lowest-energy absorption and emission peaks were computed at CAM-B3LYP-D3BJ(PCM)/6-311G(d,p) level using time-dependent density functional theory by Dr. Miquel Torrent-Sucarrat (for more details see Experimental section). Good agreements between theoretical and experimental results were obtained for the absorption and emission spectra, respectively (Computational Details section). All the energies calculated correspond to HOMO (π) $\rightarrow$ LUMO (π^*) transitions (Computational Details section). Moreover, natural population analysis (NPA) of the carbon atoms adjacent to the halogen and electron-donating groups (labeled as C2 and C3, respectively) were calculated. The charge difference between the C2 and C3 provided the initial evidence in the electron displacements of different maleimide compounds (Table 2.2).

Table 2.2 Relative fluorescence quantum yield in different solvents

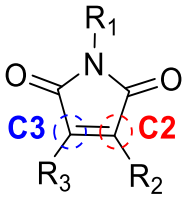

R_1	R_2	R_3	Φ_f[a]	Ground State NPA		Charge Difference
				C2	C3	
CH_3	Br	$NHCH_2CH_3$	29.7±1.4	-0.32	0.15	0.47
CH_3	Cl	$NHCH_2CH_3$	37±0.9	-0.24	0.15	0.39
CH_3	I	$NHCH_2CH_3$	7.78±0.6	-0.44	0.15	0.59
H	Br	$NH(CH_2)_3CH_3$	31.2±1.6	-0.32	0.14	0.47
H	Cl	$NH(CH_2)_3CH_3$	42.1±1.3	-0.25	0.14	0.39

*The simulation results were carried out by Dr. Miquel Torrent-Sucarrat

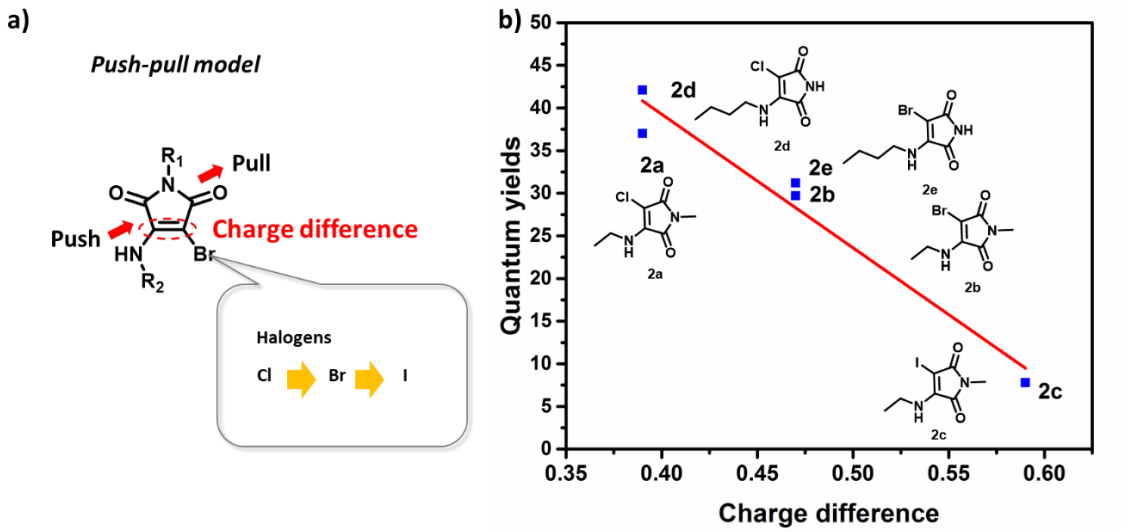

Figure 2.18 a) Schematic illustration of the charge difference between the C=C double bond based on the push-pull model of maleimide structures; b) The linear relationship of calculated charge difference between the C2 and C3 with experimental quantum yields in different halogenated amino-substituted maleimides.

To investigate the effect of the charge difference between the C2 and C3, the fluorescent quantum yields and charge difference between the C2 and C3 in the corresponding structures have been plotted in figure 2.18b. It is worth noting that the experimental quantum yield results are linearly correlated to the calculated charge differences (C2-C3) on C=C bond. The altering of the halogen from Cl to I increases the charge difference, which is linearly correlated to a decrease in the fluorescence quantum yield. This indicated that high quantum yield values are associated with a stronger electron-donating group on C3 and a stronger electron-withdrawal group on C2, which gives a large charge difference on C=C bond. Consequently, this reinforces the "push-pull" mechanism in the substituted maleimides, where a stronger electron-withdrawal group on C2 promotes the electron transfer process. In summary, the results presented here highlight the important consideration that high charge difference on the C=C bond will improve emission and extend the scope of maleimide fluorophores.

* The simulation results were carried out by Dr. Miquel Torrent-Sucarrat

2.3.5 Design and Synthesis of Alcohol Substituted Maleimides

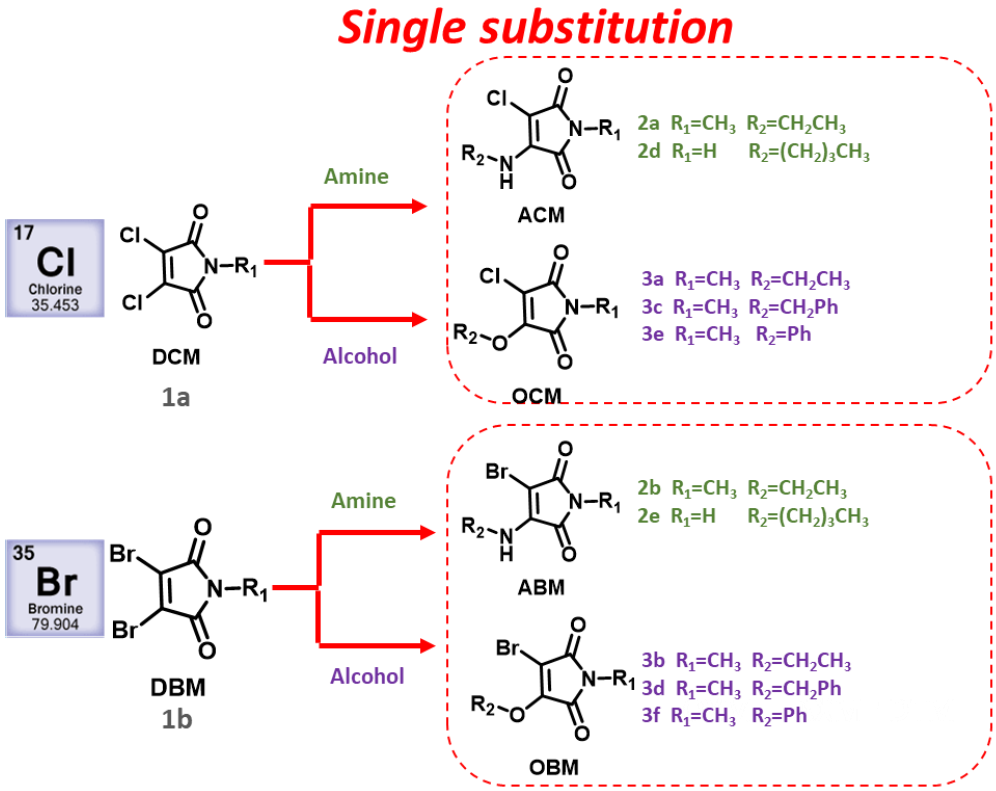

Figure 2.19 Synthesis of the different alcohol substituted maleimides and comparison of the fluorescent properties between the alcohol substituted maleimides with the amine substituted maleimides.

By changing the halogen substituents, it was clear that the optical properties are closely related to the charge difference of the C=C double bond in amino-substituted maleimides. However, the effect of the electron donor group in these systems has not yet been explored. Hence, we sought to expand the range of donor groups and decided to investigate alkoxy substituents instead of the stronger amino electron-donating group.

Due to lower reactivity, reports on alcohol substituted maleimides are very limited. In 2004, Booker-Milburn *et. al.*, reported a synthetic route by choosing sodium alkoxide as the catalyst for the substitution reaction of dichloromaleimdies/

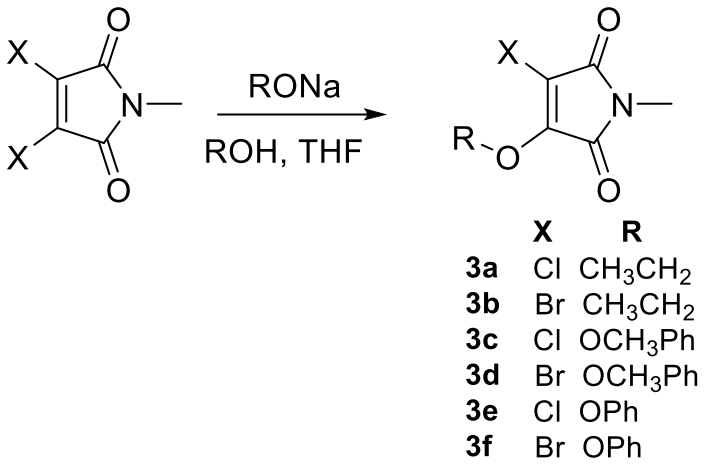

Figure 2.20 Synthetic strategy for the different alkoxy substituted methylmaleimides

dibromomaleimdies with a series of alcohols.[58] A strong base – sodium was applied to deprotonate the alcohol, followed by direct reaction with the maleimide precursor to form the singly substituted maleimide product.

Following this route, the sodium alkoxide solution was firstly prepared by reacting sodium with the reactant alcohol. The precursors **1a**-**b** were mixed with this freshly prepared sodium alkoxide solution without using additional solvent (Figure 2.20). The excess of alcohol used in this reaction should accelerate the reaction by pushing the equilibrium of the reaction to get a higher yield. The reaction was monitored by consumption of **1a**-**b** *via* TLC and was complete within 30 min to 1 h. The excess of sodium alkoxide was washed with ammonium chloride solution and water, following by purification *via* column chromatography. The singly substituted products of the *in-situ* formation of the alkoxy maleimides (**3a**-f) were confirmed by NMR spectroscopy and HR-MS (see Experimental section). All compounds exhibited good solubility in common organic solvents.

2.3.6 Fluorescence Properties of Alcohol Substituted Maleimides

The fluorescence properties of the acquired alcohol substituted maleimides have been investigated for the first time. When comparing the fluorescence of different alcohol substituted maleimides, both the ethoxy (**3a**-**b**) and benzyloxy (**3c**-**d**) substituted products showed blue emission with the λ maximum around 450-460 nm, whereas no emission was observed for the phenoxy (**3e**-**f**) derivatives (Figure 2.21a). These results are consistent with our previous reports, in which the direct conjugation of aromatic rings leads to the quenching of aminobromaleimides.[30] In addition, similar emission was observed in these alkoxymaleimides when varying the halogen from Br (**3b**, **3d**) to Cl (**3a**, **3c**), coinciding within the amino-substituted series (**2a**-**b**) (Figure 2.21b).

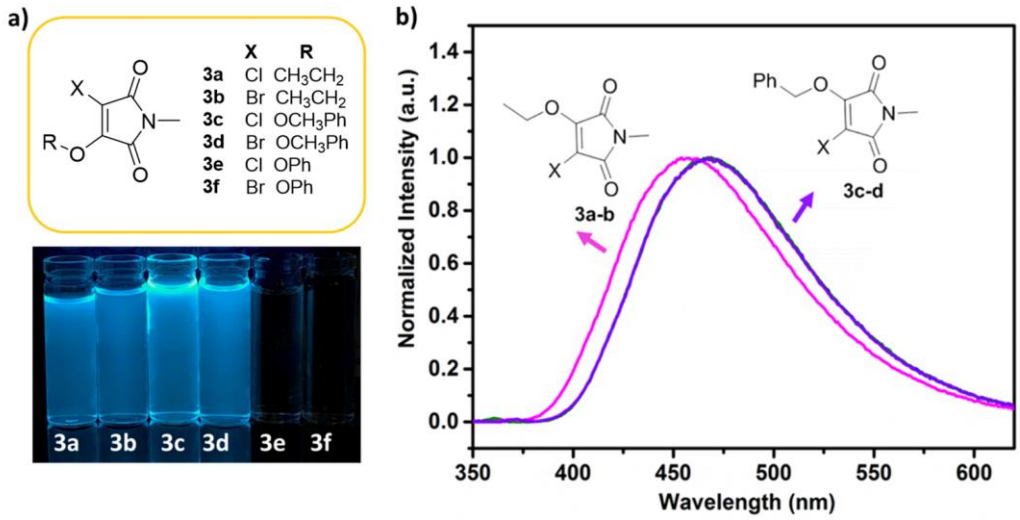

Figure 2.21 a) Photographs of the fluorescence of different alcohol substituted maleimides (**3a**-**f**) under UV light (365 nm) in diethyl ether; b) Fluorescence spectra of the alcohol substituted maleimides (**3a**-**d**) in diethyl ether (10 μM; λex 385 nm; Slit: 2.5 nm, 2.5 nm).

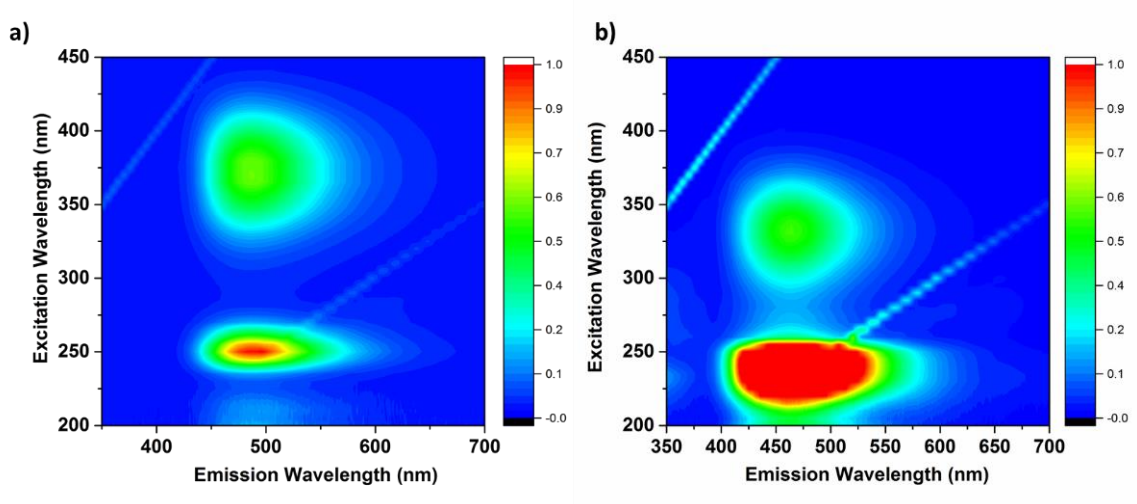

Figure 2.22 Comparison of a) 2D excitation-emission spectra (with a 5 nm step) of ACM **2a** in diethyl ether at 10 μM; with b) 2D excitation-emission spectra (with a 5 nm step) of OCM **3a** in diethyl ether at 10 μM. Peaks at λex = λem are due to Rayleigh scattering from the solution.

When comparing the 2D excitation-emission spectra of the ethylamine substituted maleimide (**2a**) with the ethanol substituted maleimide (**3a**), a clear blue-shift of the emission peak from 475 nm to 458 nm was observed (Figure 2.22). Meanwhile, the absorption of both **3a** and **3b** was blue-shifted to 330nm in the UV-vis spectra, which may be caused by the higher energy level of excited state in OCMs.

The solvatochromic properties of **3a-b** were recorded in eight solvents. The absorption spectra didn't show a dramatic shift while the emission spectra showed a characteristic red-shift in protic-solvents in comparison to the non-protic solvents (Figure 2.24). This evidence reveals that similar to the amino-substituted maleimides, the fluorescence properties of the alcohol substituted maleimides are also highly sensitive to the polarity of the solvent. Meanwhile, the solvatochromic properties were not affected when changing the halogen from Br (**3b**) to Cl (**3a**) in alcohol substituted maleimides (Figure 2.24).

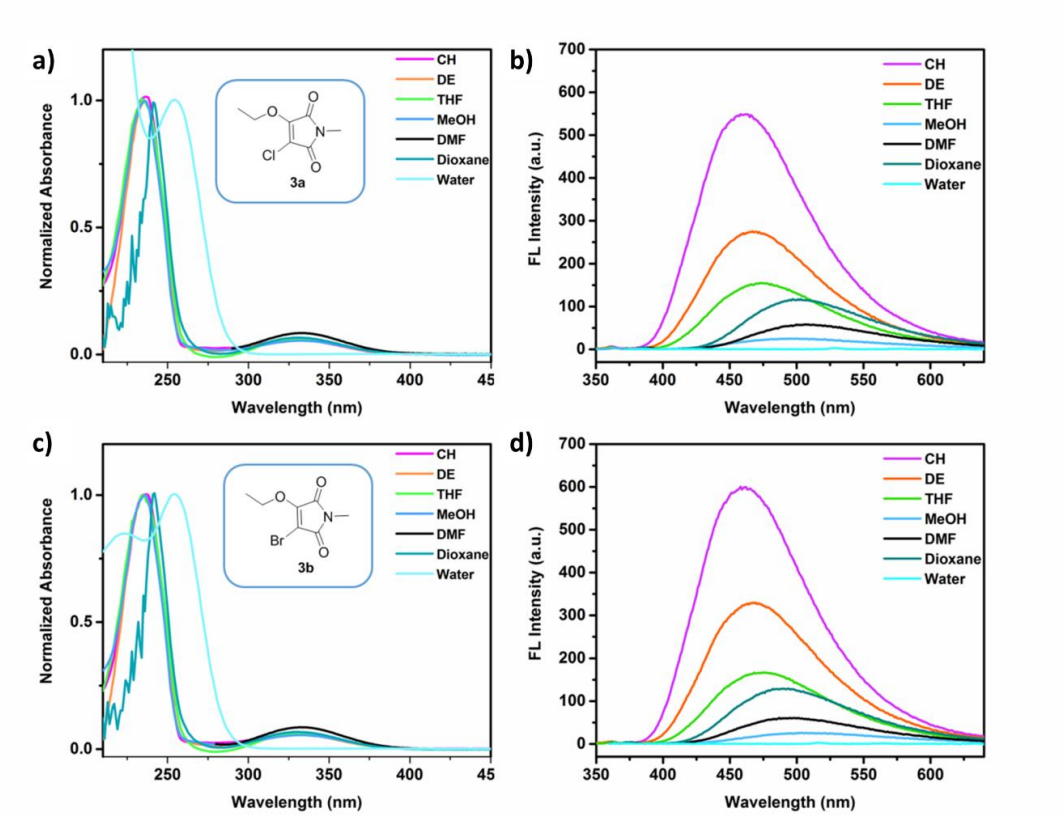

Figure 2.23 UV-Vis and fluorescence spectra of **3a-b** in seven common solvents: water, THF, diethyl ether, cyclohexane, dioxane, DMF, methanol; (20 μM, λ_{ex} 335 nm; Slit: 5 nm, 5 nm).

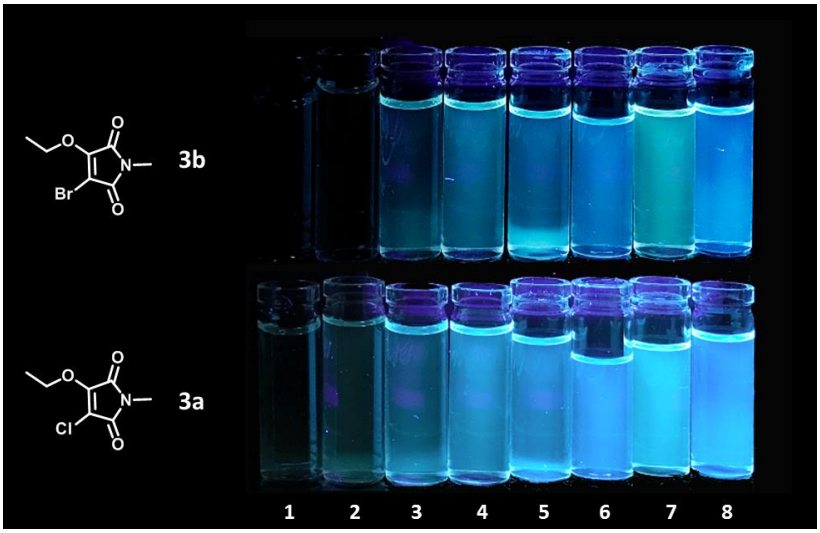

Figure 2.24 Photographs illustrating fluorescence of alkoxy maleimides (**3a-b**) in eight solvents (1–8: H_2O, MeOH, DMF, Dioxane, THF, Et_2O, CH_2Cl_2, and Cyclohexane;) under UV light (365 nm).

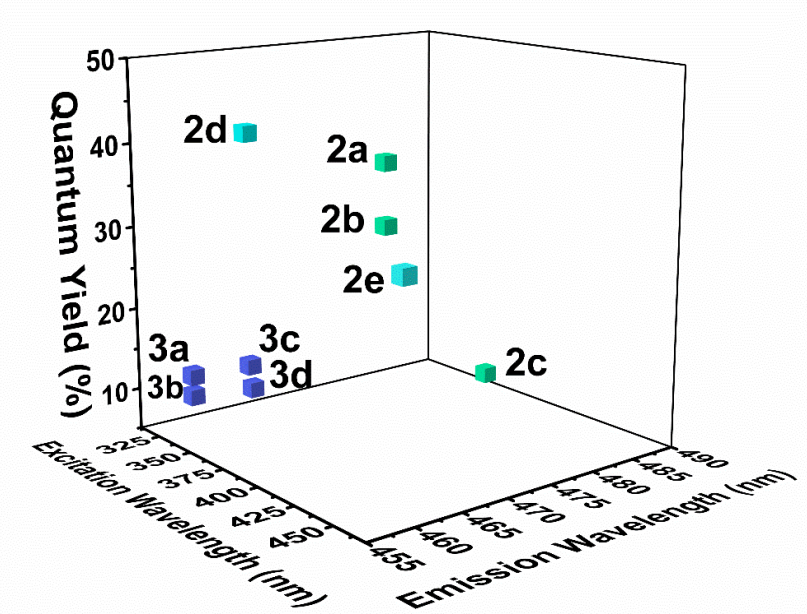

Figure 2.25 Fluorescence quantum yields of studied singly substituted maleimides (**2a-e**, **3a-d**) against excitation and emission wavelengths (10 μM in diethyl ether).

The fluorescence quantum yields of different alcohol substituted maleimides (**3a-f**) in diethyl ether were firstly compared with the amino-maleimides (Figure 2.26). The variation of the substituent from ethylamino group (**2a**) to an ethoxy (**3a**) group leads to a dramatic decrease in ($_f$ from 30% to 10% (in diethyl ether) (Figure 2.26, Table 2.3). This agrees with the hypothesis of the electron "push-pull" mechanism in substituted maleimides, indicating that a strong electron-donating group on the C=C bond is critical for obtaining a high fluorescence intensity. Moreover, a decrease in Φ_f was observed by varying the halogen from Cl (**3a**) to Br (**3b**) in alcohol substituted maleimides, which is similar to that in amine substituted compounds. The effect on Φ_f of different alcohol substituents was also compared (Table 2.3). The direct conjugation of the aromatic ring quenched the fluorescence while the phenyl group (3**c-d**) exhibited a similar Φ_f as an ethyl group (**3a-b**). These results were in accordance with observations in the aminomaleimides, suggesting the same mechanism is occurring for alcohol substituted maleimides.

Table 2.3 Fluorescence properties of synthesized compounds in different solvents

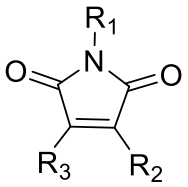

Number	R_1	R_2	R_3	Solvent	Φ_f %	ε_{max} $M^{-1}cm^{-1}$	λ_{abs} nm	λ_{ex} nm	λ_{em} nm	$\Delta\lambda$ nm
3a	CH_3	OCH_2CH_3	Cl	Diethyl Ether	12	770	230, 335	332	458	228, 123
				Cyclohexane	24	875	237, 330	332	461	224, 131
				Methanol	2	825	236, 333	330	486	250, 153
				Water	<0.1	548	236, 342	341	505	269, 163
3b	CH_3	OCH_2CH_3	Br	Diethyl Ether	10	666	230, 336	332	458	228, 122
				Cyclohexane	24	668	238, 333	332	461	223, 128
				Methanol	2	629	237, 335	332	486	249, 151
				Water	<0.1	432	236, 343	344	501	265, 158
3c	CH_3	OCH_2Ph	Cl	Diethyl Ether	12	1267	232, 335	334	464	232, 129
3d	CH_3	OCH_2Ph	Br	Diethyl Ether	9	907	233, 340	329	465	232, 125
3e	CH_3	OPh	Cl	Diethyl Ether	<0.1	586	238, 333	--	--	--
3f	CH_3	OPh	Br	Diethyl Ether	<0.1	821	243, 325	--	--	--

2.4 Summary

In summary, we have systemically designed and synthesized a library of singly substituted maleimide fluorophores with versatile fluorescent properties. Firstly, we have expanded the scope of substitution patterns of maleimide fluorophores, using readily available di-halogenated maleimides as building blocks. The synthesis of singly substituted maleimide fluorophores reported in this work offers facile access to different functionalization and tagging methods (amines and alcohols).

Meanwhile, by systematically tailoring the substitution patterns of maleimide dyes, remarkable fluorescent properties such as tunable emissions, high fluorescence quantum yields (up to 64%), large Stokes shift and solvafluorochromic properties were achieved in this chapter. More importantly, we for the first time explored the relationship between the substitution structures and optical properties. The fluorescence results provide evidence of the previously hypothesized push-pull model and computational results further confirmed that smaller charge differences on the C=C bond positively affect fluorescence intensity. As the optical properties are closely related to rational modifications made in this series of singly substituted maleimides, it is hypothesized that more remarkable changes may be realized by exploring disubstituted maleimides.

2.5 Experimental Section

2.5.1 Materials

All chemicals and reagents were purchased from either: Sigma Aldrich, Fisher Chemicals, Acros Chemicals, or Alfa Aesar and used as received. Dithiolmaleimide (**5**) was synthesized according to a previous paper.[40] Solvents were purchased from Fisher Scientific and used as received. Dry solvents were used directly from drying and degassing solvent tower delivery system.

2.5.2 Characterization Techniques

NMR Spectroscopy. ^{1}H-NMR and ^{13}C-NMR spectra were recorded NMR spectra were recorded on a Bruker Avance 300, a Bruker Avance III HD 400, or a Bruker Avance III HD 500 spectrometer at 298 K and 300, 400 and 500 MHz, respectively. Shifts are quoted in δ in parts per million and quoted relative to the internal standard trimethylsilane (TMS).

High-Resolution Mass Spectrometry. High-Resolution Mass Spectra (HR-MS) were conducted on a Bruker UHR-Q-ToF MaXis spectrometer with electrospray ionization.

Fourier-transform infrared spectroscopy. FTIR was carried out using a PerkinElmer 100 FT-IR. 16 Scans from 600 to 4000 cm^{-1} were taken at a resolution of 4 cm^{-1}, and the spectra were corrected for background absorbance.

UV-Vis spectroscopy. UV-Vis was performed on a Perkin Elmer Lambda 365 UV/vis spectrometer or an Agilent Cary 60 UV-Vis Spectrometer. Quartz cells (170 - 2000 nm) from Hellma with two polished sides were used for examining the absorption spectral data by using Thermo INSIGHT software.

Fluorescence spectroscopy. Fluorescence spectra were recorded using an Agilent Cary Eclipse Fluorescence spectrophotometer. Quartz cells with four polished sides (Starna) were used for fluorescence measurements.

2.5.3 Experimental Procedure for Di-halogen Maleimides Preparation

3,4-dichloro-1-methyl-1H-pyrrole-2,5-dione (1a):

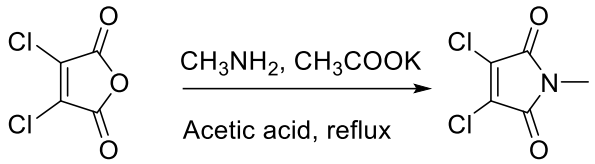

This compound was prepared by a method from the previous literature.[52] 3,4-dichloromaleic anhydride (1 g, 5.98 mmol), methylamine hydrochloride (0.605 g, 8.97 mmol), and potassium acetate (1.24 g, 8.97 mmol) were added to a solution of acetic acid (10 ml) and stirred for 4 hrs under reflux. The reaction becomes yellow, and was cooled to 25-30 ^{o}C, and poured slowly onto chilled sodium bicarbonate solution (1 M, 50 ml) until no effervesce was observed, followed by stirring for 1 hour. The solids were filtered, washed with *n*-hexane (2 x 30 ml), and dried under vacuum to obtain 3,4-dichloro-1-methyl-1H-pyrrole-2,5-dione (0.732 g, 68%). Matches literature data.[52] TLC conditions: R_f = 0.61 (petroleum ether: ethyl acetate= 4:1), Yield =68.0%.

^{1}H NMR (400 MHz, $CDCl_3$) δ= 3.12 (1H, s, H1);

^{13}C NMR (101 MHz, $CDCl_3$, ppm) δ= 162.8 (C2), 133.51 (C3), 25.1 (C1);

FTIR (neat) ν_{max} / cm^{-1} 1708 and 1617 (C=O of maleimide), 1436 and 1381 (C=C of maleimide).

3,4-diiodo-1-methyl-1H-pyrrole-2,5-dione (1c):

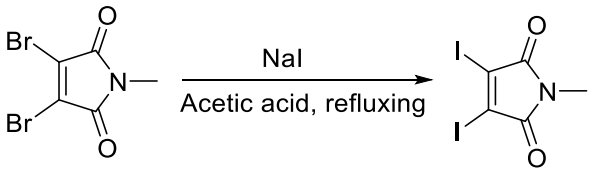

This compound was prepared by a method from the previous literature.[51] 3,4-dibromo-N-methylmaleimide (0.5 g, 1.859 mmol) and sodium iodide (1.115 g, 7.437 mmol) in acetic acid (20 ml) were heated at refluxing temperature for 2 h. Then the solution was added to water. The obtained yellow precipitate was filtered, washing with water and drying at 60 °C to obtain the 3,4-diiodo-1-methyl-1H-pyrrole-2,5-dione (0.527 g, 78.3%). Matches literature data.[2] TLC conditions: R_f = 0.53 (petroleum ether: ethyl acetate= 4:1), Yield =78 %.

^{1}H NMR (400 MHz, $CDCl_3$, ppm) δ= 3.15 (1H, s, H1).

^{13}C NMR (101 MHz, $CDCl_3$, ppm) δ=166.2 (C2), 117.1 (C3), 26.0 (C1).

HR-MS (MaXis) m/z found 385.8141 $(M+Na)^+$, calculated 385.8145;

FTIR (neat) ν_{max} / cm^{-1} 1695 and 1560 (C=O of maleimide), 1426 and 1361 (C=C of maleimide).

2.5.4 General Procedure for Synthesizing the Amine Substituted Maleimide

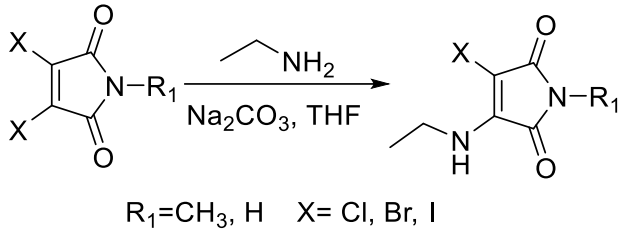

Reactions were performed according to the protocol established by a previous paper.[33] All reactions were performed in THF (20 mL) at room temperature with 2,3-dibromomaleimide/ 2,3-dibromomethylmaleimide (1 eq.), sodium carbonate (2.5 eq.) and a small excess of amine (1.05-1.1 eq.). Consumption of 2,3-dibromomaleimide was monitored by TLC, and was complete within 30 min to 2 h. The solvent was then evaporated under reduced pressure and the residue was taken up with 150 mL of CH_2Cl_2. The resultant mixture was washed with water (2 × 150 mL), dried with sodium sulfate and purified *via* column chromatography on silica gel with petroleum ether/ethyl acetate.

3-chloro-4-(ethylamino)-1-methyl-1H-pyrrole-2,5-dione (2a):

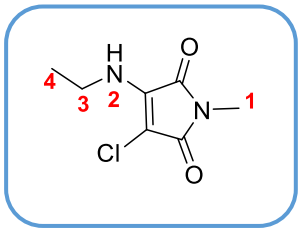

TLC conditions: R_f = 0.60 (petroleum ether: ethyl acetate= 2:1), Yield =60.5%. ^{1}H NMR (400 MHz, $CDCl_3$, ppm) δ=5.30 (1H, s, H2), 3.76 – 3.58 (2H, m, H3), 3.00 (3H, s, H1), 1.30 (3H, t, $^3J_{H-H}$ = 7.2 Hz, H4);

^{13}C NMR (101 MHz, $CDCl_3$, ppm) δ=38.1 (C3), 24.2 (C1), 16.1 (C4);

HR-MS (MaXis) m/z found 211.0247 $(M+Na)^+$, calculated 211.0245;

FTIR (neat) ν_{max} / cm^{-1} 3344 (H-N of amine), 1694 and 1629 (C=O of maleimide), 1436 and 1372 (C=C of maleimide).

3-bromo-4-(ethylamino)-1-methyl-1H-pyrrole-2,5-dione (2b):

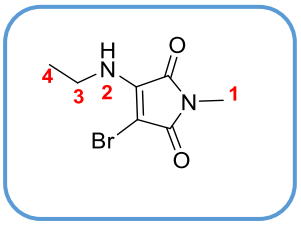

TLC conditions: R_f = 0.60 (petroleum ether: ethyl acetate= 2:1) Yield =54.3%. ^{1}H NMR (400 MHz, $CDCl_3$, ppm) δ=5.35 (1H, s, H2), 3.78 – 3.63 (2H, m, H3), 3.02 (3H, s, H1), 1.29 (3H, t, $^3J_{H-H}$ = 7.2 Hz, H4); ^{13}C NMR (101 MHz, $CDCl_3$, ppm) δ=38.0 (C3), 24.4 (C1), 15.8 (C4); HR-MS (MaXis) m/z found 256.9720 $(M+Na)^+$, calculated 256.9719;

FTIR (neat) ν_{max} / cm^{-1} 3332 (H-N of amine), 1707 and 1655 (C=O of maleimide), 1449 and 1372 (C=C of maleimide).

3- iodo-4-(ethylamino)- 1-methyl-1H-pyrrole-2,5-dione (2c):

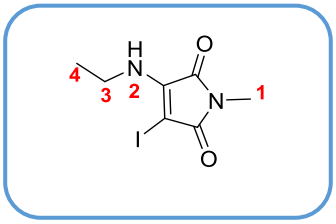

TLC conditions: R_f = 0.60 (petroleum ether: ethyl acetate= 2:1); Yield = 32.1%; ^{1}H NMR (400 MHz, $CDCl_3$, ppm) δ=5.35 (1H, s, H2), 3.78 – 3.63 (2H, m, H3), 3.02 (3H, s, H1), 1.29 (3H, t, $^3J_{H-H}$ 7 Hz, H4). ^{13}C NMR (101 MHz, $CDCl_3$, ppm) δ=38.0 (C3), 24.4 (C1), 15.8 (C4);

HR-MS (MaXis) m/z found 302.9604 $(M+Na)^+$, calculated 302.9601.

FTIR (neat) ν_{max} / cm^{-1} 3332 (H-N of amine), 1604 (C=O of maleimide), 1449 (C=C of maleimide).

3-(butylamino)-4-chloro-1-methyl-1H-pyrrole-2,5-dione (2d):

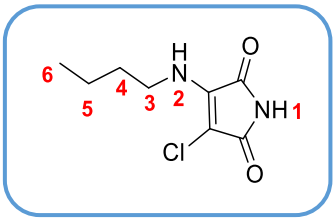

TLC conditions: R_f = 0.50 (petroleum ether: ethyl acetate= 2:1), Yield = 58.7%. ^{1}H NMR (400 MHz, $CDCl_3$, ppm) δ=7.08 (1H, s, H1), 5.31 (1H, s, H2), 3.62 (2H, td, $^3J_{H-H}$ = 14, 7 Hz, H3), 1.74 – 1.53 (2H, m, $^3J_{H-H}$ = 7 Hz, H4), 1.48 – 1.34 (2H, sex, $^3J_{H-H}$ = 7 Hz, H5), 0.97 (3H, t, $^3J_{H-H}$ = 7 Hz, H6). ^{13}C NMR (101 MHz, $CDCl_3$, ppm) δ=42.8 (C3), 32.8 (C4), 19.6 (C5), 13.6 (C6);

HR-MS (MaXis) m/z found 225.0404 $(M+Na)^+$, calculated 225.0401;

FTIR (neat) ν_{max} / cm^{-1} 3319 (H-N of amine), 3138 (H-N of maleimide) 1772 and 1707 (C=O of maleimide), 1404 and 1359 (C=C of maleimide).

3-bromo-4-(butylamino)-1H-pyrrole-2,5-dione (2e):

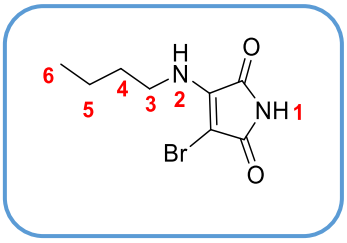

TLC conditions: R_f = 0.50 (petroleum ether: ethyl acetate= 2:1), Yield = 69.2%; ^{1}H NMR (400 MHz, $CDCl_3$, ppm) δ=7.17 (1H, s, H1), 5.41 (1H, s, H2), 3.65 (2H, dd, J = 7 Hz, H3), 1.70 – 1.58 (2H, quin, $^3J_{H-H}$ = 7 Hz, H4), 1.42 (2H, sex, $^3J_{H-H}$ =7 Hz, H5), 0.97 (3H, t, $^3J_{H-H}$ = 7 Hz, H6). ^{13}C NMR (101 MHz, $CDCl_3$) δ=42.9 (C3), 32.7 (C4), 19.5 (C5), 13.7 (C6); HR-MS (MaXis) m/z found 268.9898 $(M+Na)^+$, calculated 268.9896.

FTIR (neat) ν_{max} / cm^{-1} 3344 (H-N of amine), 3138 (H-N of maleimide) 1617 and 1707 (C=O of maleimide), 1462 and 1333 (C=C of maleimide);

2.5.5 General Procedure for Synthesizing the Alkoxymaleimides

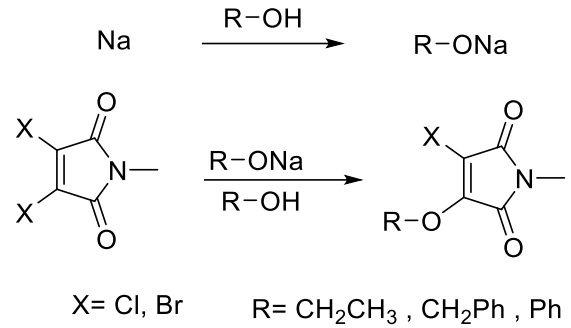

Reactions were performed according to the protocol established by a previous paper.[58] Sodium alkoxide solution was freshly prepared by the addition of sodium (2 mmol, 1 equiv) to the desired alcohol. This solution was then added dropwise to a cooled solution of the maleimide (2 mmol, 1 equiv.) in the same alcohol (10 mL). This was kept at 0 °C in an ice bath. Consumption of 2, 3-dibromo/chloro maleimide was monitored by TLC and was complete within 30 min to 1 h. Then the reaction mixture was concentrated in vacuo and separated between ethyl acetate and aqueous ammonium chloride solution. The aqueous layer was washed with ethyl acetate (50 mL×3), then the combined organic extracts washed with water (50 mL×3), brine, and dried with Na_2SO_4. Concentration *in vacuo,* followed by purification *via* column chromatography on silica gel with petroleum ether/ethyl acetate, afforded the products.

3-chloro-4-ethoxy-1-methyl-1H-pyrrole-2,5-dione (3a):

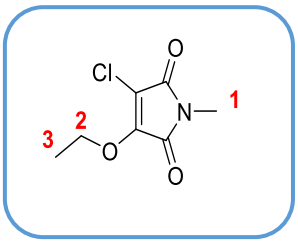

TLC conditions: R_f = 0.38 (petroleum ether: ethyl acetate= 4:1). Yield = 55.1%. ^{1}H NMR (400 MHz, $CDCl_3$, ppm) δ=4.72 (2H, q, $^3J_{H-H}$ = 7 Hz, H2), 3.05 (3H, s, H1), 1.49 (3H, t, $^3J_{H-H}$ = 7 Hz, H3). ^{13}C NMR (101 MHz, $CDCl_3$, ppm) δ=68.8 (C2), 23.9 (C1), 15.1 (C3). HR-MS (MaXis) m/z found 212.0084 $(M+Na)^+$, calculated 212.0085.

FTIR (neat) ν_{max} / cm^{-1} 1707 and 1655 (C=O of maleimide), 1436 and 1384 (C=C of maleimide), 1255 (C-O of alcohol).

3-bromo-4-ethoxy-1-methyl-1H-pyrrole-2, 5-dione (3b):

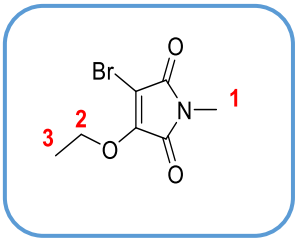

TLC conditions: R_f = 0.38 (petroleum ether: ethyl acetate= 4:1). Yield = 42.5%.; ^{1}H NMR (400 MHz, $CDCl_3$, ppm) δ=4.70 (2H, q, $^3J_{H-H}$ = 7 Hz, H2), 3.03 (3H, s, H1), 1.47 (3H, t, $^3J_{H-H}$ = 7 Hz, H3); ^{13}C NMR (101 MHz, $CDCl_3$) δ 68.7 (C2), 24.1 (C1), 15.4 (C3); FTIR (neat) ν_{max} / cm^{-1} 1720 and 1640 (C=O of maleimide), 1436 and 1382 (C=C of maleimide), 1268 (C-O of alcohol).

3-(benzyloxy)-4-chloro-1-methyl-1H-pyrrole-2,5-dione (3c):

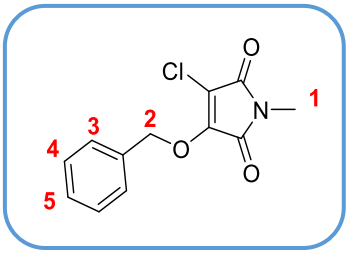

TLC conditions: R_f = 0.41 (petroleum ether: ethyl acetate= 4:1). Yield =43.7%; ^{1}H NMR (400 MHz, DMSO, ppm) δ=7.60 – 7.39 (5H, m, H3), 5.71 (2H, s, H2), 2.94 (3H, s, H3); ^{13}C NMR (101 MHz, DMSO, ppm) δ=131.24 – 125.94 (m, C3), 73.83 (C2), 24.42 (C1);

HR-MS (MaXis) *m/z* found 274.0243, calc. 274.0241 $([M+Na]^+$,100%);

FTIR (neat) ν_{max} / cm^{-1} 1720 and 1642 (C=O of maleimide), 1449 and 1397 (C=C of maleimide), 1255 (C-O of alcohol), 752 and 701 (C-H of aromatic).

3-(benzyloxy)-4-bromo-1-methyl-1H-pyrrole-2,5-dione (3d):

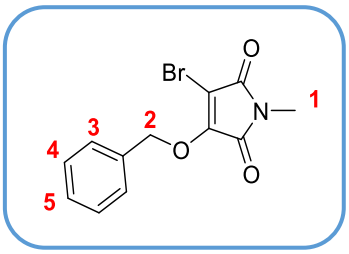

TLC conditions: R_f = 0.41 (petroleum ether: ethyl acetate= 4:1). Yield = 32.1%; ^{1}H NMR (400 MHz, DMSO, ppm) δ=7.55 – 7.35 (5H, m, H3), 5.69 (2H, s, H2), 2.90 (3H, s, H3); ^{13}C NMR (101 MHz, DMSO, ppm) δ=130.4 – 126.2 (m, C3), 73.8 (C2), 24.5 (C1); HR-MS (MaXis) *m/z* found 317.9731, calc. 317.9736 ([M+Na]$^{+}$,100%);

FTIR (neat) ν_{max} / cm^{-1} 1707 and 1642 (C=O of maleimide), 1423 and 1382 (C=C of maleimide), 1255 (C-O of alcohol), 740 and 688 (C-H of aromatic);

3-chloro-1-methyl-4-phenoxy-1H-pyrrole-2,5-dione (3e):

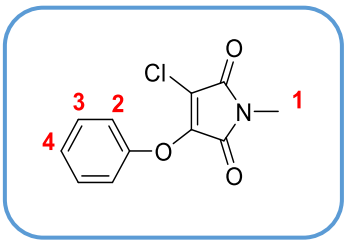

TLC conditions: R_f = 0.41 (petroleum ether: ethyl acetate= 4:1); Yield =55.1%; ^{1}H NMR (400 MHz, MeOD, ppm) δ=7.43 (2H, t, J = 8 Hz, H2), 7.28 (2H, t, J = 7 Hz, H3), 7.23 (1H, d, J = 8 Hz,), 3.03 (3H, s, H1). ^{13}C NMR (101 MHz, MeOD, ppm) δ=129.43 (C2), 125.47 (C3), 118.70 (C4), 22.87 (C1); HR-MS (MaXis) m/z found 260.0085 (M+Na)$^{+}$, calculated 260.0085; FTIR (neat) ν_{max} / cm^{-1} 1720 (C=O of maleimide), 1433 and 1392 (C=C of maleimide), 1270 (C-O of alcohol), 774 and 695 (C-H of aromatic).

3-bromo-1-methyl-4-phenoxy-1H-pyrrole-2,5-dione (3f):

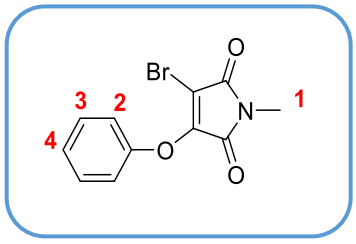

TLC conditions: R_f = 0.41 (petroleum ether: ethyl acetate= 4:1); Yield =51.0%. ^{1}H NMR (400 MHz, DMSO, ppm) δ=7.43 (2H, t, J = 7.5 Hz, H2), 7.28 (3H, dd, J = 14, 7 Hz, H2,3), 2.93 (3H, s, H1); ^{13}C NMR (101 MHz, DMSO, ppm) δ=130.2 (C2), 125.9 (C3), 119.1 (C4), 24.7 (C1). HR-MS (MaXis) m/z found 303.9586 (M+Na)$^{+}$, calculated 303.9580; FTIR (neat) ν_{max} / cm^{-1} 1720 (C=O of maleimide), 1436 and 1359 (C=C of maleimide), 1165 (C-O of alcohol), 830 and 714 (C-H of aromatic).

2.5.6 Determination of Relative Quantum Yield

Fluorescence quantum yields were measured by the relative method according to the literature.[13] Commercial fluorophore quinine sulfate was chosen as standard reference (Φ_f = 59%). All recorded absorbance (both samples and reference) were measured while keeping maximum absorbance value 0.1. Measurements were made in quartz cuvettes with a total sample volume of 3 mL.

Reference solution preparation: A solution of 0.105 M perchloric acid was prepared as the solvent. Quinine sulfate dihydrate was dissolved in this solution to a final concentration of 0.105 M. The solutions of the quinine sulfate were freshly prepared for each measurement.

Sample solution: The samples were prepared as 2 mM stocks in dioxane. The dyes were then diluted to 10 μM, and further diluted to various final concentrations.

General procedure for quantum yield measurement: A fresh solution of the quantum yield standard was used and its absorption spectrum measured. Using compound **2b** as an example, the sample and reference absorption spectra were overlaid, and the optimal excitation wavelength for the calculation was chosen to be the crossover wavelength (Figure 2.27)

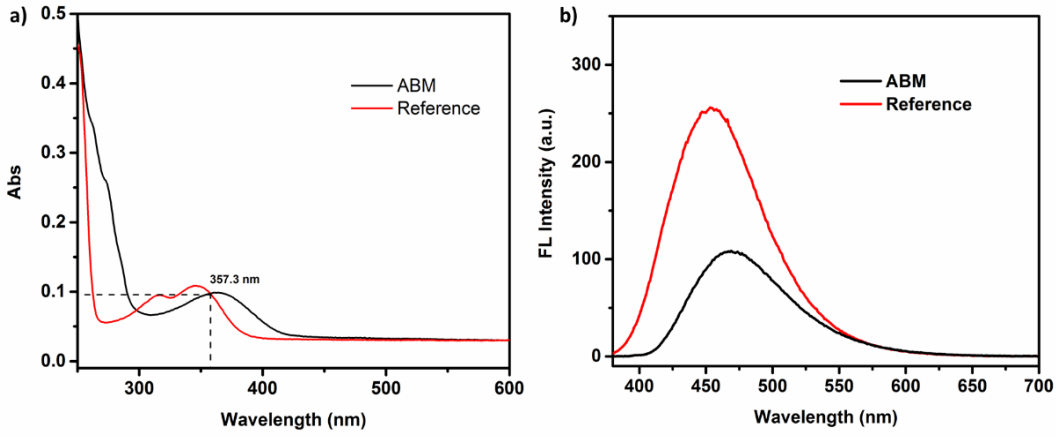

Figure 2.26 UV-Vis (a) and fluorescence emission (b) spectra of ABM (**2b**) and quinine standard.

Using this crossover wavelength as the excitation wavelength for fluorescence, the emission of both sample and reference solution was measured (Figure 2.27.) to calculate the quantum yield:

$$\Phi_{f,x} = \Phi_{f,st} \cdot \frac{F_x}{Fst} \cdot \frac{f_{st}}{f_x} \cdot \frac{n_x^2(\lambda_{em})}{n_{st}^2(\lambda_{em})}$$

in which F is the integral photon flux (emission integral), f is the absorption factor, n is the refractive index of the solvent and Φ_f is the quantum yield. The index x denotes the sample, and the index st denotes the standard. As the absorbance for the standard and sample match ($f_{st}/f_{conj}=1$), it can be neglected. Refractive indices are found for the conjugate and quinine solvents at their respective average emission wavelengths.

2.5.7 Computational Details*

The geometries for all studied systems in the ground state have been fully optimized with the CAM-B3LYP[7] functional and the 6-311G(d,p) basis set.[8,9] The dispersion effects and the solvent were included in the optimization process. The D3-Grimme's dispersion[10] with Becke-Johson damping factor[11,12] was used to evaluate the dispersion effects. The solvent was considered using the polarization continuum model (PCM)[13, 14,] and the dielectric constant of diethyl ether ($\varepsilon = 4.24$). The harmonic vibrational frequencies were also calculated at the same level of theory in order to verify that all the stationary points are minima of their potential energy surface. The time-dependent density functional theory (TD-DFT)[15-23] was applied to compute the absorption and emission (fluorescence) spectra at the ground and the first singlet excited state, respectively. The charge distribution was obtained following the natural bond orbital (NBO) partition scheme by Weinhold and co-workers.[24] All the calculations were performed using the Gaussian09 program package.[25]

* The simulation results was carried out by Dr. Miquel Torrent-Sucarrat

Table 2.4 TD-DFT excitation and emission energies and oscillator strengths of the maleimide derivatives studied in this work.[a,b]

Compound	λ_{exc} [c]	f_{exc} [d]	λ_{em} [e]	f_{em} [d]	$\Delta\lambda$ [f]
1a	302.4	0.023	468.4	0.011	166.0
1b	309.2	0.040	465.6	0.022	156.4
1c	323.2	0.078	463.7	0.058	140.5
2a	338.6	0.087	460.2	0.070	121.6
2b	339.0	0.087	458.9	0.073	119.9
2c	339.9	0.088	458.5	0.078	118.6
2d	330.3	0.121	435.3	0.104	104.9
2e	331.3	0.119	435.4	0.105	104.2
3a	307.3	0.035	442.7	0.028	135.4
3b	309.0	0.038	442.1	0.032	133.1
3c	308.0	0.031	449.7	0.022	141.7
3d	310.2	0.035	449.8	0.026	139.5
3e	306.3	0.033	445.5	0.024	139.2
3f	308.9	0.036	459.8	0.035	151

[a] All excitation and emission energies correspond to the first excited state ($\pi \rightarrow \pi^*$ transition).

[b] All values computed at CAM-B3LYP-D3BJ/6-311G(d,p) level of theory in solution using the PCM with $\varepsilon = 4.24$.

[c] Excitation wavelength, in nm.

[d] Oscillator strength.

[e] Emission wavelength, in nm.

[f] Stokes shift ($\lambda_{em} - \lambda_{exc}$).

[*] The simulation results was carried out by Dr. Miquel Torrent-Sucarrat

Table 2.5 Natural population analysis of the Carbon atoms adjacent to the electron withdrawing and donating groups (labeled as C_2 and C_3, respectively).[a]

Compound	q_{C2}	q_{C3}	Δq
1a	-0.13	-0.13	0.00
1b	-0.20	-0.20	0.00
1c	-0.32	-0.32	0.00
2a	-0.24	0.15	0.39
2b	-0.32	0.15	0.47
2c	-0.44	0.15	0.59
2d	-0.25	0.14	0.39
2e	-0.32	0.14	0.47
3a	-0.23	0.29	0.52
3b	-0.31	0.29	0.6
3c	-0.22	0.28	0.50
3d	-0.29	0.28	0.57
3e	-0.21	0.28	0.49
3f	-0.29	0.28	0.57

[a] All values computed at CAM-B3LYP-D3BJ/6-311G(d,p) level of theory in solution using the PCM with $\varepsilon = 4.24$.

* The simulation results was carried out by Dr. Miquel Torrent-Sucarrat

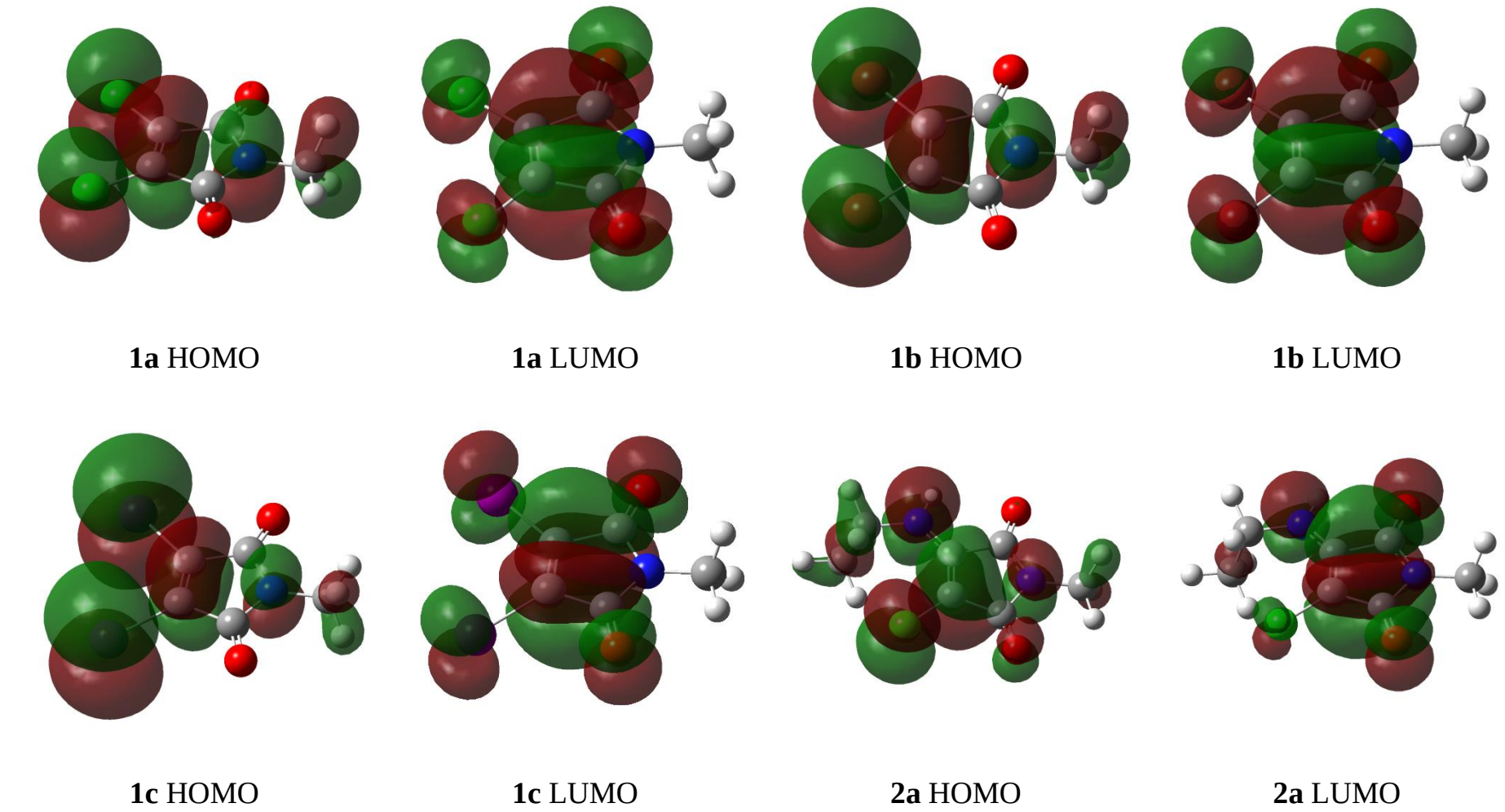

Figure 2.27 HOMO and LUMO Kohn-Sham orbitals of **1a**, **1b**, **1c** and **2a** maleimide derivatives.

* The simulation results was carried out by Dr. Miquel Torrent-Sucarrat

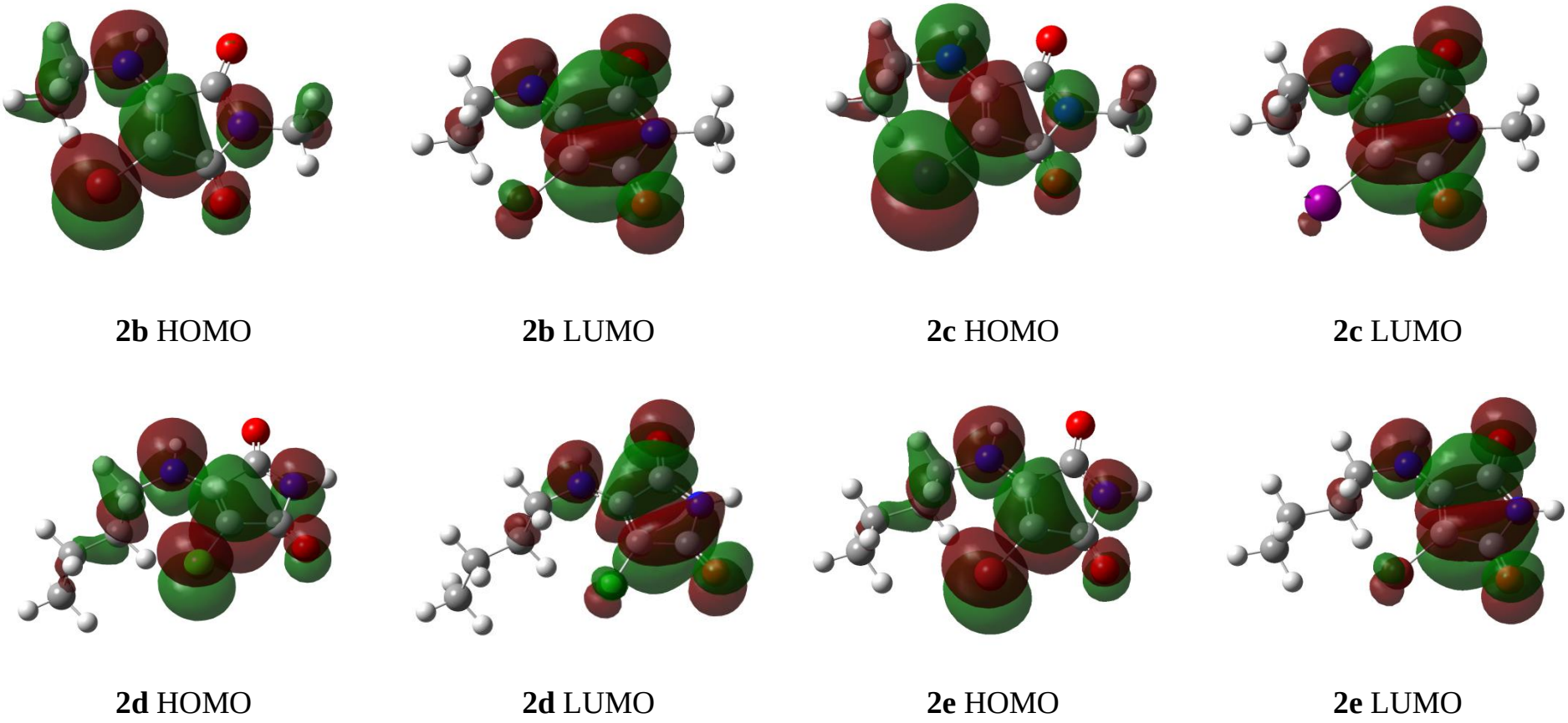

Figure 2.28 HOMO and LUMO Kohn-Sham orbitals of **2b**, **2c**, **2d** and **2e** maleimide derivatives.

* The simulation results was carried out by Dr. Miquel Torrent-Sucarrat

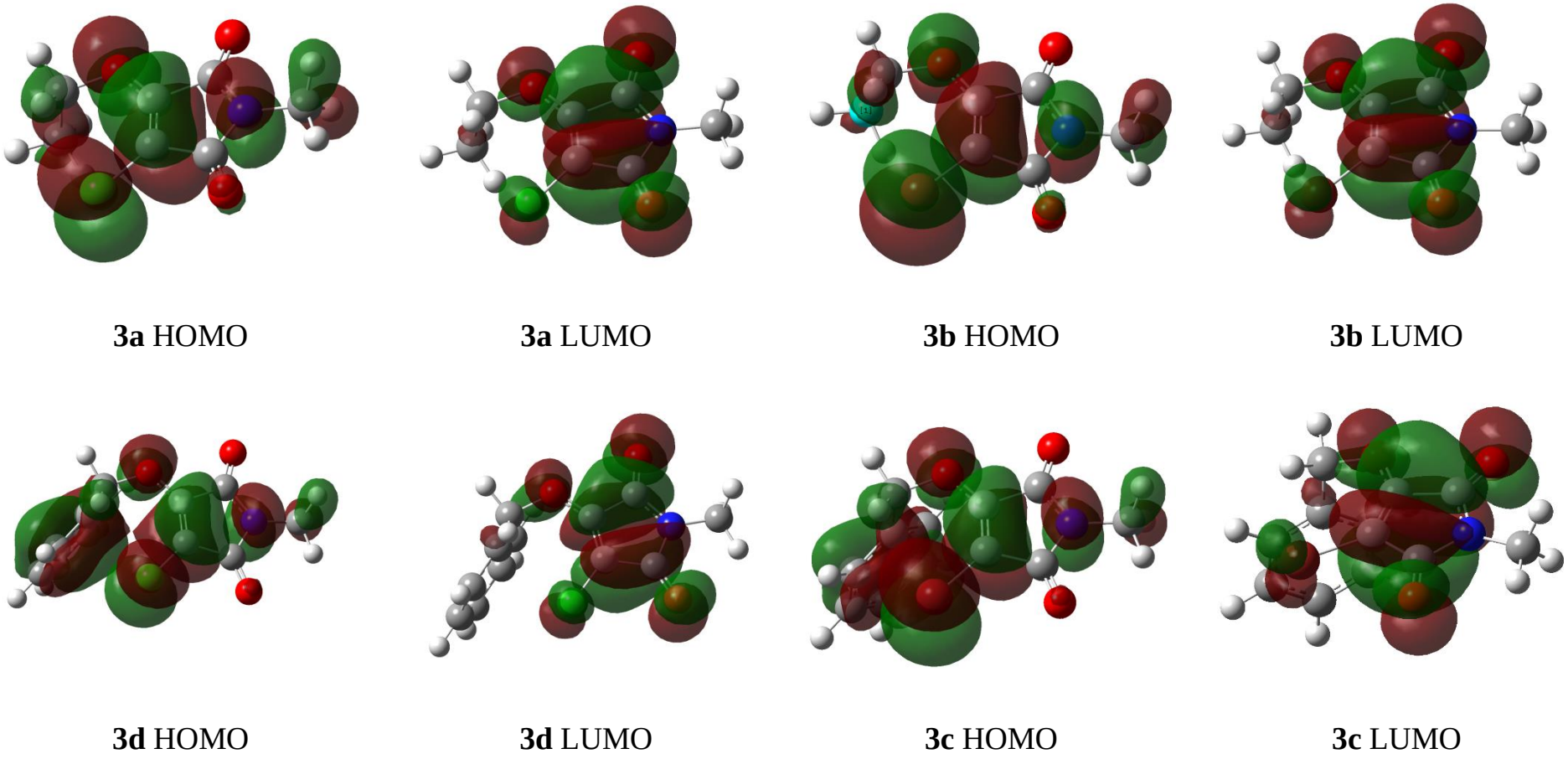

Figure 2.29 HOMO and LUMO Kohn-Sham orbitals of **3a**, **3b**, **3c** and **3d** maleimide derivatives.

* The simulation results was carried out by Dr. Miquel Torrent-Sucarrat

2.5.8 NMR Spectra of Substituted Maleimides

3-chloro-4-(ethylamino)-1-methyl-1H-pyrrole-2,5-dione (2a):

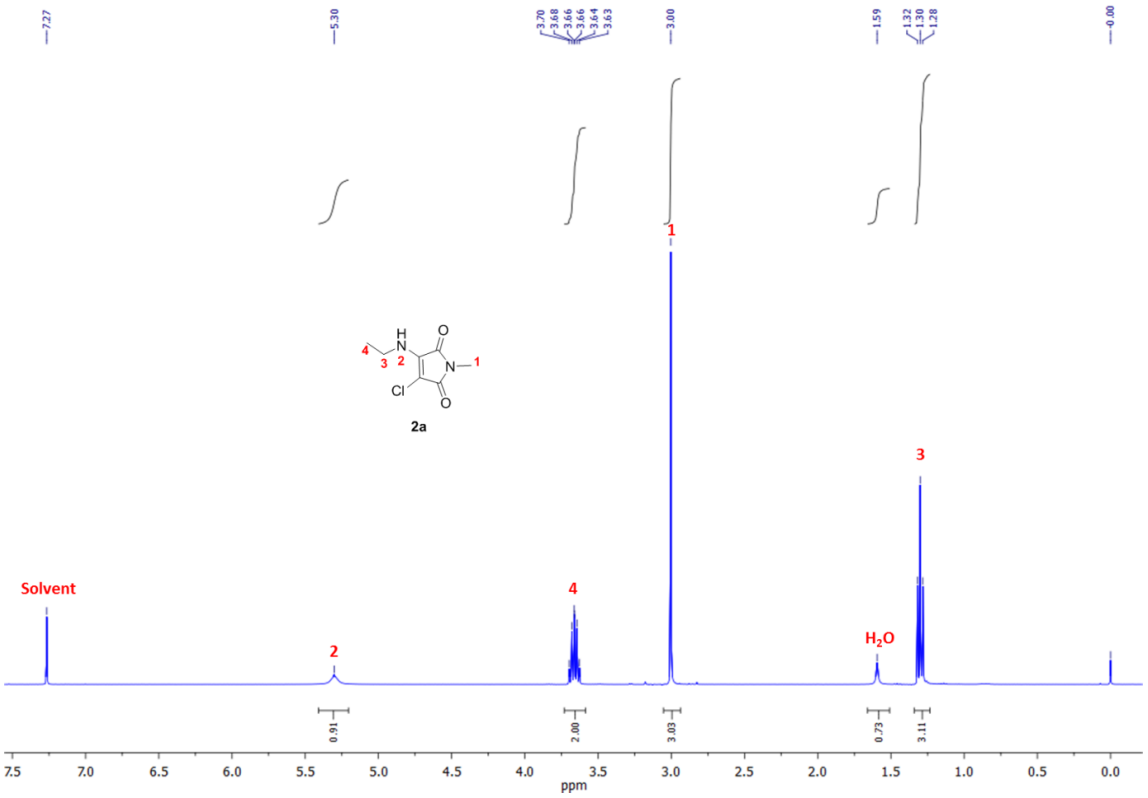

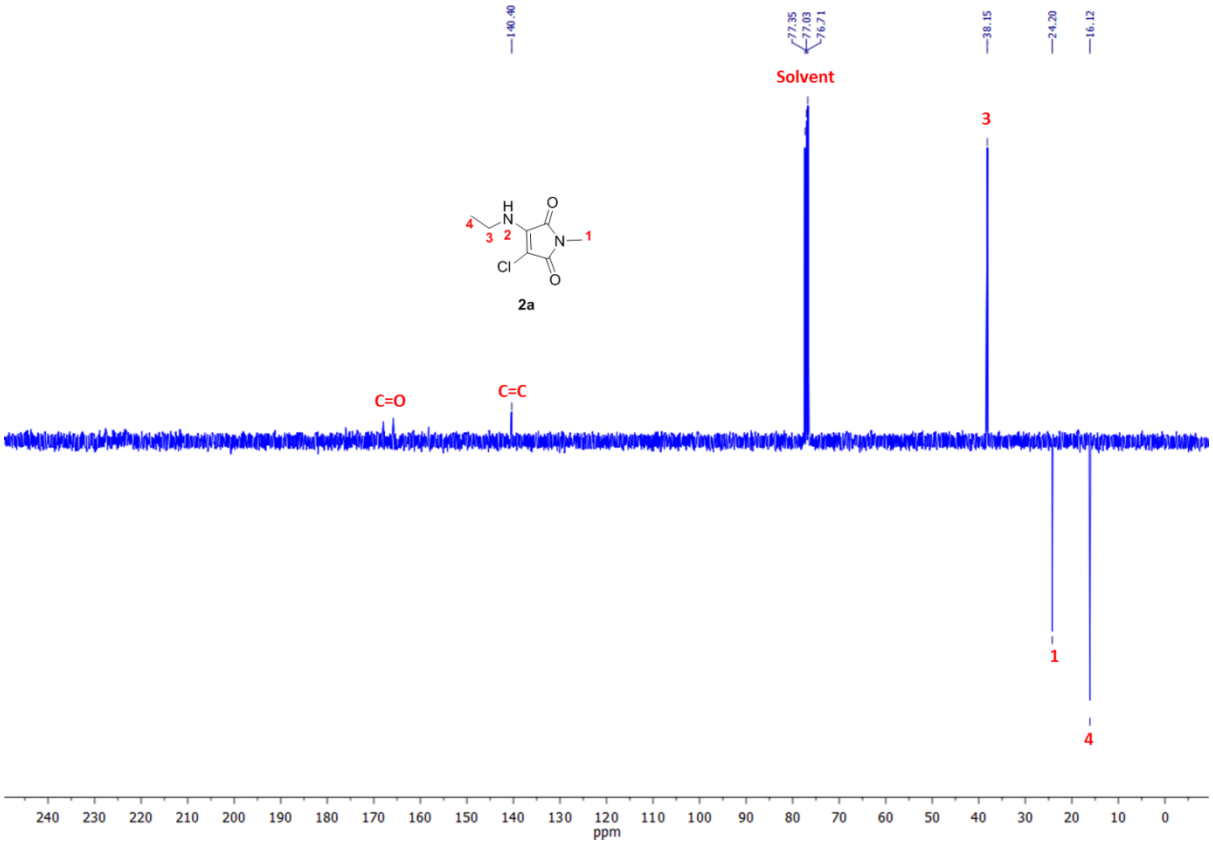

3-bromo-4-(ethylamino)-1-methyl-1H-pyrrole-2,5-dione (2b):

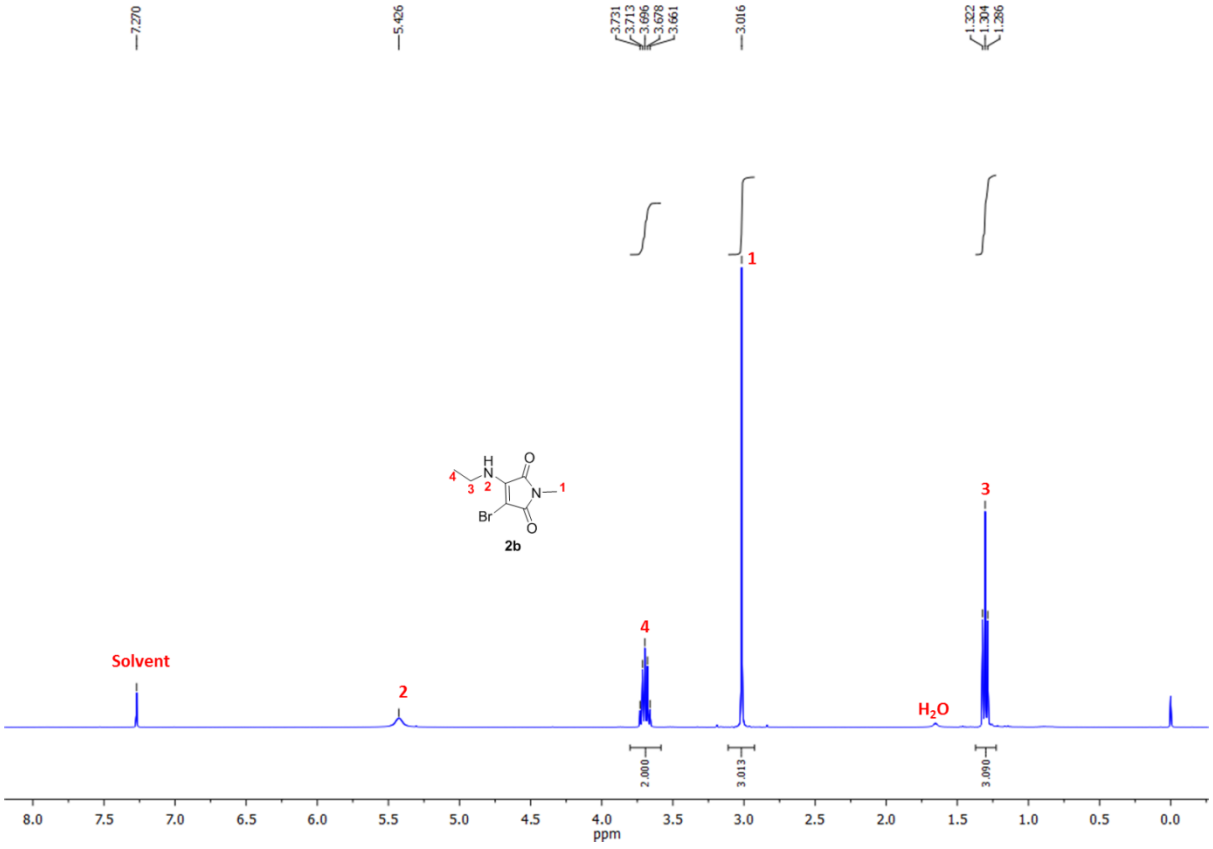

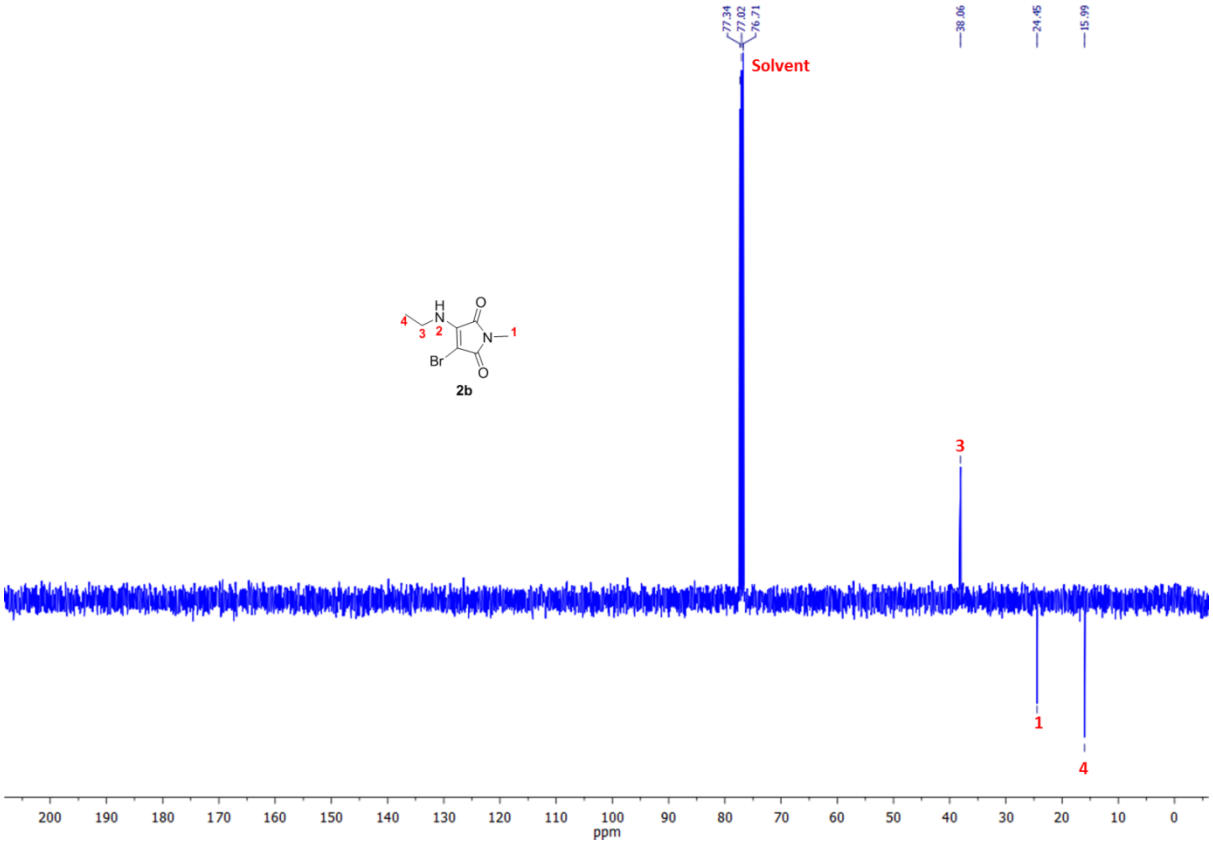

3- iodo-4-(ethylamino)- 1-methyl-1H-pyrrole-2,5-dione (2c):

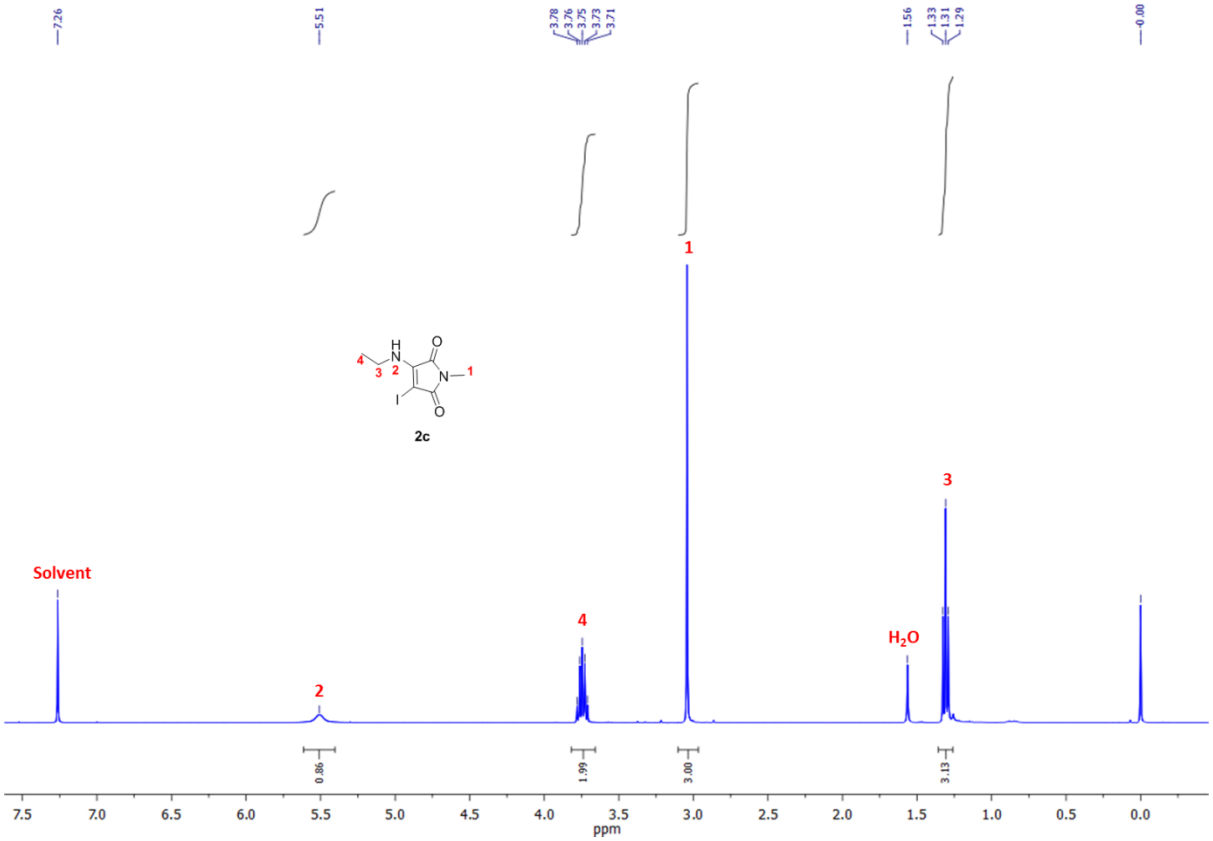

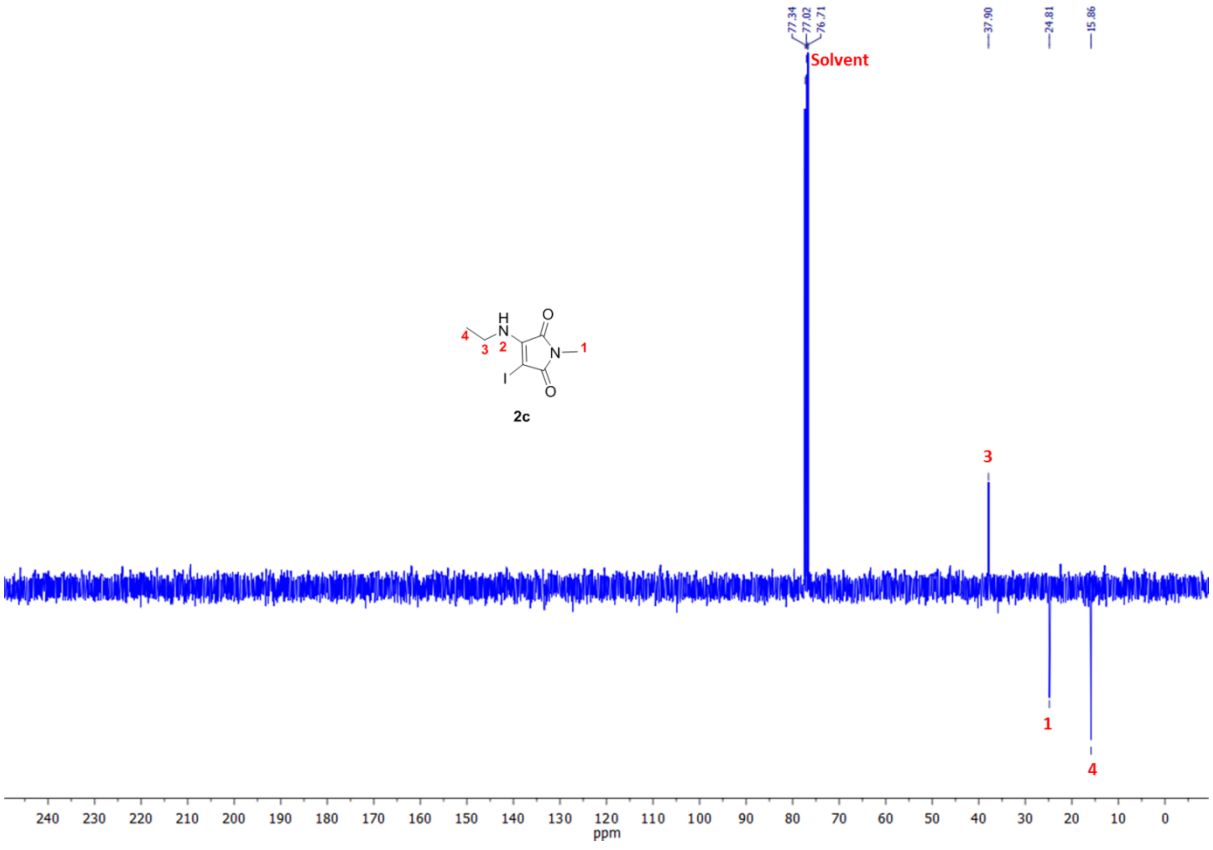

3-(butylamino)-4-chloro-1-methyl-1H-pyrrole-2,5-dione (2d):

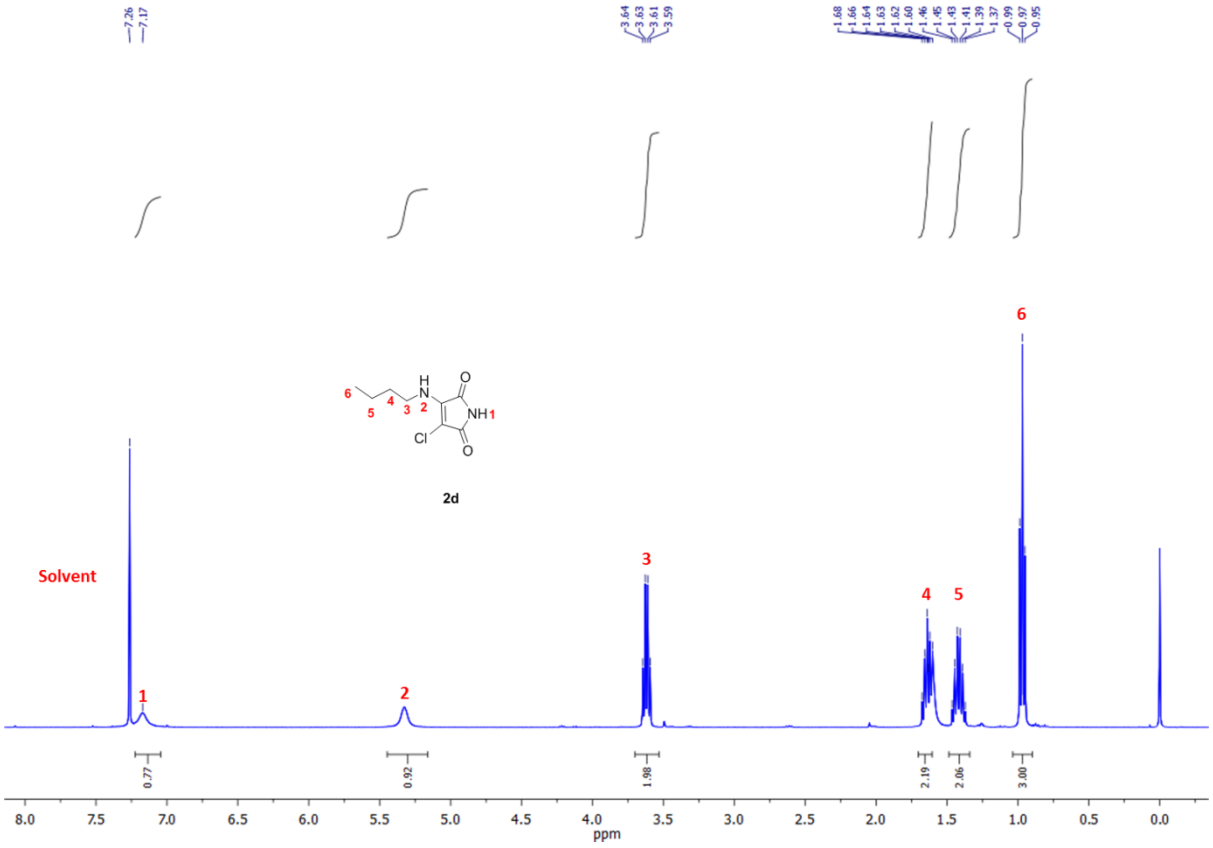

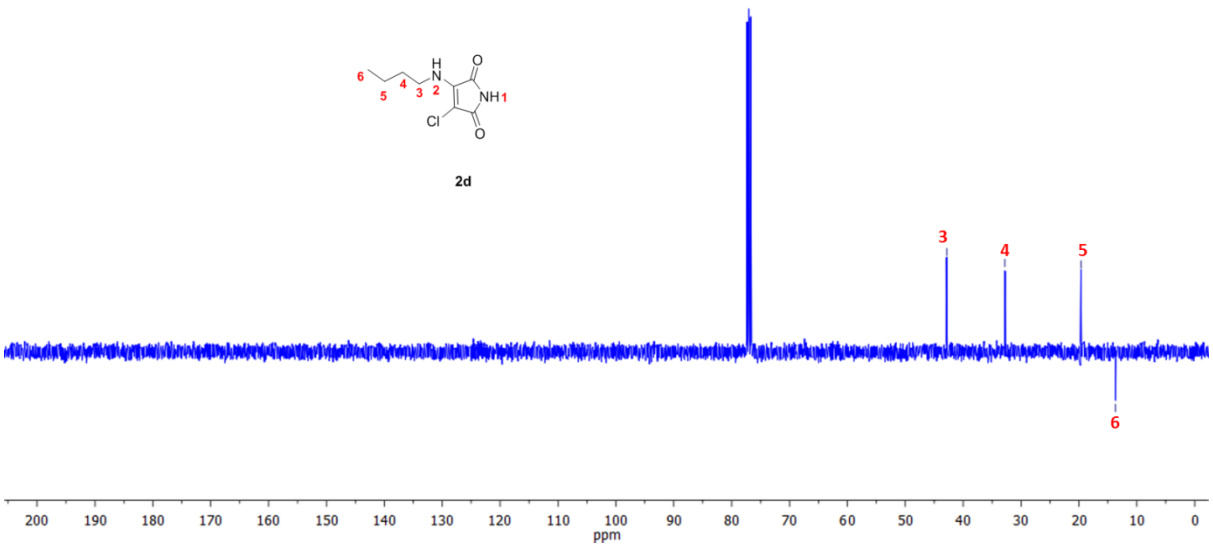

3-bromo-4-(butylamino)-1H-pyrrole-2,5-dione (2e)

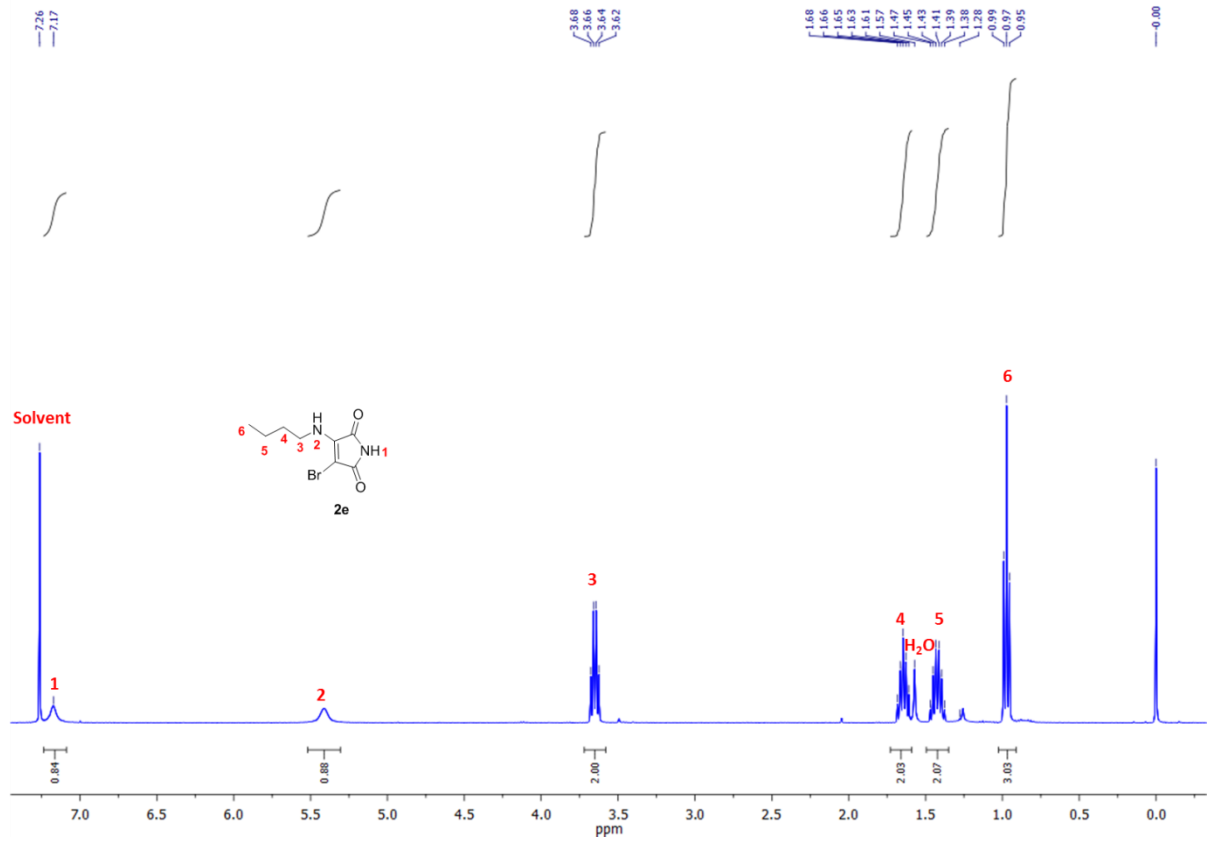

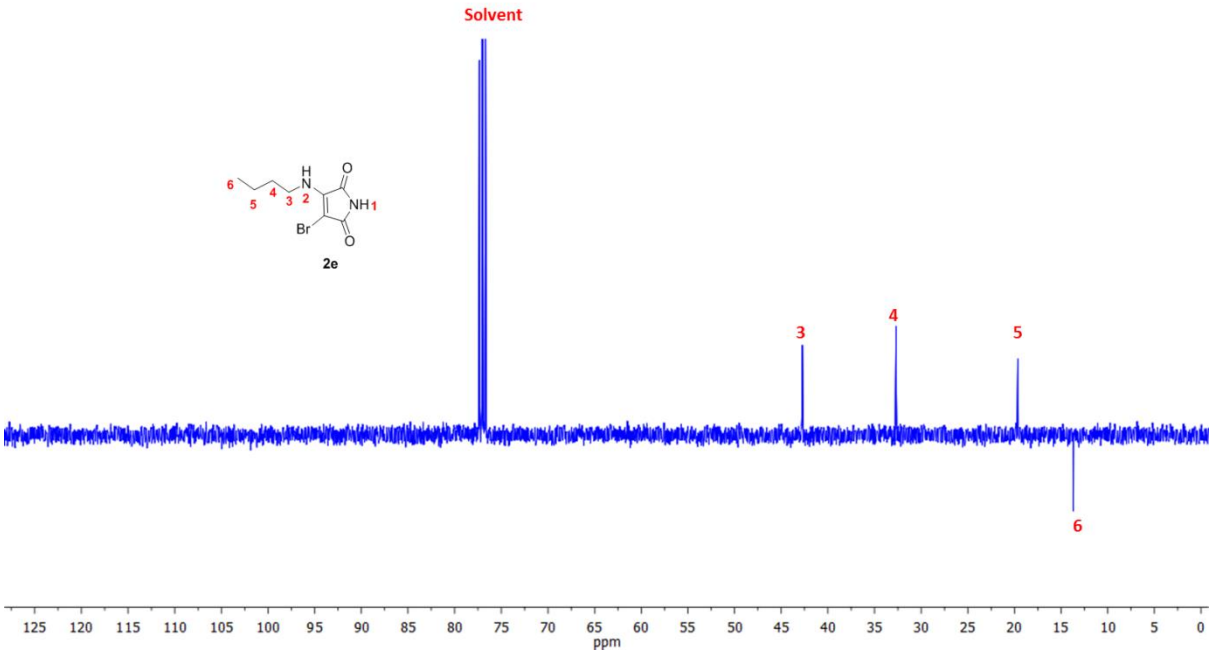

3-chloro-4-ethoxy-1-methyl-1H-pyrrole-2,5-dione (3a)

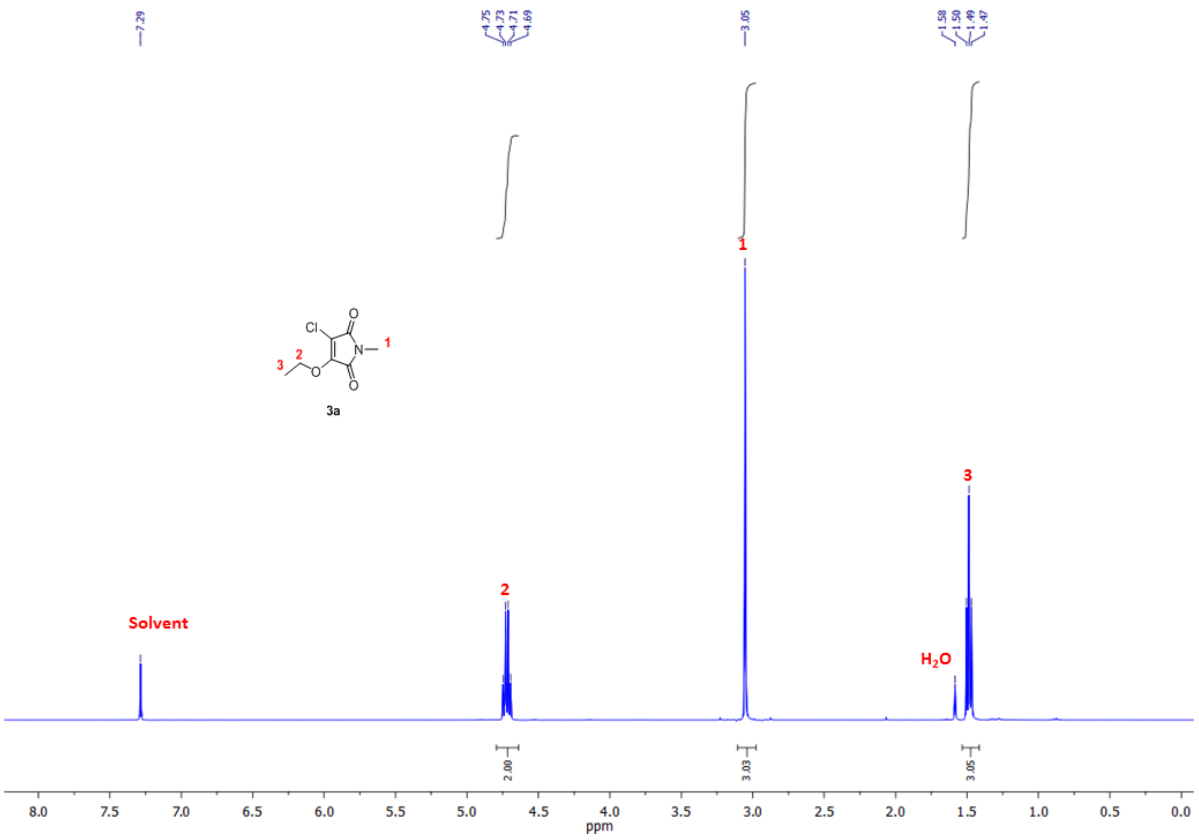

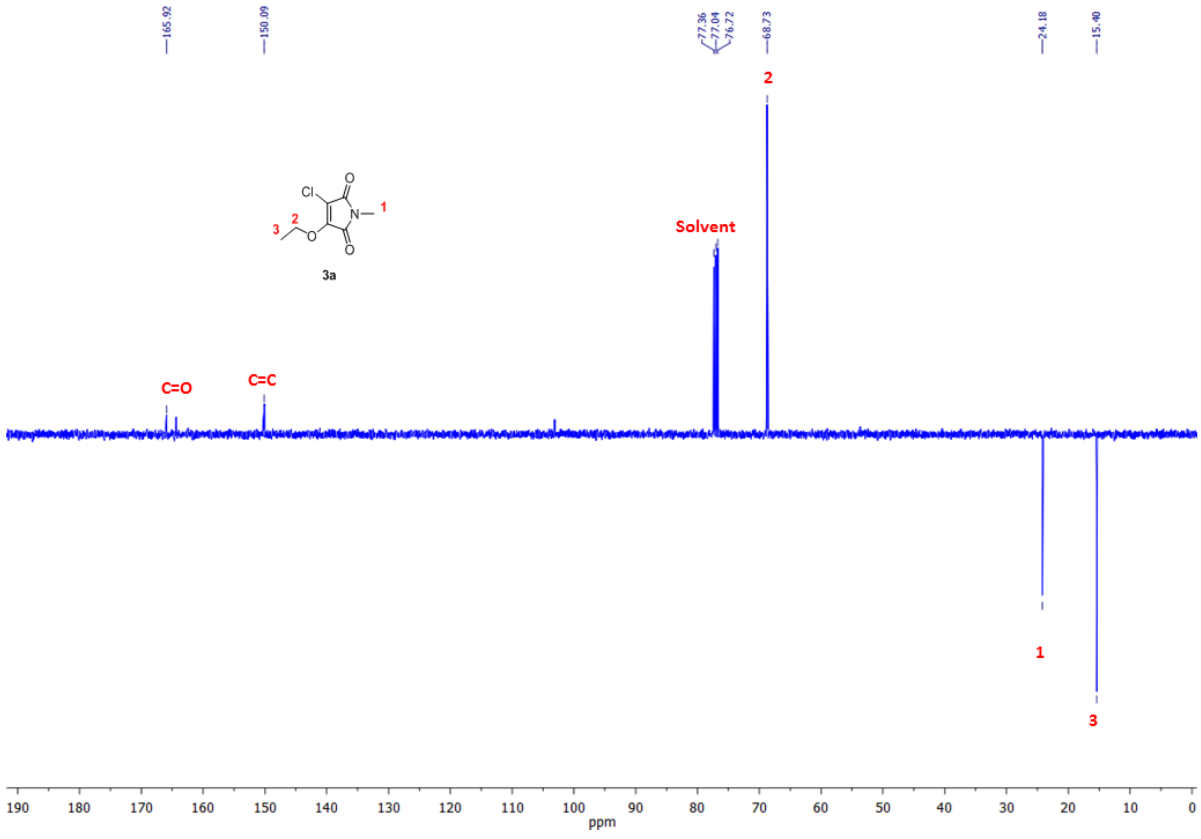

3-bromo-4-ethoxy-1-methyl-1H-pyrrole-2, 5-dione (3b)

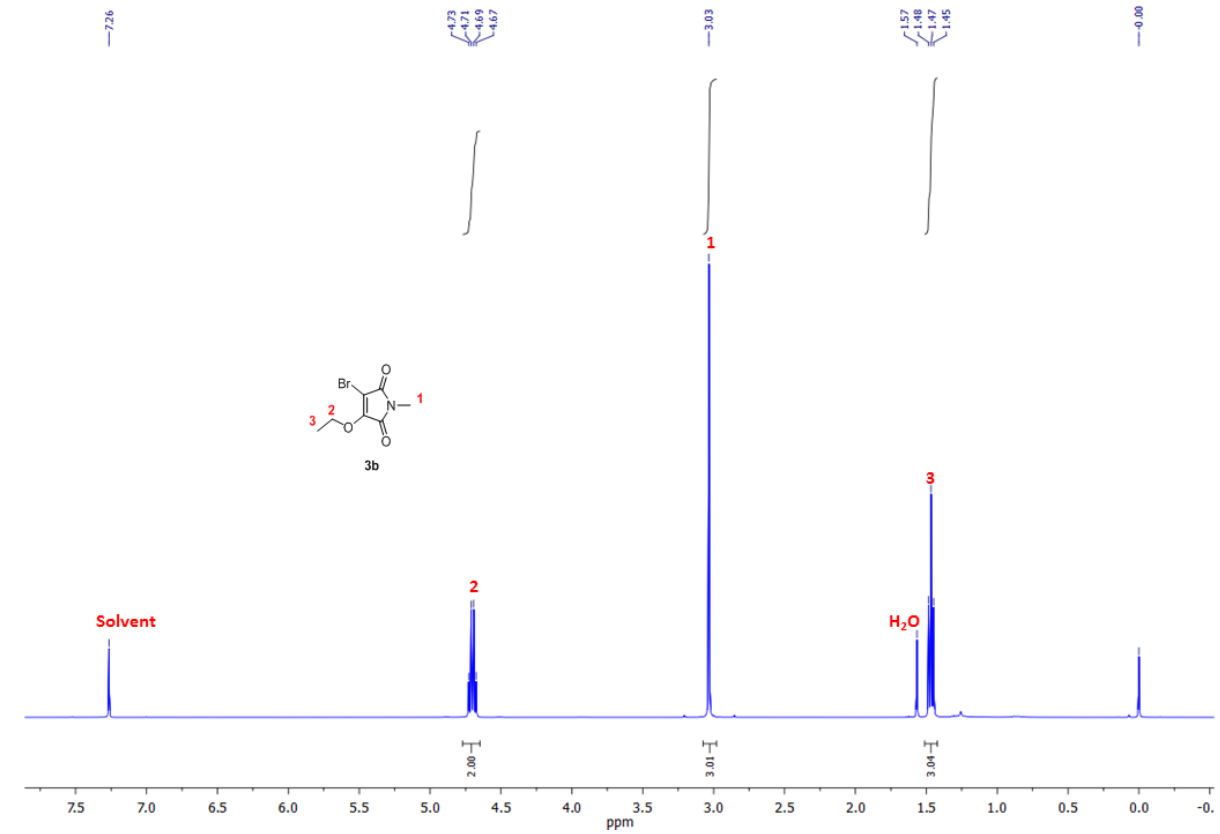

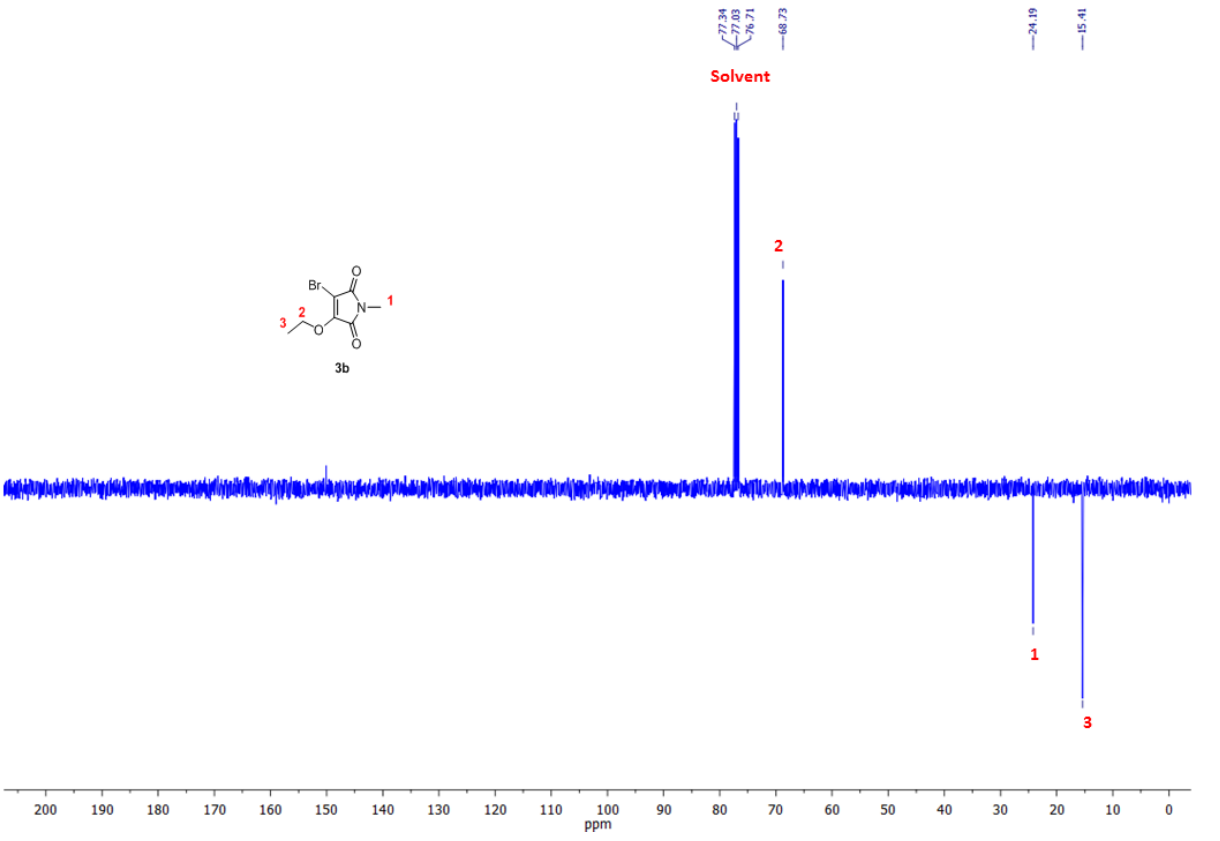

3-(benzyloxy)-4-chloro-1-methyl-1H-pyrrole-2,5-dione (3c):

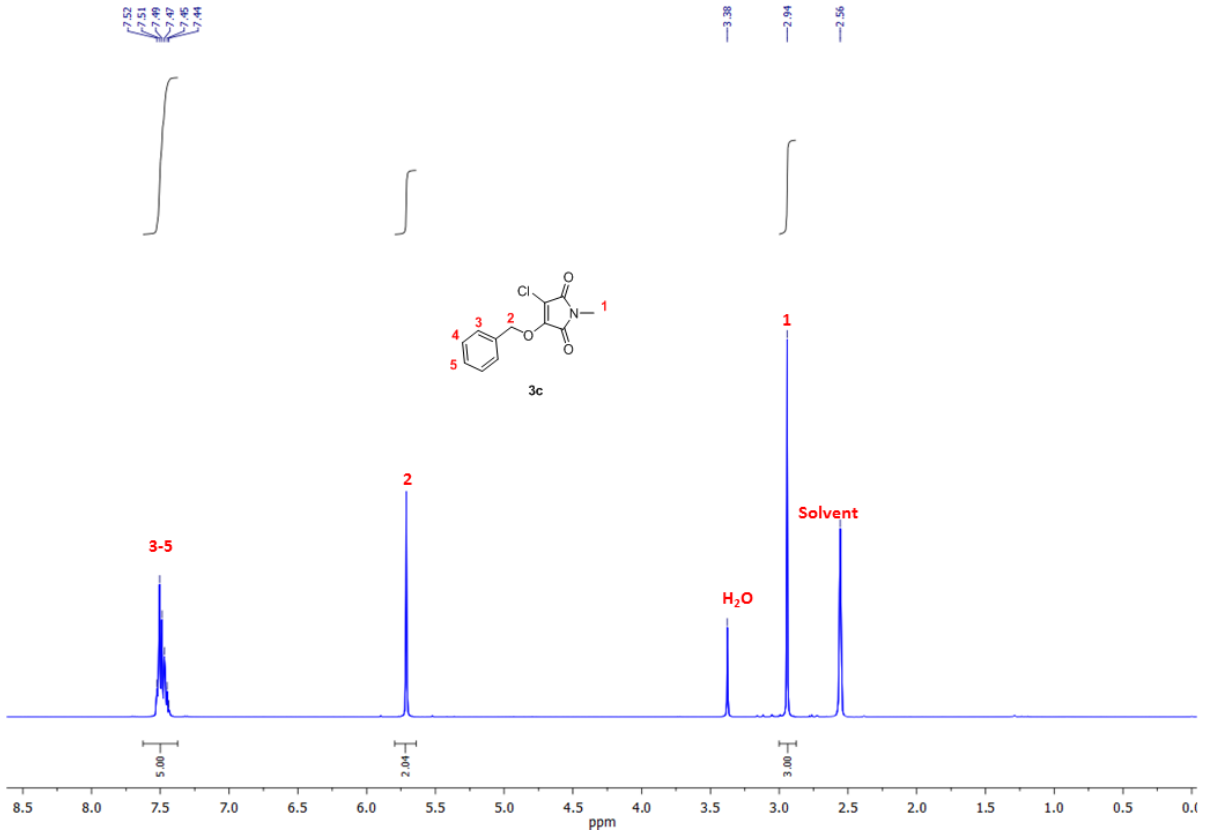

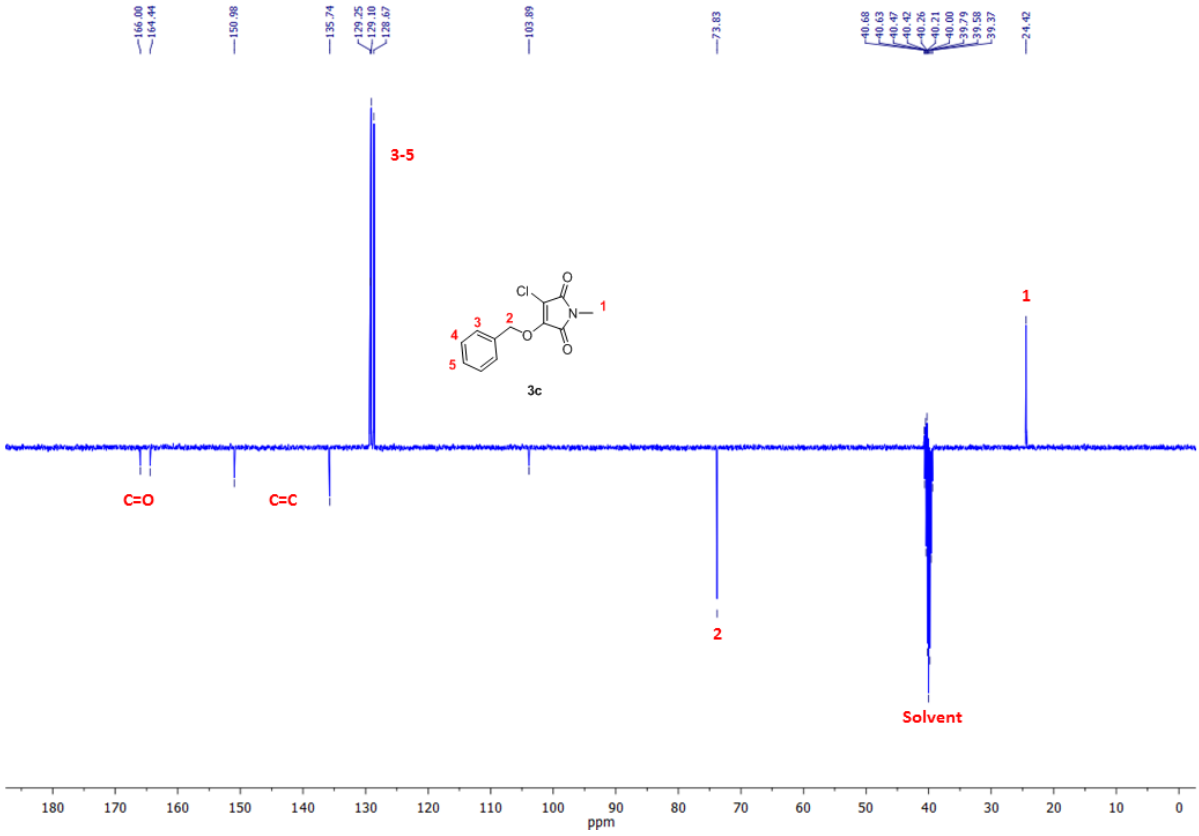

3-(benzyloxy)-4-bromo-1-methyl-1H-pyrrole-2,5-dione (3d)

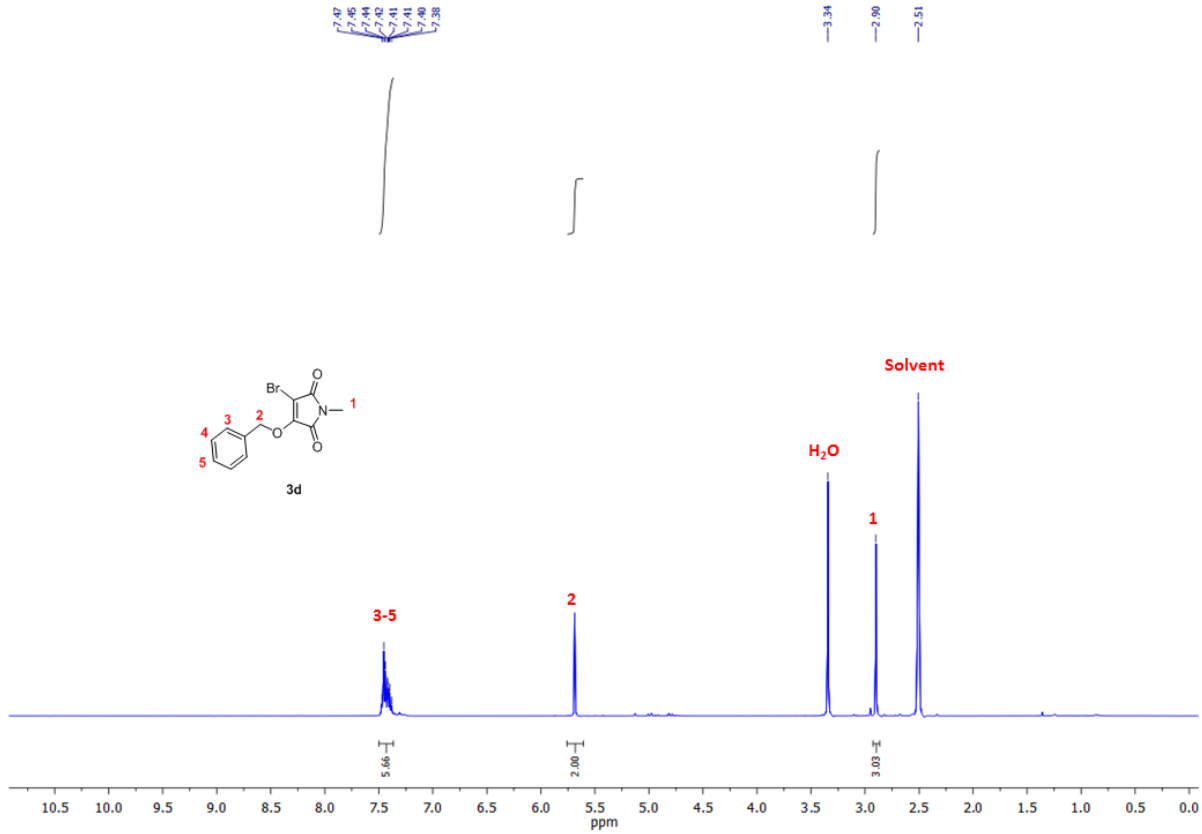

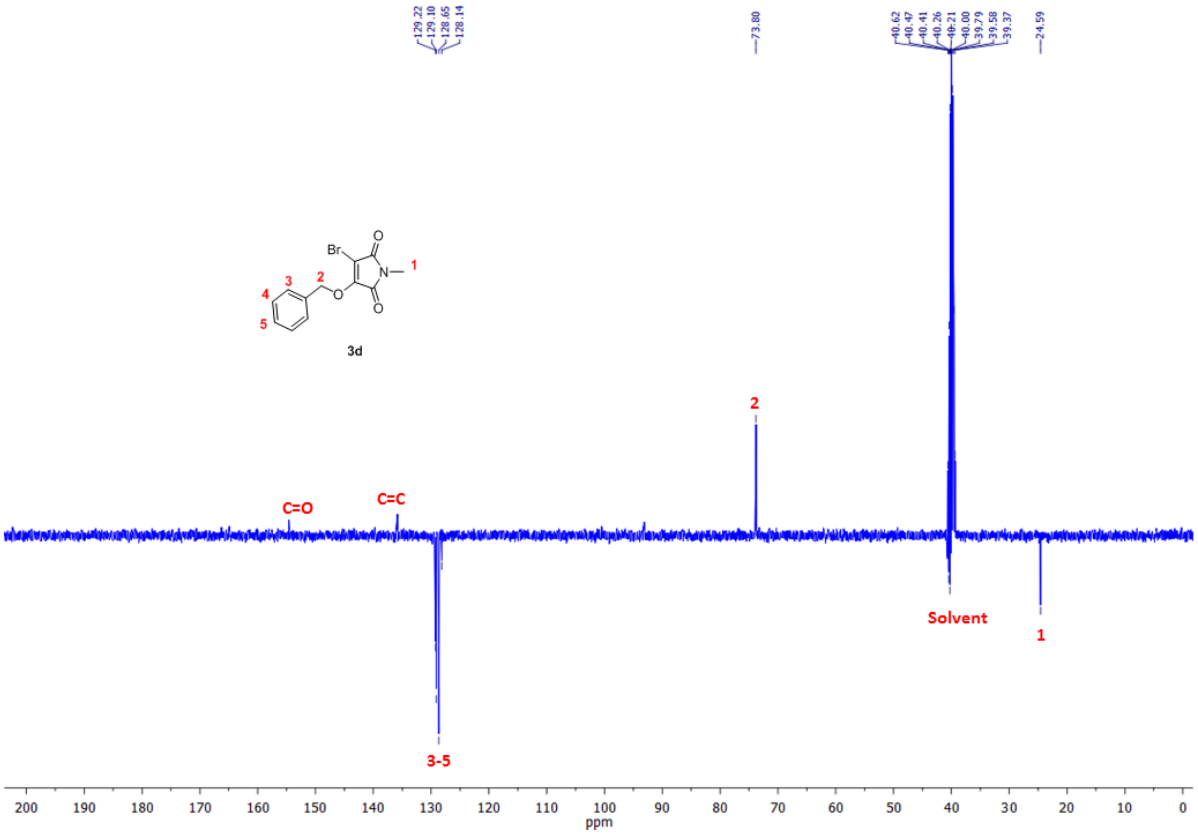

3-chloro-1-methyl-4-phenoxy-1H-pyrrole-2,5-dione (3e):

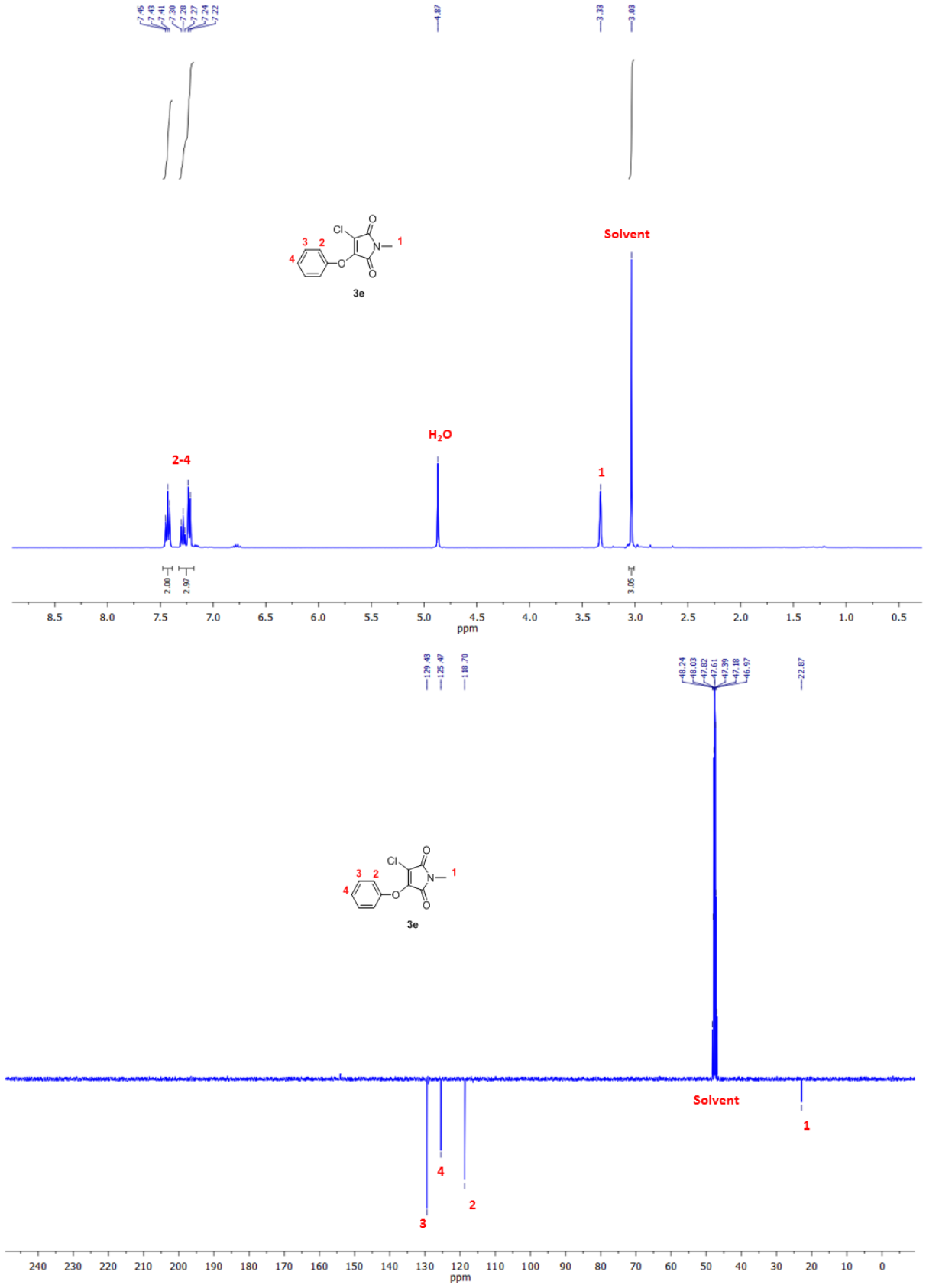

3-bromo-1-methyl-4-phenoxy-1H-pyrrole-2,5-dione (3f):

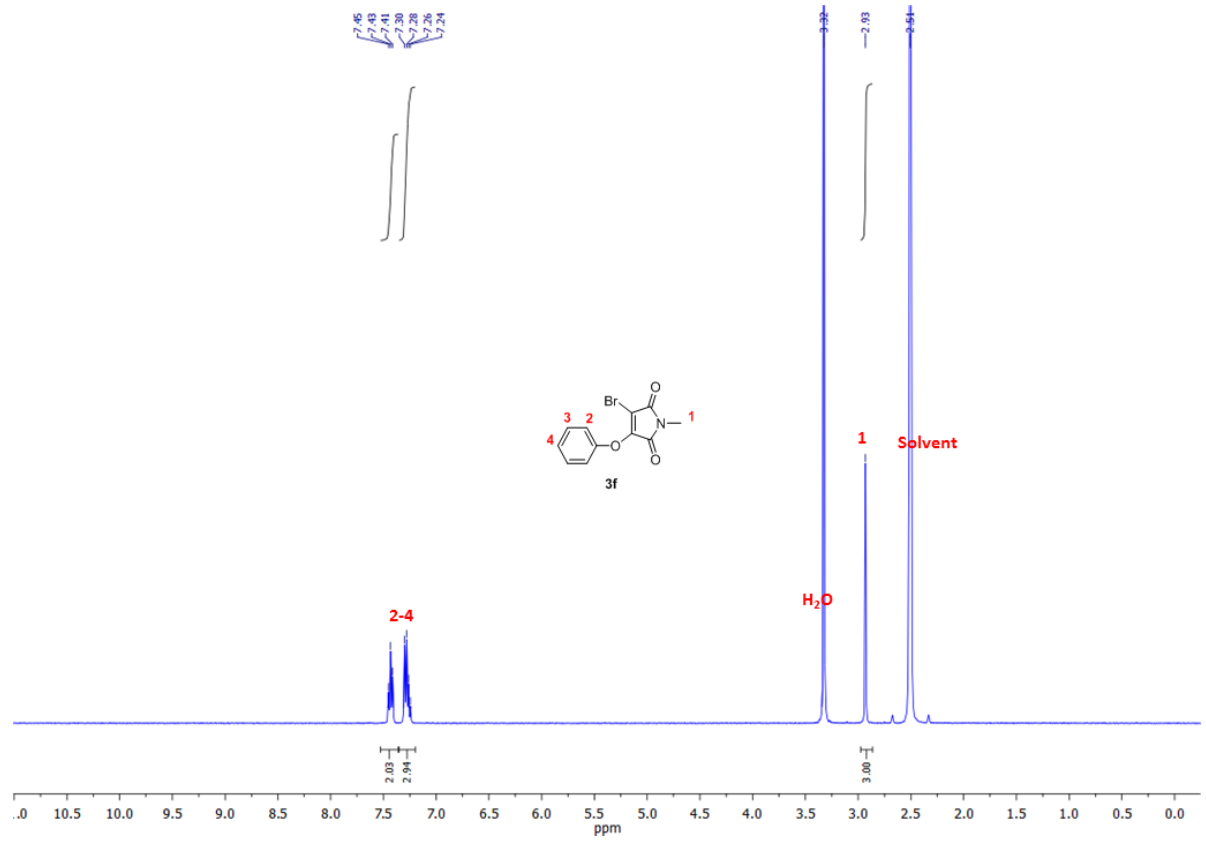

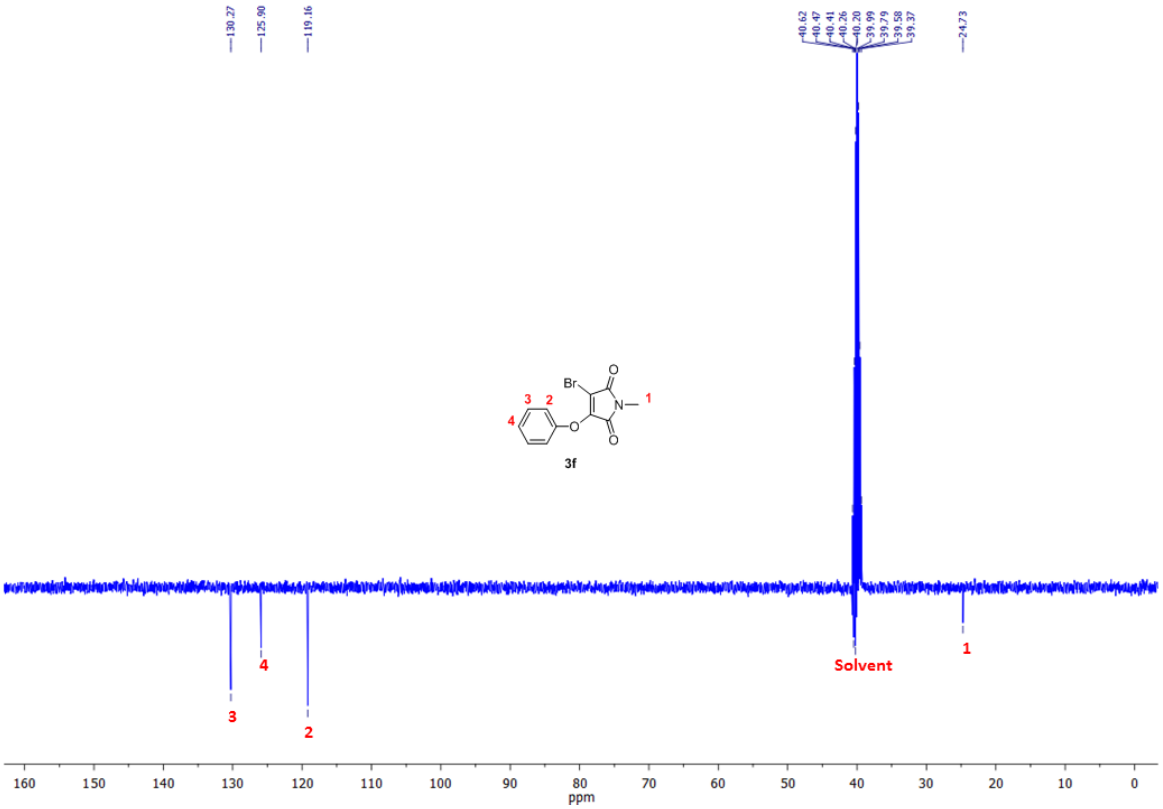

2.6 References

1. Yu, W.-T.; Wu, T.-W.; Huang, C.-L.; Chen, I. C.; Tan, K.-T., Protein sensing in living cells by molecular rotor-based fluorescence-switchable chemical probes. *Chem. Sci.* **2016,** *7* (1), 301.

2. Wu, D.; Sedgwick, A. C.; Gunnlaugsson, T.; Akkaya, E. U.; Yoon, J.; James, T. D., Fluorescent chemosensors: the past, present and future. *Chem. Soc. Rev.* **2017,** *46* (23), 7105.

3. Wieczorek, A.; Werther, P.; Euchner, J.; Wombacher, R., Green- to far-red-emitting fluorogenic tetrazine probes - synthetic access and no-wash protein imaging inside living cells. *Chem. Sci.* **2017,** *8* (2), 1506.

4. Kumar Konidena, R.; Justin Thomas, K. R.; Kumar Dubey, D.; Sahoo, S.; Jou, J. H., A new molecular design based on hybridized local and charge transfer fluorescence for highly efficient (>6%) deep-blue organic light emitting diodes. *Chem. Commun.* **2017,** *53* (86), 11802-11805.

5. Yu, J.; Rong, Y.; Kuo, C. T.; Zhou, X. H.; Chiu, D. T., Recent Advances in the Development of Highly Luminescent Semiconducting Polymer Dots and Nanoparticles for Biological Imaging and Medicine. *Anal. Chem.* **2017,** *89* (1), 42.

6. Lee, M. H.; Kim, J. S.; Sessler, J. L., Small molecule-based ratiometric fluorescence probes for cations, anions, and biomolecules. *Chem. Soc. Rev.* **2015,** *44* (13), 4185-4191.

7. Klymchenko, A. S., Solvatochromic and Fluorogenic Dyes as Environment-Sensitive Probes: Design and Biological Applications. *Acc. Chem. Res.* **2017,** *50* (2), 366.

8. Hu, J.; Liu, S., Responsive Polymers for Detection and Sensing Applications: Current Status and Future Developments. *Macromolecules* **2010,** *43* (20), 8315.

9. Kar, H.; Ghosh, S., J-aggregation of a sulfur-substituted naphthalenediimide (NDI) with remarkably bright fluorescence. *Chem. Commun.* **2016,** *52* (57), 8818.

10. Rivera-Fuentes, P.; Lippard, S. J., Metal-based optical probes for live cell imaging of

nitroxyl (HNO). *Acc. Chem. Res.* **2015,** *48* (11), 2927.

11. Fang, X.; Zheng, Y.; Duan, Y.; Liu, Y.; Zhong, W., Recent Advances in Design of Fluorescence-Based Assays for High-Throughput Screening. *Anal. Chem.* **2019,** *91* (1), 482.

12. Patra, S. K.; Sheet, S. K.; Sen, B.; Aguan, K.; Roy, D. R.; Khatua, S., Highly Sensitive Bifunctional Probe for Colorimetric Cyanide and Fluorometric H2S Detection and Bioimaging: Spontaneous Resolution, Aggregation, and Multicolor Fluorescence of Bisulfide Adduct. *J. Org. Chem.* **2017,** *82* (19), 10234.

13. Würth, C.; Grabolle, M.; Pauli, J.; Spieles, M.; Resch-Genger, U., Relative and absolute determination of fluorescence quantum yields of transparent samples. *Nat. Protoc.* **2013,** *8* (8), 1535.

14. Prasanna de Silva, A.; Nimal Gunaratne, H. Q.; Gunnlaugsson, T., Fluorescent PET(Photoinduced Electron Transfer) reagents for thiols. *Tetrahedron Lett.* **1998,** *39* (28), 5077.

15. Zhang, Y.; Huo, F.; Yin, C.; Yue, Y.; Hao, J.; Chao, J.; Liu, D., An off–on fluorescent probe based on maleimide for detecting thiols and its application for bioimaging. *Sens. Actuators. B* **2015,** *207*, 59.

16. Langmuir, M. E.; Yang, J.-R.; Moussa, A. M.; Laura, R.; LeCompte, K. A., New naphthopyranone based fluorescent thiol probes. *Tetrahedron Lett.* **1995,** *36* (23), 3989.

17. Chen, X.; Zhou, Y.; Peng, X.; Yoon, J., Fluorescent and colorimetric probes for detection of thiols. *Chem. Soc. Rev.* **2010,** *39* (6), 2120.

18. Chen, Y.; Tsao, K.; De Francesco, E.; Keillor, J. W., Ring Substituent Effects on the Thiol Addition and Hydrolysis Reactions of N-Arylmaleimides. *J. Org. Chem.* **2015,** *80* (24), 12182.

19. Tedaldi, L. M.; Smith, M. E.; Nathani, R. I.; Baker, J. R., Bromomaleimides: new reagents for the selective and reversible modification of cysteine. *Chem. Commun.* **2009,** *0* (43), 6583.

20. Marculescu, C.; Kossen, H.; Morgan, R. E.; Mayer, P.; Fletcher, S. A.; Tolner, B.; Chester, K. A.; Jones, L. H.; Baker, J. R., Aryloxymaleimides for cysteine modification, disulfide bridging and the dual functionalization of disulfide bonds. *Chem. Commun.* **2014,** *50* (54), 7139.

21. Fletcher, S. A.; Sin, P. K.; Nobles, M.; Arstad, E.; Tinker, A.; Baker, J. R., A dual optical and nuclear imaging reagent for peptide labelling via disulfide bridging. *Org. Biomol. Chem.* **2015,** *13* (37), 9559.

22. Castaneda, L.; Maruani, A.; Schumacher, F. F.; Miranda, E.; Chudasama, V.; Chester, K. A.; Baker, J. R.; Smith, M. E.; Caddick, S., Acid-cleavable thiomaleamic acid linker for homogeneous antibody-drug conjugation. *Chem. Commun.* **2013,** *49* (74), 8187.

23. Hull, E. A.; Livanos, M.; Miranda, E.; Smith, M. E.; Chester, K. A.; Baker, J. R., Homogeneous bispecifics by disulfide bridging. *Bioconjug. Chem.* **2014,** *25* (8), 1395.

24. Richards, D. A.; Fletcher, S. A.; Nobles, M.; Kossen, H.; Tedaldi, L.; Chudasama, V.; Tinker, A.; Baker, J. R., Photochemically re-bridging disulfide bonds and the discovery of a thiomaleimide mediated photodecarboxylation of C-terminal cysteines. *Org Biomol. Chem.* **2016,** *14* (2), 455.

25. Ryan, C. P.; Smith, M. E.; Schumacher, F. F.; Grohmann, D.; Papaioannou, D.; Waksman, G.; Werner, F.; Baker, J. R.; Caddick, S., Tunable reagents for multi-functional bioconjugation: reversible or permanent chemical modification of proteins and peptides by control of maleimide hydrolysis. *Chem. Commun.* **2011,** *47* (19), 5452.

26. Schumacher, F. F.; Nobles, M.; Ryan, C. P.; Smith, M. E.; Tinker, A.; Caddick, S.; Baker, J. R., In situ maleimide bridging of disulfides and a new approach to protein PEGylation. *Bioconjug. Chem.* **2011,** *22* (2), 132.

27. Wang, H.; Xu, M.; Xiong, M.; Cheng, J., Reduction-responsive dithiomaleimide-based nanomedicine with high drug loading and FRET-indicated drug release. *Chem. Commun.* **2015,**

51 (23), 4807.

28. Tang, Z.; Wilson, P.; Kempe, K.; Chen, H.; Haddleton, D. M., Reversible Regulation of Thermoresponsive Property of Dithiomaleimide-Containing Copolymers via Sequential Thiol Exchange Reactions. *ACS Macro Lett.* **2016,** *5* (6), 709.

29. Xie, Y.; Husband, J. T.; Torrent-Sucarrat, M.; Yang, H.; Liu, W.; O'Reilly, R. K., Rational design of substituted maleimide dyes with tunable fluorescence and solvafluorochromism. *Chem. Commun.* **2018,** *54* (27), 3339.

30. Mabire, A. B.; Robin, M. P.; Quan, W. D.; Willcock, H.; Stavros, V. G.; O'Reilly, R. K., Aminomaleimide fluorophores: a simple functional group with bright, solvent dependent emission. *Chem. Commun.* **2015,** *51* (47), 9733.

31. Robin, M. P.; Wilson, P.; Mabire, A. B.; Kiviaho, J. K.; Raymond, J. E.; Haddleton, D. M.; O'Reilly, R. K., Conjugation-Induced Fluorescent Labeling of Proteins and Polymers Using Dithiomaleimides. *J. Am. Chem. Soc.* **2013,** *135* (8), 2875.

32. Mabire, A. B.; Robin, M. P.; Willcock, H.; Pitto-Barry, A.; Kirby, N.; O'Reilly, R. K., Dual effect of thiol addition on fluorescent polymeric micelles: ON-to-OFF emissive switch and morphology transition. *Chem. Commun.* **2014,** *50* (78), 11492.

33. Mabire, A. B.; Robin, M. P.; Quan, W.-D.; Willcock, H.; Stavros, V. G.; O'Reilly, R. K., Aminomaleimide fluorophores: a simple functional group with bright, solvent dependent emission. *Chem. Commun.* **2015,** *51* (47), 9733-9736.

34. Grison, C. M.; Burslem, G. M.; Miles, J. A.; Pilsl, L. K. A.; Yeo, D. J.; Imani, Z.; Warriner, S. L.; Webb, M. E.; Wilson, A. J., Double quick, double click reversible peptide "stapling". *Chem. Sci.* **2017,** *8* (7), 5166.

35. Robin, M. P.; O'Reilly, R. K., Strategies for preparing fluorescently labelled polymer nanoparticles. *Polym. Int.* **2015,** *64* (2), 174.

36. Gaitzsch, J.; Chudasama, V.; Morecroft, E.; Messager, L.; Battaglia, G., Synthesis of an

Amphiphilic Miktoarm Star Terpolymer for Self-Assembly into Patchy Polymersomes. *ACS Macro. Lett.* **2016,** *5* (3), 351.

37. Yan, J.; Wang, R.; Pan, D.; Yang, R.; Xu, Y.; Wang, L.; Yang, M., Thiolactone-maleimide: a functional monomer to synthesize fluorescent aliphatic poly(amide-imide) with excellent solubility *via* in situ PEGylation. *Polym. Chem.* **2016,** *7* (40), 6241.

38. Robin, M. P.; O'Reilly, R. K., Fluorescent and chemico-fluorescent responsive polymers from dithiomaleimide and dibromomaleimide functional monomers. *Chem. Sci.* **2014,** *5* (7), 2717.

39. Robin, M. P.; Osborne, S. A. M.; Pikramenou, Z.; Raymond, J. E.; O'Reilly, R. K., Fluorescent Block Copolymer Micelles That Can Self-Report on Their Assembly and Small Molecule Encapsulation. *Macromolecules* **2016,** *49* (2), 653.

40. Robin, M. P.; Mabire, A. B.; Damborsky, J. C.; Thom, E. S.; Winzer-Serhan, U. H.; Raymond, J. E.; O'Reilly, R. K., New Functional Handle for Use as a Self-Reporting Contrast and Delivery Agent in Nanomedicine. *J. Am. Chem. Soc.* **2013,** *135* (25), 9518.

41. Mabire, A. B.; Brouard, Q.; Pitto-Barry, A.; Williams, R. J.; Willcock, H.; Kirby, N.; Chapman, E.; O'Reilly, R. K., CO2/pH-responsive particles with built-in fluorescence read-out. *Polym. Chem.* **2016,** *7* (38), 5943.

42. Robin, M. P.; Raymond, J. E.; O'Reilly, R. K., One-pot synthesis of super-bright fluorescent nanogel contrast agents containing a dithiomaleimide fluorophore. *Mater. Horiz.* **2015,** *2* (1), 54.

43. Zhu, Q.; Ye, Z.; Yang, W.; Cai, X.; Tang, B. Z., One-Pot Synthesis and Structure-Property Relationship of Aminomaleimides: Fluorescence Efficiencies in Monomers and Aggregates Easily Tuned by Switch of Aryl and Alkyl. *J. Org. Chem.* **2017,** *82* (2), 1096.

44. Imoto, H.; Nohmi, K.; Kizaki, K.; Watase, S.; Matsukawa, K.; Yamamoto, S.; Mitsuishi, M.; Naka, K., Effect of alkyl groups on emission properties of aggregation induced emission

active N-alkyl arylaminomaleimide dyes. *RSC Adv.* **2015,** *5* (114), 94344.

45. Zheng, R.; Mei, X.; Lin, Z.; Zhao, Y.; Yao, H.; Lv, W.; Ling, Q., Strong CIE activity, multi-stimuli-responsive fluorescence and data storage application of new diphenyl maleimide derivatives. *J. Mater. Chem. C* **2015,** *3* (39), 10242.

46. Imoto, H.; Kizaki, K.; Watase, S.; Matsukawa, K.; Naka, K., Color Tuning of the Aggregation-Induced Emission of Maleimide Dyes by Molecular Design and Morphology Control. *Chem. Eur. J.* **2015,** *21* (34), 12105.

47. Yeh, H.-C.; Wu, W.-C.; Chen, C.-T., The colourful fluorescence from readily-synthesised 3,4-diaryl-substituted maleimide fluorophores. *Chem. Commun.* **2003,** *0* (3), 404.

48. Lauer, M. H.; Drekener, R. L.; Correia, C. R.; Gehlen, M. H., Fluorescence from bisaryl-substituted maleimide derivatives. *Photochem. Photobiol. Sci.* **2014,** *13* (6), 859.

49. Kizaki, K.; Imoto, H.; Kato, T.; Naka, K., Facile construction of N-alkyl arylaminomaleimide derivatives as intensively emissive aggregation induced emission dyes. *Tetrahedron* **2015,** *71* (4), 643.

50. Xie, H. D.; Ho, L. A.; Truelove, M. S.; Corry, B.; Stewart, S. G., Fluorescent triphenyl substituted maleimide derivatives: synthesis, spectroscopy and quantum chemical calculations. *J. Fluoresc.* **2010,** *20* (5), 1077.

51. Dubernet, M.; Caubert, V.; Guillard, J.; Viaud-Massuard, M.-C., Synthesis of substituted bis(heteroaryl)maleimides. *Tetrahedron* **2005,** *61* (19), 4585.

52. Nirogi, R.; Dwarampudi, A.; Kambhampati, R.; Bhatta, V.; Kota, L.; Shinde, A.; Badange, R.; Jayarajan, P.; Bhyrapuneni, G.; Dubey, P. K., Rigidized 1-aryl sulfonyl tryptamines: Synthesis and pharmacological evaluation as 5-HT6 receptor ligands. *Bioorg. Med. Chem. Lett.* **2011,** *21* (15), 4577-4580.

53. Carey, F. A., Giuliano, R. M, *Organic chemistry (Ninth edition.)*. NY: McGraw-Hill: New York, 2014.

54. Mei, X.; Wang, J.; Zhou, Z.; Wu, S.; Huang, L.; Lin, Z.; Ling, Q., Diarylmaleic anhydrides: unusual organic luminescence, multi-stimuli response and photochromism. *J. Mater. Chem. C* **2017,** *5* (8), 2135.

55. Staniforth, M.; Quan, W. D.; Karsili, T. N. V.; Baker, L. A.; O'Reilly, R. K.; Stavros, V. G., First Step toward a Universal Fluorescent Probe: Unravelling the Photodynamics of an Amino-Maleimide Fluorophore. *J. Phys. Chem. A* **2017,** *121* (34), 6357.

56. Lim, C. H.; Ryan, M. D.; McCarthy, B. G.; Theriot, J. C.; Sartor, S. M.; Damrauer, N. H.; Musgrave, C. B.; Miyake, G. M., Intramolecular Charge Transfer and Ion Pairing in N,N-Diaryl Dihydrophenazine Photoredox Catalysts for Efficient Organocatalyzed Atom Transfer Radical Polymerization. *J. Am. Chem. Soc.* **2017,** *139* (1), 348.

57. Environmental Effects on Fluorescence Emission. In *Molecular Fluorescence*, p 109.

58. Booker-Milburn, K. I.; Baker, J. R.; Bruce, I., Rapid Access to Azepine-Fused Oxetanols from Alkoxy-Substituted Maleimides. *Org. Lett.* **2004,** *6* (9), 1481.

Chapter 3 Design of Novel Di-substituted Maleimides with AIE Fluorescence Effect

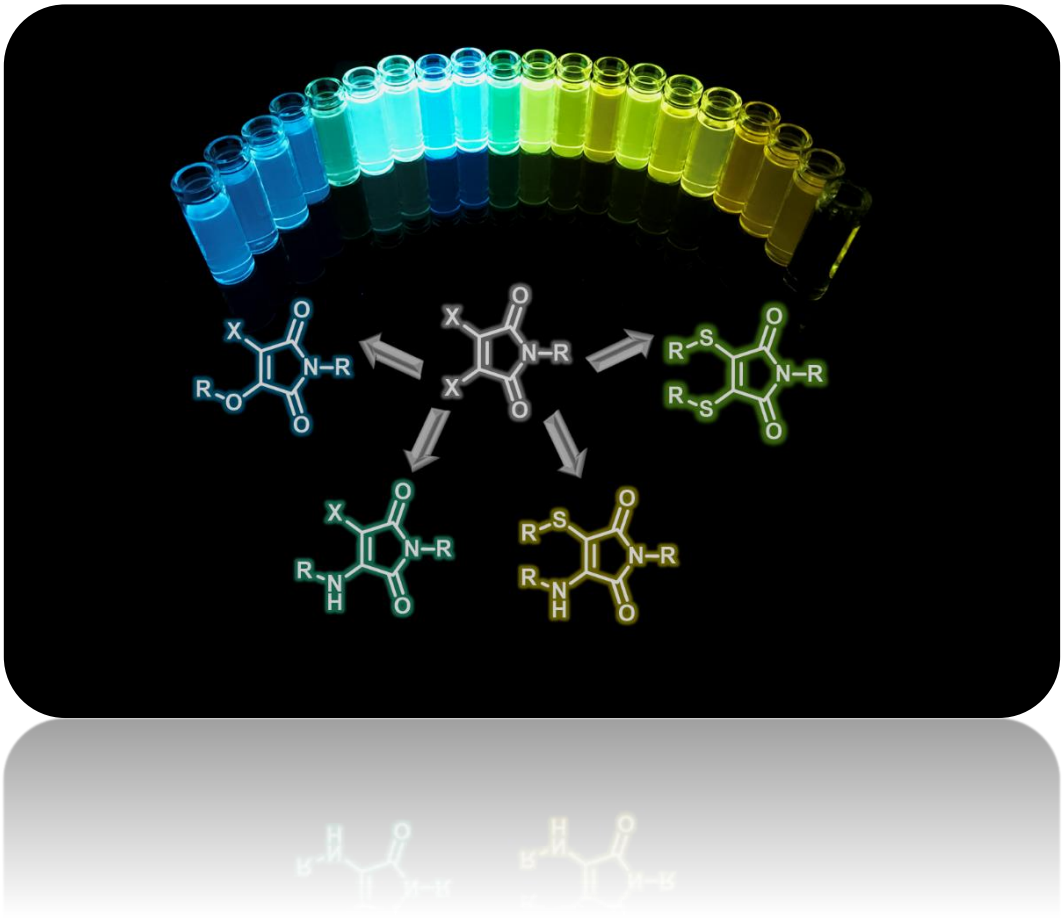

3.1 Abstract

Substituted maleimide is an intriguing class of organic fluorophore, benefiting by the strong emission, small size, and versatile chemistry. In chapter 2, we identified that the optical properties of the substituted maleimides were closely related to the substituents' structures. Therefore, it is important to explore the novel maleimide derived fluorophores through the incorporation of different functional groups, in an attempt to optimize the optical properties and expand the emission wavelength.

In this chapter, a series of unsymmetrical di-substituted maleimide bearing multiple groups were designed and synthesized, which enables a higher degree of modification. Significantly, the optical properties were investigated and compared exhibit a red-shifted emission (~50 nm) expanded from blue to yellow region. More importantly, the mechanism of the fluorescence in disubstituted maleimides was rationalized based on the DFT simulation results. The unexpected fluorescence bearing thiophenol groups were explored for the first time by the effect of aggregation state.

3.2 Introduction

3.2.1 Synthetic Strategy for Substituted Maleimides Derivatives

Maleimide derivatives, constructed by a five-member heterocyclic structure, have been long investigated as an important motif in organic synthesis and drug design fields. In recent decades, the application of maleimide derivatives have received a significant amount of attention in research areas utilising fluorescence. The unsubstituted maleimides have been firstly reported as effective fluorescence quenchers through direct conjugation to fluorophores (Figure 3.1).[1-3] The low lying n-π* transition of the maleimide ring can provide a nonradiative pathway for excited state decay and significantly reduce the emission of fluorophores. [4-6]

In 1970, Heindel *et al.* reported a facile ammonolysis method to synthesize anilinomaleimides from dimethyl acetylenedicarboxylate and aryl amines.[7] Since then, two strategies have been developed to synthesize substituted maleimide compounds: (1) one step directly forming the substituted maleimide structure from alkyne or maleic anhydrides derivatives (Figure 3.2a, b); (2) by modification of bromo/chloro maleimides (Figure 3.2c, d). These substituted maleimides are important structural motifs in several natural products and synthetic compounds, however, little focus has been given to their optical properties. In 2002, Chen's

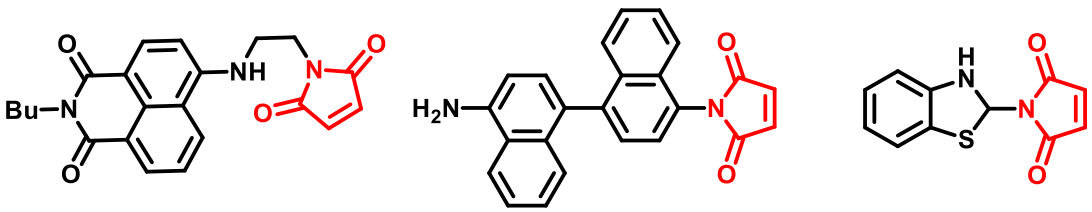

a b c

Figure 3.1 Unsubstituted maleimides structures as fluorescence quenchers for the fluorescent sensoring applications.[1, 2, 8]

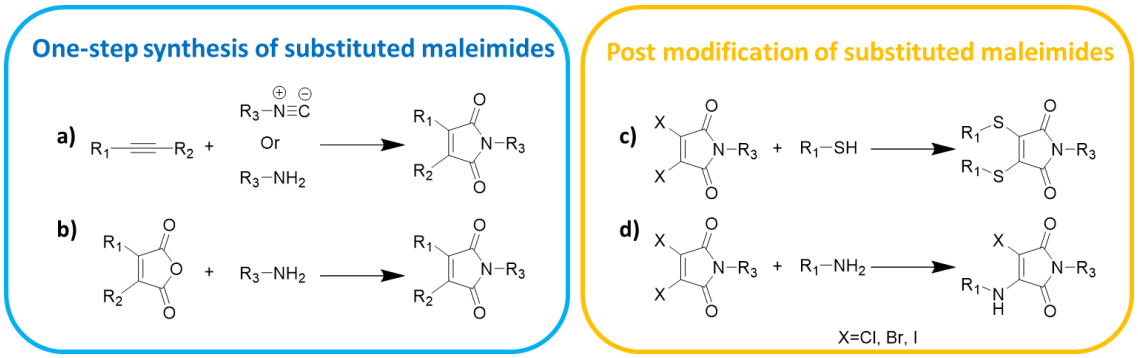

Figure 3.2 Two common strategies have been reported to synthesize substituted maleimide compounds in the literature: a-b) Strategies for the one-step synthesis of substituted maleimides.[9-11] c-d) Strategy of maleimides derivation *via* addition–elimination reactions.[12, 13]

group utilized a one-step synthesis methodology to form a series of 3,4-diaryl-substituted maleimides from easily-accessible acetonitrile derivatives.[14] Such maleimide-based structures exhibited a large variation in emission wavelength covering the entire visible region (Figure 3.3a). They altered the electron-donating or electron-withdrawing aryl substituents which determined the molecular energy level and the emission wavelength of the maleimide. Naka's group has formed several unsymmetrical maleimide structures *via* similar reactions and investigated their optical properties.[15] Interestingly, they observed red-shifted emission with aggregation-induced emission (AIE) effect in solid states of such unsymmetrical maleimide structures. Although multi-colored emission was achieved in these works, sophisticated synthetic routes and inefficient quantum yields (lower than 10%) limited their future development.

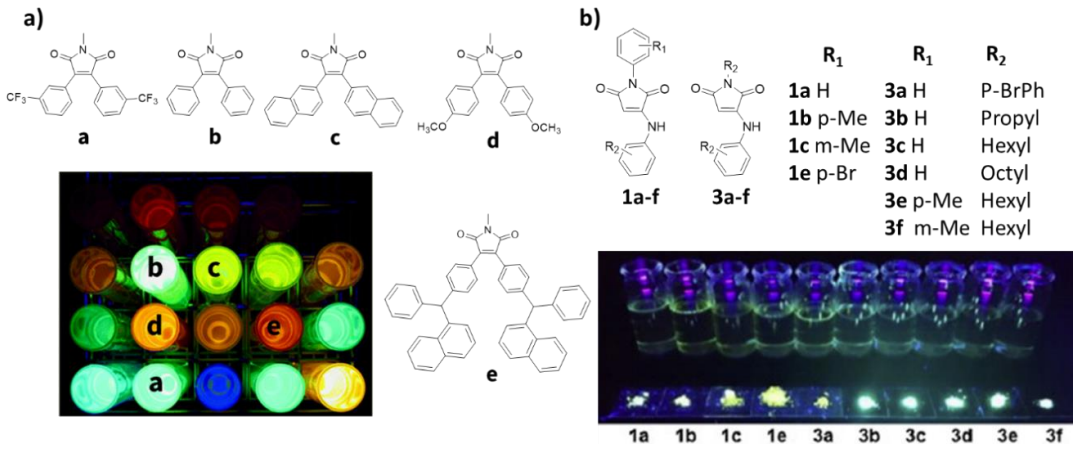

Figure 3.3 a) Reported 3,4-diaryl-substituted maleimides with different emissions wavelength;[14] b) Amino substituted maleimides with aggregation-induced emission properties in solid states.[15] Figure adapted from ref.

Further efforts have been made in an attempt to expand the maleimide fluorophores with excellent optical properties, such as a high fluorescence quantum yield and color purity, which could provide the possibility for cost-effective imaging applications. Meanwhile, the expansion of the emission towards the red or infrared region could also lead to a higher sensitivity with less background influence. Our group has determined that addition–elimination reactions of di-halogenated maleimides can be employed for the synthesis of fluorescent amino-substituted maleimides (Figure 3.2b).[12] The results demonstrated that primary amine-functionalized maleimides exhibited an intense fluorescence emission with high quantum yield (59%). Most recently, Tang *et al.* compared two synthetic methods (one or two steps synthesis) to synthesize the monoaminomaleimide and further investigated the optical properties of different mono amino-substituted maleimides.[16] They also investigated the different optical properties in monomers and the aggregate states of aminomaleimides. Red-shifted emissions were observed in aggregates state of monoaminomaleimides compared to those in monomeric forms.

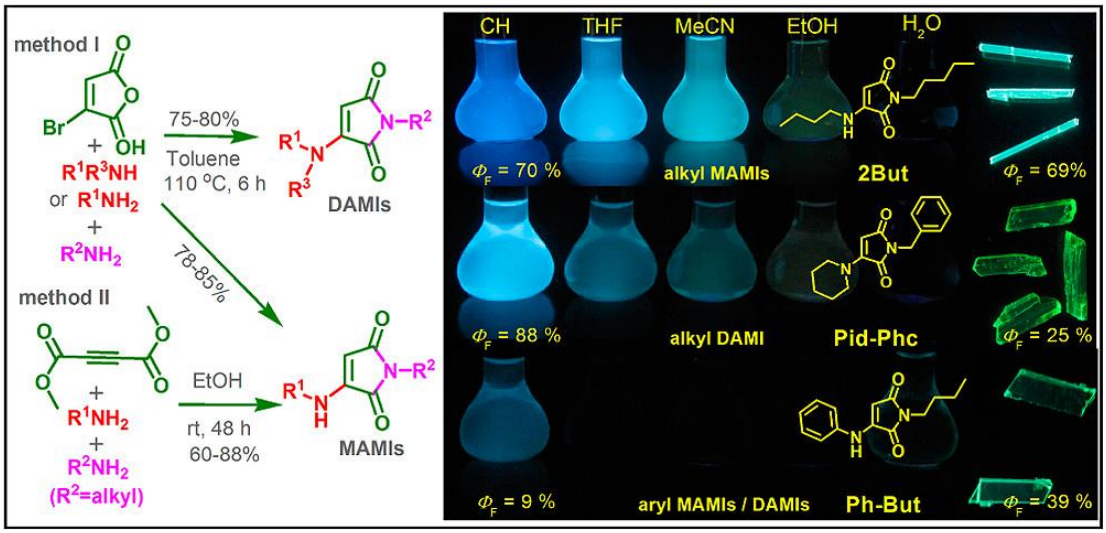

Figure 3.4 Two strategies for the synthesis of amino-substituted maleimides and the compared fluorescent properties in solution and solid states.[10] Figure adapted from ref.

3.2.2 Design of Maleimide Derivatives with Different Substitution Patterns

Owing to the versatile reactivity and facile structures, different substitution patterns were achieved by numerous reactions in the synthesis of different maleimides, including the single substitutions and double substitutions (Figure 3.5). These patterns allowed to bear the multiplex functionalizations within one molecule and hence be useful as the linker in many areas like drug design,[17, 18] material modification,[19, 20], and functionalization.[21, 22]

Single substituted maleimides, normally attaining one or two different functional groups, could be synthesized through different strategies like the addition-elimination reactions with amine or alcohol,[12] Suzuki reaction involved cross-coupling,[18, 23] and one-pot synthesis from the alkynes or anhydride.[24] Compared with single substitution pattern, the double substitution allows for higher degree of functionalization and could achieve symmetric or unsymmetrical structures. Dithiol substituted maleimides, as one of the symmetrical structures, were achieved through the one-step addition-elimination reaction

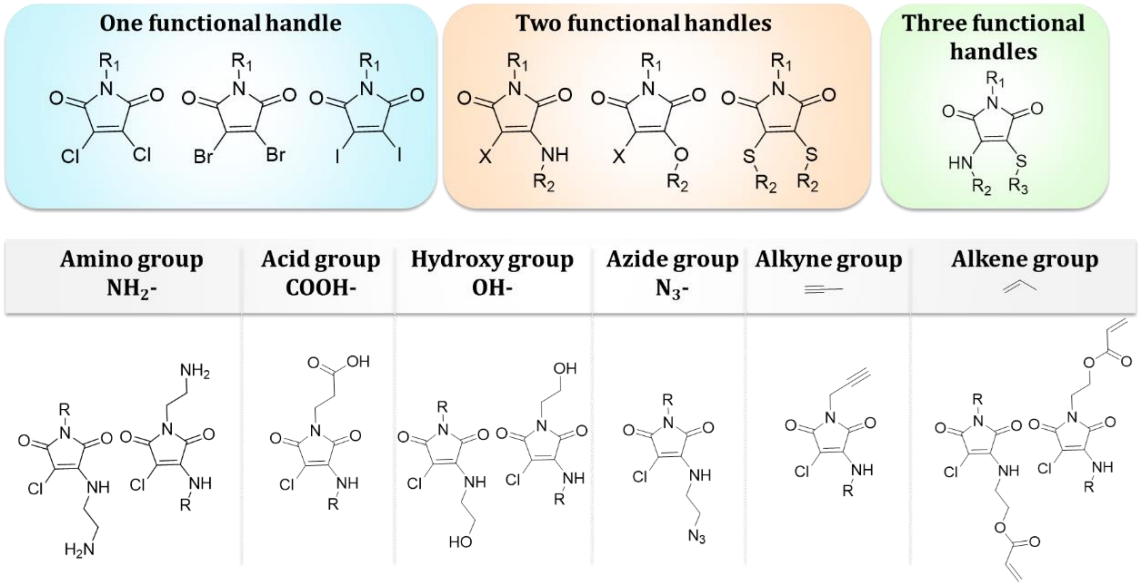

Figure 3.5 Diverse substituted maleimides structures bearing different functional groups.

of dibromo or chloro- maleimides with thiol (**1**, Figure 3.6). [25-31] Such double substitution structures have attracted much interest in protein and enzyme modifications areas as an effective crosslinker, owning to the abundant thiol or dithiol bridge in the biomolecules.[32, 33] The Awuah and Capretta groups previously managed to introduce a second amino moiety onto an aminobromomaleimides scaffold (**2**).[34, 35] Although the unsymmetrical substitution structures could be achieved, they determined that the substitution of the amino group in aminobromomaleimides precursors altered the electronic nature of the neighboring halogen due to the introduced nitrogen atom as the strong electron-donating group, which results in much harsher reaction conditions (microwave irradiation) for further addition of the second amine. Except for the addition elimination reaction, the Suzuki cross-coupling could also be applied in the synthesis of symmetrical and unsymmetrical (**3, 4**).[11, 36-44] Some other double substituted maleimides were also summarized in Figure 3.6, including the diazide substituted maleimide (**5**),[45] binol substituted maleimides (**6**)[46] phenylamino-4-phenylsulfonyl maleimides (**7**),[47] and di phosphorane maleimides (**8**).[45]

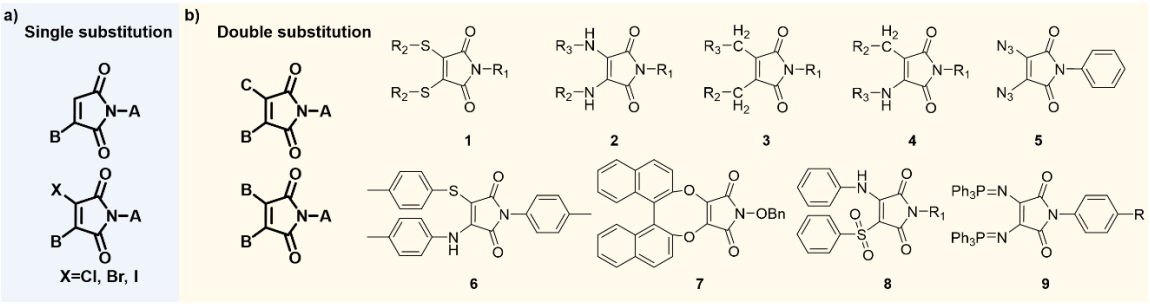

Figure 3.6 a) Single substituted maleimides patterns; b) Double substituted maleimides patterns and several reported double substituted maleimides structures.[25-31, 34, 35, 45-47]

As discussed in chapter 2, the fluorescence properties of the maleimide derivatives are closely related to the substitution groups within single substituted maleimides. To expand upon these, unsymmetrical disubstituted products that contained an amine and a thiol group were targeted in this chapter. A similar compound has been reported to date, by Naka *et. al.*, where thiophenol was able to undergo reaction with an aniline substituted maleimide (**6**). However, due to the aromatic nature of the aniline (as discussed quenching effect in chapter 2), almost no fluorescence was observed in the solution.[48]

In this chapter, we were inspired by the fast and efficient double addition elimination reaction with thiols and hence attempted to introduce a second thiol group on an aminobromaleimides and explore the involved fluorescence properties regarding the different substitution patterns.

3.3 Results and Discussion

3.3.1 Design Strategy for the Unsymmetrical Di-substituted Maleimides

In chapter 2, the design and synthesis of several single substituted maleimides were extensively investigated and the presented results highlighted an important consideration that the fluorescence properties are closely related to the substitution structures (Figure 3.7). We proposed that a more dramatic effect could be realized if we could change the substitution pattern of maleimides structures by achieving both the unsymmetrical substitution of maleimides and introducing heteroatoms. With the single substituted maleimides in hand, the further modification will be crucial in this project, not only for changing the substitution and subsequent fluorescent properties but also possible to introduce an extra functional handle and achieve the triple functionalization within one molecule.

Although amines are able to process an efficient addition–elimination reaction with di-halogenated maleimides to form the single substituted maleimides, the further reaction of amino-maleimides with a second amine is hampered, mainly due to the strong electron-donating group - amine group altered the electronic nature of the neighboring halogen through the C=C double bond, in which addition of the second amine required harsh reaction condition.[49] Naka *et. al.* reported that thiophenol was able to undergo reaction with an amino maleimide and achieved the unsymmetrical amino thiol maleimides. [48] Based on this report, in an effort to design a multi-functional maleimide with different fluorescent properties, we sought to expand the scope of the unsymmetrical amino thiol maleimides to investigate the effect on optical properties when altering the substitution patterns.

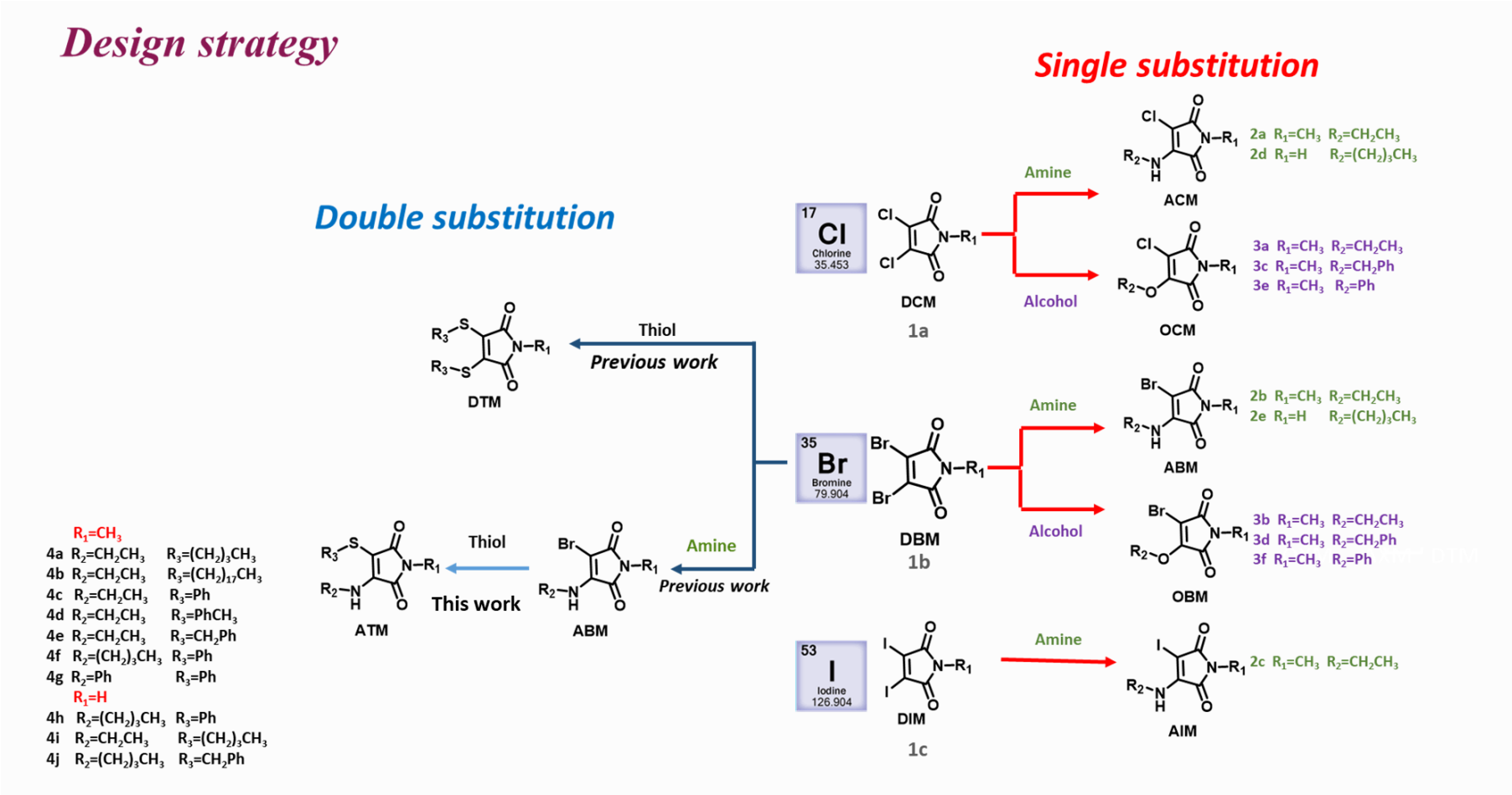

Figure 3.7 Design strategy of the different amino maleimides and amino thiol maleimides.

3.3.2 Design and Synthesis of Halogenated Aminomaleimide Derivatives

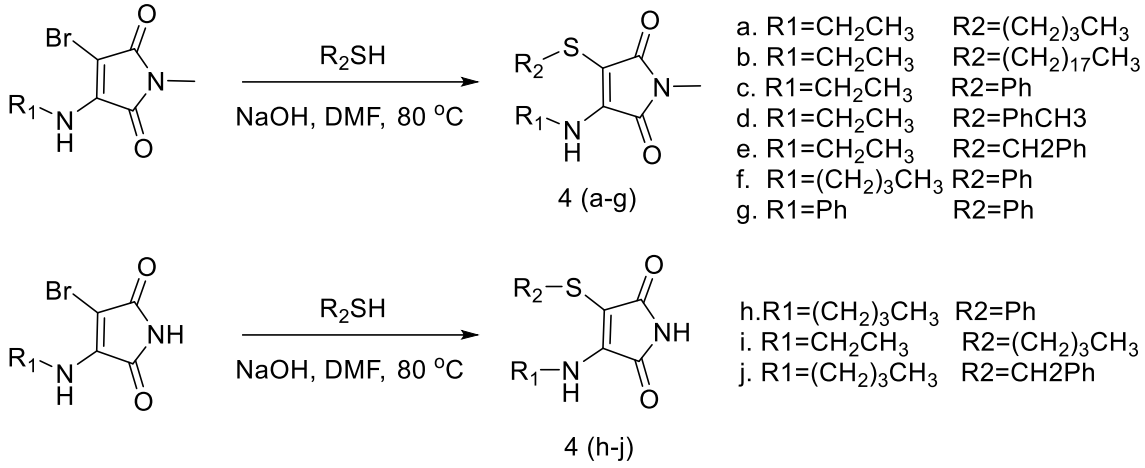

Figure 3 8 Synthetic routes for a series of different amino thiol maleimides

A library of different amino thiol maleimides was systematically synthesized by reacting to the amino-maleimides with different thiols (Figure 3.8). The amino maleimide precursors were synthesized according to the previous procedure, detailed in chapter 2. The further reactions of aminobromomaleimide with thiols were processed in DMF in the presence of NaOH as the base. Due to the decrease of the reactivity of the bromo group after the amine substitution, higher temperature (80 °C) and longer reaction time (20 h) is required. The crude product was washed with water, brine further purified by column chromatography to yield the yellow or orange products in yields 15-50%.

All acquired products were confirmed by the ^{1}H and ^{13}C NMR, HRMS and FT-IR. The detailed spectra were listed in the experimental section. After confirming the purity and structure of the compound, we then investigated the optical properties regarding the different substitution structures.

3.3.3 Fluorescence Properties of Amino thiol Maleimide Derivatives

The optical properties of the obtained amino thiol substituted maleimides (ATM) were investigated by fluorescence spectroscopy. Comparing to the related amino bromo maleimide (ABM) precursor, a clear red-shift in emission spectra was observed in ATMs after thiol modifications, showing green to yellow emission with the maximum λ_{em} ranging from 510 nm to 540 nm (Figure 3.9a, Table 3.1). In previous reports, our group found that the direct conjugation of the benzene group in the ABM structure could quench the fluorescence, due to the intramolecular electron transfer. A similar quenching phenomenon was identified in **4g** as the phenylamino substitution. Interestingly, the thiophenol substituted ABM (**4c**-**d**) did not show a similar quenching effect and on the contrary, was demonstrated a strong emission around 550 nm (Figure 3.9a). Among all synthesized ATMs, the effect of thiol structures on the emission spectra was firstly investigated in **4a**-**d**, which have identical amine substituent but different thiol groups including two alkyl thiols and two thiophenols. When comparing the emission spectra in terms of the different thiol structures (**4a**-**d**), the alkyl functionalized products (**4a**, **b**) showed emission at relatively high wavelength (*ca.* 560 nm) and covered part of

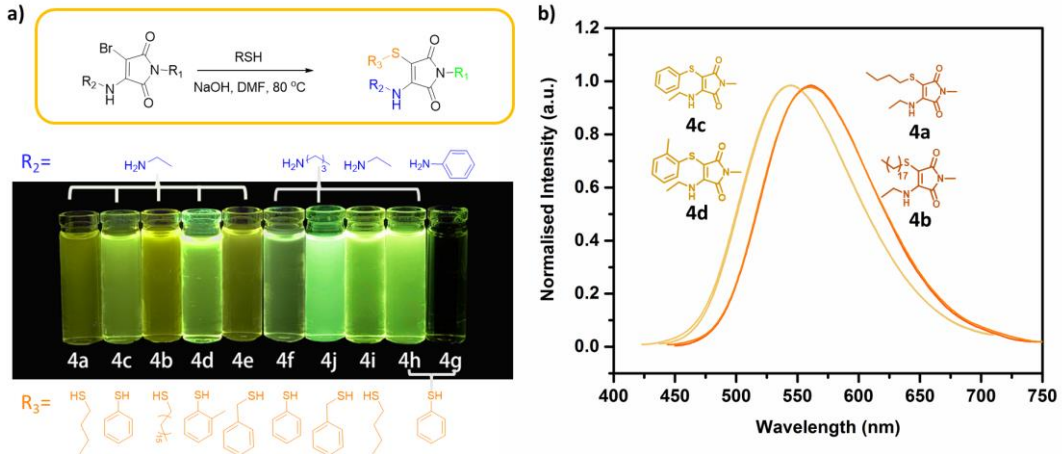

Figure 3.9 (a) Photographs of different ATMs (**4a-g**) in diethyl ether; (b) Normalized emission spectra of the studied **4a-d** in diethyl ether (10 μM λ_{ex} 385 nm; Slit: 2.5 nm, 2.5 nm)

the red wavelength region (over 600 nm) (Figure 3.9b). It was demonstrated that the different thiophenol structures (**4c**, **d**) didn't affect the emission while both showed the blue shift comparing to alkyl functionalized products (**4a**, **b**).

The absorption and 2D excitation-emission spectra of ATM (**4h**) were compared to related ABM precursor (**2e**) (Figure 3.10). The similar two peaks with higher emission wavelength were revealed in **4h**. While the similar absorptions were identified, a larger Stokes shift (*ca.* 147-165 nm, *ca.* 296-329 nm in diethyl ether) was obtained in ATM (**4h**) compared with ABM (**2e**)。

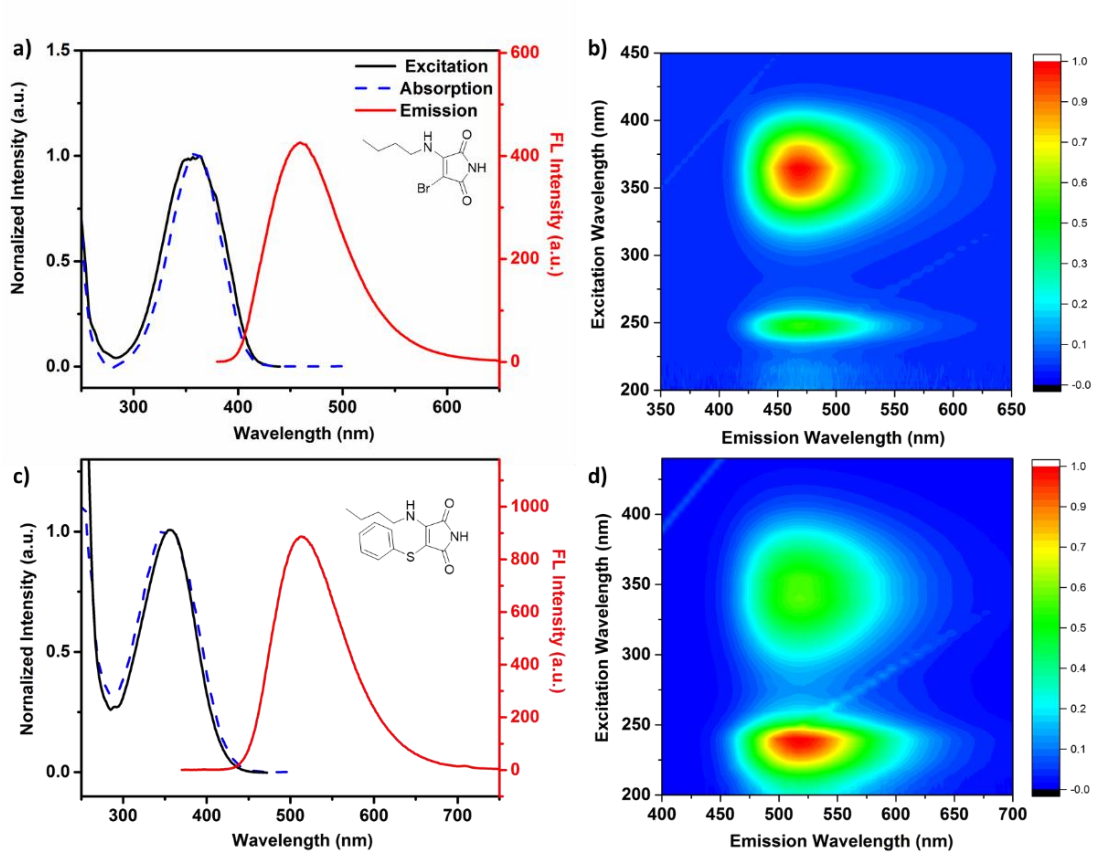

Figure 3.10 a) Excitation, emission, and absorption spectra of **2e** in diethyl ether; b) 2D excitation-emission spectra (with a 5 nm step) of **2e** in diethyl ether. c) Excitation, emission, and absorption spectra of **4h** in diethyl ether; d) 2D excitation-emission spectra (with a 5 nm step) of **4h** in diethyl ether. Peaks at $\lambda_{ex} = \lambda_{em}$ are due to Rayleigh scattering from the sample solution.

To obtain deeper insight into the solvafluorochromic properties of double substituted ATM (**4h**), the fluorescence emission was measured in eight common protic and aprotic solvents (water, methanol, DMF, dioxane, THF, diethyl ether, CH_2Cl_2, and cyclohexane), which could further provide the different microenvironment and interactions to these substituted maleimides. Compared with the blue to green emissions of its single substituted precursor ABM (**2e**), the emissions of ATM (**4h**) showed higher in wavelength (green to yellow range) (Figure 3.12). Similar to ABM**s**, fluorescence quenching effect of **ATMs** was observed in protic solvents which attributed to hydrogen bonding between the protic solvent and the carbonyl. The emission spectra in different solvents were summarized into the CIE chromaticity diagrams (CIE 1938), which clearly demonstrated the color varying in **ATM** molecules from green to yellow when increasing the polarity of the solvents (Figure 3.13). Therefore, compared with **ACM**, the further thiol modification in **ATM** also showed the color change in different solvents with expanded the emission range with higher wavelength (yellow and even red range).

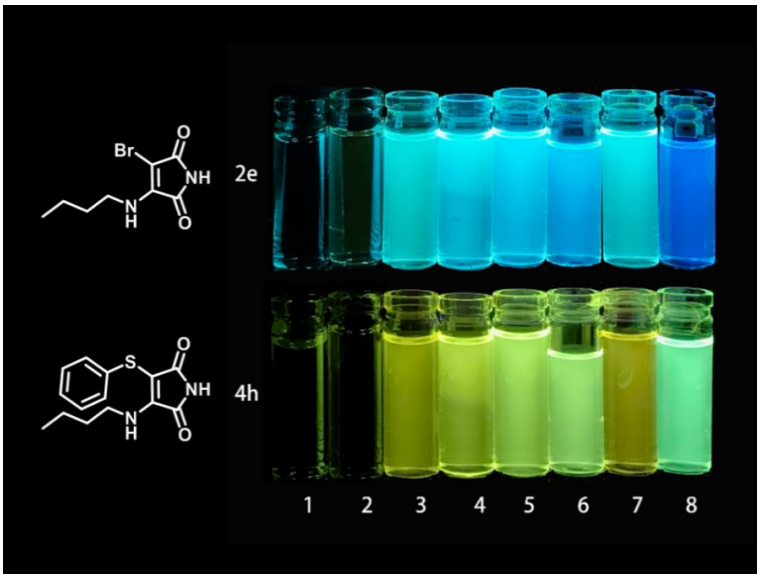

Figure 3.11 Photographs of ABM (**2e**) and ATM (**4h**) in different solvents under the 365 nm hand-held UV lamp. 1-8: water, methanol, DMF, dioxane, THF, diethyl ether, CH_2Cl_2 and cyclohexane.

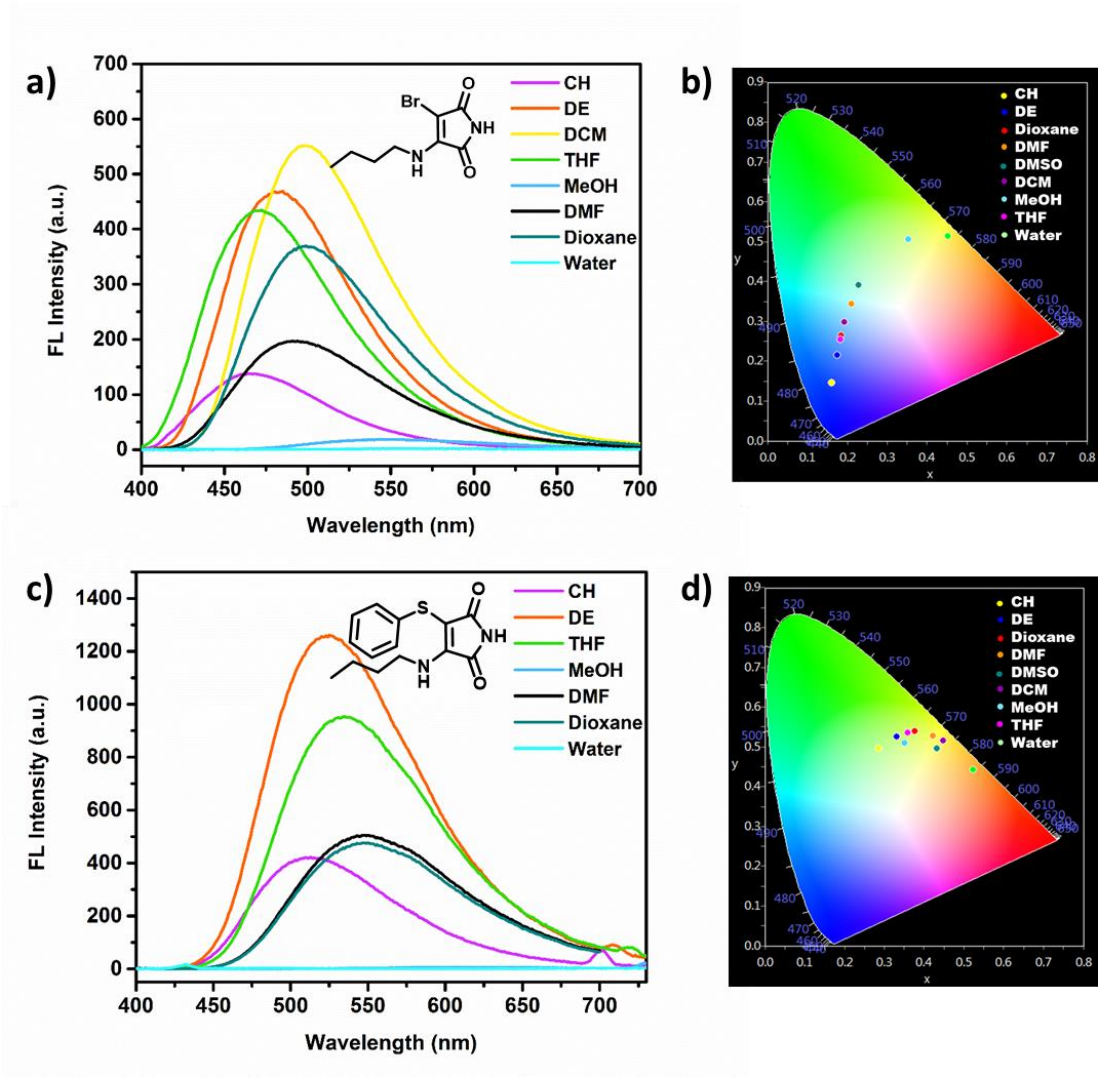

Figure 3.12 a) Emission spectra of **2e** in seven different solvents (10 μM; λ_{ex} 385 nm; Slit: 2.5 nm, 2.5 nm) b) CIE diagram of the fluorescent wavelength shift for **2e** in different solvents. a) Emission spectra of **4h** in seven different solvents (10 μM; λ_{ex} 385 nm; Slit: 2.5 nm, 2.5 nm) b) CIE diagram of the fluorescent wavelength shift for **4h** in different solvents. Solvents: H_2O, MeOH, DMF, Dioxane, THF, Et_2O (DE), and Cyclohexane (CH)

To investigate how the substituents influence the optical properties, the fluorescence quantum yields (φ_f) of **ATMs** with varying thiol substituents (**4a-e**), amine substituents (**4f-j**) and imide modification (R_1) were compared. The quantum yields were firstly studied on the effect of thiol groups in the R_3 position within the ATMs (**4a-e**) with identical amino substituent (R_2). The emission of two alkyl thiol substituted compounds (**4a** and **4b**) with relatively high emission wavelength (*ca.* 560 nm) showed poor emission intensity and Φ_f <10% (Figure 3.13, Table 3.1). Interestingly, when switching to a thiophenol group (**4c**), the emission maxima blue-shifted with an unexpected increase in quantum yield (11.7 %). To determine if the increase of quantum yield in 4c is caused by the π- π stacking of thiophenol group, the quantum yield of the *o*-toluenethiol ATM (**4d**) was compared as the methyl group in *o*-toluenethiol disturbs π- π stacking. However, these two compound (**4c**,**d**) showed a similar emission intensity and quantum yield

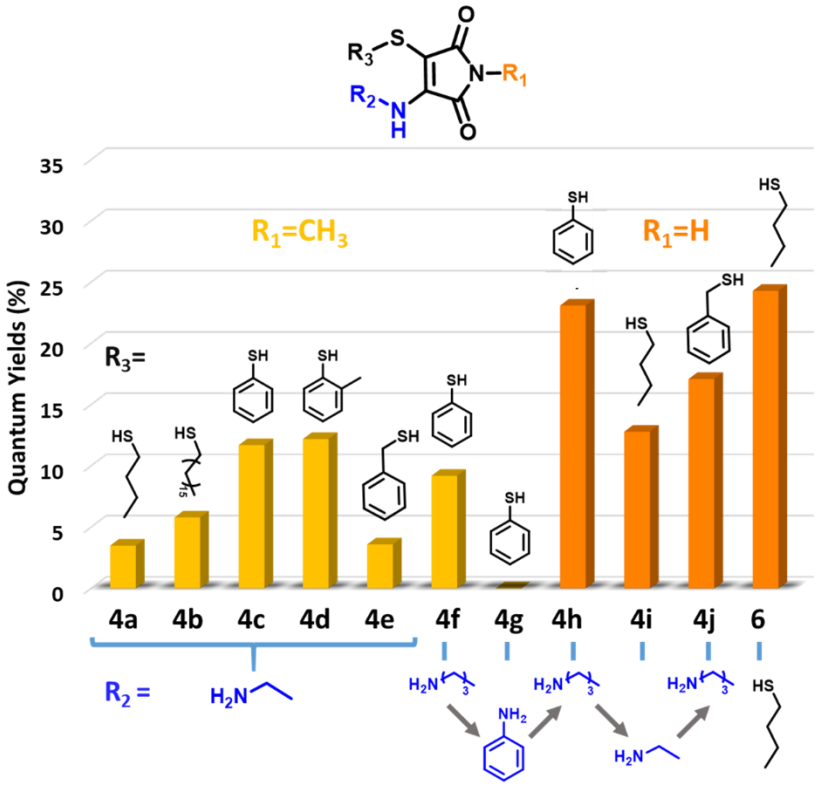

Figure 3.13 Fluorescence quantum yield of the ATM (**4a-i)** and DTM (**6)** using 59% quinine sulfate as the reference.

(Figure 3.13, Table 3.1), suggesting that the π- π stacking of benzene ring is not the main reason for the fluorescence increase. It was further proved by the lower quantum yield of **4e** which also bears the benzene motif.

Following the study on the effect of thiol groups in the R3 position, substituents on the R1 and R2 positions were also found to affect the optical properties significantly in the **ATMs**. Specifically, compounds with hydrogen at the R1 position (**4h-j**) showed increased quantum yields compared with compounds with methyl at R1 (**4a-g**). These results were consistent with previously reported aminobromomaleimides, which the hydrogen at the R1 position increase the fluorescence quantum yield.[12]

When considering the amine group in the R2 position in ATMs, the direct conjugation of an aniline group (**4g**) caused dramatic quenching of the fluorescence (Φ_f <0.1 %) while the n-butylamine group showed higher quantum yields (**4h**). These results lead to the conclusion that the fluorescence of **ATMs** still originates from the aminomaleimide moiety analogous to **ABMs**, in which the amino group on C=C double bond acts as the donor moiety in a donor-acceptor skeleton.

Table 3.1 Fluorescent properties of aminothiol maleimides in different solvents

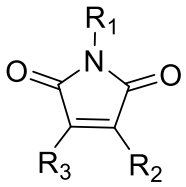

Number	R_1	R_2	R_3	Solvent	Φ_f%	ε_{max} $M^{-1}cm^{-1}$	λ_{abs} nm	λ_{ex} nm	λ_{em} nm	$\Delta\lambda$ nm
4a	CH_3	$NHCH_2CH_3$	$S(CH_2)_3CH_3$	Diethyl Ether	3.5	1917	240, 379	377	544	165
4b	CH_3	$NHCH_2CH_3$	$S(CH_2)_{16}CH_3$	Diethyl Ether	5.8	2790	232, 383	377	543	160
4c	CH_3	$NHCH_2CH_3$	SPh	Diethyl Ether	11.7	1761	230, 370	364	530	160
4d	CH_3	$NHCH_2CH_3$	$SPhCH_3$	Diethyl Ether	12.2	2595	236, 370	367	531	161
4e	CH_3	$NHCH_2CH_3$	SCH_2Ph	Diethyl Ether	3.6	2130	238, 381	378	545	164
4f	CH_3	$NH(CH_2)_3CH_3$	SPh	Diethyl Ether	9.2	3898	246, 368	359	528	160
4g	CH_3	NHPh	SPh	Diethyl Ether	<0.1	4202	230, 398	--	--	--
4h	H	$NH(CH_2)_3CH_3$	SPh	Diethyl Ether	23.1	2685	230, 355	355	512	157
				Cyclohexane	36.7	4743	241, 355	347	502	147
				Methanol	0.3	4269	241, 370	364	593	223
				Water	0.2	1617	236, 376	--	--	--
4i	H	$NHCH_2CH_3$	$S(CH_2)_3CH_3$	Diethyl Ether	12.8	4363	227, 378	369	525	147
4j	H	$NHCH_2CH_3$	SCH_2Ph	Diethyl Ether	17.1	2276	224, 370	367	522	152
5	H	$S(CH_2)_3CH_3$	S(CH2)3CH3	Diethyl Ether	24.3	6275	246, 400	403	488	88

3.3.4 Simulation of Optical Properties in Amino-thiol Maleimides*

The interesting optical properties draw our attention on the role of thiol groups regarding the ATM molecules. In order to study the possible mechanism underlying the optical properties of this series, the time-dependent density functional theory (TD-DFT)[15-23] was applied to compute the absorption and emission (fluorescence) spectra at the ground and the first singlet excited state, respectively (detailed in Experiments and Methods sections). Nice agreements between theoretical and experimental results are obtained with root-mean-square deviation values for the absorption and emission spectra, respectively (Table 3.4 in Computational Details section). The HOMO and LOMO orbitals of **4a-j** were summarized in computational section (Figure 3.17 - 3.20).

From Figure 3.14, the electron density of HOMO and LOMO in **2d** was mainly centered on the maleimide ring which originated the fluorescence of the maleimides and achieved

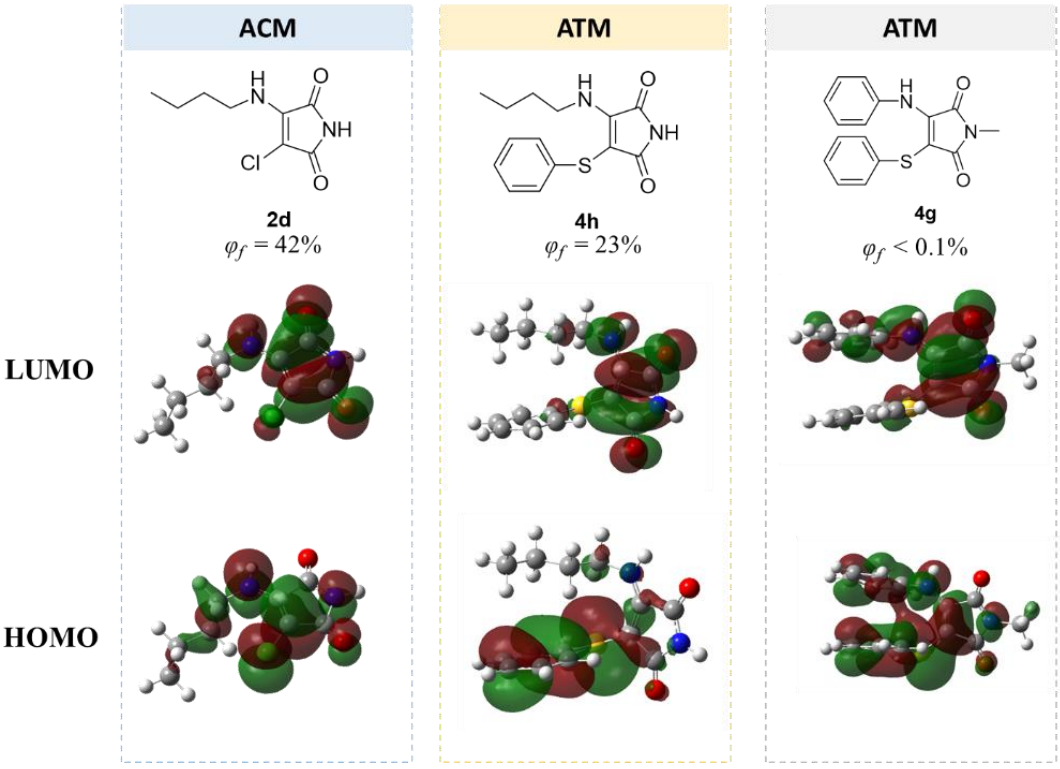

Figure 3.14 HOMO and LUMO Kohn-Sham orbitals of ACM (**2d**) and ATM (**4h, g**) with different fluorescence quantum yields. *

* The simulation results were carried out by Dr. Miquel Torrent-Sucarrat

high fluorescence quantum yields. Comparing with ACM (**2d**), the electron density in LOMO orbitals in ATM (**4h**) was similar in **2d**, without the effect of the thiophenol substitution. However, the thiophenol group distorts part of the electron density from the maleimide ring in the HOMO orbital of **4h**, which partially decreases the efficiency of the fluorescence process originating from the maleimide motif.

When directly conjugating a benzene group on the amine side in the double substituted maleimides (**4g**), a dramatic fluorescence decrease was identified. It was noted that the electron density on the maleimide ring was largely distorts by aniline group in both HOMO and LOMO orbitals, which will largely influence the electron transfer within the "donor-acceptor" skeleton. Therefore, according to the simulated HOMO and LUMO orbitals, we could have brief ideas on the effect of the substituents in double substituted maleimides.

In chapter 2, we rationalized such relation by modeling the fluorescence quantum yields with related charge difference on C=C bond in maleimides rings, resulting in a linear relationship in amino-substituted maleimides systems. Therefore, in this chapter, the charge difference in ATMs (**4a-j**) was calculated and plotted in figure 3.15. The simulation results demonstrated that all ATMs showed smaller charge difference on C=C bond compared with amino-substituted maleimides, which explained the relatively low quantum yields among ATM molecules. However, when comparing within the ATM structures, we found that the charge difference on C=C bond did not fit well with the experimental quantum yields results, suggesting that the other driving forces influenced the quantum yields. Apart from the structure effect, it has been reported that the aggregation state could also influence the optical properties of the small molecule fluorophores. Therefore, we hypothesized that the unexpected fluorescence of ATM bearing thiophenol groups may be caused by the aggregation state.

* The simulation results were carried out by Dr. Miquel Torrent-Sucarrat

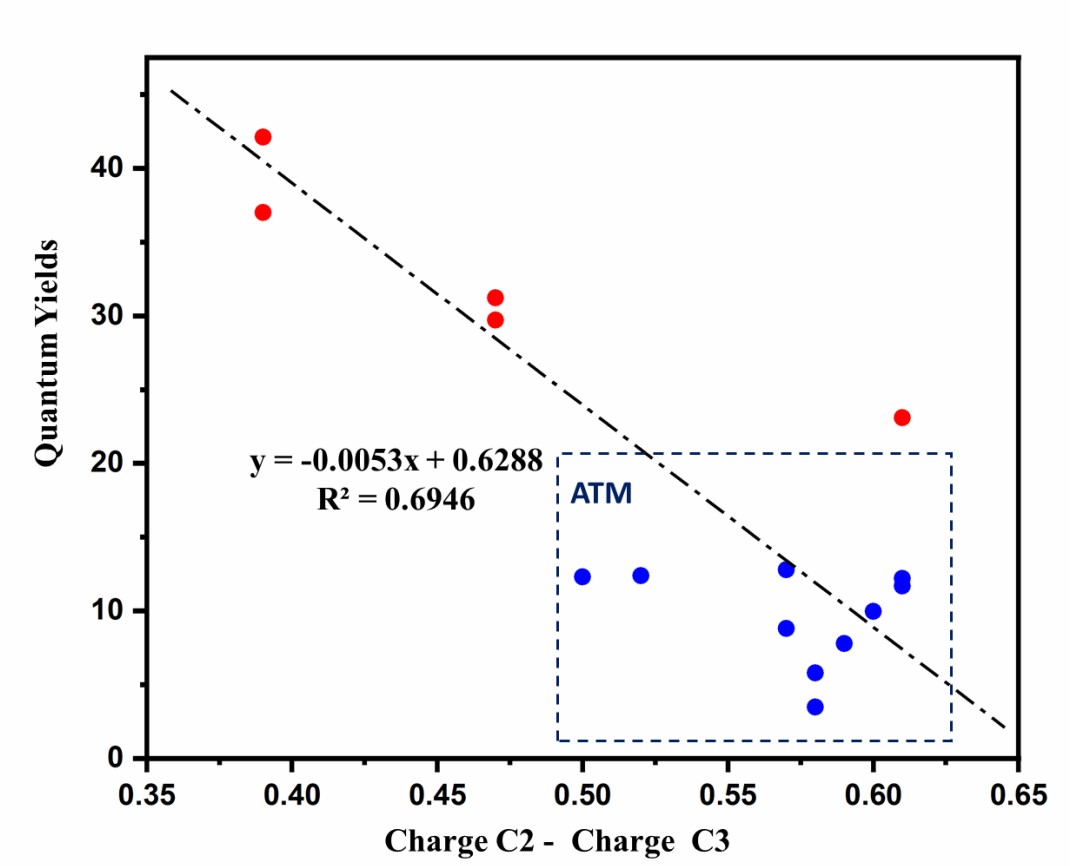

Figure 3.15 The fluorescence quantum yield is plotted as a function of charge difference on C=C bond from the simulation results (blue: single substituted maleimides, orange: amino thiol maleimides).

* The simulation results were carried out by Dr. Miquel Torrent-Sucarrat

3.3.5 Aggregation States Enhanced Fluorescence in Amino-thiol Maleimides

To prove this assumption, quantum yields and fluorescence lifetimes of the thiophenol functionalized ATM (**4h**) in the solid and solution state was evaluated, in comparison to their analogous ABM (**2e**) (Figure 3.16). The absolute quantum yields in the solid state were measured by absolute method using the integrating sphere. The **4h** processes a higher quantum yield (**4h** 8% versus **2e** 1%) and longer fluorescence lifetime (**4h** 2.97 ns versus **2e** 0.65 ns) in solid-state, as the opposite situations were observed in solution states. The unexpected increase of fluorescence quantum yield and lifetime in solid state in ATM leads to the assumption that the twisted benzene ring in thiophenol group can be retained in the solid-state and diminished aggregation caused quenching (ACQ) in the solid-state.

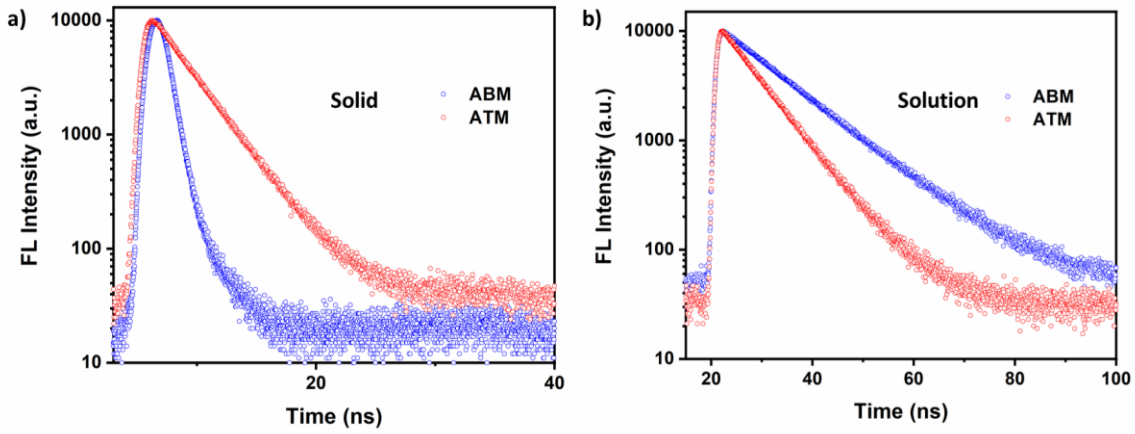

Figure 3.16 Fluorescent lifetimes of ATM (**4h**) and ABM (**2e**) in solid and solution states (10 μM in dioxane).

To study this further, the fluorescence of **4h** and **2e** were compared in a mixed solvent system of hexane (non-solvent) and dichloromethane (good solvent). By slowly increasing the ratio of the non-solvent, it is expected to subsequently prompt the small molecules aggregate in the solution. It is showed that the fluorescent intensity of **4h** gradually increased with the addition of non-solvent while aminomaleimide **2e** did not

present the same trend (Figure 3.17). These results suggest that quenching in the solid-state can be prevented by introducing an aromatic thiol adjacent to the donor group resulting in dual-state emission (DSE).[50] This trend aligns with previous reports in which maleimides with three aromatic motifs showed aggregation-induced emission (AIE).[10, 48]

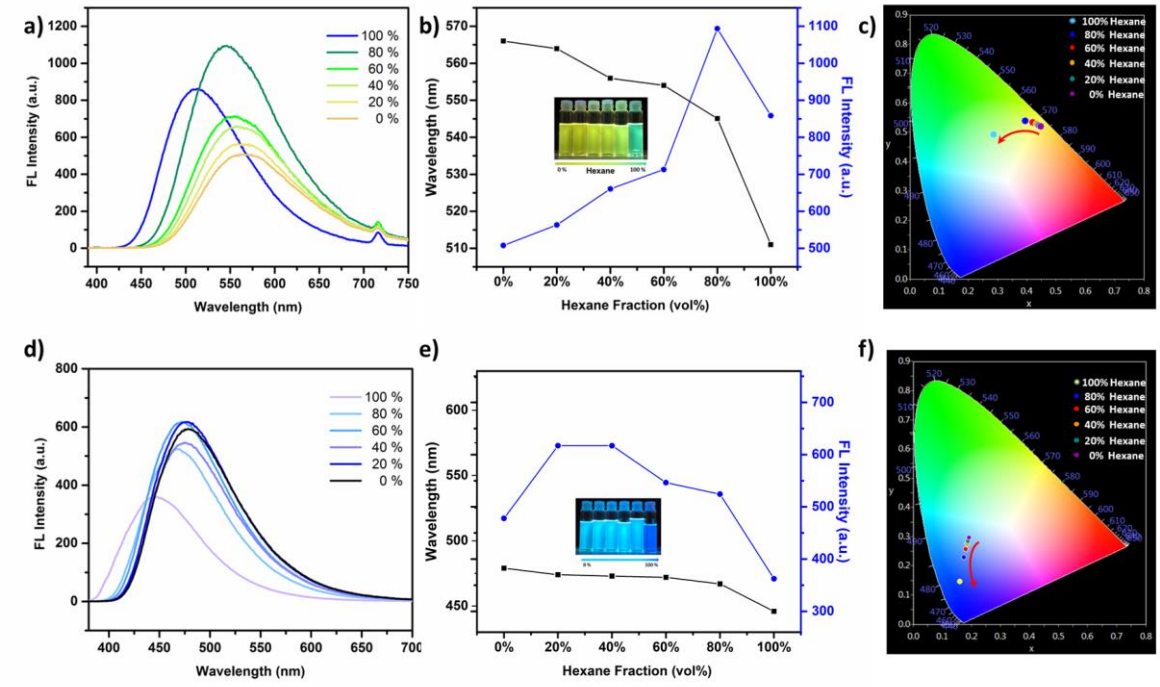

Figure 3. 17 a) Fluorescence spectra of thiophenol substituted aminomaleimide (**4h**) in different ratios of hexane/CH_2Cl_2 solution (0-100% hexane); b) Intensity and wavelength changes in different ratios of hexane/CH_2Cl_2 solutions; (insert images are **4h** under UV light in the solutions); c) CIE diagram of the fluorescent wavelength shift for **4h** upon changing the solvent quality. d) Fluorescence spectra of aminobromomaleimide (**2e**) in different ratios of hexane/CH_2Cl_2 solution (0-100% hexane); e) Intensity and wavelength changes in different ratios of hexane/CH_2Cl_2 solutions; f) CIE diagram of fluorescent wavelength shift for **2e** upon changing the solvent quality.

3.4 Summary

In conclusion, we successfully synthesized a series of novel di-substituted unsymmetrical maleimides by two-step addition elimination reactions involving different thiol and amine groups. Such reaction brings multiple functional groups into one molecule and enables a higher degree of modification for this class of dye. Significantly, we investigated the effect on optical properties *via* altering the substitution patterns, which exhibit a red-shifted emission (~50 nm) expanded from blue to yellow region. More importantly, the mechanism of the fluorescence in ATMs was rationalized based on the DFT simulation results. The unexpected fluorescence in ATM bearing thiophenol groups was explored for the first time by the effect of aggregation state.

Based on this chapter, we found that the substitution pattern of maleimide based fluorophores plays a key role in varying fluorescent properties. In this regard, the fluorescent properties of maleimide structures could be predicted and tuned for various applications.

3.5 Experimental Section

3.5.1 Materials

All chemicals and reagents were purchased from either: Sigma Aldrich, Fisher Chemicals, Acros Chemicals or Alfa Aesar and used as received. Dithiolmaleimides (**5**) was synthesized according to a previous paper.[26] Solvents were purchased from Fisher Scientific and used as received. Dry solvents were used directly from drying and degassing solvent tower delivery system.

3.5.2 Characterization Techniques

NMR Spectroscopy. ^{1}H-NMR and ^{13}C-NMR spectra were recorded NMR spectra were recorded on a Bruker Avance 300, a Bruker Avance III HD 400, or a Bruker Avance III HD 500 spectrometer at 298 K and 300, 400 and 500 MHz, respectively. Shifts are quoted in δ in parts per million and quoted relative to the internal standard trimethylsilane (TMS).

High-Resolution Mass Spectrometry. High-Resolution Mass Spectra (HR-MS) were conducted on a Bruker UHR-Q-ToF MaXis spectrometer with electrospray ionization.

Fourier-transform infrared spectroscopy. FTIR was carried out using a PerkinElmer 100 FT-IR. 16 Scans from 600 to 4000 cm^{-1} were taken at a resolution of 4 cm^{-1}, and the spectra were corrected for background absorbance.

UV-Vis spectroscopy. UV-Vis was performed on a Perkin Elmer Lambda 365 UV/vis spectrometer or an Agilent Cary 60 UV-Vis Spectrometer. Quartz cells (170 - 2000 nm) from Hellma with two polished sides were used for examining the absorption spectral data by using Thermo INSIGHT software.

Fluorescence spectroscopy. Fluorescence spectra were recorded using an Agilent Cary Eclipse Fluorescence spectrophotometer. Fluorescence lifetime and absolute fluorescence quantum yield were performed on an Edinburgh Instruments FLS920

steady-state spectrometer fitted with an integrating sphere. Solution measurement were carried out in solution using 1 cm path length quartz cuvettes with four transparent polished faces.

3.5.3 Synthetic Procedure for aminothiomaleimide synthesis

Aminobromomaleimide (2 mmol, 1 equiv.) was dissolved in DMF (30 mL) followed by the addition of NaOH (3 mmol, 1.5 equiv). The mixture was stirred for 5 minutes and then thiol (2 mmol, 1 equiv.) was added dropwise. Upon complete addition, the solution was allowed to warm to 80 °C and left to stir for 20 hours. Then the reaction mixture was concentrated in vacuo and dissolved in ethyl acetate. The organic solution washed with water, brine, and dried over anhydrous Na_2SO_4. The solution was filtered and concentrated *in vacuo*, and the crude product was purified by column chromatography (petroleum ether: ethyl acetate = 10:1-3:1) to yield the yellow product.

3-(butylthio)-4-(ethylamino)-1-methyl-1H-pyrrole-2,5-dione (4a):

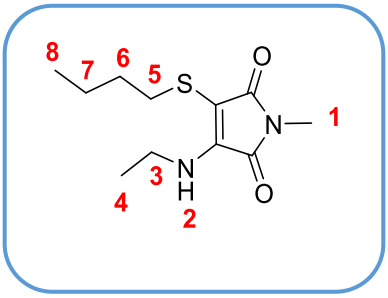

TLC conditions: R_f = 0.63 (petroleum ether: ethyl acetate= 2:1); Yield =36.8%; ^{1}H NMR (400 MHz, $CDCl_3$, ppm) δ=5.54 (1H, s, H2), 3.88 – 3.79 (2H, m, H3), 3.01 (3H, s, H1), 2.71 – 2.65 (2H, t, $^3J_{H-H}$ = 7 Hz, H5), 1.61 – 1.51 (2H, quin, $^3J_{H-H}$ = 7 Hz,H6), 1.41 (2H, sex, $^3J_{H-H}$ = 7 Hz, H7), 1.30 (3H, t, $^3J_{H-H}$ = 7 Hz, H4), 0.91 (3H, t, $^3J_{H-H}$ = 7 Hz, H8); ^{13}C NMR (101 MHz, $CDCl_3$, ppm) δ=38.4 (C3), 35.7 (C5), 31.9 (C6), 24.1 (C1), 21.8 (C7), 15.4 (C4), 13.6 (C8);

HR-MS (MaXis) *m/z* found 265.0983, calc. 265.0981 ($[M+Na]^+$, 100%);

FTIR (neat) ν_{max} / cm^{-1} 3307 (H-N of amine), 1708 and 1617 (C=O of maleimide), 1436 and 1371 (C=C of maleimide).

3-(ethylamino)-1-methyl-4-(octadecanethio)-1H-pyrrole-2,5-dione (4b):

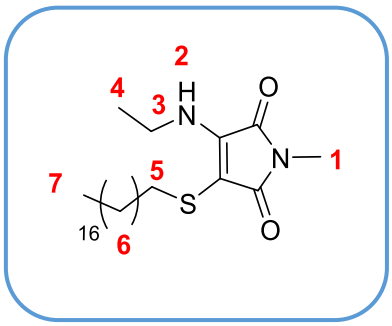

TLC conditions: R_f = 0.39 (petroleum ether: ethyl acetate= 2:1); Yield =18.2 %; ^{1}H NMR (400 MHz, $CDCl_3$, ppm) δ=5.53 (1H, s, H2), 3.82 (2H, p, $^3J_{H-H}$ = 7 Hz, H3), 3.00 (3H, s, H1), 2.69 – 2.64 (2H, m, H5), 1.32 – 1.19 (34H, m, H6+H4), 0.88 (3H, t, *J* = 7 Hz, H7); ^{13}C NMR (1 MHz, $CDCl_3$, ppm) δ=38.5 (C3), 36.2 (C5), 31.9- 29.8 (C6), 24.2 (C4), 22.9 (C6), 15.3 (C7), 14.0 (C1);

HR-MS (MaXis) *m/z* found 461.3171, calc. 461.3172 ($[M+Na]^+$, 100%);

FTIR (neat) ν_{max} / cm^{-1} 3320 (H-N of amine), 1700 and 1621 (C=O of maleimide), 1463 and 1391 (C=C of maleimide).

3-(ethylamino)-1-methyl-4-(phenylthio)-1H-pyrrole-2,5-dione (4c):

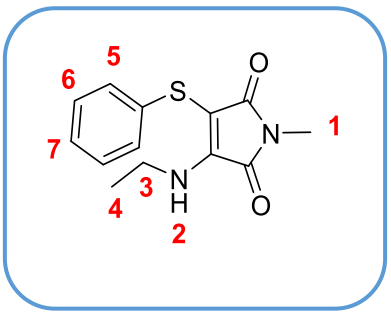

TLC conditions: R_f = 0.42 (petroleum ether: ethyl acetate= 2:1); Yield =50.9%; ^{1}H NMR (400 MHz, CD_3CN, ppm) δ= 7.30 (2H, dd, $^3J_{H-H}$ = 10, 4 Hz, H5), 7.23 (2H, dd, $^3J_{H-H}$ = 5, 3 Hz, H6), 7.19 – 7.14 (1H, m, H7), 3.70 (2H, p, $^3J_{H-H}$ = 7 Hz, H3), 2.96 (3H, s, H1), 1.16 (t, $^3J_{H-H}$ = 3H, 7 Hz, H4). ^{13}C NMR (101 MHz, CD_3CN, ppm) δ=129.6 (C5), 126.0 (C6), 125.8 (C7), 38.3 (C3), 24.1 (C1), 15.4 (C4).

HR-MS (MaXis) *m/z* found 285.0667, calc. 285.0668 ($[M+Na]^{+,}$ 100%);

FTIR (neat) ν_{max} / cm^{-1} 3313 (H-N of amine), 1696 and 1614 (C=O of maleimide), 1437 and 1390 (C=C of maleimide), 792 and 683 (C-H of aromatic).

3-(ethylamino)-1-methyl-4-(o-tolylthio)-1H-pyrrole-2,5-dione (4d):

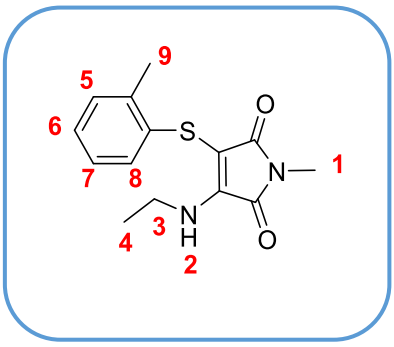

TLC conditions: R_f = 0.47 (petroleum ether: ethyl acetate= 2:1); Yield =55.6%; ^{1}H NMR (400 MHz, CD_3CN, ppm) δ=7.17 (1H, t, $^3J_{H-H}$ = 8 Hz,H5), 7.12 (1H , d, $^3J_{H-H}$ = 7.5 Hz, H6), 7.06 (2H, t, $^3J_{H-H}$ = 6 Hz,H7,H8), 3.65 (2H, p, $^3J_{H-H}$ = 7 Hz, H3), 2.97 (3H, s,H1), 2.38 (3H, s, H9), 1.13 (1H, t, $^3J_{H-H}$ = 7 Hz,H4);^{13}C NMR (101 MHz, CD_3CN, ppm) δ =130.6 (C5), 127.1 (C7), 125.4 (C6), 125.2 (C8), 38.3 (C3), 24.1 (C1), 19.3 (C9), 15.4 (C4);

HR-MS (MaXis) *m/z* found 299.0827, calc. 299.0825 ($[M+Na]^{+,}$100%);

FTIR (neat) ν_{max} / cm^{-1} 3327 (H-N of amine), 1703 and 1602 (C=O of maleimide), 1436 and 1383 (C=C of maleimide), 797 and 744 (C-H of aromatic).

3-(benzylthio)-4-(ethylamino)-1-methyl-1H-pyrrole-2,5-dione (4e):

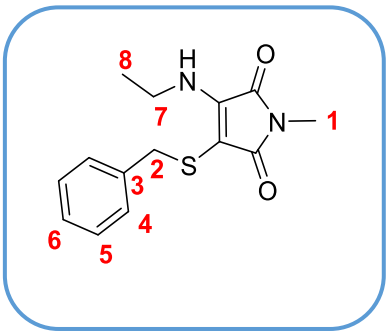

TLC conditions: R_f = 0.39 (petroleum ether: ethyl acetate= 2:1); Yield =11.9%; ^{1}H NMR (400 MHz, DMSO) δ 7.23 (5H, ddd, J = 26, 16, 7 Hz, H 4-6), 3.78 (2H, s, H3), 3.27 (2H, dd, J = 13, 6 Hz, H7), 2.88 (3H, s, H1), 0.90 (3H, t, J = 7 Hz, H8); ^{13}C NMR (101 MHz, DMSO, ppm) δ 129.2 (C4), 128.7, 127.3 (C5, C6), 37.8 (C7), 24.1 (C1), 15.0 (C8);

HR-MS (MaXis) *m/z* found 299.0825, calc. 299.0825 ([M+Na]$^{+,}$ 100%);

FTIR (neat) ν_{max} / cm^{-1} 3306 (H-N of amine), 1707 and 1604 (C=O of maleimide), 1345 (C=C of maleimide, 757 and 641 (C-H of aromatic).

3-(butylamino)-1-methyl-4-(phenylthio)-1H-pyrrole-2,5-dione (4f):

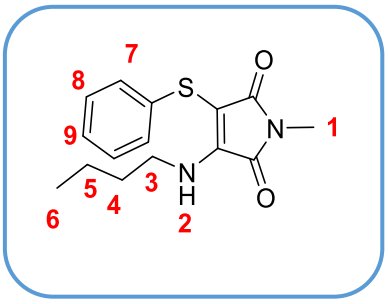

TLC conditions: R_f = 0.23 (petroleum ether: ethyl acetate= 2:1). Yield =42.3%. ^{1}H NMR (400 MHz, DMSO, ppm) δ=7.28 (2H, t, *J* = 7 Hz, H7), 7.13 (3H, dd, *J* = 14, 7 Hz, H8-9), 3.52 (2H, d, *J* = 6 Hz, H3), 2.91 (3H, s, H1), 1.52 – 1.33 (2H, m, H4), 1.17 (2H, dd, *J* = 14, 7 Hz, H5), 0.71 (3H, t, *J* = 7 Hz, H6); ^{13}C NMR (101 MHz, DMSO) δ 129.5 (C7), 125.4 (C8), 125.3 (C9), 42.6 (C3), 32.2 (C4), 24.5 (C1), 19.6 (C5), 13.9 (C6);

HR-MS (MaXis) *m/z* found 289.1015, calc. 289.1016 ([M+Na]$^{+,}$ 100%);

FTIR (neat) ν_{max} / cm^{-1} 3332 (H-N of amine), 1681 and 1604 (C=O of maleimide), 1436 and 1384 (C=C of maleimide), 740 and 688 (C-H of aromatic).

1-methyl-3-(phenylamino)-4-(phenylthio)-1H-pyrrole-2,5-dione (4g):

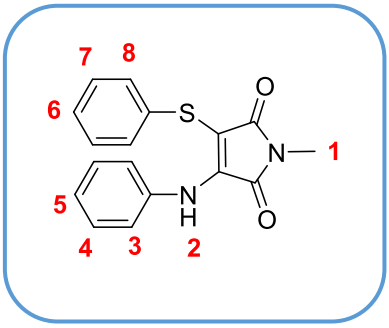

TLC conditionss: R_f = 0.44 (petroleum ether: ethyl acetate= 2:1); Yield =44.2%; ^{1}H NMR (400 MHz, DMSO, ppm) δ= 10.10 (1H, s, H2), 7.18 – 6.99 (8H, m, H4-8), 6.91 (H2, d, J = 7 Hz, H3), 2.97 (3H, s, H1); ^{13}C NMR (101 MHz, DMSO, ppm) δ 129.1 (C5), 128.0 (C8), 126.3 (C4), 125.8 (C7), 125.5 (C5), 124.8 (C6), 24.6 (C1); HR-MS (MaXis) *m/z* found 333.0678, calc. 333.0668 ([M+Na] $^{+,}$ 100%);

FTIR (neat) ν_{max} / cm^{-1} 3281 (H-N of amine), 1694 and 1604 (C=O of maleimide), 1449 (C=C of maleimide), 740 and 688 (C-H of aromatic).

3-(butylamino)-4-(phenylthio)-1H-pyrrole-2,5-dione (4h):

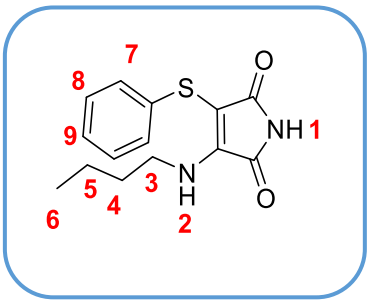

TLC conditions: R_f = 0.23 (petroleum ether: ethyl acetate= 2:1); Yield = 50.1%; ^{1}H NMR (400 MHz, DMSO, ppm) δ=10.75 (1H, s, H1), 8.32 (1H, s, H2), 7.29 (2H, t, $^{3}J_{H-H}$ = 7 Hz, H7), 7.18 – 7.06 (3H, m, H8, H9), 3.51 (2H, d, $^{3}J_{H-H}$ = 7 Hz, H3), 1.49 – 1.33 (2H, m, H4), 1.22 – 1.08 (2H, m, H5), 0.72 (3H, t, $^{3}J_{H-H}$ = 7 Hz, H6); ^{13}C NMR (101 MHz, DMSO, ppm) δ 129.5 (C7), 125.3 (C8, C9), 42.4 (C3), 32.2 (C4), 19.6 (C5), 13.9 (C6);

HR-MS (MaXis) *m/z* found 299.0872, calc. 299.0825 ([M+Na] $^{+,}$ 100%);

FTIR (neat) ν_{max} / cm^{-1} 3216 (H-N of amine), 1720 and 1617 (C=O of maleimide), 1345 (C=C of maleimide), 740 and 688 (C-H of aromatic).

3-(butylthio)-4-(ethylamino)-1H-pyrrole-2,5-dione (4i):

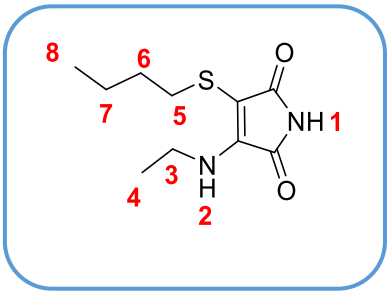

TLC conditions: R_f = 0.39 (petroleum ether: ethyl acetate= 2:1); Yield =18.9%; ^{1}H NMR (400 MHz, $CDCl_3$, ppm) δ=7.2 (1H, s, H1), 5.5 (1H, s, H2), 3.8 (2H, p, $^3J_{H-H}$ = 7 Hz, H3), 2.7 – 2.5 (2H, m, H5), 1.6 – 1.5 (2H, m, H6), 1.4 – 1.3 (2H, m, H7), 1.2 (3H, $^3J_{H-H}$ = 7 Hz, H4), 0.8 (3H, $^3J_{H-H}$ = 7 Hz, H8). ^{13}C NMR (101 MHz, $CDCl_3$, ppm) δ 171.1, 166.3 (C=O), 38.4 (C3), 35.6 (C5), 31.9 (C6), 21.9 (C7), 15.4(C4), 13.6 (C8);

HR-MS (MaXis) *m/z* found 229.1007, calc. 229.1005 ($[M+H]^{+,}$ 100%)

FTIR (neat) ν_{max} / cm^{-1} 3319 (H-N of amine), 3164 (H-N of maleimide), 1707 and 1617 (C=O of maleimide), 1359 (C=C of maleimide).

3-(benzylamino)-4-(butylthio)-1H-pyrrole-2,5-dione (4j):

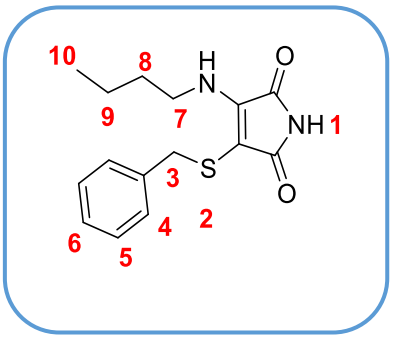

TLC conditions: R_f = 0.42 (petroleum ether: ethyl acetate= 2:1). Yield =26.4%. ^{1}H NMR (400 MHz, MeOD, ppm) δ=7.23 (5H, ddd, $^3J_{H-H}$ = 25, 16, 7; H 4, 5, 6), 3.8 (2H, s, H3), 3.25 (2H, t, $^3J_{H-H}$ = 7 Hz, H7), 1.49 – 1.19 (4H, m, H8, 9), 0.9 (3H, t, $^3J_{H-H}$ = 7 Hz, H10); ^{13}C NMR (101 MHz, MeOD, ppm) δ 128. 7, 127.8, 126.7 (C6, 5, 4), 42.0 (C7), 39.3 (C8), 31.2 (C9), 19.4 (C10);

HR-MS (MaXis) *m/z* found 313.0981, calc. 313.0981 ($[M+Na]^{+,}$100%);

FTIR (neat) ν_{max} / cm^{-1} 3315 (H-N of amine), 1711 and 1620 (C=O of maleimide), 1359 (C=C of maleimide, 765 and 705 (C-H of aromatic).

3.5.4 NMR Spectra of Substituted Maleimides

3-(butylthio)-4-(ethylamino)-1-methyl-1H-pyrrole-2,5-dione(4a)

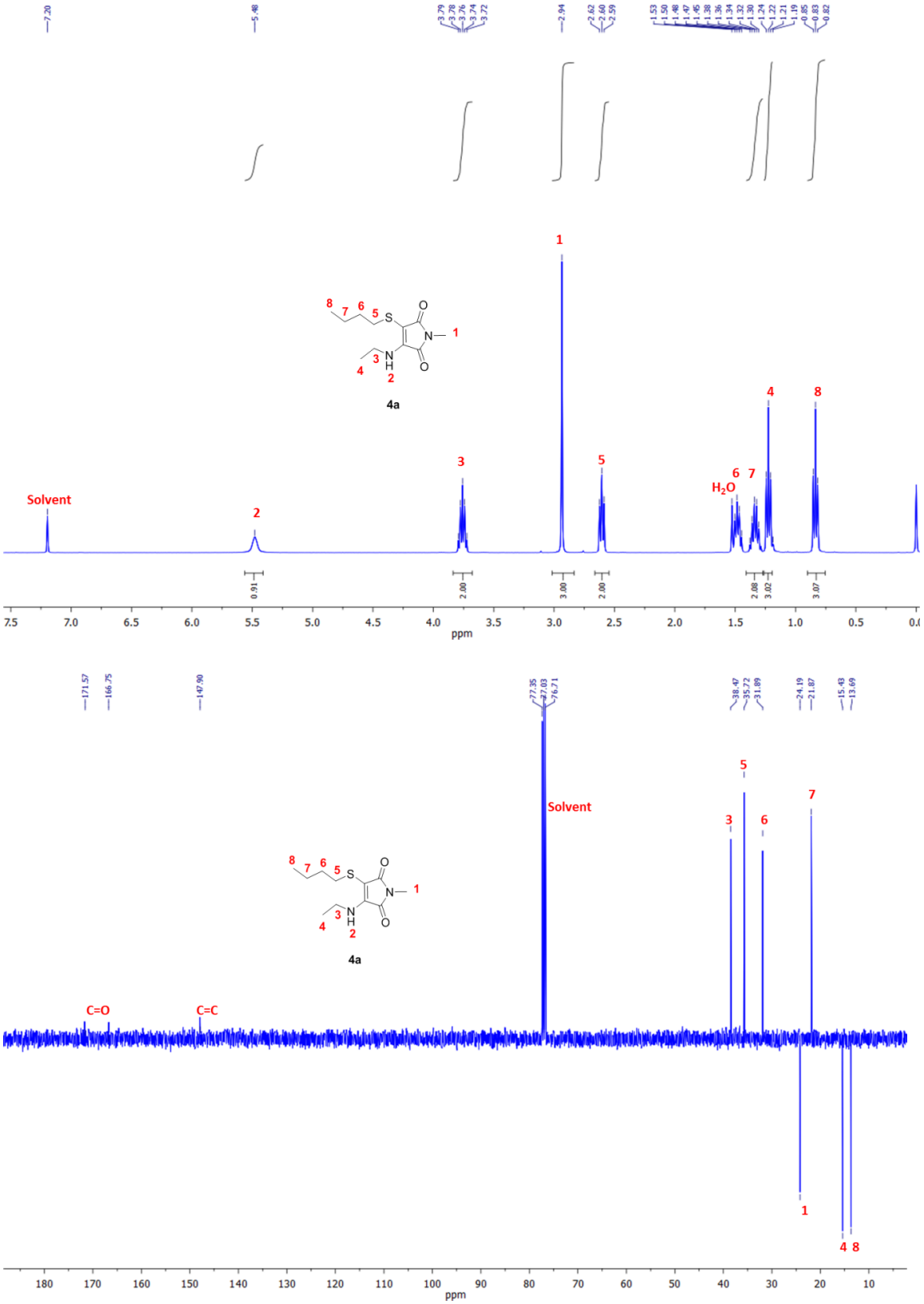

3-(ethylamino)-1-methyl-4-(octadecylthio)-1H-pyrrole-2,5-dione (4b)

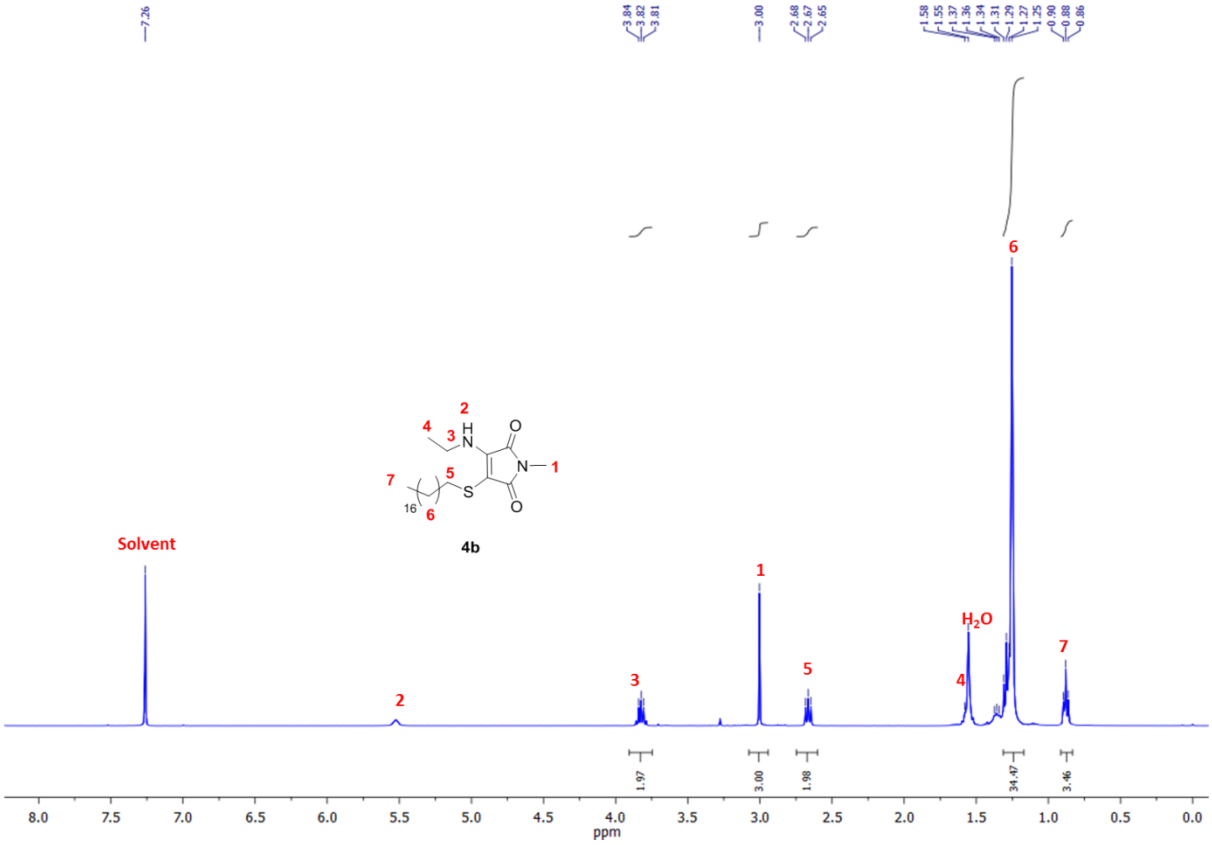

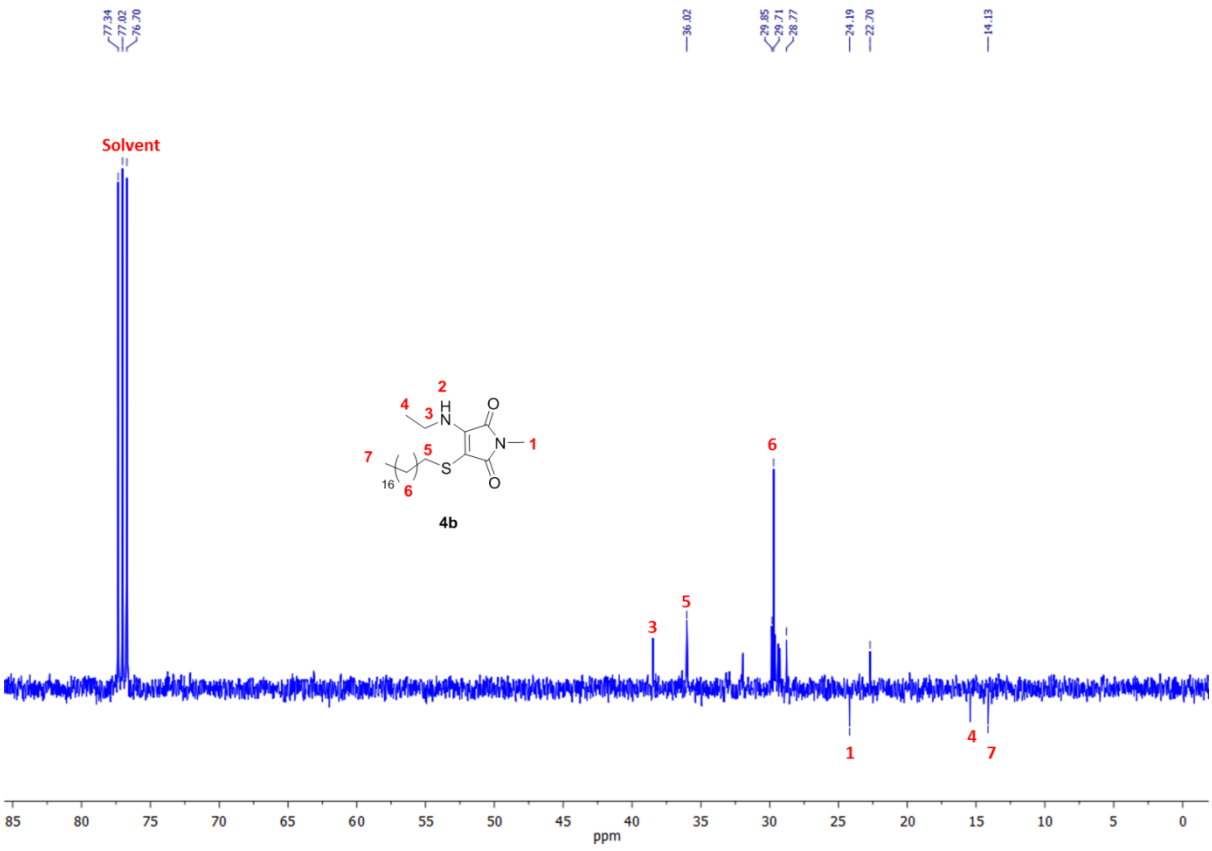

3-(ethylamino)-1-methyl-4-(phenylthio)-1H-pyrrole-2,5-dione(4c)

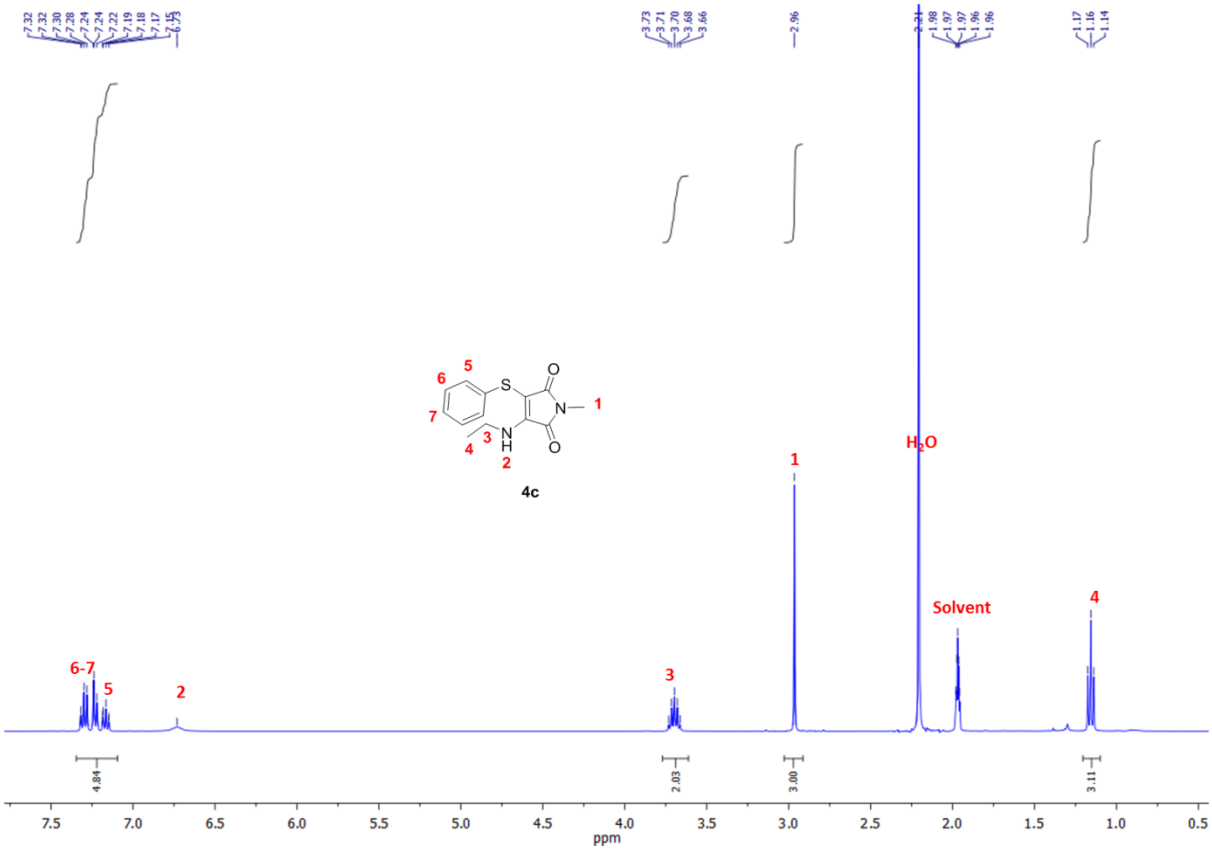

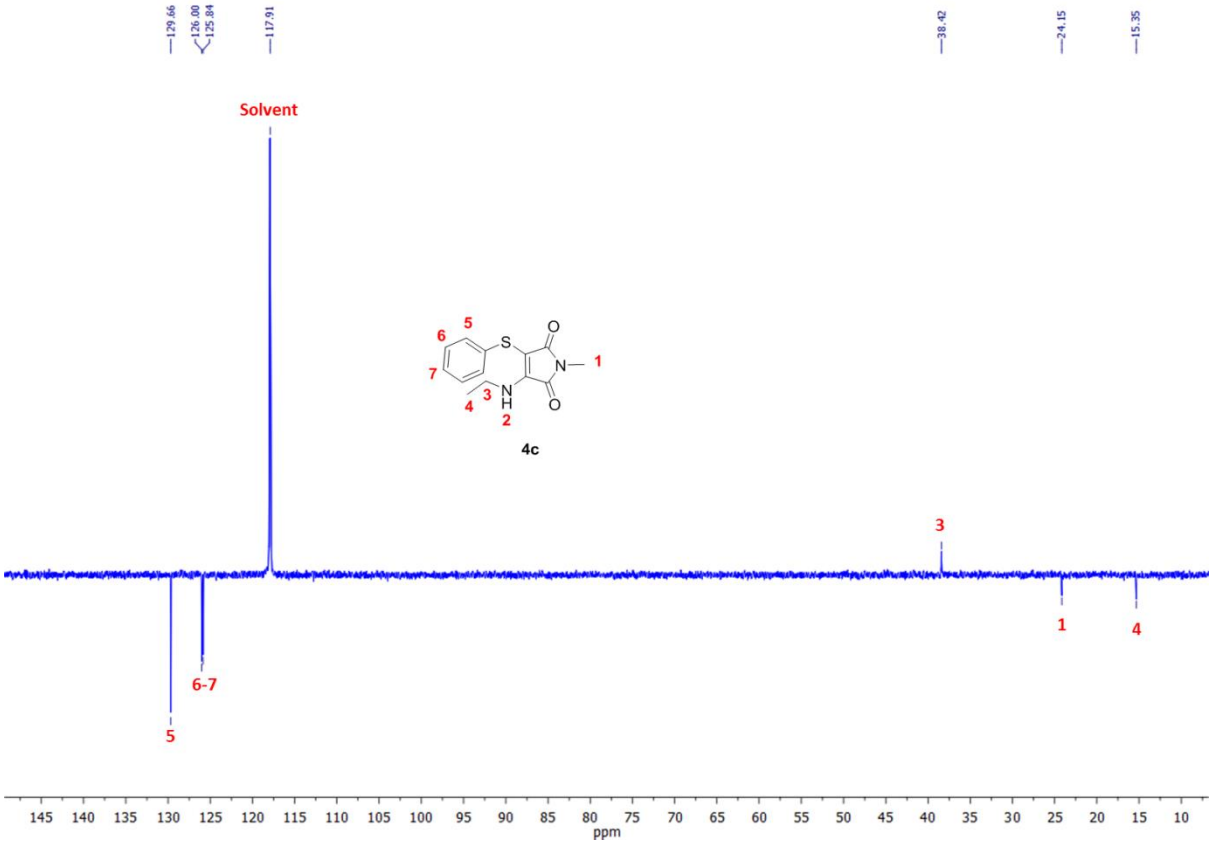

3-(ethylamino)-1-methyl-4-(o-tolylthio)-1H-pyrrole-2,5-dione(4d)

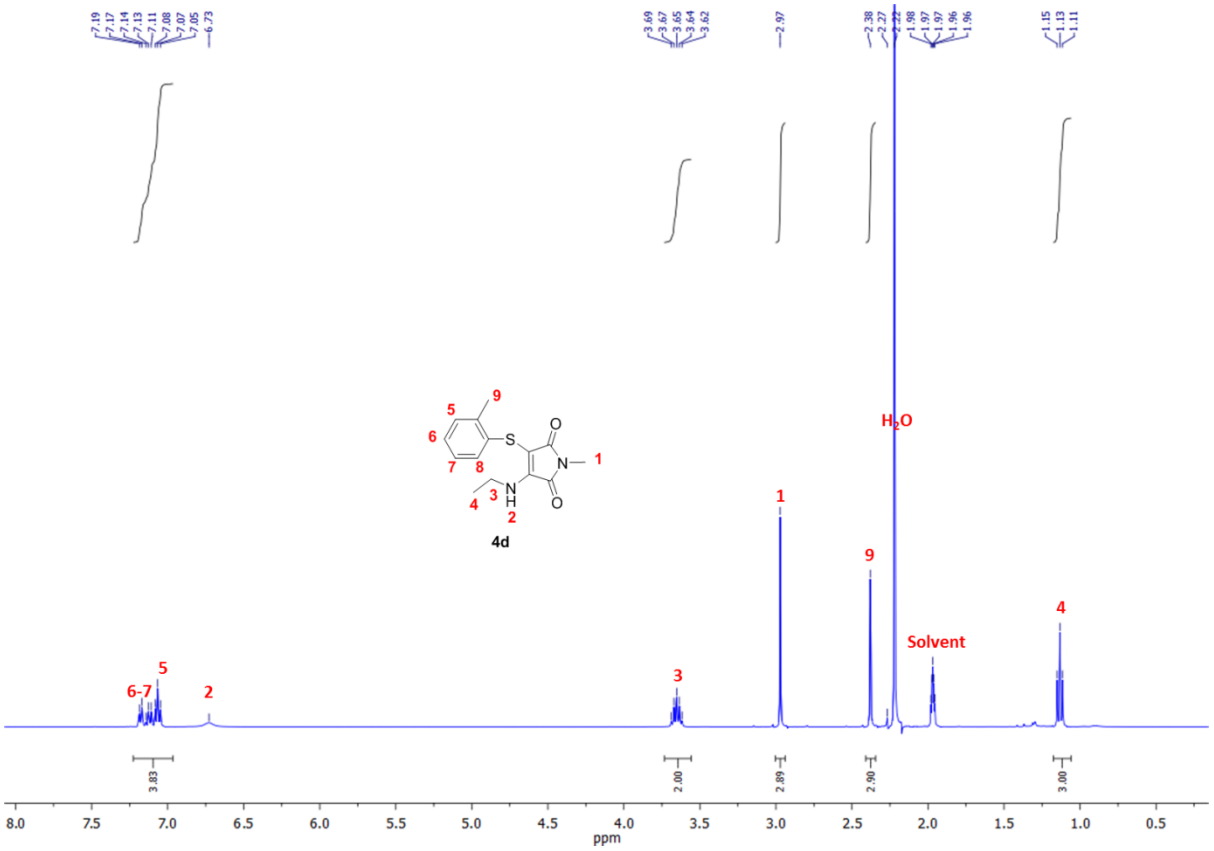

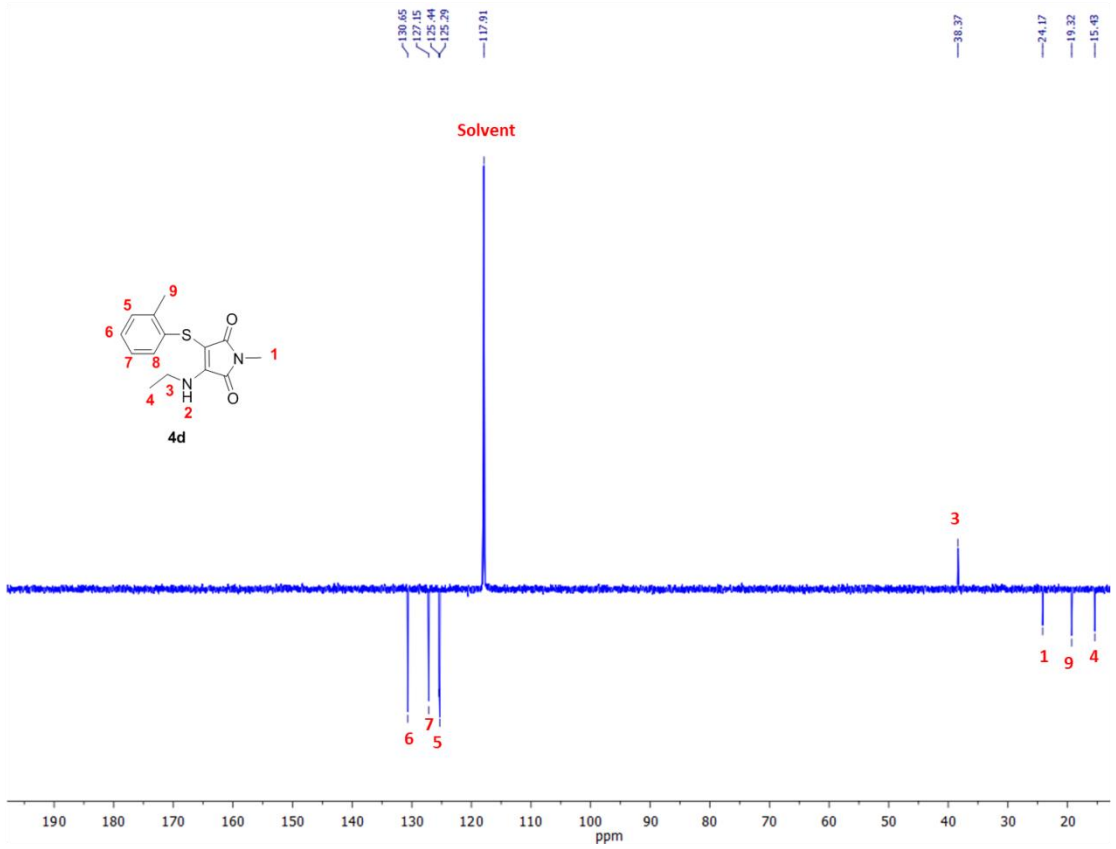

3-(benzylthio)-4-(ethylamino)-1-methyl-1H-pyrrole-2,5-dione (4e)

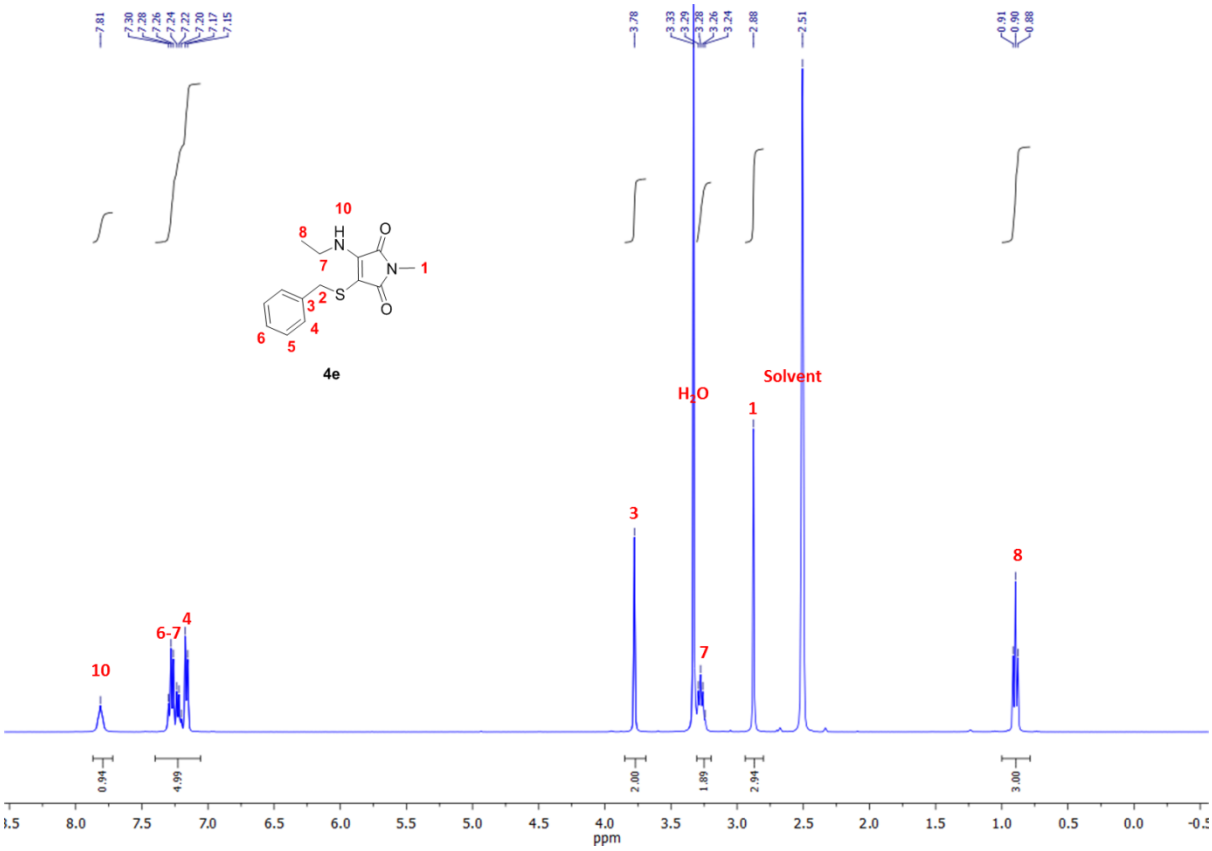

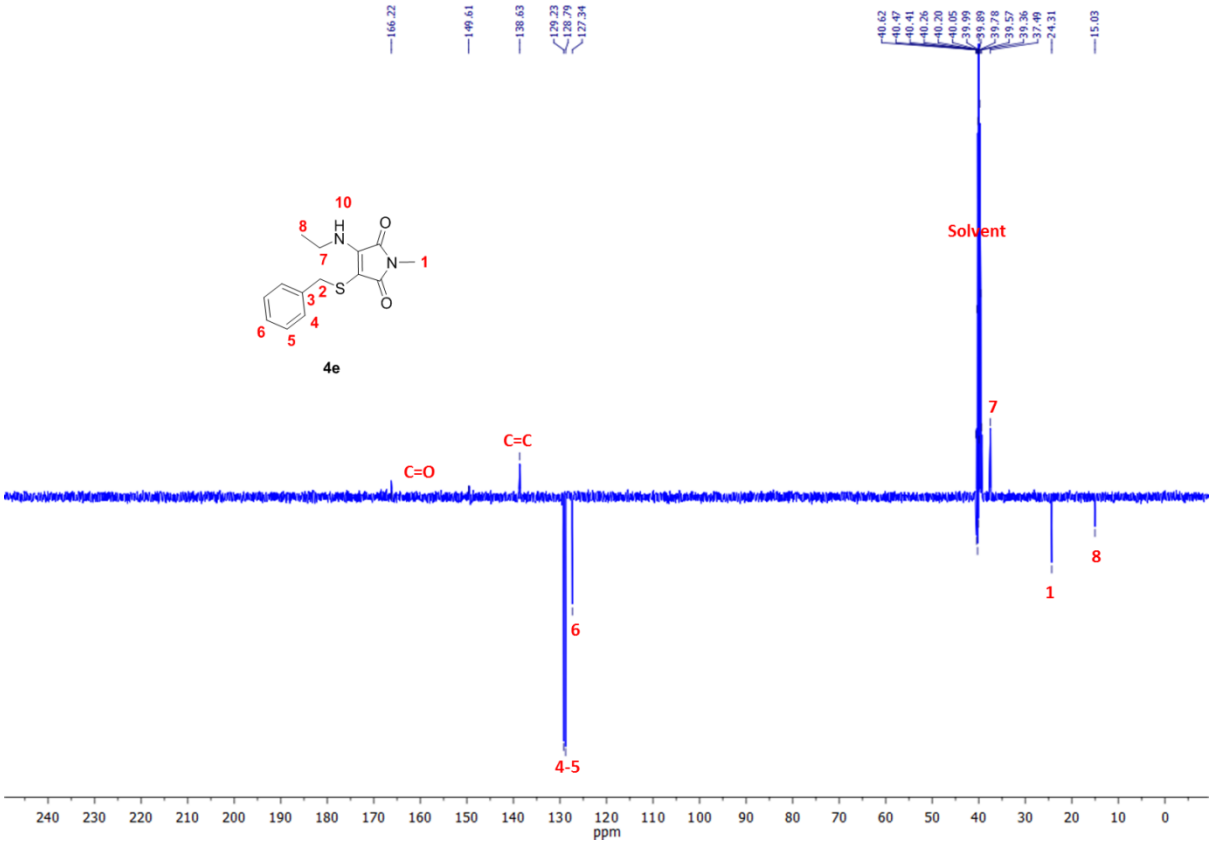

3-(butylamino)-1-methyl-4-(phenylthio)-1H-pyrrole-2,5-dione (4f):

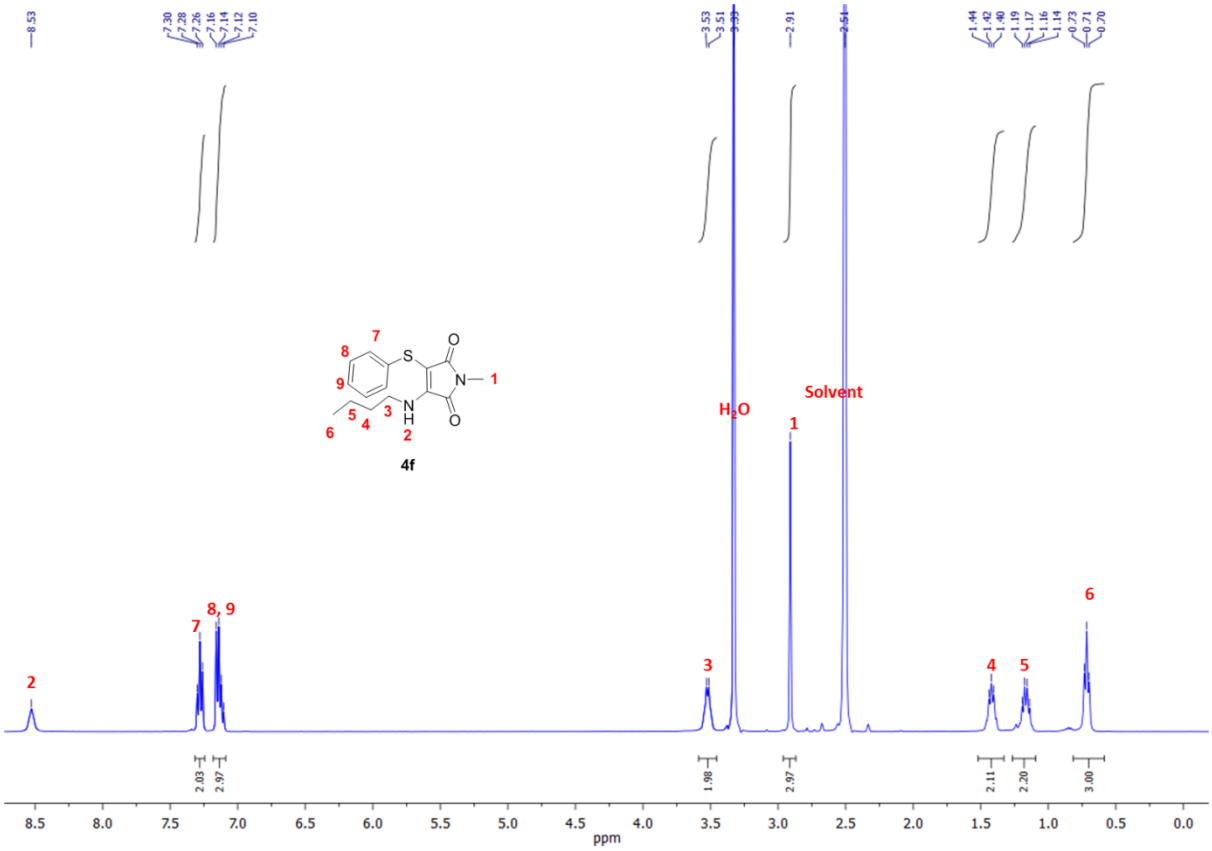

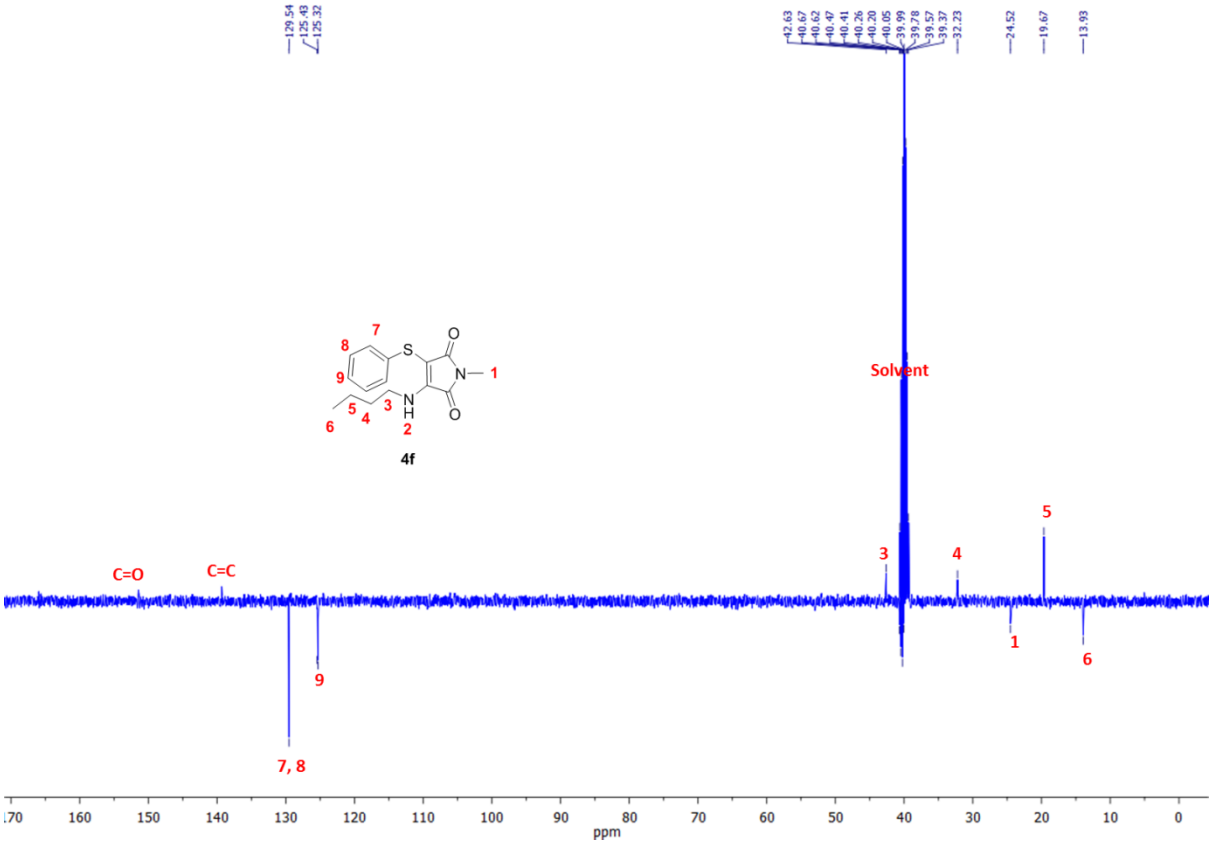

1-methyl-3-(phenylamino)-4-(phenylthio)-1H-pyrrole-2,5-dione (4g)

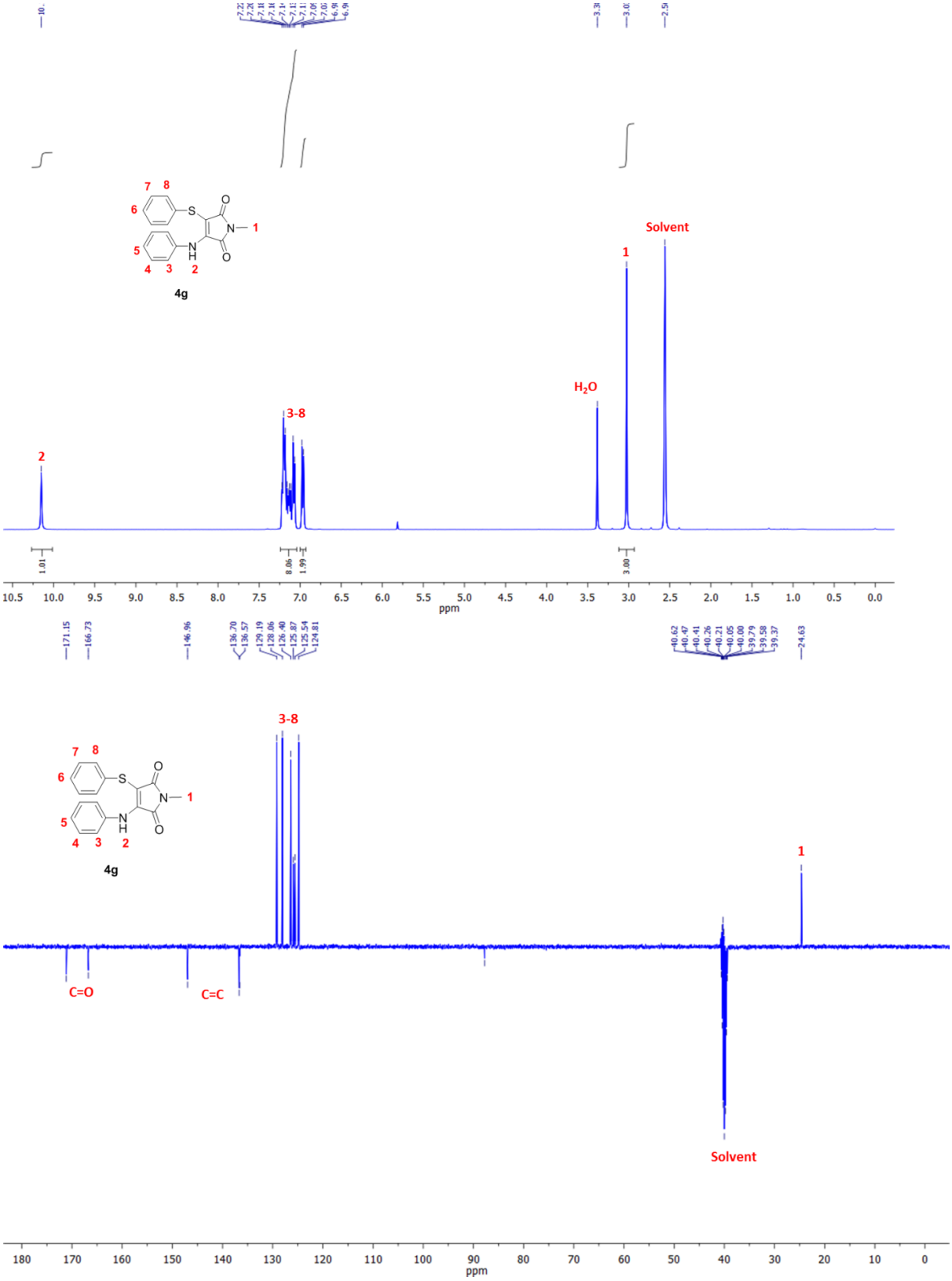

3-(butylamino)-4-(phenylthio)-1H-pyrrole-2,5-dione (4h)

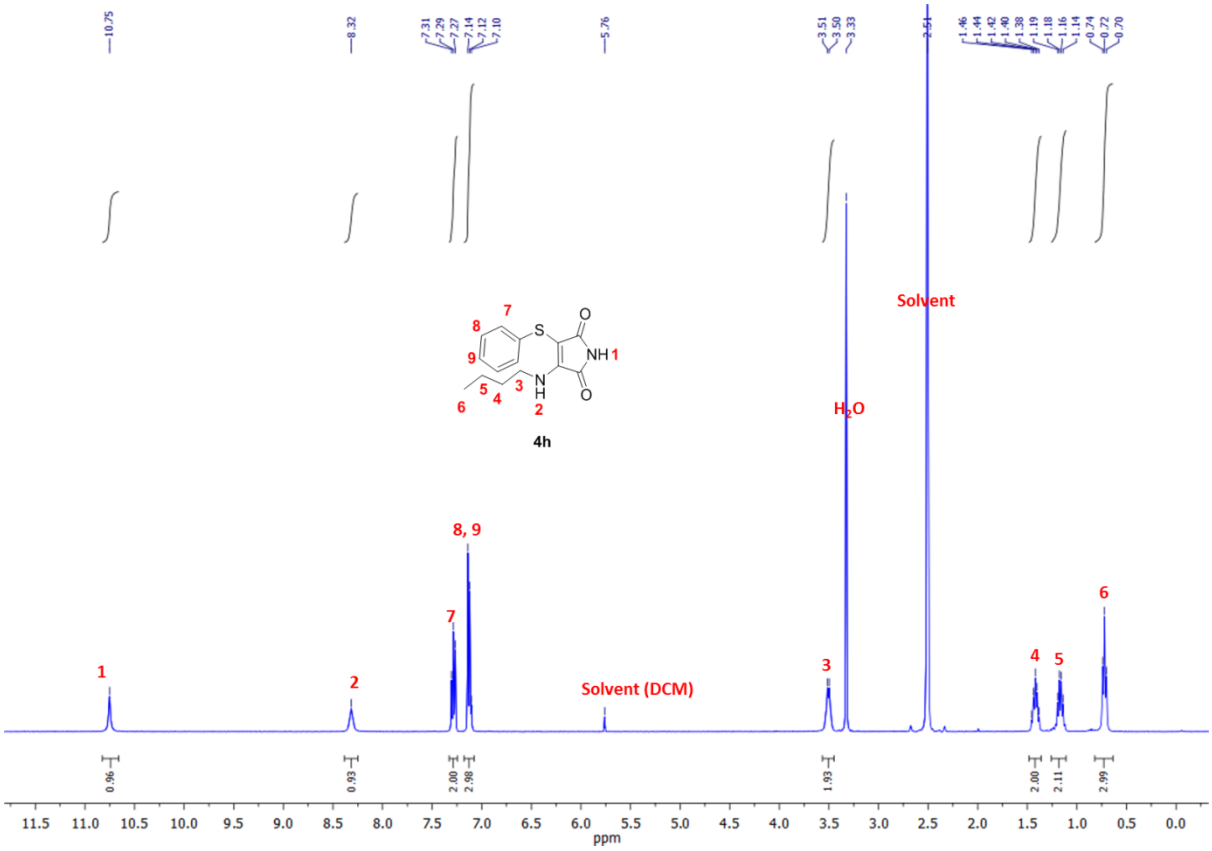

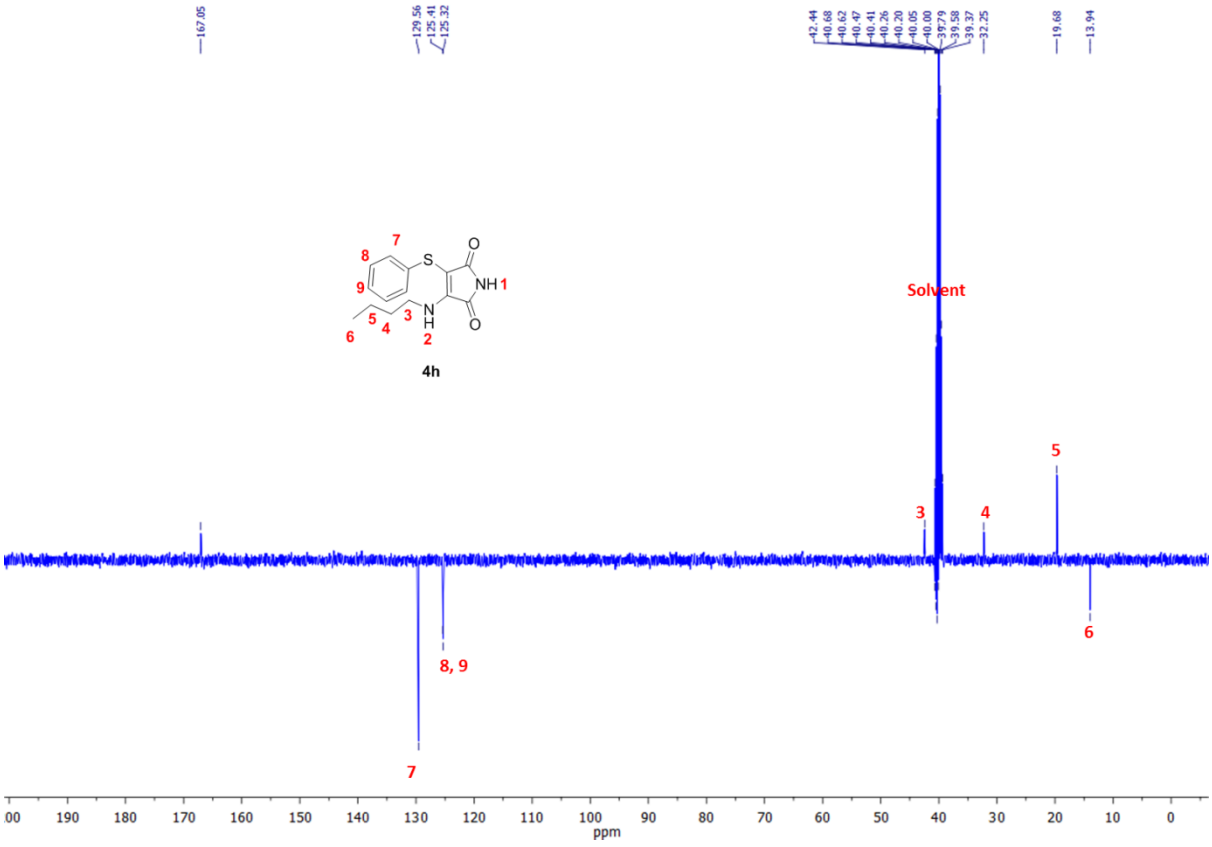

3-(butylthio)-4-(ethylamino)-1H-pyrrole-2,5-dione (4i)

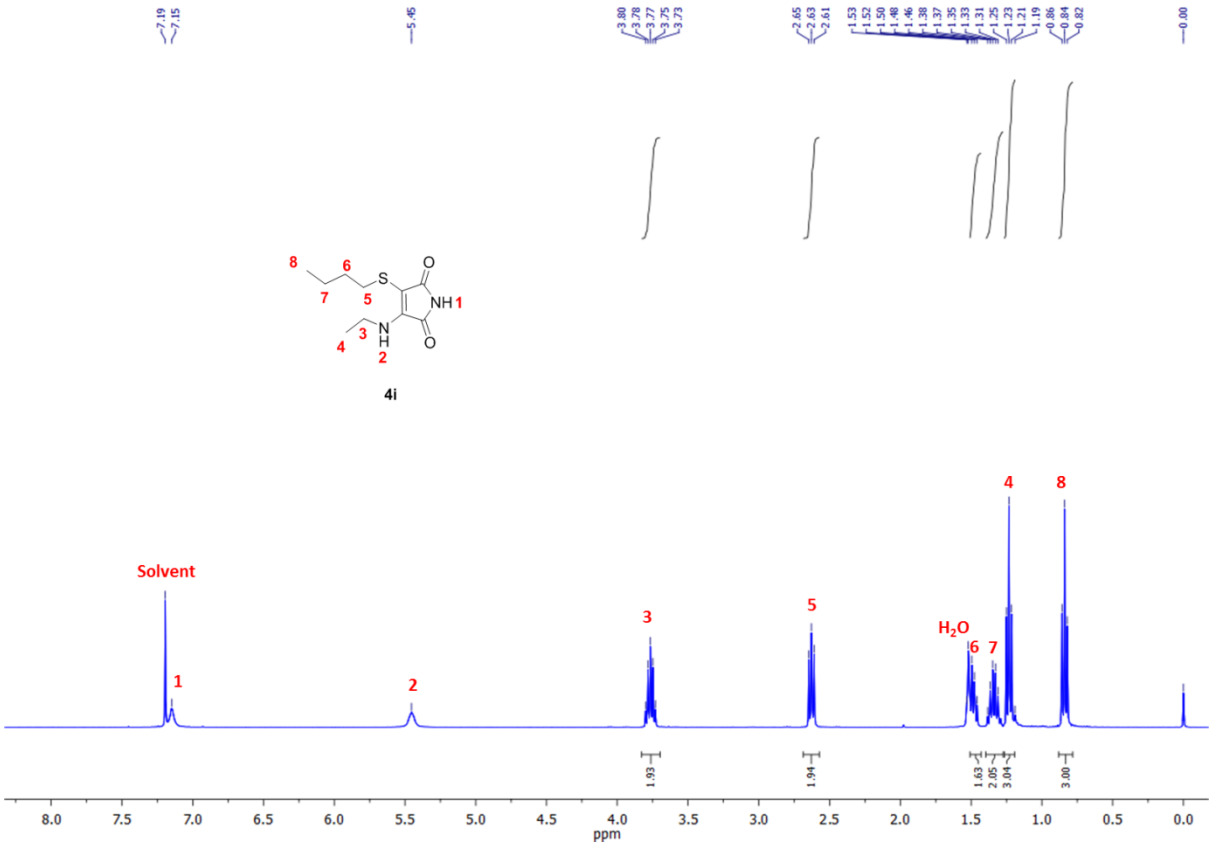

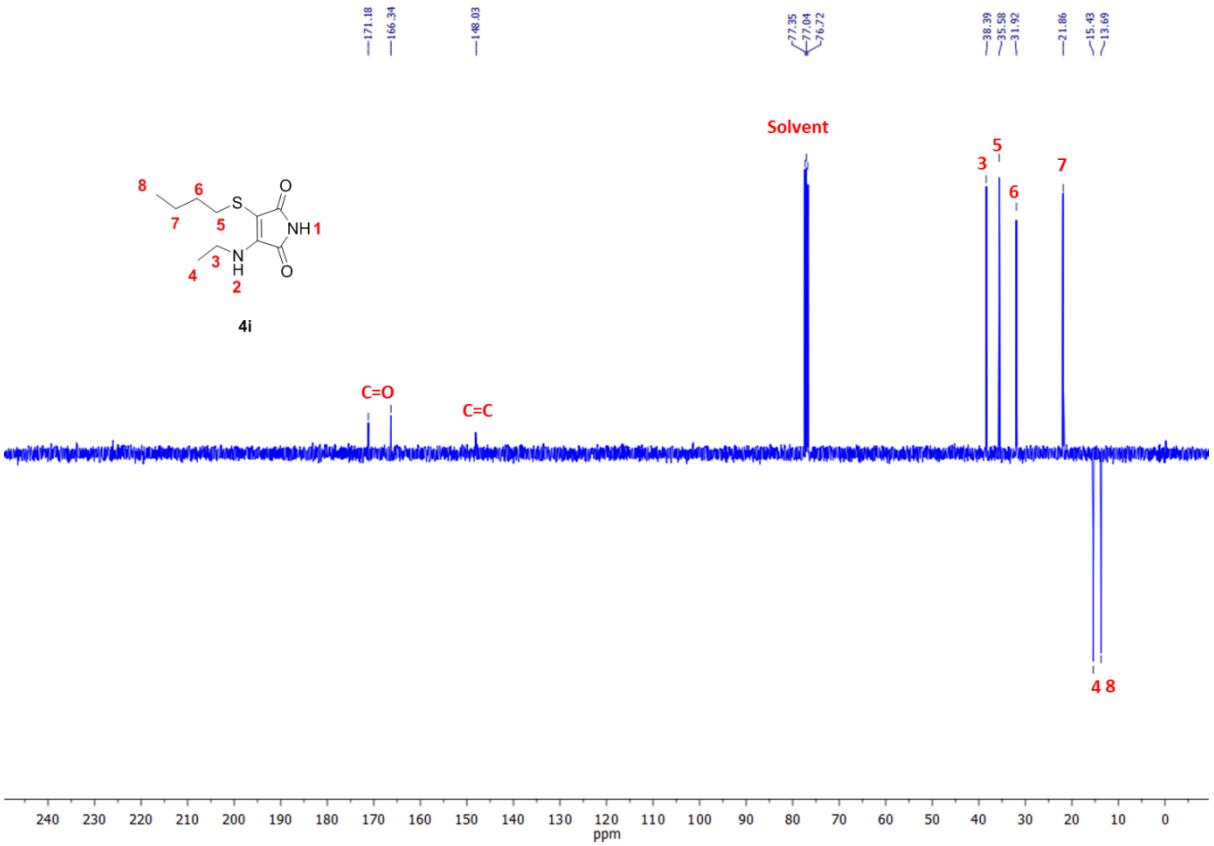

3-(benzylamino)-4-(butylthio)-1H-pyrrole-2,5-dione (4j)

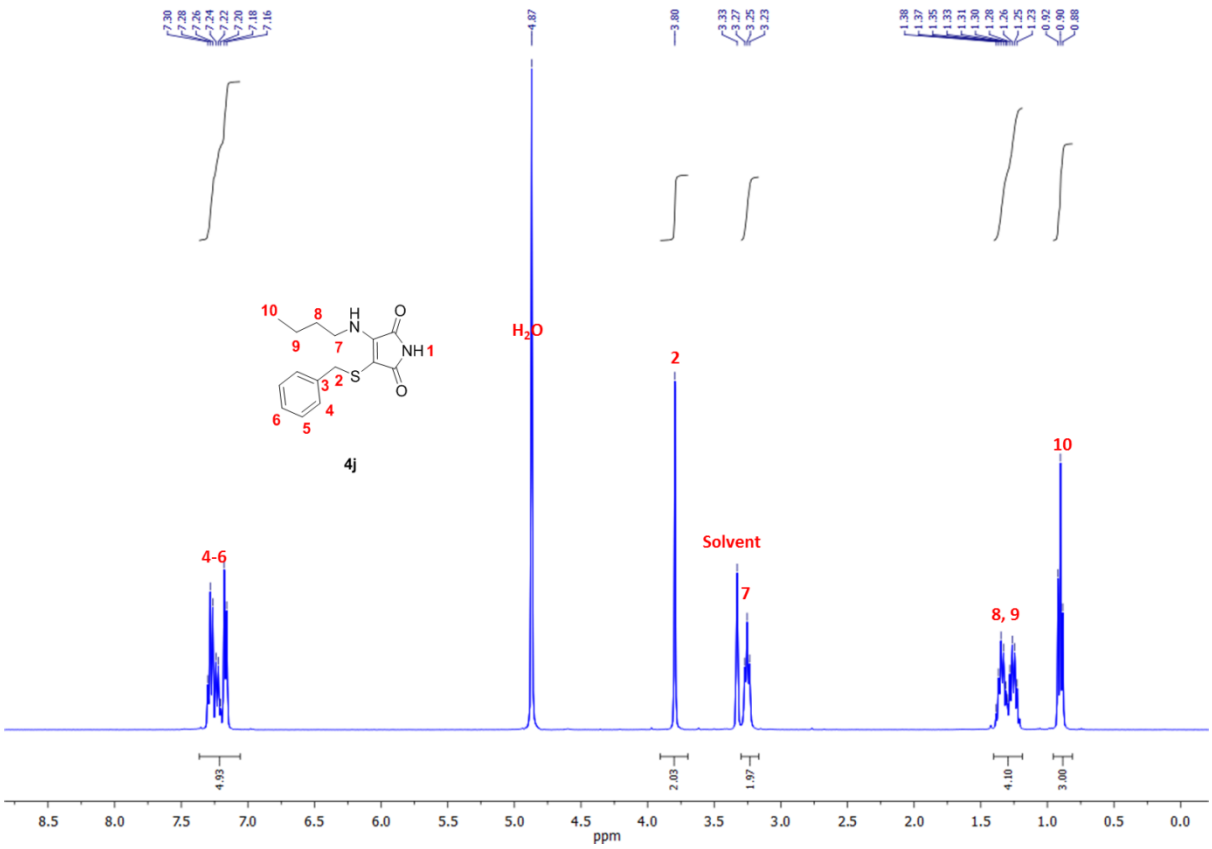

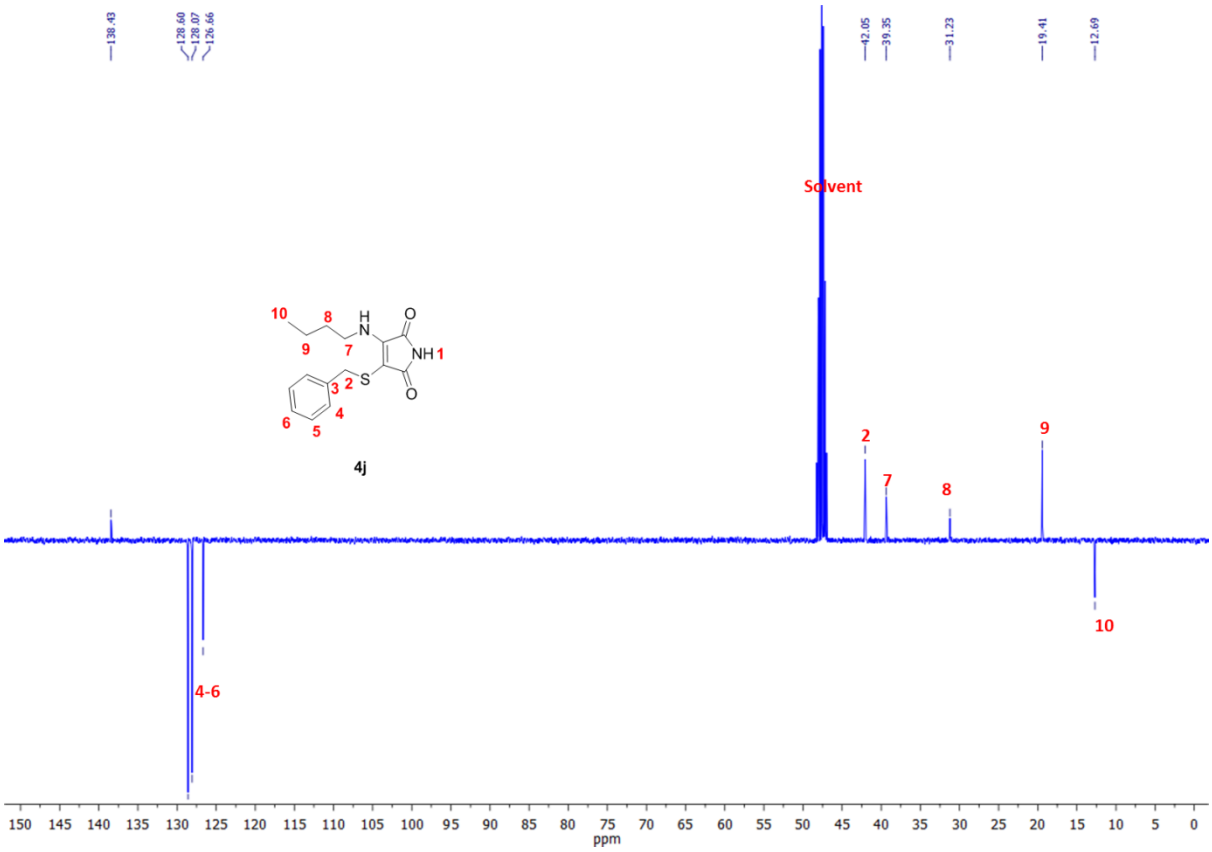

3.5.5 Computational Details

The geometries for all studied systems in the ground state have been fully optimized with the CAM-B3LYP[7] functional and the 6-311G(d,p) basis set.[8,9] The dispersion effects and the solvent were included in the optimization process. The D3-Grimme's dispersion[10] with Becke-Johson damping factor[11,12] was used to evaluate the dispersion effects. The solvent was considered using the polarization continuum model (PCM)[13, 14] and the dielectric constant of diethyl ether ($\varepsilon = 4.24$). The harmonic vibrational frequencies were also calculated at the same level of theory in order to verify that all the stationary points are minima of their potential energy surface. The time-dependent density functional theory (TD-DFT)[15-23] was applied to compute the absorption and emission (fluorescence) spectra at the ground and the first singlet excited state, respectively. The charge distribution was obtained following the natural bond orbital (NBO) partition scheme by Weinhold and co-workers.[24] All the calculations were performed using the Gaussian09 program package.[25]

* The simulation results were carried out by Dr. Miquel Torrent-Sucarrat

Table 3.2 TD-DFT excitation and emission energies and oscillator strengths of the maleimide derivatives studied in this work.[a,b]

Compound	λ_{exc} [c]	f_{exc} [d]	λ_{em} [e]	f_{em} [d]	$\Delta\lambda$ [f]
4a	334.0	0.090	551.5	0.084	217.5
4b	333.8	0.090	552.9	0.085	219.0
4c	328.3	0.067	510.4	0.065	182.1
4d	328.1	0.068	511.5	0.065	183.4
4e	336.2	0.095	550.6	0.089	214.5
4f	336.8	0.064	510.0	0.065	173.2
4g	373.5	0.088	508.2	0.098	134.7
4h	316.7	0.087	491.4	0.084	174.8
4i	327.2	0.115	528.8	0.106	201.5
4j	326.3	0.104	537.6	0.105	211.3

[a] All excitation and emission energies correspond to the first excited state ($\pi \rightarrow \pi^*$ transition).

[b] All values computed at CAM-B3LYP-D3BJ/6-311G(d,p) level of theory in solution using the PCM with $\varepsilon = 4.24$.

[c] Excitation wavelength, in nm.

[d] Oscillator strength.

[e] Emission wavelength, in nm.

[f] Stokes shift ($\lambda_{em} - \lambda_{exc}$).

[*] The simulation results were carried out by Dr. Miquel Torrent-Sucarrat

Table 3.3 Natural population analysis of the Carbon atoms adjacent to the electron withdrawing and donating groups (labeled as C_2 and C_3, respectively).[a]

Compound	q_{C2}	q_{C3}	Δq
4a	-0.40	0.18	0.58
4b	-0.40	0.18	0.58
4c	-0.42	0.19	0.61
4d	-0.42	0.19	0.61
4e	-0.40	0.18	0.59
4f	-0.42	0.19	0.61
4g	-0.38	0.16	0.53
4h	-0.42	0.19	0.61
4i	-0.40	0.17	0.57
4j	-0.42	0.19	0.60

[a] All values computed at CAM-B3LYP-D3BJ/6-311G(d,p) level of theory in solution using the PCM with $\varepsilon = 4.24$.

* The simulation results were carried out by Dr. Miquel Torrent-Sucarrat

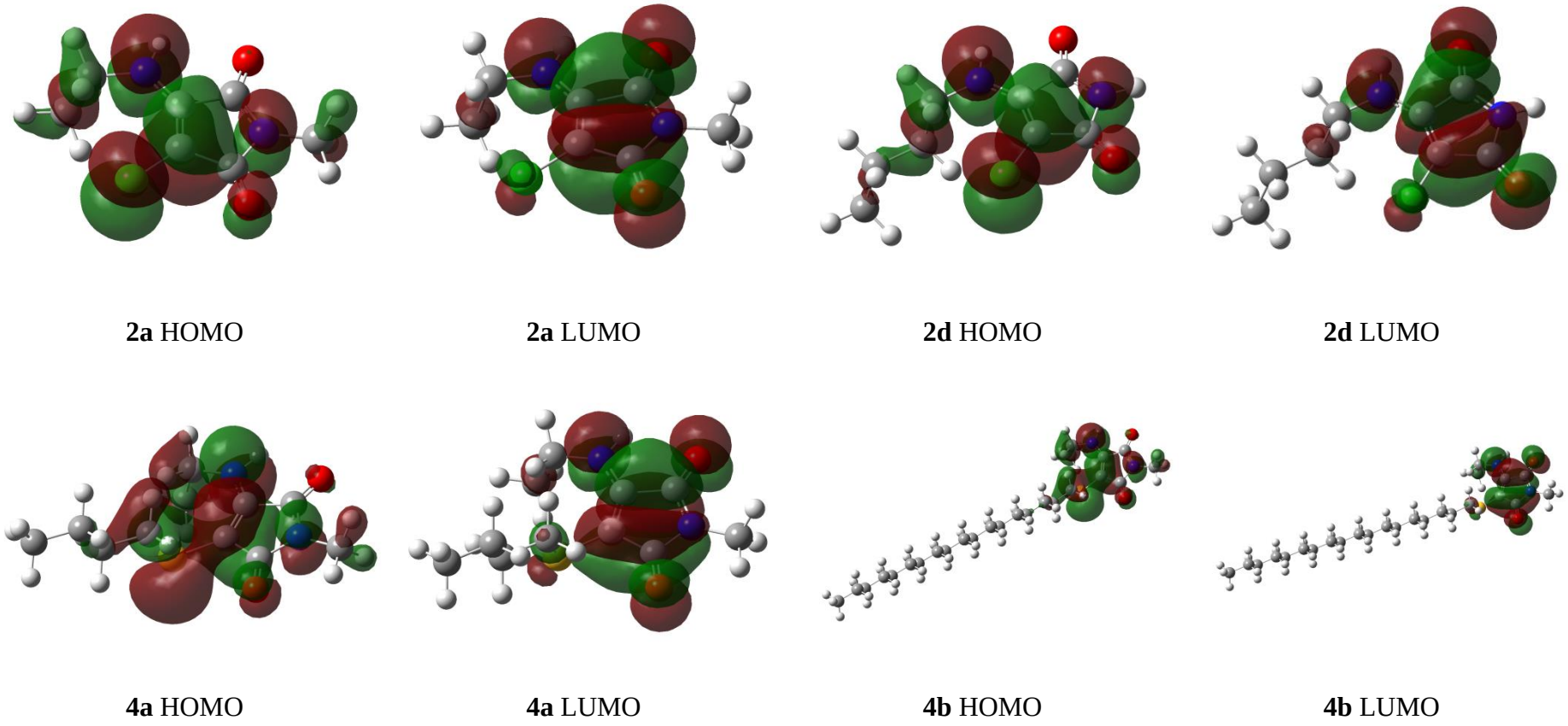

Figure 3. 18 HOMO and LUMO Kohn-Sham orbitals of **3e**, **3f**, **4a**, and **4b** maleimide derivatives.

* The simulation results was carried out by Dr. Miquel Torrent-Sucarrat

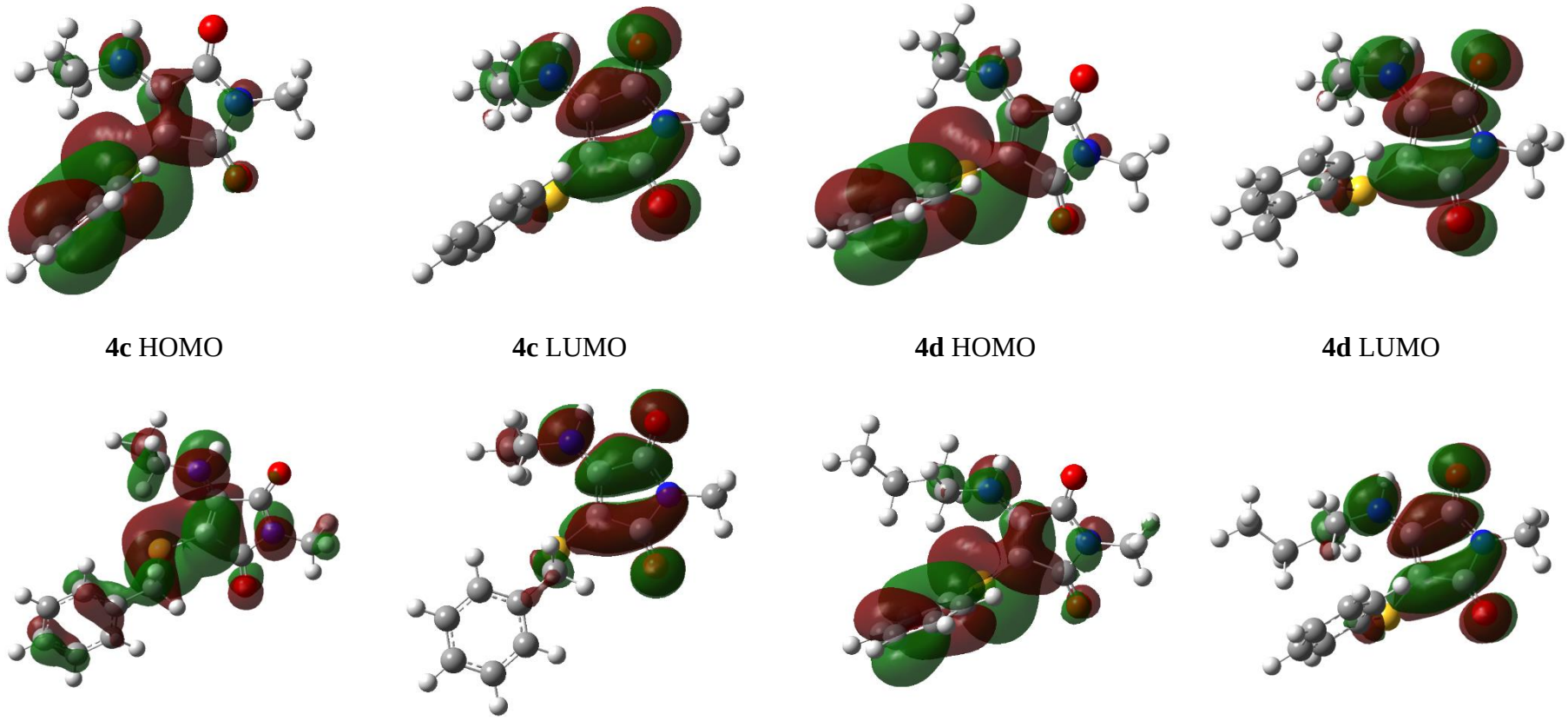

Figure 3.19 HOMO and LUMO Kohn-Sham orbitals of **4c**, **4d**, **4e** and **4f** maleimide derivatives.

* The simulation results were carried out by Dr. Miquel Torrent-Sucarrat

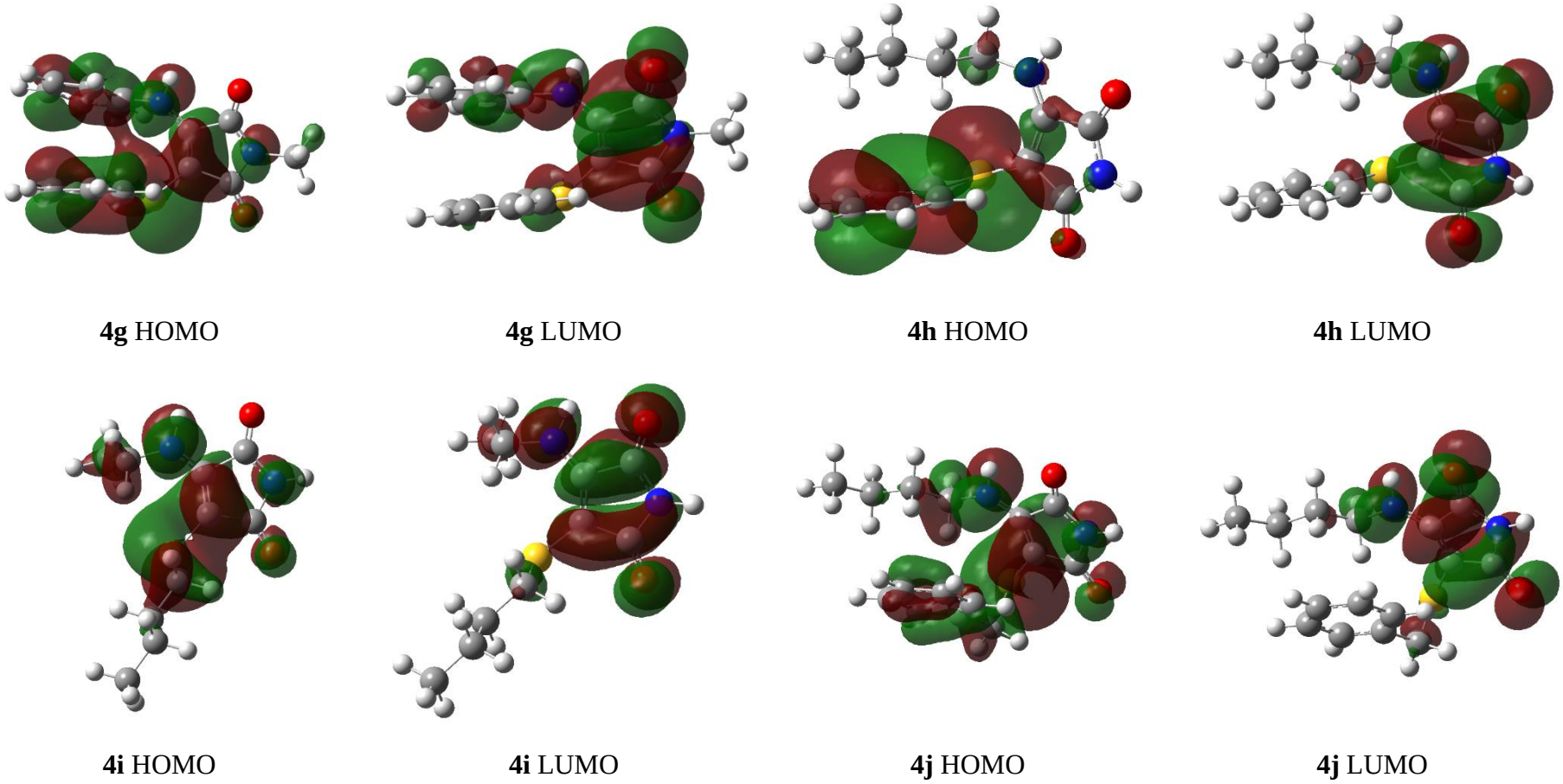

Figure 3.20 HOMO and LUMO Kohn-Sham orbitals of **4g**, **4h**, **4i** and **4j** maleimide derivatives.

* The simulation results were carried out by Dr. Miquel Torrent-Sucarrat

3.6 References

1. Prasanna de Silva, A.; Nimal Gunaratne, H. Q.; Gunnlaugsson, T., Fluorescent PET(Photoinduced Electron Transfer) reagents for thiols. *Tetrahedron Lett.* **1998,** *39* (28), 5077.

2. Patra, S. K.; Sheet, S. K.; Sen, B.; Aguan, K.; Roy, D. R.; Khatua, S., Highly Sensitive Bifunctional Probe for Colorimetric Cyanide and Fluorometric H2S Detection and Bioimaging: Spontaneous Resolution, Aggregation, and Multicolor Fluorescence of Bisulfide Adduct. *J. Org. Chem.* **2017,** *82* (19), 10234.

3. Zhang, Y.; Huo, F.; Yin, C.; Yue, Y.; Hao, J.; Chao, J.; Liu, D., An off–on fluorescent probe based on maleimide for detecting thiols and its application for bioimaging. *Sens. Actuators. B* **2015,** *207*, 59.

4. Langmuir, M. E.; Yang, J.-R.; Moussa, A. M.; Laura, R.; LeCompte, K. A., New naphthopyranone based fluorescent thiol probes. *Tetrahedron Lett.* **1995,** *36* (23), 3989.

5. Chen, X.; Zhou, Y.; Peng, X.; Yoon, J., Fluorescent and colorimetric probes for detection of thiols. *Chem. Soc. Rev.* **2010,** *39* (6), 2120.

6. Chen, Y.; Tsao, K.; De Francesco, E.; Keillor, J. W., Ring Substituent Effects on the Thiol Addition and Hydrolysis Reactions of N-Arylmaleimides. *J. Org. Chem.* **2015,** *80* (24), 12182.

7. Heindel, N. D., Maleimide syntheses by amine reaction with acetylenedicarboxylate esters. *J. Org. Chem* **1970,** *35* (9), 3138.

8. Tang, W.; Wang, J., Mechanism for toluene detection of flower-like ZnO sensors prepared by hydrothermal approach: Charge transfer. *Sensors and Actuators B: Chemical* **2015,** *207*, 66.

9. Fletcher, S. A.; Sin, P. K.; Nobles, M.; Arstad, E.; Tinker, A.; Baker, J. R., A dual optical and nuclear imaging reagent for peptide labelling via disulfide bridging. *Org. Biomol. Chem.* **2015,** *13* (37), 9559.

10. Zhu, Q.; Ye, Z.; Yang, W.; Cai, X.; Tang, B. Z., One-Pot Synthesis and Structure-Property Relationship of Aminomaleimides: Fluorescence Efficiencies in Monomers and Aggregates Easily Tuned by Switch of Aryl and Alkyl. *J. Org. Chem.* **2017,** *82* (2), 1096.

11. Ambrogi, M.; Ciogli, A.; Mancinelli, M.; Ranieri, S.; Mazzanti, A., Atropisomers of arylmaleimides: stereodynamics and absolute configuration. *J. Org. Chem.* **2013,** *78* (8), 3709.

12. Mabire, A. B.; Robin, M. P.; Quan, W. D.; Willcock, H.; Stavros, V. G.; O'Reilly, R. K., Aminomaleimide fluorophores: a simple functional group with bright, solvent dependent emission. *Chem. Commun.* **2015,** *51* (47), 9733.

13. Robin, M. P.; O'Reilly, R. K., Fluorescent and chemico-fluorescent responsive polymers from dithiomaleimide and dibromomaleimide functional monomers. *Chem. Sci.* **2014,** *5* (7), 2717.

14. Yeh, H.-C.; Wu, W.-C.; Chen, C.-T., The colourful fluorescence from readily-synthesised 3,4-diaryl-substituted maleimide fluorophores. *Chem. Commun.* **2003,** *0* (3), 404.

15. Kizaki, K.; Imoto, H.; Kato, T.; Naka, K., Facile construction of N-alkyl arylaminomaleimide derivatives as intensively emissive aggregation induced emission dyes. *Tetrahedron* **2015,** *71* (4), 643.

16. Chen, P. Z.; Weng, Y. X.; Niu, L. Y.; Chen, Y. Z.; Wu, L. Z.; Tung, C. H.; Yang, Q. Z., Light-Harvesting Systems Based on Organic Nanocrystals To Mimic Chlorosomes.

Angew Chem Int Ed **2016,** *55* (8), 2759.

17. Zhang, Y.; Chen, F.; Yang, Y.; Tang, C.-Z.; Tian, F.; Peng, L.; Wang, L.-X., An unexpected metal-free DMAP catalyzed Michael addition–elimination domino reaction between 2-naphthols and bromomaleimides for the effective construction of 3-arylmaleimides. *Tetrahedron Lett.* **2016,** *57* (11), 1261.

18. Gu, G.; Wang, H.; Liu, P.; Fu, C.; Li, Z.; Cao, X.; Li, Y.; Fang, Q.; Xu, F.; Shen, J.; Wang, P. G., Discovery and structural insight of a highly selective protein kinase inhibitor hit through click chemistry. *Chem. Commun.* **2012,** *48* (22), 2788.

19. Richards, D. A.; Fletcher, S. A.; Nobles, M.; Kossen, H.; Tedaldi, L.; Chudasama, V.; Tinker, A.; Baker, J. R., Photochemically re-bridging disulfide bonds and the discovery of a thiomaleimide mediated photodecarboxylation of C-terminal cysteines. *Org Biomol Chem* **2016,** *14* (2), 455.

20. Hull, E. A.; Livanos, M.; Miranda, E.; Smith, M. E.; Chester, K. A.; Baker, J. R., Homogeneous bispecifics by disulfide bridging. *Bioconjug. Chem.* **2014,** *25* (8), 1395.

21. Chan, L.-H.; Lee, Y.-D.; Chen, C.-T., Achieving saturated red photoluminescence and electroluminescence with readily synthesized maleimide-arylamine copolymers. *Tetrahedron* **2006,** *62* (41), 9541.

22. Liu, T.-Z.; Chen, Y., Synthesis, optical and electrochemical properties of luminescent polymers containing 1,2-diphenylmaleimide and thiophene segments. *Polymer* **2005,** *46* (23), 10383.

23. Bouissane, L.; Sestelo, J. P.; Sarandeses, L. A., Synthesis of 3,4-Disubstituted Maleimides by Selective Cross-Coupling Reactions Using Indium Organometallics. *Org. Lett.* **2009,** *11* (6), 1285.

24. Imoto, H.; Nohmi, K.; Kizaki, K.; Watase, S.; Matsukawa, K.; Yamamoto, S.; Mitsuishi, M.; Naka, K., Effect of alkyl groups on emission properties of aggregation induced emission active N-alkyl arylaminomaleimide dyes. *RSC Adv.* **2015,** *5* (114), 94344.

25. Smith, M. E. B.; Schumacher, F. F.; Ryan, C. P.; Tedaldi, L. M.; Papaioannou, D.; Waksman, G.; Caddick, S.; Baker, J. R., Protein Modification, Bioconjugation, and Disulfide Bridging Using Bromomaleimides. *J. Am. Chem. Soc.* **2010,** *132* (6), 1960.

26. Robin, M. P.; Mabire, A. B.; Damborsky, J. C.; Thom, E. S.; Winzer-Serhan, U. H.; Raymond, J. E.; O'Reilly, R. K., New Functional Handle for Use as a Self-Reporting Contrast and Delivery Agent in Nanomedicine. *J. Am. Chem. Soc.* **2013,** *135* (25), 9518.

27. Robin, M. P.; Wilson, P.; Mabire, A. B.; Kiviaho, J. K.; Raymond, J. E.; Haddleton, D. M.; O'Reilly, R. K., Conjugation-Induced Fluorescent Labeling of Proteins and Polymers Using Dithiomaleimides. *J. Am. Chem. Soc.* **2013,** *135* (8), 2875.

28. Schumacher, F. F.; Nunes, J. P.; Maruani, A.; Chudasama, V.; Smith, M. E.; Chester, K. A.; Baker, J. R.; Caddick, S., Next generation maleimides enable the controlled assembly of antibody-drug conjugates via native disulfide bond bridging. *Org. Biomol. Chem.* **2014,** *12* (37), 7261.

29. Grison, C. M.; Burslem, G. M.; Miles, J. A.; Pilsl, L. K. A.; Yeo, D. J.; Imani, Z.; Warriner, S. L.; Webb, M. E.; Wilson, A. J., Double quick, double click reversible peptide "stapling". *Chem. Sci.* **2017,** *8* (7), 5166.

30. Bai, T.; Du, J.; Chen, J.; Duan, X.; Zhuang, Q.; Chen, H.; Kong, J., Reduction-responsive dithiomaleimide-based polymeric micelles for controlled anti-cancer drug delivery and bioimaging. *Polym. Chem.* **2017,** *8* (46), 7160.

31. Gaitzsch, J.; Chudasama, V.; Morecroft, E.; Messager, L.; Battaglia, G., Synthesis

of an Amphiphilic Miktoarm Star Terpolymer for Self-Assembly into Patchy Polymersomes. *ACS Macro. Lett.* **2016,** *5* (3), 351.

32. Castaneda, L.; Maruani, A.; Schumacher, F. F.; Miranda, E.; Chudasama, V.; Chester, K. A.; Baker, J. R.; Smith, M. E.; Caddick, S., Acid-cleavable thiomaleamic acid linker for homogeneous antibody-drug conjugation. *Chem Commun* **2013,** *49* (74), 8187.

33. Youziel, J.; Akhbar, A. R.; Aziz, Q.; Smith, M. E.; Caddick, S.; Tinker, A.; Baker, J. R., Bromo- and thiomaleimides as a new class of thiol-mediated fluorescence 'turn-on' reagents. *Org Biomol Chem* **2014,** *12* (4), 557.

34. Awuah, E.; Capretta, A., Development of methods for the synthesis of libraries of substituted maleimides and alpha,beta-unsaturated-gamma-butyrolactams. *J. Org. Chem.* **2011,** *76* (9), 3122.

35. Leismann, H.; Marzolph, G.; Scharf, H.-D.; Behruzi, M., Darstellung und Eigenschaften sowie Lichtstabilität des Diaminomaleinimids und einiger seiner Derivate. *Chem. Ber.* **1983,** *116* (7), 2591.

36. Xie, H. D.; Ho, L. A.; Truelove, M. S.; Corry, B.; Stewart, S. G., Fluorescent triphenyl substituted maleimide derivatives: synthesis, spectroscopy and quantum chemical calculations. *J. Fluoresc.* **2010,** *20* (5), 1077.

37. El Yahyaoui, A.; Félix, G.; Heynderickx, A.; Moustrou, C.; Samat, A., Convenient synthesis of photochromic symmetrical or unsymmetrical bis(heteroaryl)maleimides via the Suzuki–Miyaura cross-coupling reaction. *Tetrahedron* **2007,** *63* (38), 9482.

38. Song, D.; Sun, S.; Tian, Y.; Huang, S.; Ding, Y.; Yuan, Y.; Hu, A., Maleimide-based acyclic enediyne for efficient DNA-cleavage and tumor cell suppression. *J. Mater. Chem. B* **2015,** *3* (16), 3195.

39. Zhu, C.; Xu, G.; Ding, D.; Qiu, L.; Sun, J., Copper-Catalyzed Diazo Cross-/Homo-Coupling toward Tetrasubstituted Olefins and Applications on the Synthesis of Maleimide Derivatives. *Org. Lett.* **2015,** *17* (17), 4244.

40. Fleming, C.; Remón, P.; Li, S.; Simeth, N. A.; König, B.; Grøtli, M.; Andréasson, J., On the use of diarylmaleimide derivatives in biological contexts: An investigation of the photochromic properties in aqueous solution. *Dyes Pigm.* **2017,** *137*, 410.

41. Souffrin, A.; Croix, C.; Viaud-Massuard, M.-C., Efficient and General Protocol for Sonogashira Cross-Coupling Reactions of Maleimides. *Eur. J. Org. Chem.* **2012,** *2012* (13), 2499.

42. Hu, W.; Zheng, J.; Li, J.; Liu, B.; Wu, W.; Liu, H.; Jiang, H., Assembly of Polysubstituted Maleimides via Palladium-Catalyzed Cyclization Reaction of Alkynes with Isocyanides. *J. Org. Chem.* **2016,** *81* (24), 12451.

43. Jafarpour, F.; Shamsianpour, M.; Issazadeh, S.; Dorrani, M.; Hazrati, H., Palladium-catalyzed direct arylation of maleimides: A simple route to bisaryl-substituted maleimides. *Tetrahedron* **2017,** *73* (13), 1668.

44. Jafarpour, F.; Shamsianpour, M., Palladium-catalyzed cross-dehydrogenative coupling of maleimides with simple arenes: a fast track to highly substituted maleimides. *RSC Adv.* **2016,** *6* (105), 103567.

45. Mao, Y.; Maley, I.; Watson, W. H., Syntheses and structures of N-phenylmaleimidetriazoles and by-products. *J. Chem. Crystallogr.* **2005,** *35* (5), 385.

46. Brenet, S.; Baptiste, B.; Philouze, C.; Berthiol, F.; Einhorn, J., BINOL-Fused Maleimides - A New Class ofC2-Symmetric Chiral Imides. *Eur. J. Org. Chem.* **2013,** *2013* (6), 1041.

47. Deichmeister, M. V.; Pinkhasova, A. Z., Synthesis and investigation of merocyanine dyes. *Chem. Heterocycl. Compd. (N. Y., NY, U. S.)* **1971,** *7* (10), 1295.

48. Imoto, H.; Kizaki, K.; Watase, S.; Matsukawa, K.; Naka, K., Color Tuning of the Aggregation-Induced Emission of Maleimide Dyes by Molecular Design and Morphology Control. *Chem. Eur. J.* **2015,** *21* (34), 12105.

49. Awuah, E.; Capretta, A., Development of Methods for the Synthesis of Libraries of Substituted Maleimides and α,β-Unsaturated-γ-butyrolactams. *The Journal of Organic Chemistry* **2011,** *76* (9), 3122.

50. Mei, X.; Wang, J.; Zhou, Z.; Wu, S.; Huang, L.; Lin, Z.; Ling, Q., Diarylmaleic anhydrides: unusual organic luminescence, multi-stimuli response and photochromism. *J. Mater. Chem. C* **2017,** *5* (8), 2135.

Chapter 4 Photo Switchable Barcoding: Manipulating the Fluorescence Lifetime at the Sub-Cellular Scale

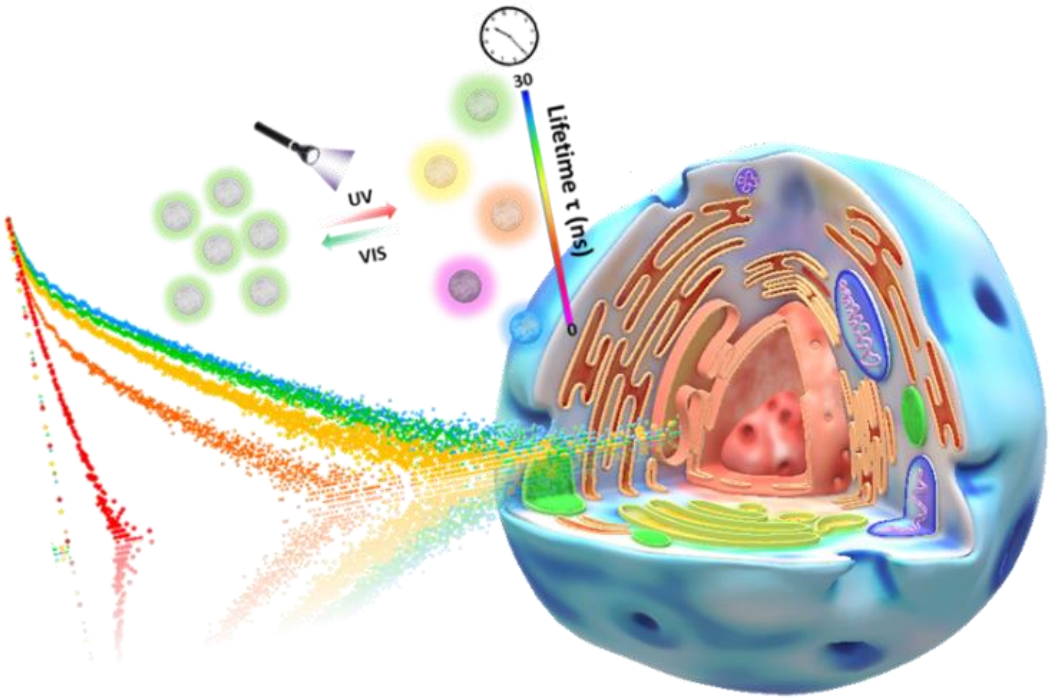

4.1 Abstract

Fluorescence barcoding is a pivotal technique for the investigation of the microscale world, from information micro-storage to the observation of biological processes. One of the forefront techniques in this area is using the fluorescence lifetime as the readout modality, which is independent of sample concentration and measurement methods, hence providing more reproducible and quantitative outputs compared to conventional fluorescent barcoding. However, as an intrinsic photophysical property, fluorescence lifetime has previously been difficult to spatially and temporally control using external stimuli and challenging to monitor the coding progression and evolution of specific coding areas in real-time.

In this chapter, a two-component photo-switchable nanogel was designed which exhibited variable fluorescence lifetime upon photoisomerization involved energy transfer processes. This light-responsive fluorescence lifetime could be visually mapped using fluorescence lifetime imaging microscopy, allowing selective storage and reading of information at the microscale. To exploit the applicability of reversible barcoding in a biologically relevant context, the lifetime barcoding nanogel was investigated in live-cell and selective labeling of sub-cellular organelles. Most importantly, the reversibility of this system further provides a strategy for increasing image contrast without the need for extra-long fluorescence lifetime which paves the way for better resolution in fluorescence lifetime imaging microscopy.

4.2 Introduction

4.2.1 Micro Barcoding

With increasing attention directed to exploring microscale events, more effective tools are needed to fully understand processes at the micro-level.[1] Micro-barcoding is a versatile technique that provides multiplex and high-throughput information storage for micro- and nanoscale applications across the fields of biological, medicinal, and material sciences (Figure 4.1).[2, 3] Among them, optical multiplexing or fluorescent barcoding has recently attracted increasing interest, largely owing to its high sensitivity, fast signaling, and minimally invasive nature.[4-8] However, current fluorescent barcoding techniques mainly rely on the use of spectral multiplexing and fluorescence intensity encoding, which are typically susceptible to spectral overlap of the encoding elements. Moreover, obtaining a quantitative readout is a major challenge as a consequence of the variability of sample concentration and external microenvironment.

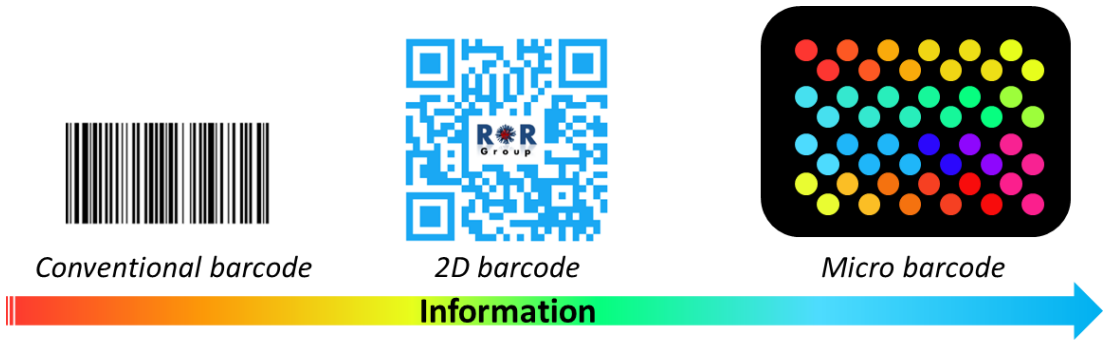

Figure 4.1 The evolution of the commonly used barcoding techniques for information storage.

4.2.2 Fluorescence Lifetime Barcoding

One of the forefront techniques to provide reproducible output in the micro barcoding area is utilizing fluorescence lifetime, an intrinsic photophysical property that is independent of the local fluorophore concentration and the method used for measurement.[9, 10] Fluorescence lifetime imaging microscopy (FLIM) is a state-of-the-art microscopy technique that provides an absolute measurement of fluorescence lifetime based on direct detection of the local fluorescence lifetime pixel-by-pixel at the cellular scale, without the influence of photobleaching or concentration (Figure 4.2).[11-14] Studying fluorescence lifetime with microscopic imaging techniques could be used as a straightforward technology to minimize the limitations in traditional fluorescence barcoding, providing a reproducible and quantitative readout over time.[10, 15, 16]

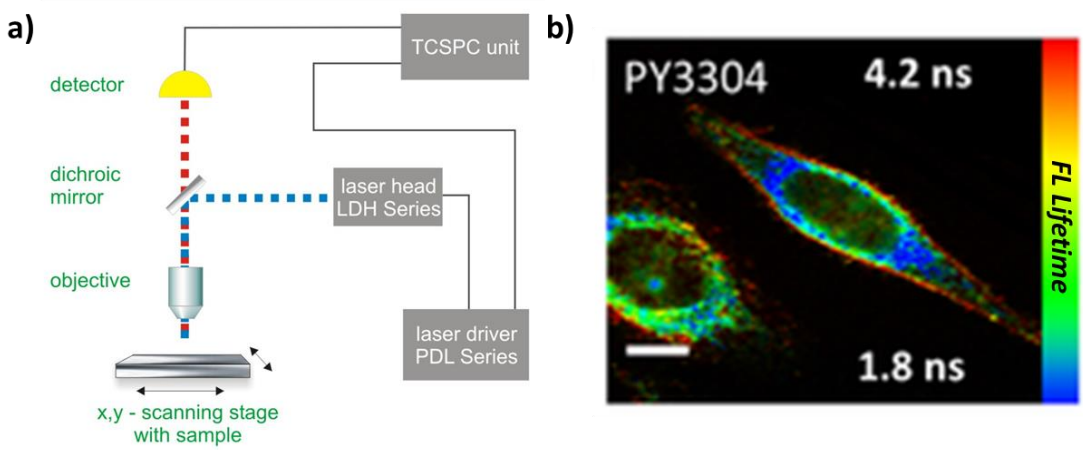

Figure 4.2 a) A schematic illustration of a typical fluorescence lifetime imaging microscope equipped with Time-Correlated Single Photon Counting (TCSPC); b) An example FLIM image of live HeLa cells stained with polarity-sensitive dyes.[17] Figure adapted from PicoQuant company (a) and ref 17 (b).

Despite these advances, there are relatively few examples where the fluorescence lifetime can be finely controlled to achieve multiplex outputs. Until now, the application of fluorescence lifetime in micro-barcoding has been mainly exploited using inorganic fluorescent materials containing lanthanides and transition metals ions, in which the fluorescence lifetime can be modulated by altering their structural configuration and composition during synthesis (Figure 4.3).[18-22] However, the use of polymeric nanoparticles is rarely exploited in the fluorescent lifetime barcoding area to date.[23] The potential toxicity of heavy metal ions used in inorganic barcoding materials raises some concerns in regards to biological-relevant applications.[24] Moreover, the inorganic matrices applied in barcoding are less responsive to external stimuli, as the fluorescent lifetime is generally inflexible and unadjustable in real-time.[25] Therefore, spatiotemporal manipulation of the coding progression and selective highlighting of specific coding areas is limited.

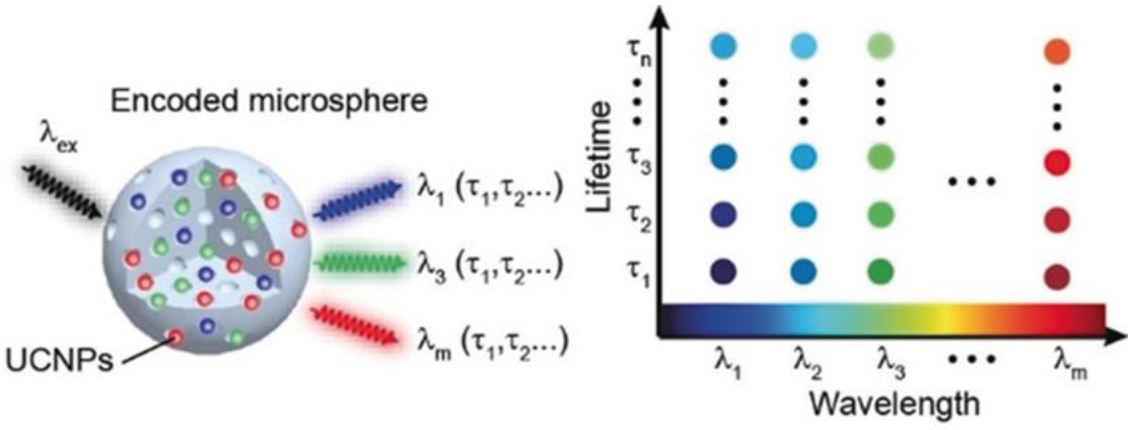

Figure 4.3 Wavelength and Lifetime barcoding strategy based on the inorganic upconversion nanoparticles (UCNPs)[19]. Figure adapted from ref 19.

4.2.3 Light Responsive Materials

Light, as a non-invasive stimulus, is a perfect tool to achieve external manipulation without the need for physical contact, hence being ideal for information imprinting, real-time labeling, and selective tracking.[26-30] Illumination responsive molecules are commonly based on a reversible photoisomerization process, in which the dynamic chemical and physical properties are in response to the light irradiation.[31] Spiropyran derivatives, as one of the most commonly used photochromic molecules, undergo a photo-cyclic reaction in which the six-member ring opens or closes *via* light illumination. (Figure 4.4) This photo-controllable reaction leads to two isomerization products, which have dramatic differences in hydrophilicity and absorption properties.

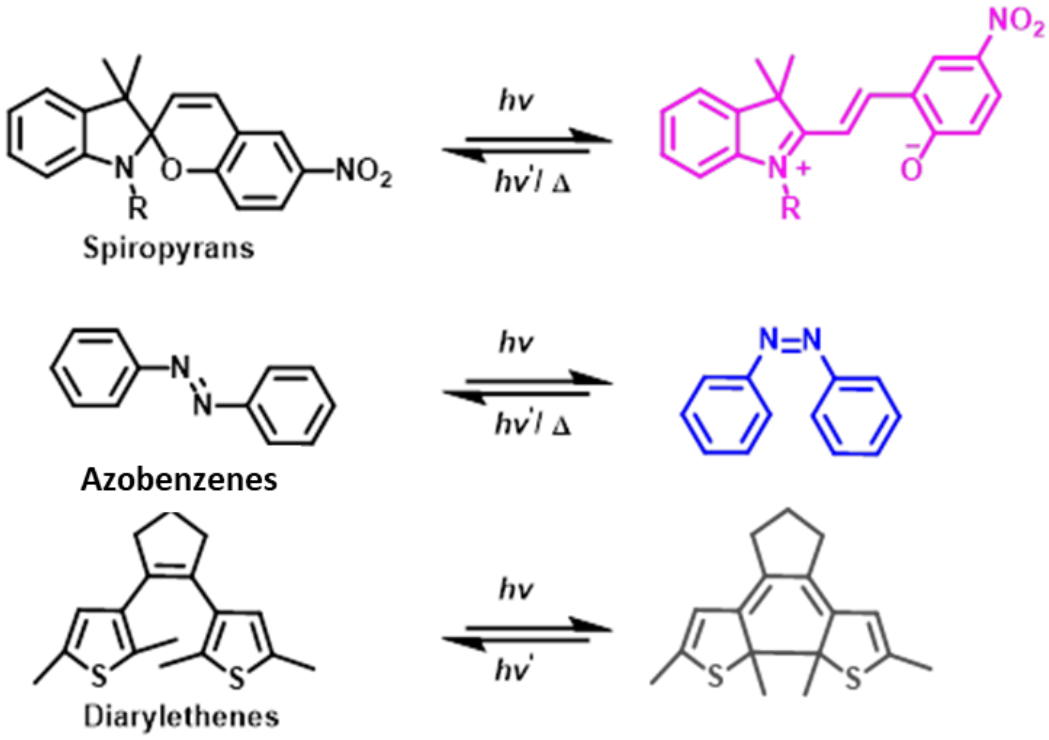

Figure 4.4 Three reported photochromic compounds involving reversible photoisomerization.

Due to these dynamic changes in chemical and physical properties, the multi-state of the light-responsive materials offer great advantages in information storage and bio-imaging, especially in optical anti-counterfeiting.[32-35] Meanwhile, photoresponsive fluorescence properties can enable excellent localization precision during the dynamic process, which was largely applied in the super-resolution imaging field. In 2018, the Françisco group reported a novel borondipyrromethene (BODIPY) based photochemical barcode system in which the multiple but distinguishable fluorescence information of the compound could be imprinted in vivo with unprecedented spatial and temporal control (Figure 4.5).[25] Though promising, changing the fluorescent lifetime during the photoisomerization processes has received little attention, mainly due to the prevalence of using small-molecule fluorophores in two-component systems which exhibit short fluorescence lifetime, limiting the applicability of this technique.[36]

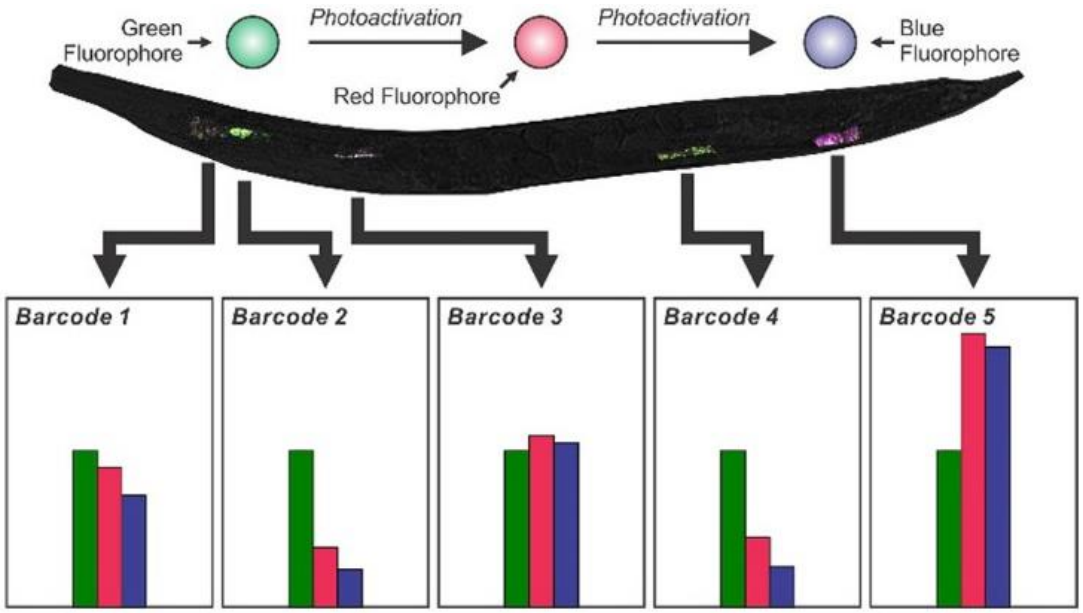

Figure 4.5 Real-time monitoring of the borondipyrromethene (BODIPY) based photochemical barcodes in different stages of the living nematode.[25] Figure adapted from ref 25.

4.2.4 Fluorescent Lifetime of Substituted Maleimides in Polymeric Nano-assemblies

Substituted maleimides represent a versatile class of fluorophore distinguished by their small size, bright fluorescence emission and the ease with which their fluorescent properties can be tuned by carefully selecting the nature of the substituents and modifying the fluorophore microenvironment.[37-39] As previously reported by our group (Figure 4.6), the encapsulation of dithiomaleimides (**DTM**) in a hydrophobic

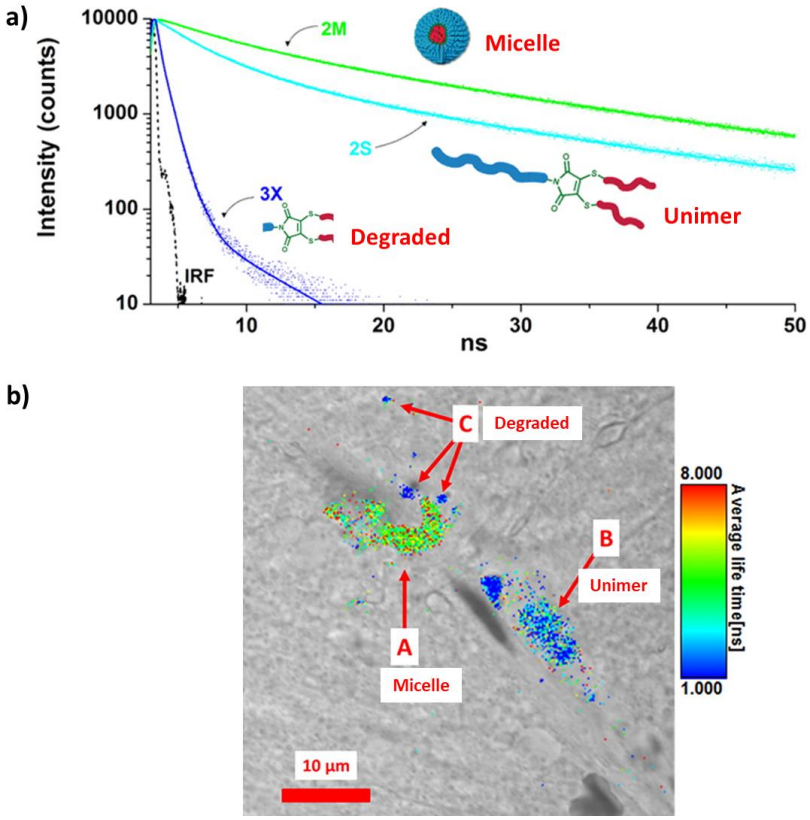

Figure 4.6 a) Fluorescence lifetime decays of the DTM fluorophores in different assembly states. b) FLIM image of the DTM functionalized nanoparticles in rat hippocampal tissue. Different color indicating the different assembly states of the polymeric nanoparticles.[40] Figure adapted from ref 40.

environment, such as the core of an amphiphilic polymeric assembly, significantly increases the fluorescence lifetime by eliminating both self-quenching caused by **DTM** dye aggregation and collisional quenching from the surrounding solvent.[40, 41] In comparison to inorganic fluorophores, small molecule fluorophores like substituted maleimides are promising due to lower cell toxicity and easily tuneable fluorescent properties, therefore representing a potential tool for barcoding applications.[14, 42-44]

In this study, we designed a lifetime photo-responsive barcoding system based on a two-component nanogel involving substituted maleimides and a spiropyran (**SP**) switch. Through inducing switchable photoisomerization processes *via* irradiation with the ultraviolet light, a fluorescence energy transfer event was observed from the **DTM** fluorophore to the ring-opened form of the **SP** photochrome, allowing reversible alteration of the fluorescence lifetime of the maleimide fluorophore and hence achieving lifetime coding in a controllable, non-invasive fashion. Moreover, a self-correction method could be used to increase the sensitivity of the fluorescence lifetime imaging microscopy, providing a higher level of information stored in the micro-scale. As a proof-of-concept, the switchable nanogel was functionalized with a mitochondrion targeting linker and lifetime photoswitch. This was visualized at both the cellular and subcellular scales in living cells showing applicability for monitoring cellular functions.

4.3 Results and Discussion

4.3.1 Design and Synthesis of the Monomers

Fluorescence lifetime, as a direct measurement of the time-resolved fluorescence decay, is closely related to the structure of a molecule and the interaction with its micro-environment.[45] In this study, the tailoring of fluorescence lifetime relies on modulating the FRET process, which has been proved to be a practical tool for controlling the fluorescence properties through long-range dipole-dipole coupling.[46] An effective applicable FRET system requires a suitable distance and appropriate spectral overlap between the two molecules.[47] To ensure that spectral criteria are met, the correct selection of the FRET building blocks is paramount. Dithiomaleimide was chosen as a fluorescence donor owning to its strong emission and sufficiently long fluorescence lifetime in a hydrophobic environment.[40, 41, 48]

Compared with commonly used small-molecule fluorophores, the uniquely long fluorescence lifetime of dithiomaleimide dyes in hydrophobic environments allow both (i) a relative wide lifetime range for more diverse fluorescence lifetimes with minimum overlap and (ii) to achieve high resolution in a biologically relevant context, representing a distinct advantage over commonly used organic dyes, whose lifetimes are usually interfered by cellular autofluorescence, introducing unwanted noise.

A photochromic molecule, like spiropyran (**SP**) derivatives, is able to undergo a conformational change in response to light irradiation at certain wavelengths.[49] Hence, the incorporation of the photochromic **SP** as the FRET acceptor could realize a photoswitchable FRET process based on the light-responsive absorption spectrum

which overlaps well with the **DTM** emission. Therefore, selectively varying the spectral overlap between the donor and acceptor will control the efficiency of the FRET process, leading to further regulation of the fluorescence lifetime (Figure 4.7).

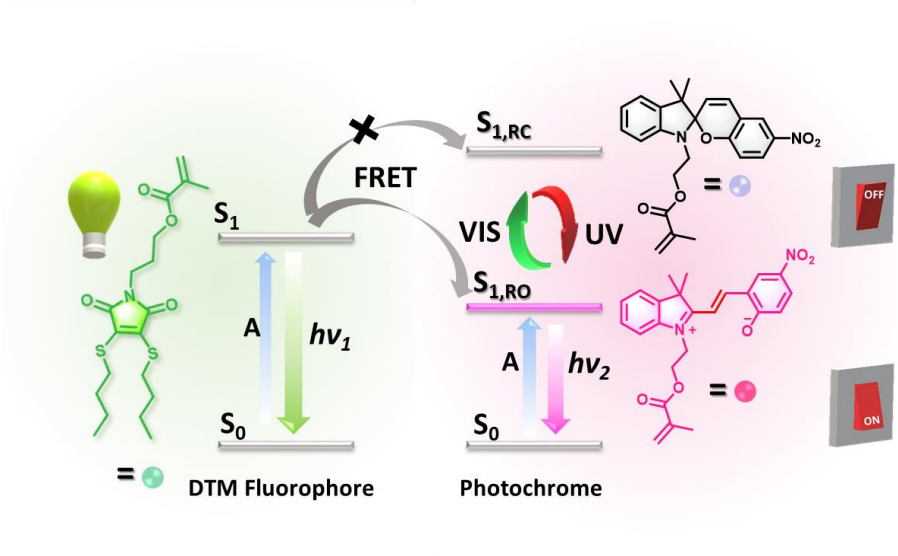

Figure 4.7 Schematic illustration of energy transfer between the singlet state of **DTMMA** and the different singlet states in ring-opened and closed stated of **SPMA** as the switch.

4.3.2 Synthesis of the Dithiomaleimide and Spiropyran Monomers

The methacrylate **DTM** monomer was synthesized over four steps (Figure 4.8), leading to the fluorescent **DTM** intermediate with the hydroxyl functional handle. The final product 3-(3,4-bis (butylthio) -2,5-dioxo-2,5-dihydro-1H-pyrrol-1-yl) propyl methacrylate (**DTMMA**) was synthesized through an esterification reaction. The methacrylate **SP** monomer was synthesized through the four steps reactions followed over four steps following a previously reported method (Figure 4.9).[50, 51] All synthesized compounds were characterized by ^{1}H-NMR, ^{13}C-NMR spectra, and HRMS.

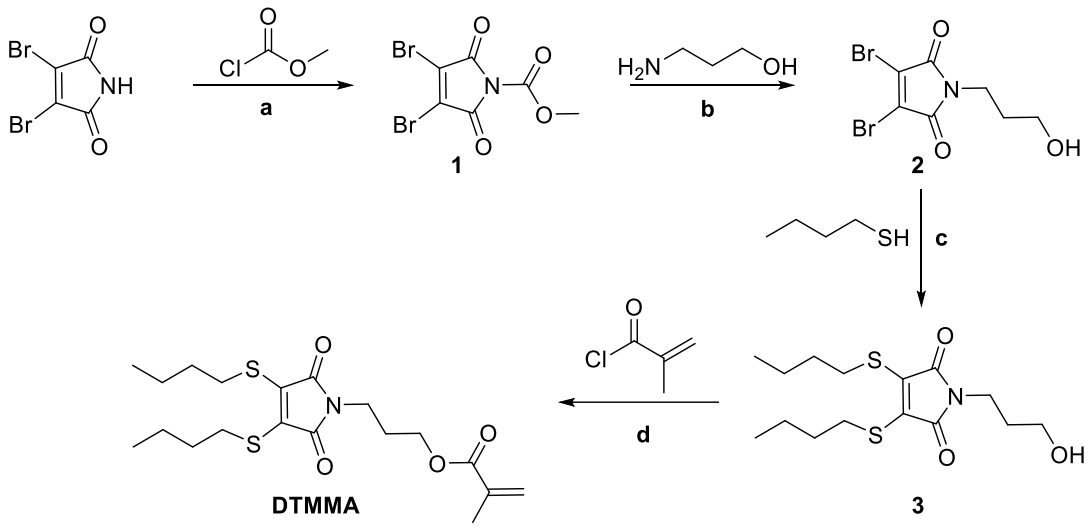

Figure 4.8 Synthetic route for monomer **DTMMA**. (a) N-methyl morpholine (NMM), THF, room temperature, 4 h; (b) CH_2Cl_2, room temperature, overnight; (c) Triethylamine, THF, room temperature, 16 h; (d) Triethylamine, CH_2Cl_2, room temperature, overnight.

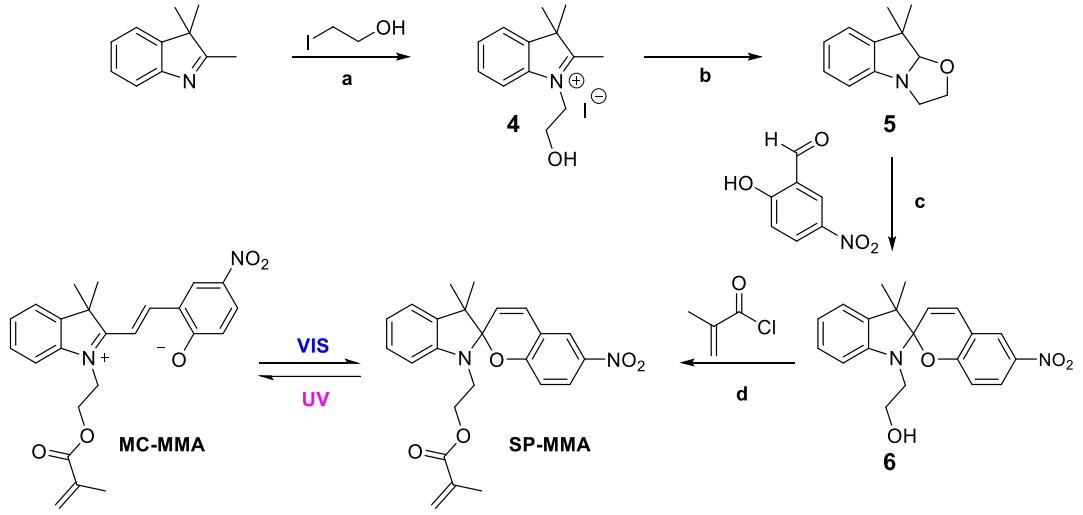

Figure 4.9 Synthetic route for monomer **SPMA**. (a) MeCN,, reflux, 24 h; (b) KOH solution, room temperature, 30 minutes; (c) Ethanol, reflux, 4 h; (d) Triethylamine, CH_2Cl_2, room temperature, overnight.

4.3.3 Preparation of Two-component Nanogels

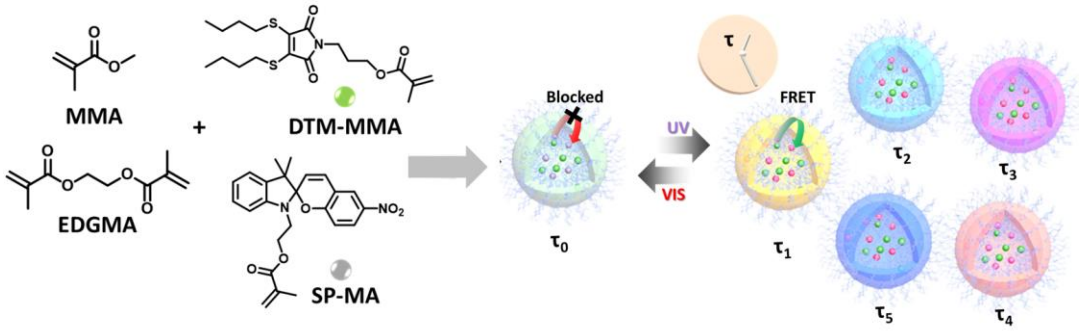

Figure 4.10 Schematic representation of the preparation of light-triggered fluorescence lifetime switchable nanogels *via* emulsion polymerization

In order to protect the DTM and SP from being influenced by the microenvironment, emulsion polymerization was selected as a straightforward technique to prepare a stable cross-linked polymer network. Methacrylate **DTM** and **SP** monomers were copolymerized in a nanogel *via* a simple one-pot micro-emulsion polymerization, with methyl methacrylate (MMA) as the hydrophobic matrix and ethyleneglycol dimethacrylate (EGDMA) as crosslinker (Figures 4.10).[52] The MMA emulsion was initially stabilized in water by sodium dodecyl sulfate (SDS) and potassium persulfate was chosen to initiate the polymerisation at 70 °C. The resulting nanogels were purified by filteration through a 0.45 μm Nylon syringe filter and dialysis (MWCO 3.5 kDa) against water to remove the remaining KPS.

The Degree of functionalization (DoF) and Cross-linking density (CLD) were calculated using following equations:

Degree of functionalization of **SPMA**:

$$DoF(mol\%) = \frac{[SPMA]}{[MMA + SPMA + DTMMA]} \times 100 \qquad (4.1)$$

Degree of functionalization of **DTMMA**:

$$DoF(mol\%) = \frac{[DTMMA]}{[MMA + SPMA + DTMMA]} \times 100 \qquad (4.2)$$

Cross-linking density of EGDMA:

$$CLD(wt\%) = \frac{2 \times Mass_{EGDMA}}{Mass_{MMA}} \times 100 \qquad (4.3)$$

In order to understand the effect of energy transfer on fluorescence lifetime properties, we constructed a series of crosslinked nanogels with different ratios of **DTMMA** and **SPMA** formed *in situ* during the polymerization (**N1-5**).

Table 4.1 Chemical composition and size characteristics of polymeric nanogel.

No.	SPMA DoF	DTMMA DoF	DoF Total	CLD	DLS[a]	
					D_h(nm)	PD
1	0.00	0.05	0.05	0.01	26.1±0.3	0.12
2	0.05	0.05	0.10	0.01	24.4±0.5	0.12
3	0.20	0.05	0.25	0.01	26.8±0.4	0.09
4	0.40	0.05	0.45	0.01	32.9±0.5	0.09
5	0.20	0.00	0.20	0.01	22.3±0.3	0.09

a. D_h and PD were average values measured 4 times from DLS analysis.

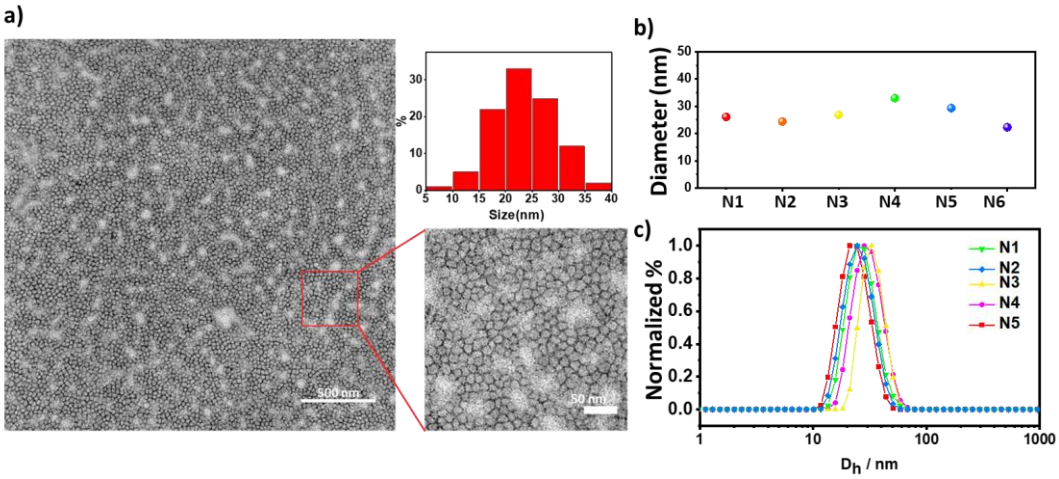

Figure 4.11 a) Dry state TEM images of nanogel (**N4**), which illustrate the spherical morphology and histogram of observed size distributions (stained with 1 wt. % uranyl acetate in water); b) Size distributions and c) corresponding hydrodynamic diameters of nanogels with variable **SMPA** and **DTMMA** ratios, obtained by DLS (detection angle = 173°) carried out in water at 25 °C (DoF: Degree of functionalization, D_h: hydrodynamic diameters, PD: Dispersity).

The hydrodynamic diameters of the nanogels in water were measured by dynamic light scattering (DLS). The relative amount of the hydrophobic SMPA monomer affected the size of the nanogel, resulting in the observed range of hydrodynamic diameters (22 to 32 nm). All samples had a low polydispersity (PD<0.15) (Table 4.1). Dry state transmission electron microscopy (TEM) further confirmed the spherical morphology of the nanogel with the uniform morphology (Figure 4.11a). Choosing N4 as the example, the size distribution from TEM was mainly located in the 15-30 nm range which compared well with the hydrodynamic diameters calculated from DLS measurement (33 nm). The small difference between the results could be a result of the drying process in TEM sample preparation.

4.3.4 Evaluation of the Energy Transfer in the Photoisomerization Process

As the FRET donor, the fluorescence emission of a nanogel containing only DTM was first investigated by steady-state fluorescence measurements. As the fluorescent donor, **DTM** was protected by the crosslinked polymeric environment from quenching by the protic solvent, leading to green emission in the range of 450-600 nm. The relative quantum yield (φ_d) of the nanogel containing only DTM (**N1**) in aqueous solution was calculated using 5-(6)-carboxyfluorescein (5(6)-FAM) as the standard reference (φ_{st}=92%). The emission of both 5(6)-FAM and **N1** were excited at 445 nm and the integration of the emission was linearly related to the absorption at the same wavelength. By comparing the slope of the reference and **N1**, the relative quantum yield of **N1** was calculated as 51% in aqueous solution (Figure 4.12).[52]

As mentioned above, an applicable FRET system requires a suitable distance and appropriate spectral overlap between the donor and acceptor molecules. In the nanogel

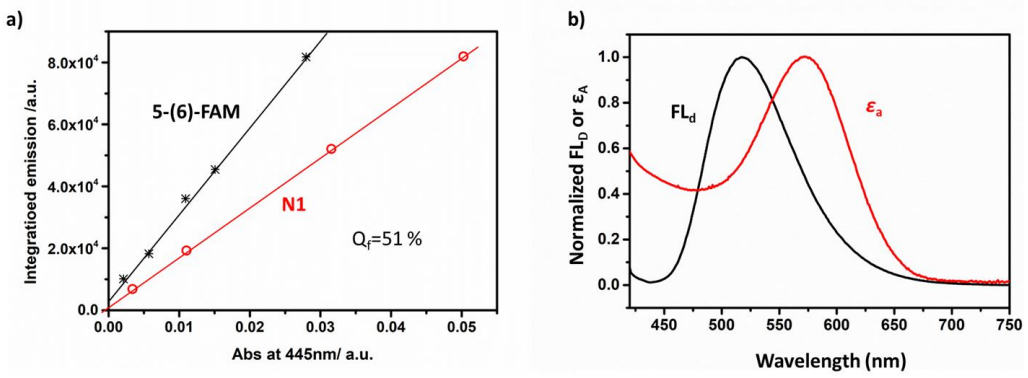

Figure 4.12 Estimation of Relative Quantum Yield of the nanogel **N1**. a) A linear fit of the integrated emission of **N1** and 5-(6)-FAM with absorption at 445 nm; b) Fluorescent emission of **N1** (black line) and the molar extinction coefficient of ring-opened form of SPMA (red line).

system, the DTM as the fluorescence donor emits between 450 to 600 nm, which overlaps well with the absorption of the FRET donor **SP** in its ring opened form after UV (365 nm) light irradiating (Figure 4.13). Therefore, the photoisomerization of **SP** leads to a change in the absorption at 500 to 600 nm which overlap well the emission spectrum of **DTM**, offering an ideal scenario for an effective FRET system to be achieved (Figure 4.13). While the ring closed form of SP was formed by vis light (520-550 nm) irradiation, the absorption peak around 580 nm of **SP** was switched off which blocked the effective FRET path.

The energy transferability between the donor (**DTM**) and acceptor (ring-opened **SP**) was quantitatively determined as the Förster radius (R_0) which is the distance at which50% FRET efficiency is achieved.[53, 54] The overlap integral of the fluorescence

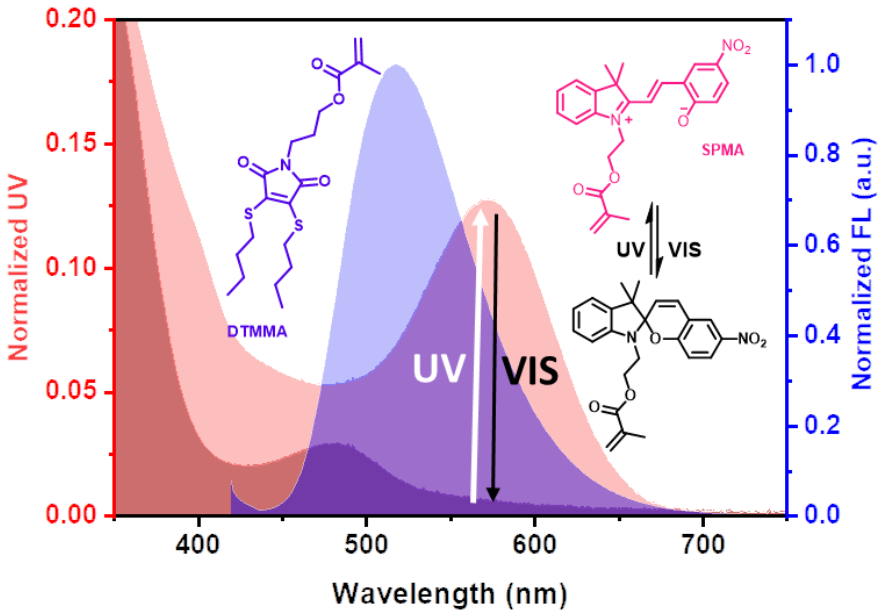

Figure 4.13 Spectra overlap between the emission of the **DTMMA** (blue) and absorption of the **SPMA** (open and closed form, red).

emission spectrum of the donor and the absorption spectrum of the acceptor was calculated as $J(\lambda)$ which is dependant on the normalized donor fluorescence spectrum ($F_d(\lambda)$) and the molar extinction coefficient (M^{-1} cm^{-1}) of the acceptor ($\varepsilon_a(\lambda)$) according to the following equations. The R_0 of the **DTM** and ring-opened form of **SP** was estimated to be 18 Å (Table 4.2).

$$J(\lambda) = \int \varepsilon_a(\lambda) F_d(\lambda)\, \lambda^4 d\lambda \qquad (4.4)$$

ε_a: The molar extinction coefficient of the acceptor. $F_d(\lambda)$:The fluorescence intensity of the donor in the absence of the acceptor. λ: The wavelength. R_o the critical Förster distance for 50% FRET efficiency, is defined by following equations.[49, 53-55]

$$R_0 = \left\{ \frac{9ln10\langle\kappa^2\rangle\varphi_d J(\lambda)}{128\pi^5 n^4 NA} \right\}^{\frac{1}{6}}$$

$$= 0.02108 \left[\frac{\kappa^2 \phi_d J(\lambda)}{n^4} \right]^{1/6} \qquad (4.5)$$

$<\kappa^2>$: The average squared orientational part of dipole-dipole interaction between donor and acceptor. Here, $<\kappa^2>$ was assumed to be 2/3 which corresponded to the random orientation of donor and acceptor during the excited state.[56] φ_d :The fluorescent quantum yield of the donor fluorophore, in this system φ_d is the fluorescence quantum yield of the nanogel containing only DTM (**N1**) calculated *via* the relative method. n: The refractive index. In this system, n is 1.45 for MMA. N_A: Avogadro constant.

Table 4.2 Photophysical data of FRET between **DTM** and ring-opened **SP**.

Donor	**Acceptor**	φ_d	$J(\lambda)$ **(M^{-1} $cm^{-1}nm^4$)**	R_0 **(nm)**	$D_{effective}$ **(nm)**
DTMMA	SPMA	0.51	5.4E+12	1.8	≤3.6

4.3.5 Simulation of the Energy Transfer in Photoisomerization Process*

To gain further insight into the energy transfer interactions between **SP** (Ring opened form and closed-form) and **DTM**, time-dependent density functional theory (TD-DFT) calculations were carried out. To obtain the most stable conformations of **DTMMA** and ring-closed **SPMA**, a Monte Carlo conformational search was performed using the OPLS force field (for each system 1000 conformational search steps were performed)[57, 58]. The 20 lowest-energy structures were selected and re-optimized using the B3LYP[59, 60] and CAM-B3LYP[61] functionals and the 6-311G(d,p) basis set.[62, 63] It is worth noting that both DFT methods coincided with the same lowest-energy structures. Additional optimization processes were also performed using the M06-2X[64] and PBE1PBE[65] functionals and the 6-311G(d,p) basis set. The dispersion effects (in exception of the M06-2X functional) and the solvent were included in all the optimization processes. The D3-Grimme's dispersion[66] with Becke-Johson damping factor[67, 68] was used to evaluate the dispersion effects. The solvent was considered using the polarization continuum model (PCM)[69, 70] and the dielectric constant of cyclohexane (ε= 2.0165). The ring-opened **SPMA** geometry was obtained from the modification of the lowest-energy ring-closed **SPMA** conformation. The harmonic vibrational frequencies were also calculated to verify that all the stationary points were minima of their potential energy surface (Figure 4.14).

* The simulation results were carried out by Dr. Miquel Torrent-Sucarrat

These structures (**DTMMA** and ring-closed and ring-opened **SPMA**) were used for the TD-DFT calculations[71, 72] (B3LYP, CAM-B3LYP, M06-2X, and PBE1PBE) to describe the absorption and emission (geometry optimization of the first singlet excited

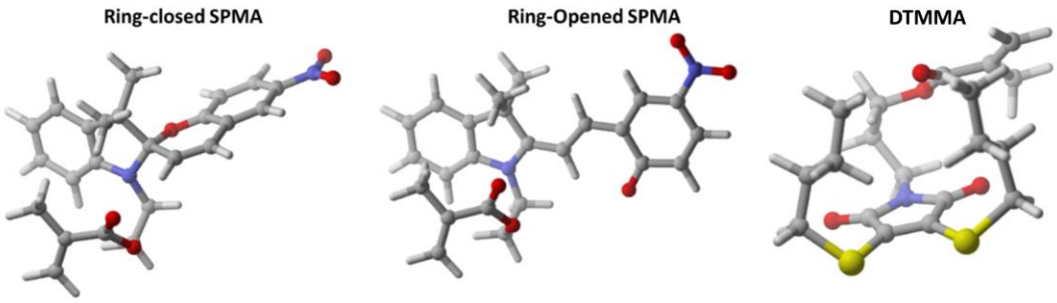

Figure 4.14 Optimized conformations of **DTMMA** and **SPMA** performed a Monte Carlo conformational search using the OPLS force field.

state) processes. In the TD-DFT calculations, 50 excited states were considered. The Macromodel[73] and Maestro[74] software packages were used to carry out the conformational search. All the remaining calculations (geometry optimizations, frequencies, and TD-DFT) were performed using the Gaussian 16 program package.[75] The B3LYP and PBE1PBE functionals predicted very similar excitation and emission energies. The lowest-energy absorption values corresponded to HOMO → LUMO transitions, which mainly represent π bonding and π* antibonding interactions. In **DTMMA** and ring-closed **SPMA** systems, the π conjugation was found to be mainly located on the dithiomaleimide ring and the phenyl of the indoline unit, respectively. Conversely, in the ring-opened **SPMA**, the π conjugation was placed along almost across the whole structure. The photophysical parameters obtained from the CAM-

* The simulation results were carried out by Dr. Miquel Torrent-Sucarrat

B3LYP and M06-2X functionals indicated a blue shift displacement between 50 and 100 nm with respect to the obtained B3LYP and PBE1PBE results.

According to the theoretical TD-DFT results, the values of the first singlet excited states of **DTM** and ring-closed and ring-opened **SP** structures are 2.7, 3.1, and 2.4 eV, respectively. (Figure 4.15) These results indicated that the FRET from **DTM** to the ring-closed **SP** was blocked and the only allowed FRET was to the ring-opened **SP** conformation.

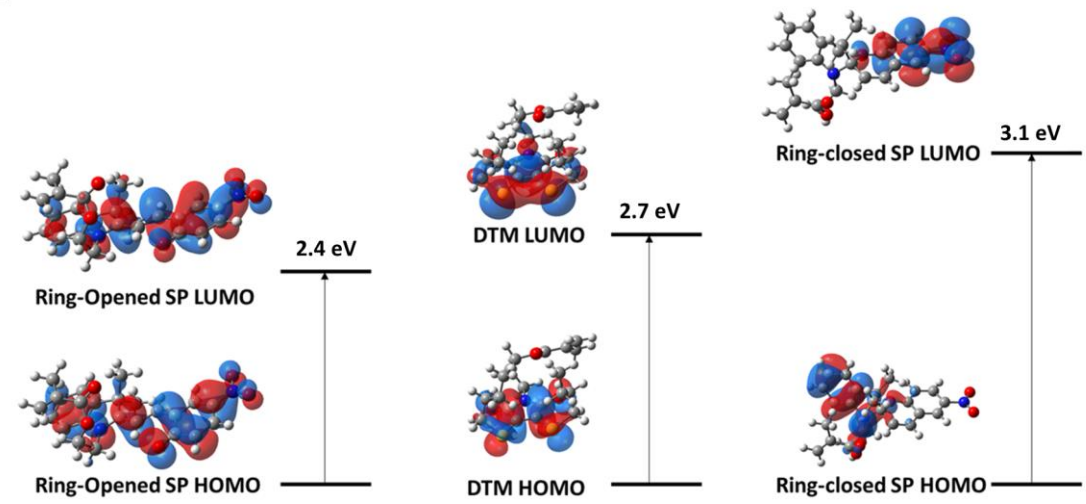

Figure 4.15 Schematic illustration of HOMO and LUMO isosurfaces of **DTMMA** and **SPMA** with their first singlet excitation energies in a non-polar environment based on DFT and TD-DFT calculations.

*The simulation results were carried out by Dr. Miquel Torrent-Sucarrat

4.3.6 Photophysical Behaviour of Nanogels *via* Light Manipulation

The high quantum yield of nanogel **N1** in aqueous solution proved that the fluorescence of maleimides was maintained in the hydrophobic environment of the nanogel and this could provide a fluorescent platform for further manipulation. As a comparison, the nanogel containing **DTM** and **SP** (**N2-4**) was investigated. Upon irradiating the nanogel solution (**N2-4**) under UV light (365 nm, Figure 4.16a), the green emission of **DTM** channel ($\lambda_{em,max}$=520 nm) was observed to decrease gradually while a new peak around

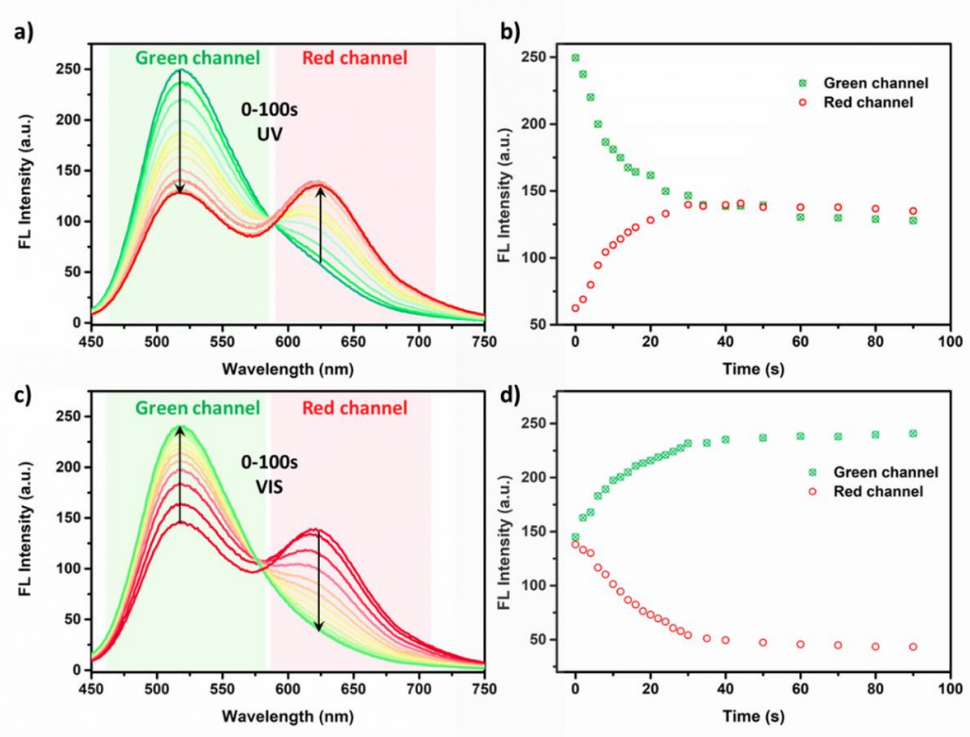

Figure 4.16 a) Emission spectra of nanogel **N4** after UV light irradiation for 0-100 s; b) Emission intensity changes at DTM channel (510 nm) and SP channel (610 nm) after UV light irritating for 0-100 s c) Emission spectra of nanogel **N4** after vis light irradiation for 0-100 s; d) Emission intensity changes at DTM channel (510 nm) and SP channel (610 nm) after vis light irritating for 0-100 s (λ_{ex}=410 nm, slit width: Ex. = 1 nm, Em. = 1 nm; C_{N4}=0.5 mg mL^{-1}).

610 nm emerged The quenching effect in the **DTM** emission indicated an effective FRET donor/acceptor pair forming between the **DTM** and ring-opened form of **SP**. As anticipated, the recovery of **DTM** emission was observed following visible light irradiation (λ ≥550 nm) in which the FRET process was blocked by switching the **SP** back to the ring closed form (Figure 4.17a). The kinetics of fluorescence intensity against UV irradiation time in **N4**, for example, indicated the photoconversion process complete within 31 s of UV irradiation recovered within 40 s of vis light irradiation (Figure 4.16b). Such switching of fluorescence emission by alternation of UV and Vis irradiations could be repeated for 5 cycles (Figure 4.17b). A slight decrease in intensity in the red channel and an increase in the green channel were observed after irradiating the sample with light 10 times presumably as a consequence of the irreversible photo-oxidation side reaction in SP molecules.

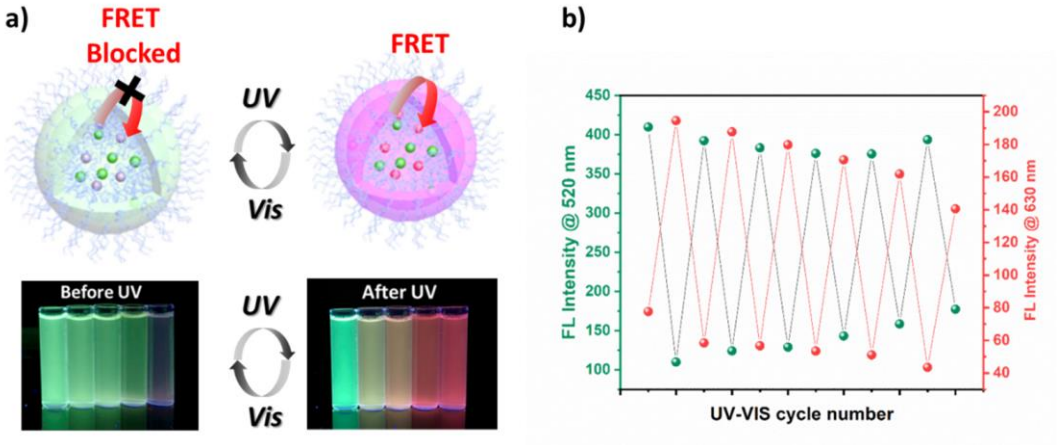

Figure 4.17 a) Fluorescence images of light-switchable nanogel solution (**N1-5**) before and after UV for 120 s; b) Fluorescence intensity cycling upon UV/Vis irradiation (the DTM channel was recorded at 520 nm and the SP channel was recorded at 630 nm, irradiation time: 120 s);

Different quenching effects on **DTM** emission in nanogels **N2-4** were observed after UV irradiation owing to the different efficiency of the FRET process (Figure 4.18 a-d).

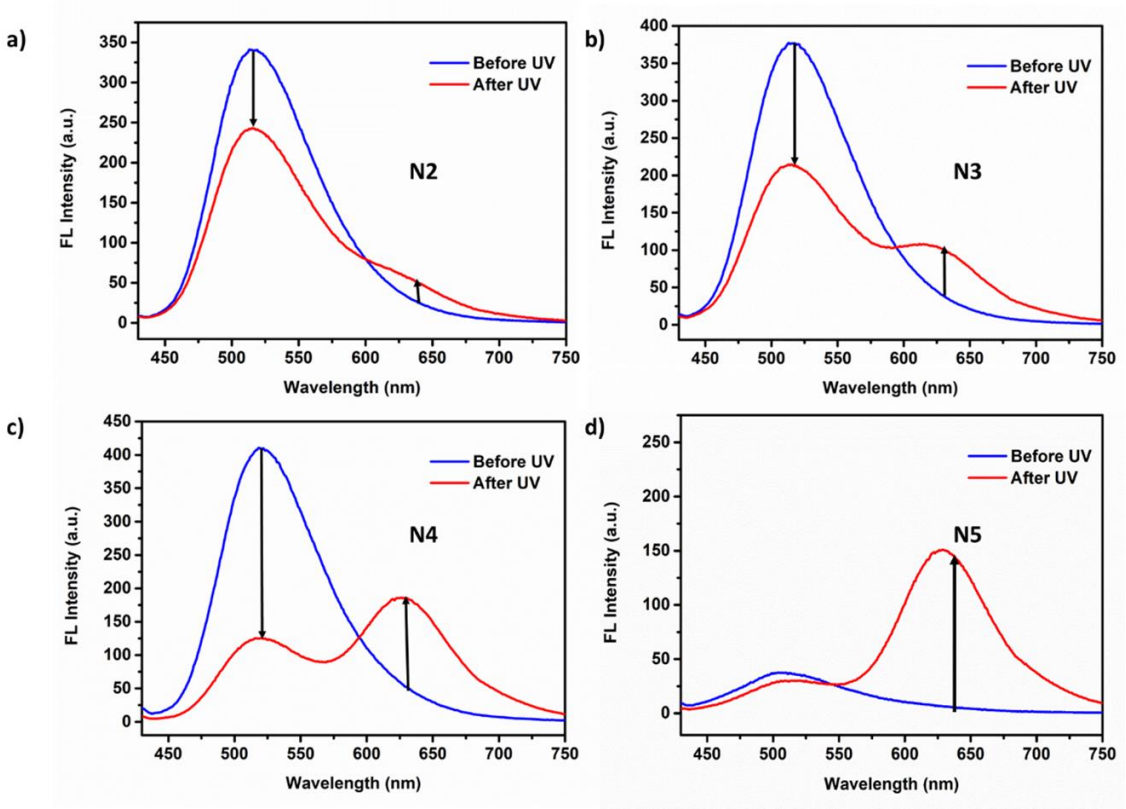

Figure 4.18 a)-d) Steady-state emission of nanogel **N2-N5** before and after UV for 120 s (λ_{ex}=410 nm, slit width: Ex. = 1 nm, Em. = 1 nm; C=0.5 mg/mL**).**

By increasing the **SP** from 0.025 mmol (**N2**) to 0.2 mmol (**N5**), the higher ratio of **SP**/**DTM** in these nanogels led to an enhanced quenching effect in the **DTM** channel (510 nm) as a result of the expanded spectral overlap. The different ratio of **SP**/**DTM** also led to the diverse emission colour from green to red after UV irradiating of the nanogels by which different energy transfer efficiency and photoswitch contrast could be selectively controlled. The colour change was calculated and summarized in CIE1931 colour spaces (Figure 4.19).

$$x = \frac{\mathrm{X}}{\mathrm{X} + \mathrm{Y} + \mathrm{Z}} \quad (4.6)$$

$$y = \frac{\mathrm{Y}}{\mathrm{X} + \mathrm{Y} + \mathrm{Z}} \quad (4.7)$$

$$y = \frac{\mathrm{Z}}{\mathrm{X} + \mathrm{Y} + \mathrm{Z}} = 1 - x - y \quad (4.8)$$

Where X, Y, Z are the Tristimulus values in the CIE 1931 systems, and x, y are the chromaticity coordinates. From Figure 4.19b, the increase of **SPMA** ratio resulted in a red shift of the emission colour which was consist with the emission observed under a UV lamp. Therefore, by tuning the ratio of the two monomers (**DTMMA** and **SPMA**), the emission colour was able to be selective varied from green to red.

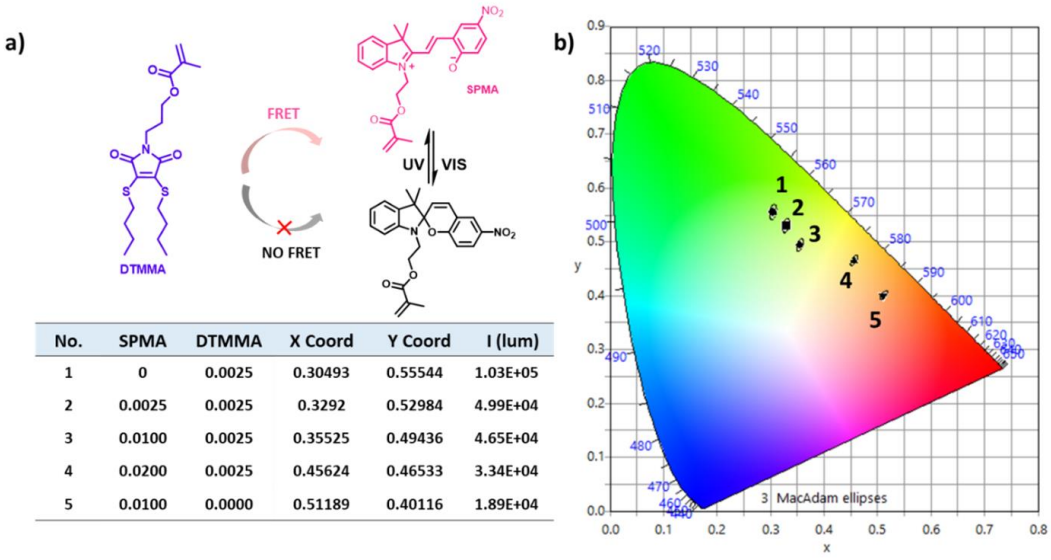

No.	SPMA	DTMMA	X Coord	Y Coord	I (lum)
1	0	0.0025	0.30493	0.55544	1.03E+05
2	0.0025	0.0025	0.3292	0.52984	4.99E+04
3	0.0100	0.0025	0.35525	0.49436	4.65E+04
4	0.0200	0.0025	0.45624	0.46533	3.34E+04
5	0.0100	0.0000	0.51189	0.40116	1.89E+04

Figure 4.19 a) Calculated CIE 1931 coordinate of the different nanogel (**N1-5**) from emission spectra; b) The summarized color change of N1-5 in CIE 1931 spectra after UV irradiation.

4.3.7 Light Stimulated Reversible Fluorescence Lifetime Performance

Based on the above preliminary results, we further investigated the fluorescence lifetime changing during this reversible photoisomerization process. A fluorescence lifetime imaging microscope (FLIM), equipped with a time-correlated single-photon counting (TCSPC) apparatus, was utilized in this study to investigate the fluorescence lifetime, and employed as the information decoding technique for further visualization of the localized fluorescence lifetime variation. FLIM is a state-of-the-art microscopy technique that provides an absolute measurement of fluorescence lifetime based on direct detection of the local fluorescence lifetime pixel-by-pixel at the cellular scale, which means there is negligible effect of photobleaching or concentration.[11-14]

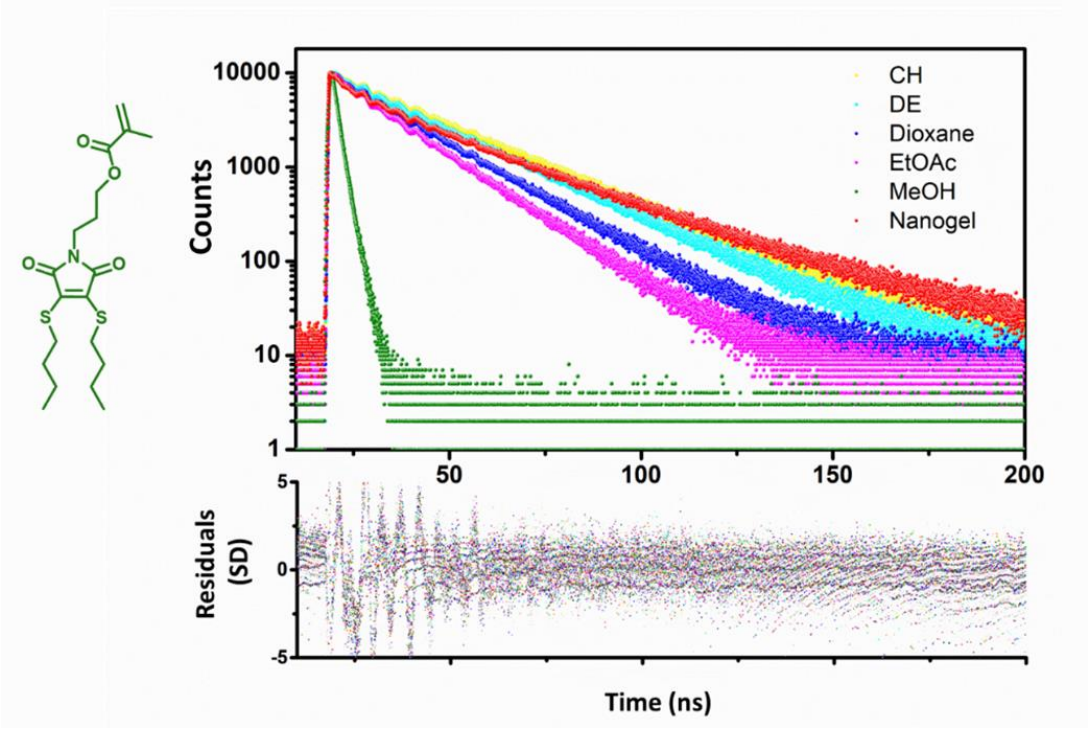

Figure 4.20 Fluorescence lifetime decay of the **DTMMA** small molecule in different solvents with fitting and residuals (bottom). CH: cyclohexane, DE: Diethyl ether, EtOAc: Ethyl acetate, MeOH: Methanol, Nanogel: **N1** (λ_{ex}=375 nm, λ_{em}=510 nm, Slit: ex=1 nm, em=1 nm).

The time-resolved fluorescence decay of fluorescent donor (**N1**) was firstly measured in the time range 1-100 ns excited by the pulsed laser (405 nm), and fitted by a sum of three exponential decays with a calculated intensity-averaged lifetime ($\tau_{Av,I}$) as 28 ns (Figure 4.20). A similar fluorescence decay was observed in a cyclohexane solution of small molecule **DTM** monomer, proving the hydrophobic environment in the nanogel

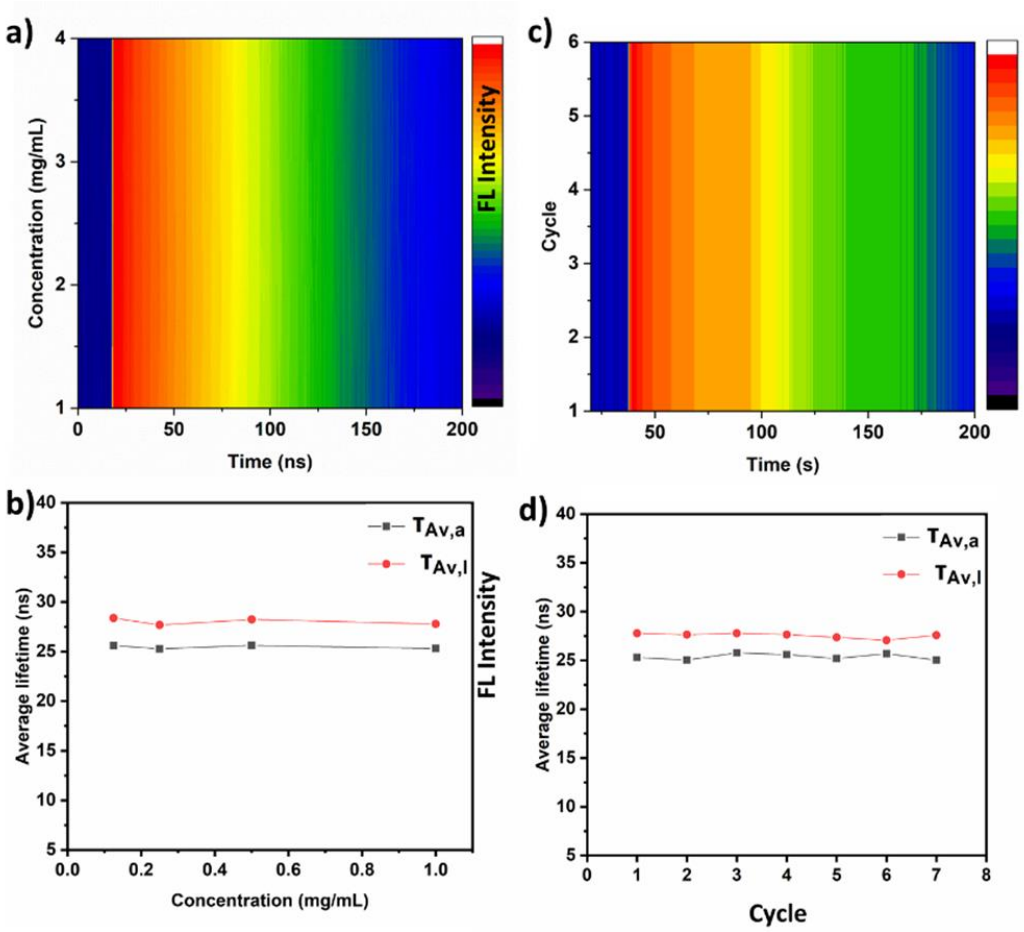

Figure 4.21 a) Fluorescence lifetime decay and b) average fluorescence lifetime of **N1** at different concentrations (1- 4 mg mL^{-1}) in water monitored under excitation with a pulsed laser (λ_{ex}=375 nm). c) Fluorescence lifetime decay and d) average fluorescence lifetime of **N1** upon alternating UV (120 s) and visible light (120 s) irradiation for 7 times (λ_{ex}=375 nm, C_{N1}=0.5 mg mL^{-1}). (χ^2<1.5)

prevents the **DTM** being quenched by water.[41] Meanwhile, nearly identical fluorescence decays of **N1** were observed when changing the concentration (1-4 mg/mL) or reversibly exposing the nanogel to UV and visible light (6 cycles), leading to a stable and sufficient lifetime platform for further manipulation (Figure 4.21).

To this end, time-resolved fluorescence decay of the nanogel (**N2-4**) was conducted *in situ* after irradiating with UV for 120 s. By varying the emission channels in 2D time-resolved fluorescence decay spectra, a decrease of the fluorescence lifetime of **N4** solution in the **DTM** channel ($\lambda_{em,max}$=520 nm, Figure 4.22) was observed, while a new fluorescence decay of ring-opened SP appeared from 600 nm to 650 nm, in comparison with **N1** solution. The overall trend indicates that the fluorescence lifetime was successfully influenced by the FRET process between the **DTM** and ring-opened **SP**. The determination of the intensity average lifetimes ($\tau_{Av,I}$) and amplitude average lifetimes ($\tau_{Av,A}$) were conducted using the following equations (Details in experimental part):

$$\tau_{Av,I} = \frac{\sum A_i \tau_i^2}{\sum A_i \tau_i}$$

$$\tau_{Av,A} = \frac{\sum A_i \tau_i}{\sum A_i}$$

The average fluorescence lifetime histograms of **N1-4** were recorded after the excitation pulse over time and this provided a real-time method to monitor the changes in lifetime (Figure 4.23a). As depicted in figure 4.23b-c, the $\tau_{Av,I}$ in **N1-4** can be tuned from 15 to 28 ns respectively after UV irradiation which is linearly related to the ratio of the two monomers (Table 4.3). Herein, the ratio of the two monomers plays an

important role in rationally designing the fluorescence lifetime after UV irradiation. Meanwhile, the overall decay of lifetime in **N4** solution, as the example, was fully reversible for 4 cycles by altering the UV and visible light without any measurable decrease (Figure 4.24).

The fluorescence lifetimes of the nanogel **N1-N4** in solution state were further visualized by FLIM, in which the different colour reflected the simultaneous lifetime (Figure 4.25). Meanwhile, the FL lifetime histogram was further calculated from the

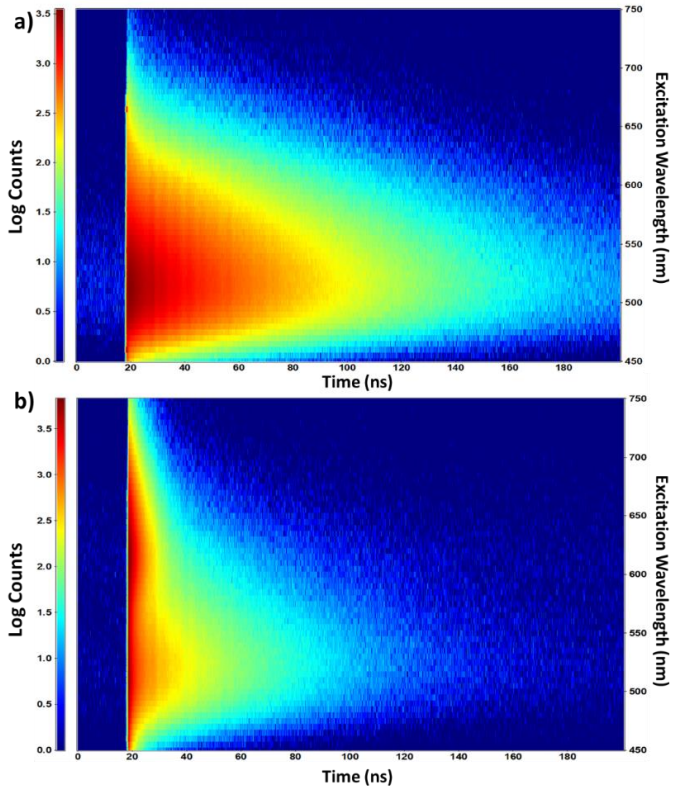

Figure 4.22 a) 2D Fluorescence lifetime decay of **N1** after UV irradiation (120 s); b) 2D Fluorescence lifetime decay of **N4** after UV irradiation (120 s); 2D Fluorescence lifetime was recorded under the continuous excitation of the nanogel solution (C =0.5 mg mL^{-1}) with a pulsed laser (λ_{ex}=375 nm). Fluorescence lifetime decays were monitored at different emission wavelengths with 5 nm steps.

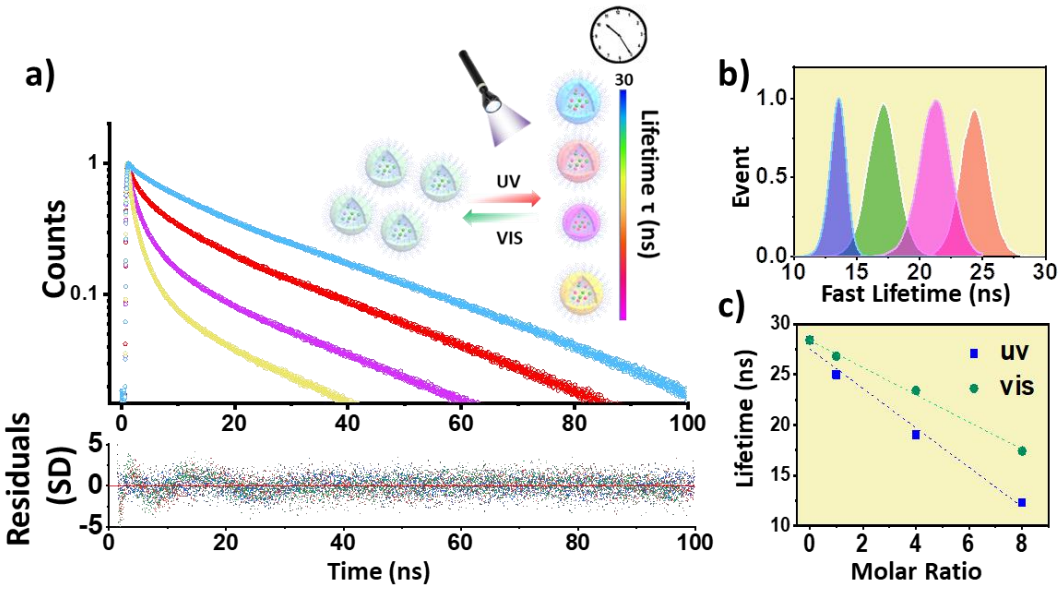

Figure 4.23 a) Fluorescence decay of nanogels (**N2-5**) after UV irradiation for 120 s (λ_{ex} = 405 nm); Bottom: corresponding residuals. The sum of the three-exponential fitting with calculated averaged lifetime evaluation is given in Table 4.3. b) Fluorescence lifetime histogram of the nanogel solutions (N1-N4) after UV irradiation (λex = 410 nm); c The average lifetime (τAv,I) of nanogel solution (N4) after UV irradiating for 0–50 s.

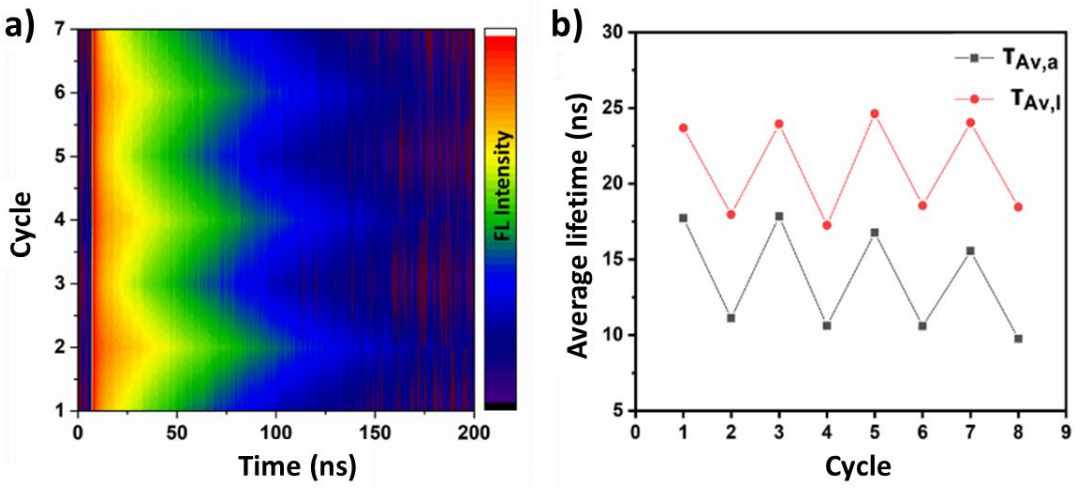

Figure 4.24 a) Reversible 2D Fluorescence decay and b) average fluorescence lifetime of **N4** upon alternating the UV and Vis irradiation for over a total of 6 cycles (λ_{ex} = 375 nm, λ_{em} = 520 nm);

acquired FLIM image. The manipulation of the fluorescence lifetime was also confirmed by monitoring the lifetime histogram changing before and after UV irradiation. A dramatic shift of the lifetime peak in **N4** was observed from the lifetime histogram and the changing of the lifetime was further able to be reversed by visible light irradiation. The reversibility of the fluorescent lifetime from the FLIM images and histograms were coincidence with observation in fluorescence emission results, which the long lifetime was observed after visible irradiation while short lifetime appeared after UV light irradiation. These results further proved the ability to control the fluorescence lifetime in this nanogel system *via* light irradiation.

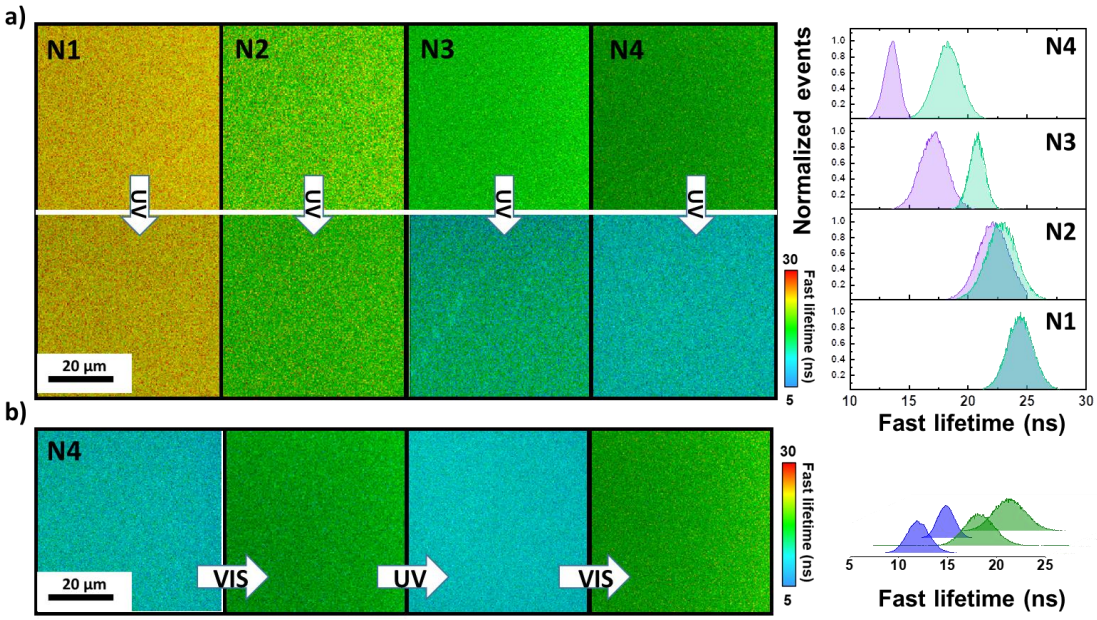

Figure 4.25 a) Fluorescence lifetime map of nanogels solution (**N1-4**, 1 mg/mL) before and after UV irradiation for 120s (λ_{ex} = 405 nm, λ_{em} = 520 nm) b) FLIM maps showing the reversible lifetime of **N4** in solution through alternating the UV and Vis irradiation (λ_{ex} = 405 nm, irradiation time: 120 s).

Table 4.3 Photophysical decay and the exponential fitting of the nanogels before and after light illumination. (λ_{ex}=410 nm)

	Parameter[a] τ		Value /ns	Std. Dev.[b] /ns	A[c] %	χ^2	$\tau_{Av,I}$ /ns	Std. Dev. /ns	$\tau_{Av,A}$ /ns	Std. Dev. /ns
N1	Vis	1	31.10	0.06	0.63	1.00	28.4	0.052	22.1	0.019
		2	7.80	0.12	0.32					
		3	0.90	0.08	0.05					
	UV	1	32.00	0.22	0.52	1.08	28.3	0.048	19.0	0.017
		2	6.80	0.25	0.33					
		3	1.10	0.12	0.16					
N2	Vis	1	30.80	0.05	0.44	1.07	26.8	0.042	16.0	0.025
		2	6.24	0.02	0.38					
		3	1.17	0.02	0.19					
	UV	1	29.00	0.16	0.43	1.05	25.0	0.043	14.4	0.089
		2	6.00	0.15	0.31					
		3	1.31	0.04	0.26					
N3	Vis	1	28.00	0.075	0.34	1.09	23.4	0.042	11.8	0.039
		2	5.52	0.071	0.35					
		3	1.13	0.019	0.31					
	UV	1	25.40	0.051	0.19	1.20	19.0	0.043	7.0	0.035
		2	4.39	0.048	0.34					
		3	1.23	0.029	0.46					
N4	Vis	1	27.00	0.06	0.22	1.28	20.8	0.037	8.0	0.025
		2	4.82	0.039	0.34					
		3	1.08	0.009	0.44					
	UV	1	23.20	0.061	0.11	1.55	15.2	0.022	4.0	0.017
		2	3.22	0.046	0.33					
		3	0.82	0.019	0.46					

[a.] Fluorescent lifetimes before and after UV and visible light irradiation. The different numbers represent the fitting exponents;

[b.] Standard deviation of fluorescence lifetimes of each exponents;

[c.] Percentage of the fitting exponents contributed to the fluorescence lifetime.

4.3.8 Remotely Controllable Fluorescence Lifetime Encryption

In order to determine the localization of nanogel with encoded information, multimode encryption capability was investigated by incorporating the nanogel in polyvinyl alcohol (PVA) film as a model under the microscope. The investigation of the lifetime encryption was performed using the micro-sized spherical PVA film containing unknown nanogel solution. The FLIM images of two droplet films were collected before and after UV irradiation for 120 s. Consequently, the overall lifetime histogram before UV irradiation only showed one peak, from which the lifetime of two droplet films are selectively identified by choosing the region of interests (ROI). The two histograms of ROI A and ROI B demonstrated a comparable lifetime before UV irradiation, therefore the nanogel information is effectively "hidden" in this state while no information was presented (Figure 4.23). After UV irradiation, a new peak emerged in the "read" state histogram which can be selectively separated by choosing the same ROIs. A dramatic change of lifetime was located in ROI B, in which the average lifetime was calculated as 10 ns corresponding to **N4**. The unchanged lifetime observed in ROI A (21 ns) was identified as **N1**, as coincident with the results from confocal laser scanning microscopy (CLSM). Although the information was both visualized by CLSM and FILM after UV irradiation, a more quantitate result was achieved through FLIM as the lifetime information could be accurately extracted by selecting ROIs, without the need to control the concentration. The construction of such a system is proof-of-principle demonstrating the selective storage and extracting information *via* light-triggered responsive lifetime storage.

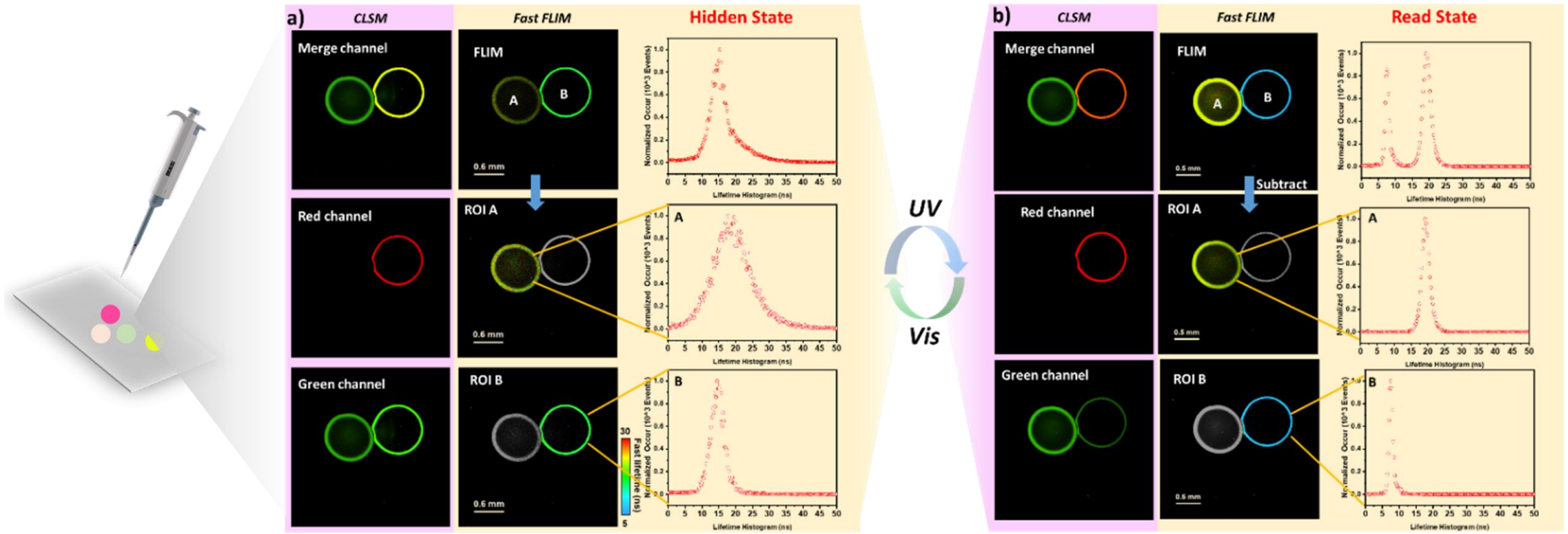

Figure 4.26 FLIM and CLSM imaging used to identify the relative position and any nanogel information incorporated in the PVA film. Different areas of the nanogel were selected as regions of interest (ROI) and analysis of the corresponsive fluorescence lifetime for each ROI is shown. Left column: CLSM images of two nanogel droplet films with different channels (Green channel: λ_{ex}:405 nm, λ_{em}:480-550 nm; red channel: λ_{ex}:405 nm, λ_{em}:600-700 nm); Right column: FLIM images of two nanogel droplet films with overall lifetime histogram and separated ROI with a subtracted lifetime histogram. (a) “Hidden” state (Before UV irradiation); (b) “Read” state (After UV irradiation)

4.3.9 Lifetime Barcoding in Living Cell

Having demonstrated the capability of dynamic lifetime barcoding in selective information encryption, the reversible nanogel was applied in the visualization of living cells using FLIM. In order to minimize the influence of the cell medium on the nanogel's reversibility, the crosslinking rate was increased to 50% to achieve a denser core (**N6**). The size of the nanogel analyzed by DLS decreased to 22 nm after increasing the crosslinking ratio (Table 4.4).

The cytotoxicity of the nanogels was first investigated in the A549 cell line (lung cancer fibroblasts) using a 10% PrestoBlue viability assay following the supplier instructions after 24 h incubation with nanogel solution at 37 °C and 5% CO_2. No measurable cytotoxicity was found for the nanogel with or without a fluorescent unit, up to a concentration of 2 $mg \cdot mL^{-1}$ (Figure 4.24). Nanogel containing only MMA and EGDMA was chosen as a positive/negative control to explore the cytotoxicity of the **SPMA** and **DTMMA**. (Red: **N6**, blue: control). Comparing with the control nanogel, the slight decrease of the cell viability in **N4** was observed which may be caused by the incorporation of the functional dye **DTMMA** and **SPMA**.

Table 4.4 Chemical composition and size characteristics of polymeric nanogel with different crosslink rate.

No.	SPMA			DTMMA			DoF	CLD[c]	DLS[d]	
	mg	mmol	DoF[a]	mg	mmol	DoF[b]	Total		D_h(nm)	PD
5	4.20	0.0100	0.20	0.00	0.0000	0.00	0.20	0.01	22±0.5	0.09
6	8.40	0.0200	0.40	1.00	0.0025	0.05	0.45	0.50	23±0.4	0.05

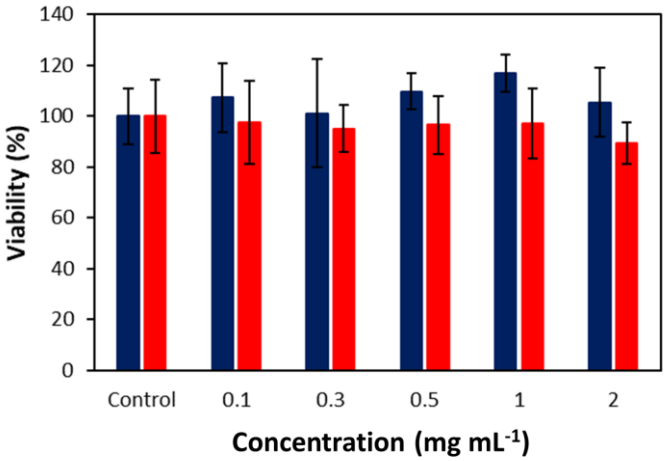

Figure 4.27 Evaluation of the cytotoxicity of nanogel **N4** in A549 lung cancer cells. Cell viability was assessed by 10% PrestoBlue viability assay following the supplier instructions after 24 h incubation with nanogel solution at 37 ºC and 5% CO_2. The fluorescence intensity (FI) was detected in a FluoStar Omega microplate reader (BMG Labtech) (λ_{ex} = 530 nm, λ_{em} = 590 nm). Cell data are reported as viability % in comparison to the control sample. Red: N4 solution; Black: control nanogel solution. Error bars represent standard deviation from 3 replicate samples.

Nanogels **N6** (CLD=50%) were further incubated into live A549 cells with 5% CO_2 and kept at 37 ºC during the whole experiment. CLSM was used as a control to investigate the fluorescence signal, whereas FLIM microscopy was employed to obtain quantitative photophysical values such as fluorescence lifetime, fluorescence count rate, and total number of photons. From the CLSM images, nanogel **N6** showed homogeneous distribution in the cell cytoplasm, maintaining its switchable properties (Figure 4.25). The maintained switchable property in **N6** in live cells showed the nanogel was efficiently incorporated into live cells and is not negatively affected by the cell medium.

* The cell viability experiments were carried out by Dr. Maria C. Arno

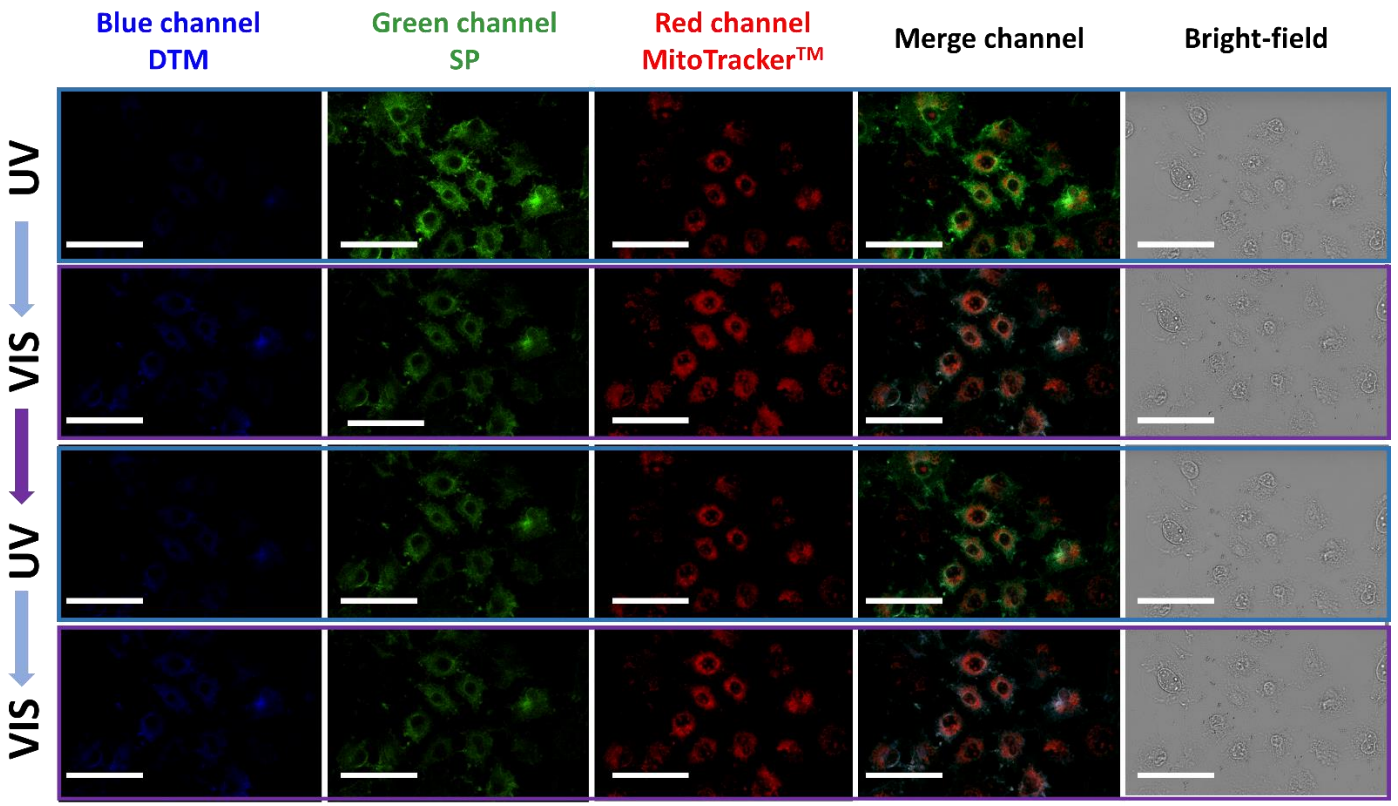

Figure 4.28 CLSM images of the nanogel in the live A549 cells co-incubated with MitoTracker Red using confocal microscopy. The intracellular images between different rows were acquired by alternating the UV and Vis irradiation. (Blue channel: DTM, λex = 405 nm; Green channel: Ring-opened form of SP, λex = 405 nm; Red channel: MitoTracker Red, λex = 630 nm; Scale bar = 60 μm).

* The cell incubations were carried out by Dr. Maria C. Arno

4.3.10 Functionalization of the Nanogel for Mitochondrion Tracking

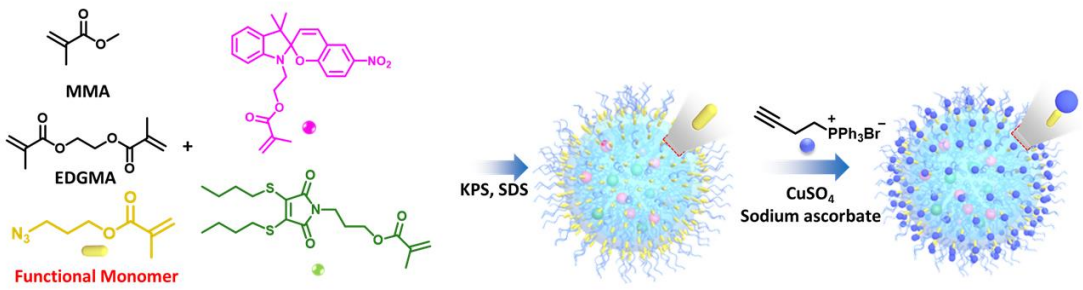

Figure 4.29 Design strategy of the triphenylphosphonium functionalized nanogel.

After achieving the remote control of the lifetime in different nanogel solution, we then sought to investigate the intracellular encoding and decoding process in more detailed cell structures, for example in subcellular organelles. Organelles play a specific and essential role in cellular processes,[76] and therefore monitoring the microenvironment within specific organelles is key to understanding their roles in cells. Due to their superior tolerance to functionalization, polymer-based nanomaterials have been successfully applied in many areas for specific targeting.[77] Among then, triphenylphosphonium (TPP) has been investigated as a specific moiety for mitochondrion targeting and monitoring.[78-80]

In order to incorporate the TPP tracker into our nanogel system, a hydrophobic monomer bearing an azide functionality was synthesized (Figure 4.26). Due to the similar hydrophobicity with MMA, the incorporation of azide monomer had only a slight influence on the size of the nanogels, as observed by DLS results (Figure 4.27).

Further post- polymerization modification of the azide nanogel (N_3-**N6**) was conducted with a triphenylphosphine alkyne *via* azide-alkyne cycloaddition (TPP-**N6**).

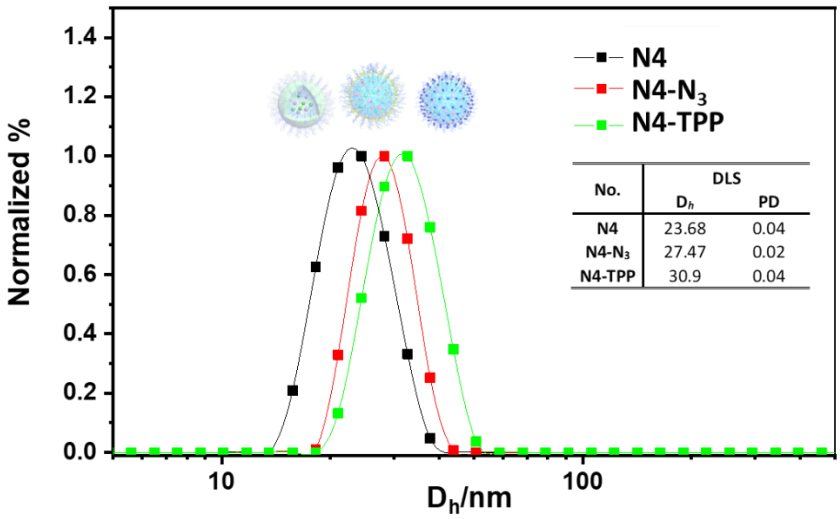

Figure 4.30 Intensity-weighted size distribution and corresponding hydrodynamic diameters obtained of unmodified nanogel (black), azide functionalized nanogel (red) and TPP functionalized nanogel (green) at 1 mg mL^{-1}, obtained by DLS (detection angle = 173°).

The incorporation of the functional group resulted in an increase of the nanogel size from 23.6 nm to 30.9 nm (Figure 4.27). This may cause by the incorporation of the positively charged triphenylphosphonium group which changed the hydrodynamic diameters of the nanogel. The incorporation of the PPh_3 group was further confirmed by ^{1}H NMR and ^{31}P NMR spectroscopy. In ^{1}H NMR, a new multiplet was observed around 7.5–8.1 ppm after TTP functionalization corresponded to the aromatic protons of triphenylphosphonium unit (Figure 4.28). A new peak in ^{31}P NMR spectrum was observed which attributed to the organic phosphorus peak in triphenylphosphonium unit (Figure 4.29).

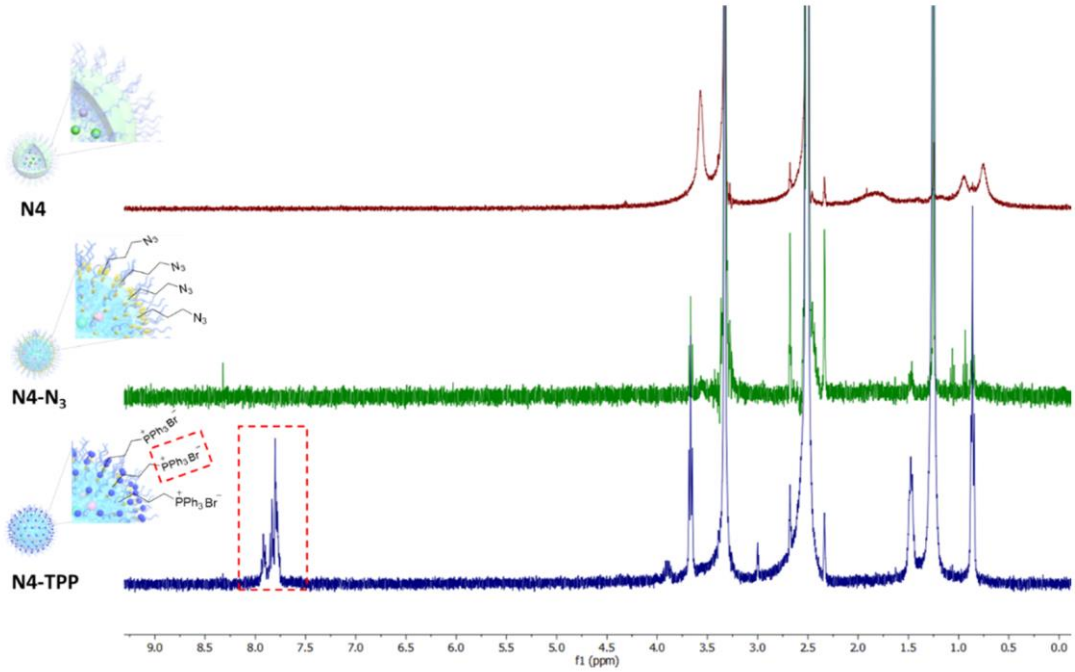

Figure 4.31 Overlaid ^{1}H NMR spectra of nanogel with different functionality to confirm the TPP functionality (*d*-DMSO, 400 MHz, 298K).

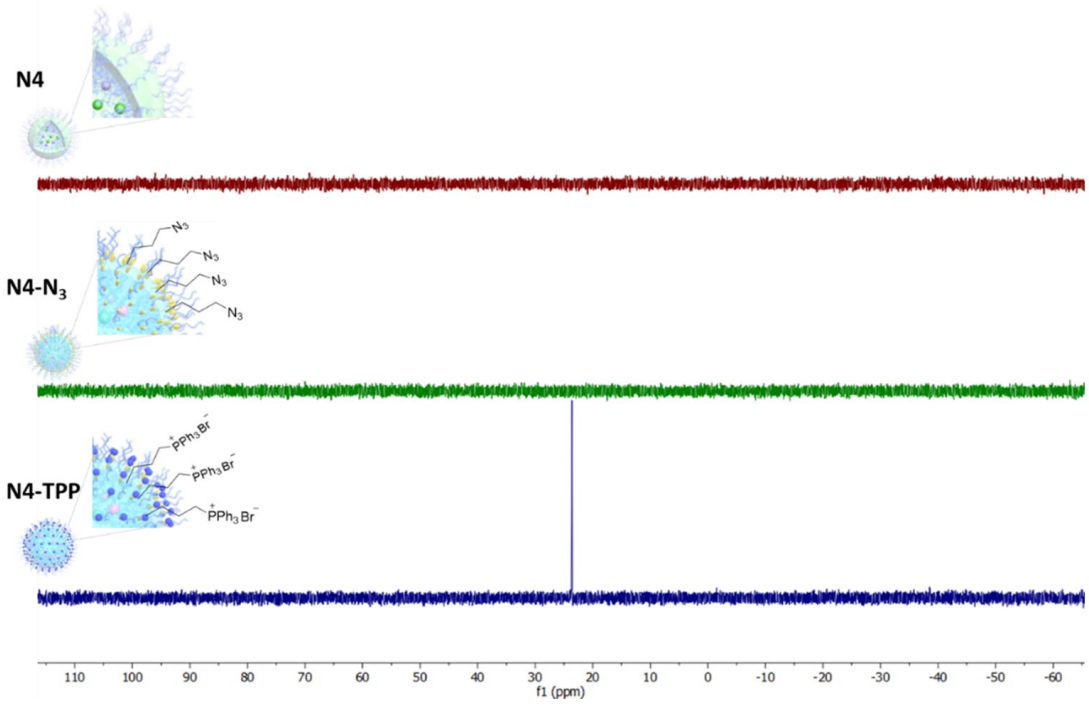

Figure 4.32 ^{31}P NMR of nanogel with different functionality to confirm the TPP functionality (*d*-DMSO, 376 MHz , 298K).

The FT-IR of the nanogel further confirmed the coupling of TPP unit *via* click reaction (Figure 4.30). In azide functionalized nanogel, the increase of the peak around 2100-2200 cm^{-1} corresponded to the stretching vibrations of azide group in **N6-N_3** nanogel. This peak was further decreased after the click reaction with (But-3-yn-1-yl) triphenylphosphonium bromide which further confirmed the successful modification of TTP group.

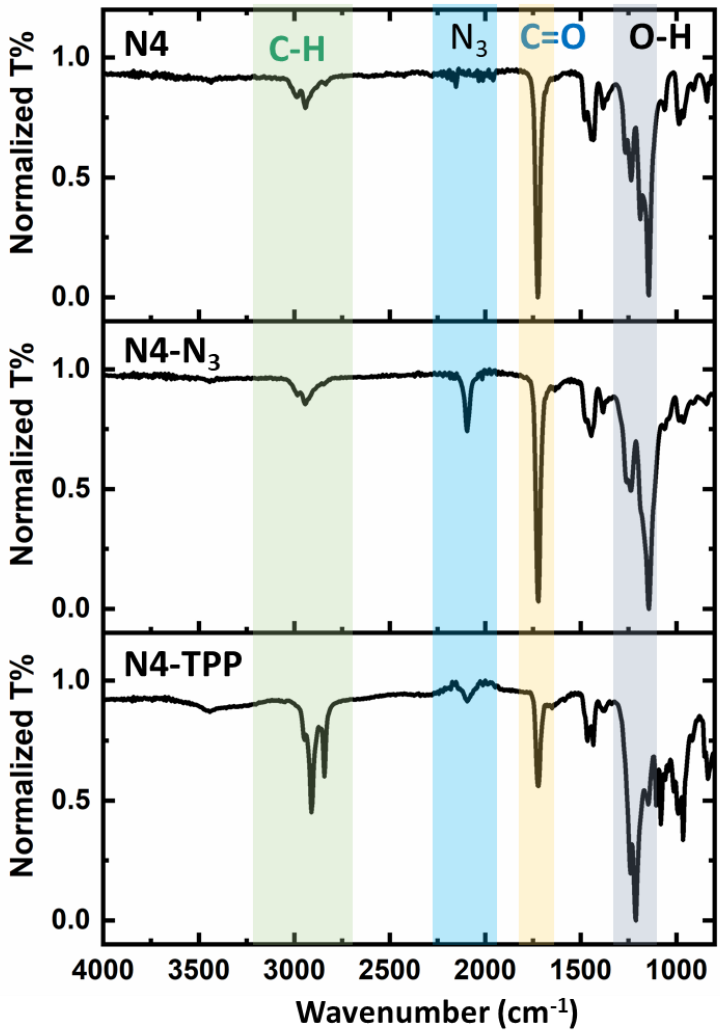

Figure 4.33 The functionalization of nanogel azide and TPP was first assessed by FT-IR spectra. 16 Scans were recorded from 600 to 4000 cm^{-1} at a resolution of 4 cm^{-1}

4.3.11 Reversible Fluorescence Lifetime Barcoding for Mitochondrion Tracking in Living Cells.

The functionalized nanogel (TPP-**N6**) was incubated in live A549 cells along with commercial MitoTracker Red for comparison (Figure 4.34). From CLSM, a large overlap was observed by comparing the DTM and SP channels in TPP-**N6** along with the red channel of commercial Mito Tracker. The overlap of the green and red channels was quantified *via* Pearson Correlation Coefficient (PCC). The PCC was calculated by the following equation and analysized by imageJ with the Coloc2 plugins.

$$r = \frac{\sum(R_i - R_{av}) \cdot (G_i - G_{av})}{\sqrt{\sum(R_i - R_{av})^2 \cdot \sum(G_i - G_{av})^2}}$$

R_i : the intensity of the red fluorophore in individual pixels;

G_i intensities for the Green fluorophore in the same pixels.

The PCC nanogel with TTP tracker (TPP-**N6**) is 0.85 which is much higher than **N4** without the TPP modification (0.57), indicating the successful nanogel localization inside the mitochondria, in contrast to the control sample without the TPP (Figure 4.31). More importantly, the nanogel showed similar reversible properties as previous nanogels (**N6**) and the incorporation of the tracker group did not influence the reversibility (Figure 4.34).

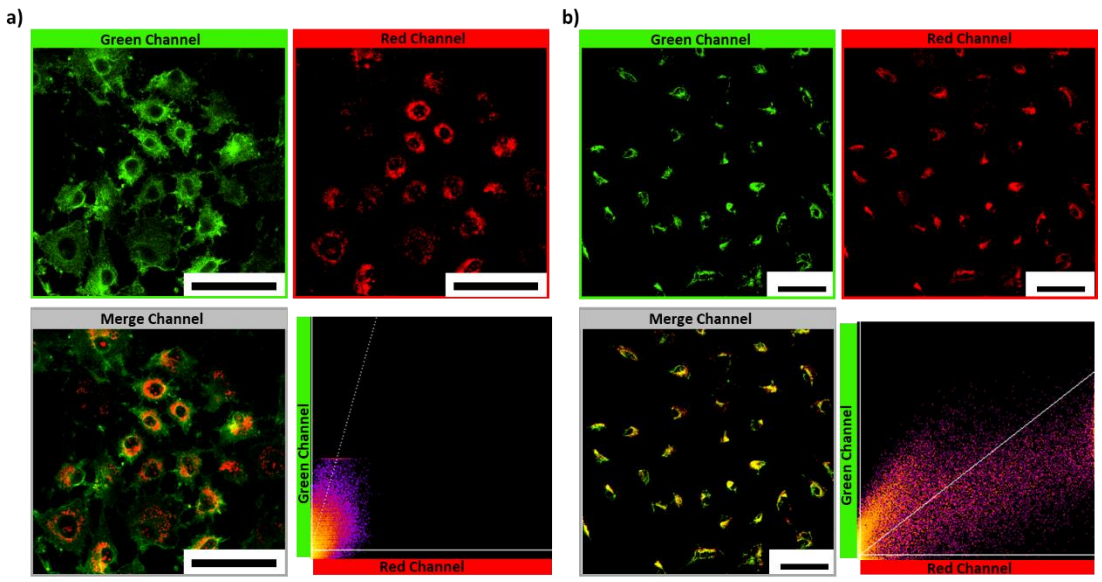

Figure 4.34 a) Schematic illustration of functional nanogel synthesizing strategy and post-polymerization modification strategy for mitochondria tracking. b) Co-localization of nanogel (TPP-**N6**, green channel) with MitoTracker Red (Red channel) in live A549 cells. Green channel: the ring-opened form of **SP** (λ_{ex}=405 nm); Red channel: MitoTracker Red (λ_{ex}=630 nm). The intensity correlation plots of TPP-**N6** and MitoTracker Red was processed on imageJ and analyzed the Pearson Correlation Coefficient using Coloc2 plugins.

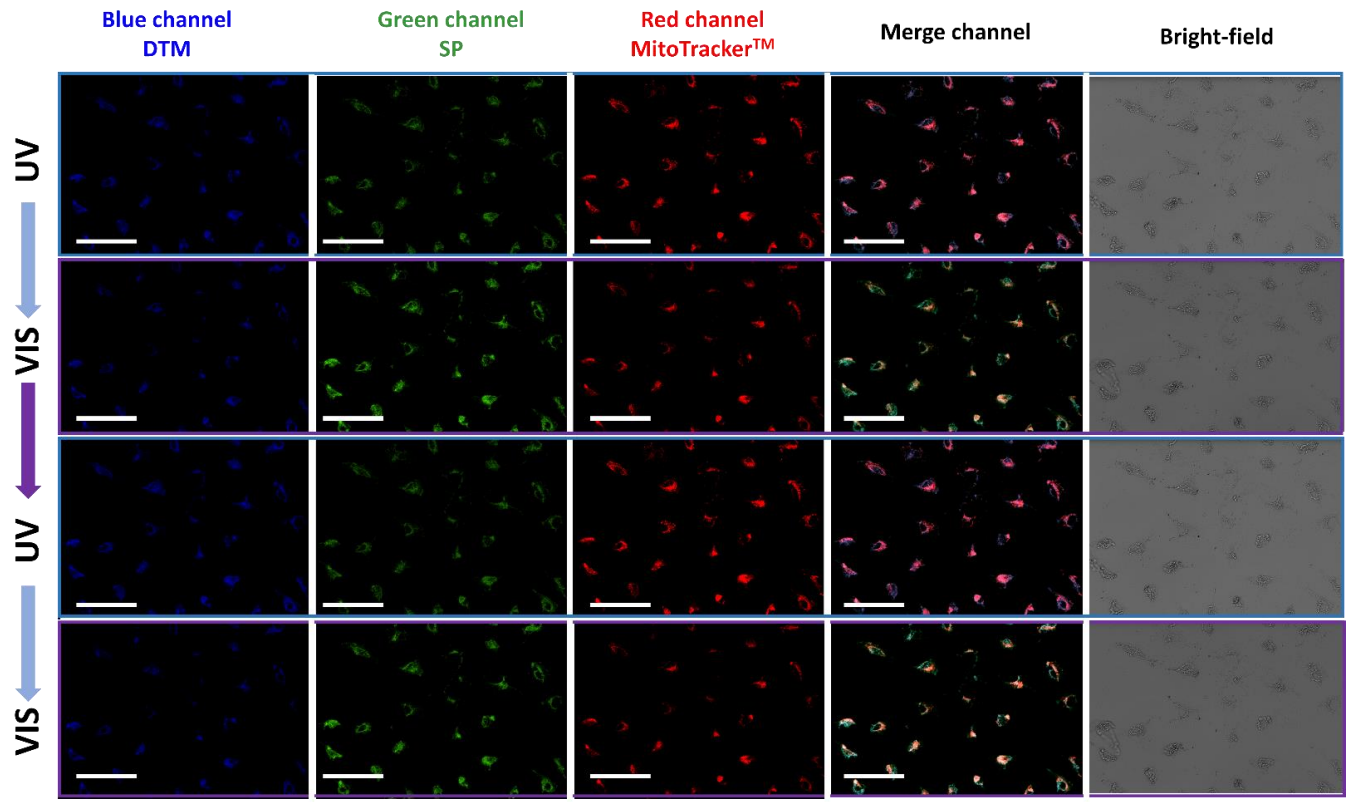

Figure 4.35 Subcellular imaging of the nanogel (**N6-TPP**) in the live A549 cells co-incubated with MitoTracker Red using CLSM. The intracellular images between different rows were acquired by alternating the UV and Vis irradiation. (Blue channel: DTM, λ_{ex} = 405 nm; Green channel: Ring-opened form of SP, λ_{ex} = 405 nm; Red channel: MitoTracker Red, λ_{ex} = 630 nm; Scale bar = 60 μm).

* The cell incubations were carried out by Dr. Maria C. Arno

Different from traditional lifetime barcoding materials that require very long lifetimes (μs-ms) to minimize the effect of autofluorescence in cellular environment, the reversible nature of the lifetime in this nanogel system provides a new strategy to amplify the signal to noise by deducting the two FLIM images between the reversible states. As an example, the FLIM image of TPP-**N6** after UV irradiation (Figure 4.36 a, UV2) was deducted from the FLIM image before UV irradiation (Figure 4.36 a, Vis1), resulting in the amplified image, in which the difference in lifetime was doubled

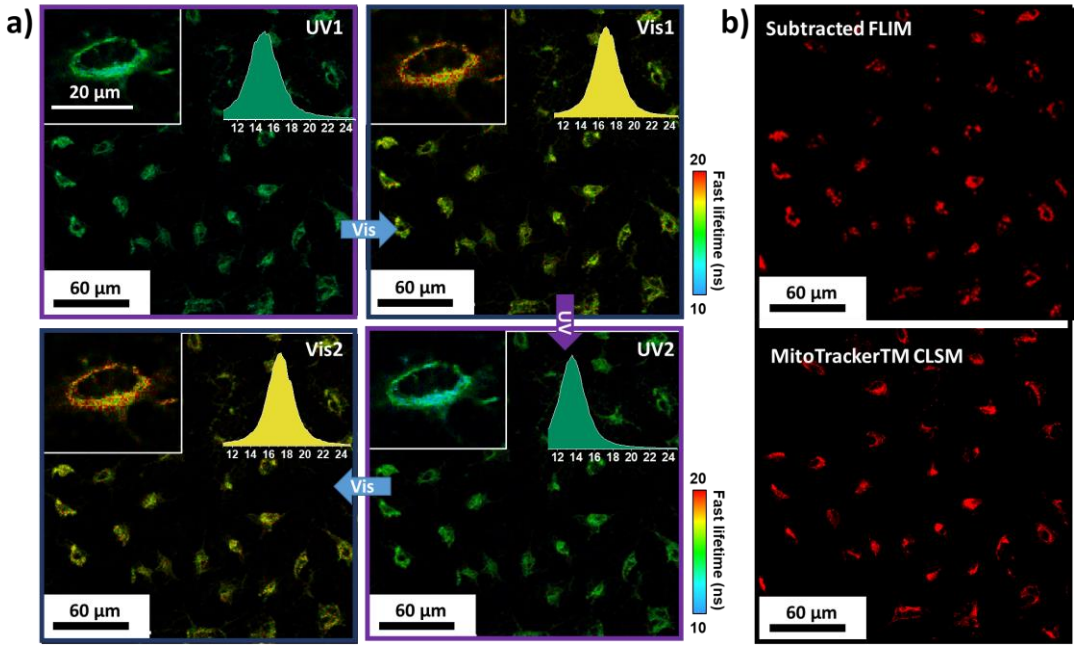

Figure 4.36 b) FLIM images of the nanogel with mitochondria tracker (TPP-**N6**) in live A549 cells under the stimulation of remote UV and Vis manipulation (Irradiation time: 120 s). The insert images are the lifetime histograms of the nanogel in whole image range; c) The subtracted FLIM image (top) which TPP-**N6** in live A549 cells before UV irradiation was subtracted with the same range after UV irradiation calculated by ImageJ. The subtracted image (top) was compared with the CLSM (bottom) of MitoTracker Red (Red channel).

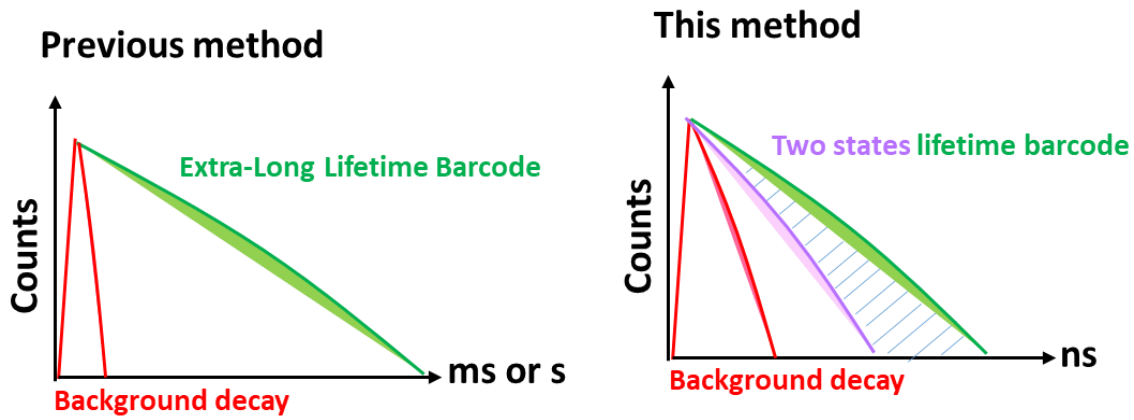

Figure 4.37 a) Schematic illustration of the lifetime amplify strategy using the reversible method compared with the previous method required for the extra-long lifetime.

(Figure 4.33b, subtracted FLIM). Due to the unchanged lifetime of the autofluorescence in the background, it could be completely subtracted while the reversible nanogel was magnified. By comparing the subtracted FLIM images with the CLSM image of MitoTracker Red, a more obvious overlap was observed without any background influence (Figure 4.37).

So far, fluorescence lifetime barcoding has been mostly carried on using inorganic fluorescent materials containing lanthanides and transition metals ions, which extra-long lifetime can minimize background fluorescence lifetime. However, inorganic barcoding materials raise some concerns in regard to biosafety and are not readily responsive to external stimuli, limiting the flexibility and application of this technique. In this study, we designed a photo-responsive lifetime barcoding polymeric nanogel system where the fluorescence lifetime can be remotely manipulated using UV and visible light. The multistate of the programmable lifetime information provides a self-

correction strategy to minimize the background lifetime in live-cell and sub-cellular organelles and the sensitivity of the fluorescence lifetime imaging can further increased without the need for extra-long lifetimes.

4.4 Summary

In summary, a strategy to remotely control fluorescence lifetime in a polymeric nanogel system was designed *via* a photoisomerization induced FRET process. The dynamic control over fluorescence lifetime has been successfully achieved *via* FRET between substituted maleimides and a spyropyran photoswitch. A series of nanogels with the same structure and surface chemistries but a broad range of dynamic lifetimes suitable for multiplex system coding and counting was synthesized. The described nanogel system was further used for lifetime barcoding, in which the multistate of the fluorescence was tracked and selectively visualized in a controllable and non-invasive manner *via* FLIM. By extracting simultaneously lifetime as the readout, the nanogel system was further proved to be able to selectively decode with quantitative results, providing higher level of micro-scale information storage with quantifying output. Meanwhile, the introduction of an azide functional handle by copolymerization allowed for further functionalization of the nanogel surface *via* click chemistry. As a proof-of-concept, a mitochondrial tracker was attached to the nanogel to achieve the live-cell lifetime barcoding at the subcellular scale *via* remote control of the fluorescence. the reversible lifetime as the self-correction manner is cable to eliminate the background influence in FLIM and could further increase the sensitivity of the imaging without need the extra-long lifetime.

4.5 Experimental Section

All synthesized compounds were confirmed by ^{1}H-NMR and ^{13}C-NMR spectra recorded on a Bruker Avance 300 or a Bruker Avance III HD 400 at 298k and 300, 400 MHz, respectively. Shifts (δ) are quoted in parts per million and quoted relative to an internal standard of trimethylsilane (TMS). High-resolution mass spectra were recorded on a Waters Xevo G2-XS QTof Quadrupole Time-of-Flight mass spectrometer.

4.5.1 Materials

All chemicals and reagents were purchased from either: Sigma Aldrich, Fisher Chemicals, Acros Chemicals or Alfa Aesar. Solvents were purchased from Fisher Scientific and used as received. Dry solvents were used directly from drying and degassing solvent tower delivery system. Commercially available monomer methyl methacrylate (MMA) and ethylene glycol dimethacrylate (EGDMA) were purified *via* passing through a column of basic alumina prior to use. Experimental procedures for the preparation of azide functionalized monomer (3-azidopropyl methacrylate) was reported previously.[81] (But-3-yn-1-yl) triphenylphosphonium bromide was synthesized following the previous reports.[82]

4.5.2 Characterization Techniques

NMR Spectroscopy. ^{1}H-NMR and ^{13}C-NMR spectra were recorded on a Bruker Avance 300 or a Bruker Avance III HD 400 at 298k and 300, 400 MHz, respectively. Shifts (δ) are quoted in parts per million and quoted relative to an internal standard of trimethylsilane (TMS).

High-Resolution Mass Spectrometry. HRMS spectra were recorded by the MS Analytical Facility Service at the University of Birmingham on a Waters Xevo G2-XS QTof Quadrupole Time-of-Flight mass spectrometer.

Fourier-transform infrared spectroscopy. FTIR was carried out using an Agilent Technologies Cary 630 FTIR spectrometer. 16 Scans from 600 to 4000 cm^{-1} were taken at a resolution of 4 cm^{-1}, and the spectra were corrected for background absorbance.

***Dynamic Light Scattering*.** Hydrodynamic diameters (D_h) and size distributions (PD) of nano-objects were determined by dynamic light scattering (DLS) using a Malvern Zetasizer Nano ZS with a 4 mW He-Ne 633 nm laser module operating at 25 °C. Measurements were carried out at an angle of 173°, and results were analyzed using Malvern DTS v7.03 software. All determinations were repeated 4 times with 15 measurements recorded for each run. D_h values were calculated using the Stokes-Einstein equation where particles are assumed to be spherical.

Transmission Electron Microscopy. Dry-state stained transmission electron microscopy (TEM) imaging was performed on a JEOL JEM-1400 microscope

operating at an acceleration voltage of 80 kV. All dry-state samples were diluted with deionized water to appropriate analysis concentration (0.1 mg/mL) and then deposited onto formvar-coated copper grids. After roughly 1 min, the excess sample was blotted from the grid and the grid was stained with an aqueous 1 wt% uranyl acetate (UA) solution for 1 min prior to blotting, drying and microscopic analysis.

Atomic Force Microscopy. AFM was performed on a JPK Nanowizard 4 system at room temperature in the supplied acoustic enclosure and vibration isolation using Nanosensor PPP-NCHAuD tips with a force constant of around 42 $N \cdot m^{-1}$. For data acquisition and handling, Nanowizard Control and Data Processing Software V.6.1.117 in QI mode with a setpoint of 25 nN was used. Samples were prepared on freshly cleaved mica by drop-casting a solution of 0.1 $mg \cdot mL^{-1}$ sample in water, settling for 2 min, removing of excess solution and subsequent drying under compressed air overnight.

UV-Vis spectroscopy. UV-Vis was performed on an Evolution 350 UV-Vis spectrophotometer equipped with Xenon Flash Lamp light source and Dual Matched Silicon Photodiodes detector. Quartz cells (170 - 2000 nm) from Hellma with two polished sides were used for examining the absorption spectral data by using Thermo INSIGHT software.

Light irradiation

The UV (365 nm, 6 W) and light-emitting diode (White LED lamps, 2 W) were used as light sources for UV and visible light irradiation, respectively.

Fluorescence steady-state and lifetime measurement and imaging

Steady-State Fluorescence Spectroscopy. All steady-state spectra were obtained with an Agilent Cary Eclipse Fluorescence spectrophotometer equipped with Photomultiplier tube (PMT) detector with a scan rate of 600 nm per minute. The emission kinetics were measured on an Edinburgh Instruments FS5 spectrofluorometer equipped with a Xenon lamp. The samples were measured in deionized water and the acquired data were analyzed in Origin 2019 (Origin Labs).

Fluorescence Lifetime Spectroscopy. Time correlated single photon counting (TCSPC) was employed to obtain all fluorescence lifetime spectra. This was done with an Edinburgh Instruments FS5 spectrofluorometer equipped with 375 ± 10 nm ps pulsed diode laser source (PicoQuant) using 10 mm path length quartz cuvettes with four transparent polished faces (Starna Cells). The emission wavelength was chosen with a monochromator at 510 ± 4 nm. The signal level was kept below 5% of the light source repetition rate. Instrument response functions (IRF) were determined from the scatter signal solution of Ludox HS-40 colloidal silica (10% particles in water w/w). The analysis was performed on Fluoracle software (Edinburgh Instruments).

Fluorescence lifetime imaging microscopy (FLIM). FLIM was performed on LSM upgrade kit (PicoQuant) mounted on a FV3000 (Olympus) confocal microscope with a IX-81 inverted base (Olympus) and the 20x and 60x oil lens (Olympus) were used for imaging. The FV3000 system was driven with the FV31S-SW Viewer software platform (Olympus) with scan rates of 1 μs pixel^{-1} at 515 by 512 pixels. FLIM images

and spectra were detected by single-photon avalanche diodes using a 520/60 bandpass filter (AHF analysentechnik) with a 405 nm (PicoQuant) pulsed diode laser driven at 2.5 MHz. FWHM for the 405 nm laser head was 59 ps and maximum power was 0.3 mW (attenuated by variable neutral density filters to prevent count pile up and maintain counting rates below 1% bin occupancy). Acquired images containing fluorescence lifetime were analyzed using fast-FLIM method implemented in SymPhoTime software (PicoQuant) and ImageJ. All IRF deconvolved exponential fits were performed with the number of exponents selected for completeness of fit as determined by boot-strap chi-squared analysis in SymPhoTime software, typically three.

Cell Culture and Fluorescence Imaging

Cell Viability Assay. A549 were purchased from Public Health England. Cells were cultured in F12K medium with addition of 10% FBS and 100 U mL^{-1} pen/strep at 37 °C and 5% CO_2. Cells were seeded on 12-well plates at 2000 cells cm^{-2} and left to adhere and proliferate for 72 h. The medium was then replaced with the nanogel samples (**N6** or nanogel without **SPMA** and **DTMMA** as control) in a concentration range from 0 to 2 mg mL^{-1}. Briefly, a solution of nanogels in water (100 mg mL^{-1}) was sterile filtered through a 0.22 μm filter. This solution was then diluted with cell culture medium (with the addition of 10% FBS and 100 U mL^{-1}pen/strep) to a final concentration of 10 mg mL^{-1}. This stock solution was then used to prepare the dilutions directly on the well plates containing cells. After 24 h, the solution was removed and cells were washed with PBS (1 mL × 3) and incubated with 10% PrestoBlue viability assay following the

supplier instructions. The fluorescence intensity (FI) was detected in a FluoStar Omega microplate reader (BMG Labtech) (λ_{ex} = 530 nm, λ_{em} = 590 nm). Cell data are reported as viability % in comparison to the control sample. Experiments were performed in triplicate.

***Live-cell imaging and Colocalization*.** A549 cells were cultured in F12K medium with addition of 10% FBS and 100 U mL^{-1} pen/strep at 37 °C and 5% CO_2. Cells were seeded in glass-bottom microdishes (Thermofisher Scientific) at 5000 cells cm^{-2} and incubated for 24 h at 37 °C in 5% CO_2. After that, cells were pre-treated with commercial MitoTracker™ Deep Red (20 $\mu g \cdot mL^{-1}$) for 30 min prior to incubation with different nanogels at 1 mg mL^{-1} for one to two hours. Upon washing with cell medium three times, the resulting cells were transferred to an Olympus FV3000 confocal microscope equipped with an incubator to keep live cells at 37 °C in a 5% CO_2 atmosphere during image acquisition. Live cells were imaged with a 60× oil-immersion objective with scan rates of 1 μs $pixel^{-1}$ at 515 by 512 pixels both on Olympus FV3000 Microscopy for fluorescent images and PicoQuant LSM Upgrade Kit for fluorescence lifetime images. The original images were processed using CellSens software (Olympus), SymPhoTime 64 (PicoQuant) and ImageJ with Coloc2 plugins.

4.5.3 Synthesis of Dye-functionalized Monomers

*Methyl 3,4-dibromo-2,5-dioxo-2,5-dihydro-1H-pyrrole-1-carboxylate (**1**).*

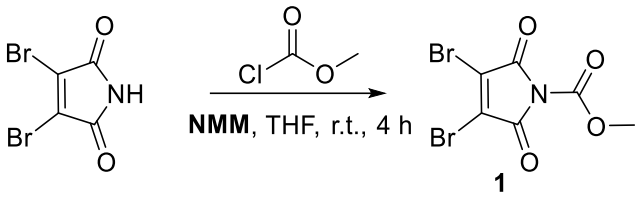

1

To a stirred solution of 3,4-dibromomaleimide (3 g, 11.76 mmol) in dry THF (40 mL) was added N-methyl morpholine (1.11g, 11.76 mmol). The solution was stirred for 15 minutes and then the methyl chloroformate (0.91 mL, 11.76 mmol) was added dropwise. The reaction was stirred under a nitrogen atmosphere for 40 minutes. Dichloromethane (200 mL) was added and the mixture was washed with water (200 mL×3) and dried over anhydrous Na_2SO_4. The solvent was removed under reduced pressure and the crude product was dried without further purification.

*3,4-dibromo-1-(3-hydroxypropyl)-1H-pyrrole-2,5-dione (**2**).*

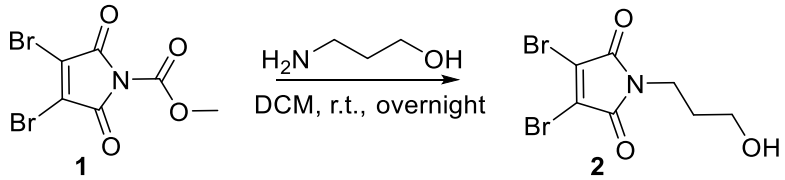

1 **2**

Methyl 3,4-dibromo-2,5-dioxo-2,5-dihydro-1H-pyrrole-1-carboxylate **1** (2 g, 6.4 mmol) was dissolved in dry DCM (50 mL) and 3-amino-1-propanol (0.48 g, 6.7 mmol) was added. The reaction was stirred under a nitrogen atmosphere for 24 hours. Dichloromethane (150 mL) was added and the mixture was washed with NH_4Cl solution (100 mL), water (200 mL×3) and dried over anhydrous Na_2SO_4. The solvent

was removed under reduced pressure and the product was purified by flash chromatography (3:1, *n*-hexanes: EtOAc) as a white solid. Yield: 73%.

^{1}H NMR (300 MHz, Chloroform-*d*) δ 3.78 (t, *J* = 6.6 Hz, 2H), 3.64 (t, *J* = 5.8 Hz, 2H), 1.93 – 1.78 (m, 2H). ^{13}C NMR (101 MHz, Chloroform-*d*) δ 164.3, 129.4, 59.3, 36.5, 31.0. HRMS(MaXis) m/z [M]: 310.8792, calculated 310.8793.

*3,4-bis(butylthio)-1-(3-hydroxypropyl)-1H-pyrrole-2,5-dione (**3**)*[41].

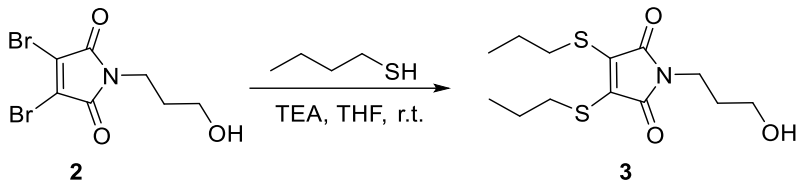

2 **3**

3,4-dibromo-1-(3-hydroxypropyl)-1H-pyrrole-2,5-dione **2** (1 g, 3.2 mmol) and butanethiol (576 mg, 6.4 mmol) was dissolved in THF (50 mL) and cooled to 0 °C for 10 minutes. Then, triethylamine was added dropwise to the cooled solution and the reaction was stirred for 16 hours at room temperature. Dichloromethane (150 mL) was added and the mixture was washed with water (200 mL×3) and dried over anhydrous Na_2SO_4. The solvent was removed under reduced pressure and the product was purified by flash chromatography (2:1, *n*-hexane: EtOAc) as a orange oil. Yield: 56 %.

^{1}H NMR (300 MHz, Chloroform-*d*) δ 3.74 – 3.64 (m, 1H), 3.65 – 3.55 (m, 1H), 3.36 – 3.25 (m, 2H), 1.87 – 1.73 (m, 1H), 1.71 – 1.59 (m, 2H), 1.54 – 1.39 (m, 2H), 0.95 (t, *J* = 7.3 Hz, 3H). ^{13}C NMR (101 MHz, Chloroform-*d*) δ 59.0, 34.8, 32.5, 31.6, 31.3, 21.7. HRMS(MaXis) m/z $[M+Na]^+$: 354.1171, calculated 354.1174.

*3-(3,4-bis(butylthio)-2,5-dioxo-2,5-dihydro-1H-pyrrol-1-yl)propyl methacrylate (**DTMMA**).*

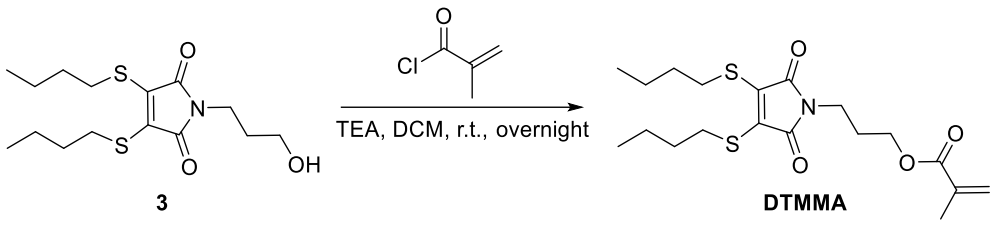

3,4-bis(butylthio)-1-(3-hydroxypropyl)-1H-pyrrole-2,5-dione **6** (600 mg, 1.8 mmol) was dissolved in dry DCM (10 mL) and triethylamine (494 μL, 2.2 mmol) was added. The reaction mixture was cooled to 0 °C for 10 minutes and the methacryloyl chloride (220 μL, 2.2 mmol) was added to the solution dropwise over 30 minutes. The solution was then stirred at room temperature overnight under a nitrogen atmosphere. 50 mL DCM was then added to the solution and followed by washing with water (50 mL ×3) and dried with anhydrous Na_2SO_4. The solvent was removed under reduced pressure to give a orange oil that was purified by flash chromatography (4:1, hexane:EtOAc) as the prange oil. Yield: 35 %.

^{1}H NMR (300 MHz, Chloroform-*d*) δ 6.10 (dt, *J* = 1.9, 0.9 Hz, 1H), 5.56 (t, *J* = 1.6 Hz, 1H), 4.15 (t, *J* = 6.1 Hz, 2H), 3.63 (t, *J* = 6.9 Hz, 2H), 3.28 (t, 4H), 2.05 – 1.96 (m, 2H), 1.68 – 1.54 (m, 4H), 1.52 – 1.37 (m, 4H), 0.93 (t, *J* = 7.3 Hz, 6H). ^{13}C NMR (101 MHz, Chloroform-*d*) δ 167.3, 166.6, 136.2, 135.7, 125.7, 61.9, 35.7, 32.5, 31.5, 27.6, 21.7, 18.3, 13.6. HRMS(MaXis) m/z $[M+Na]^+$: 422.1440, calculated 422.1436.

*1-(2-hydroxyethyl)-2,3,3-trimethyl-3H-indol-1-ium iodide (**4**).*

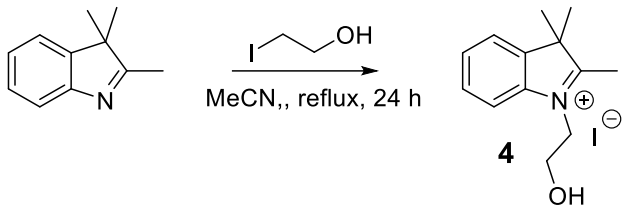

2,3,-trimethyl-3H indole (5 g, 31.5 mmol) and 2-iodoethanol (7.5 g, 44 mmol) was dissolved in MeCN (50 mL). The solution was refluxed under nitrogen for 24 hours. The reaction mixture was cooled to room temperature and product precipitated by the addition of hexane. The purple solid was filtered and dried without further purification. Yield: 95%.

*9,9-dimethyl-2,3,9,9a-tetrahydrooxazolo[3,2-a]indole (**5**).*

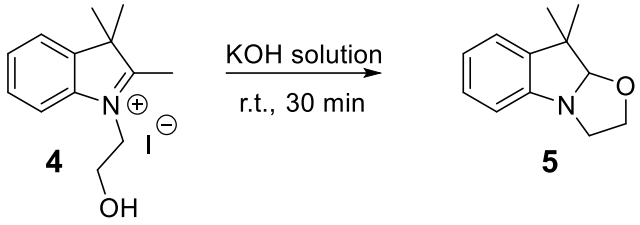

1-(2-hydroxyethyl)-2,3,3-trimethyl-3H-indol-1-ium iodide (7 g, 21 mmol) was suspended in degassed water (50 mL) under a nitrogen flow and potassium hydroxide (4 g, 70 mmol) was added. The solution was sonicated for 5 minutes and stirred at room temperature for 30 min under a nitrogen atmosphere. Then the reaction mixture was extracted with diethyl ether. The combined organic layer was washed with brine and dried over anhydrous Na_2SO_4. The solvent was evaporated to afford **2** as an orange oil. Yield: 97%. ^{1}H NMR (300 MHz, Chloroform-*d*) δ 7.11 – 6.94 (m, 2H), 6.85 (td, *J* =

7.4, 1.0 Hz, 1H), 6.68 (dt, *J* = 7.9, 0.7 Hz, 1H), 3.83 – 3.72 (m, 1H), 3.70 – 3.58 (m, 1H), 3.58 – 3.37 (m, 2H), 1.35 (s, 3H), 1.31 (s, 3H), 1.11 (s, 3H). ^{13}C NMR (101 MHz, Chloroform-*d*) δ 150.5, 140.0, 127.5, 122.4, 121.7, 112.0, 109.0, 63.0, 50.1, 47.0, 28.1, 20.8, 17.6. HRMS (MaXis) m/z $[M+H]^+$ found 203.1311, calculated 203.1310.

*2-(3',3'-dimethyl-6-nitrospiro[chromene-2,2'-indolin]-1'-yl)ethan-1-ol (**6**)*

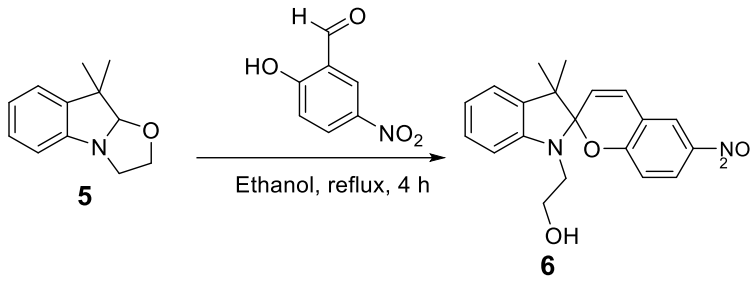

5 **6**

9,9-dimethyl-2,3,9,9a-tetrahydrooxazolo[3,2-a]indole **2** (5 g, 16.7 mmol) and 2-Hydroxy-5-nitrobenzaldehyde (2.79 mg, 16.7 mmol) were dissolved in 20 mL ethanol. The reaction was left to reflux under nitrogen atmosphere for 4 hrs. The solvent was removed under reduced pressure to give a purple solid that was purified by flash chromatography (1:1, *n*-hexane:EtOAc) Yield: 89%.

^{1}H NMR (300 MHz, Chloroform-*d*) δ 8.00 – 7.86 (m, 2H), 7.13 (td, *J* = 7.6, 1.3 Hz, 1H), 7.03 (dd, *J* = 7.3, 1.3 Hz, 1H), 6.89 – 6.77 (m, 2H), 6.69 (d, *J* = 8.6 Hz, 1H), 6.60 (d, *J* = 7.8 Hz, 1H), 5.81 (d, *J* = 10.4 Hz, 1H), 3.82 – 3.60 (m, 2H), 3.39 (ddd, *J* = 14.9, 7.4, 5.4 Hz, 1H), 3.26 (dt, *J* = 14.9, 5.1 Hz, 1H), 1.65 (s, 1H), 1.22 (s, 3H), 1.13 (s, 3H). ^{13}C NMR (101 MHz, Chloroform-*d*) δ 159.3, 147.0, 135.9, 128.3, 127.9, 126.0, 122.8, 122.0, 121.9, 120.0, 118.6, 115.6, 106.9, 106.7, 60.9, 60.4, 52.9, 46.1, 25.9, 20.0. HRMS(MaXis) m/z $[M+H]^+$: found 353.1503, calculated 353.1501.

*2-(3',3'-dimethyl-6-nitrospiro[chromene-2,2'-indolin]-1'-yl)ethyl methacrylate (**SPMA**)*

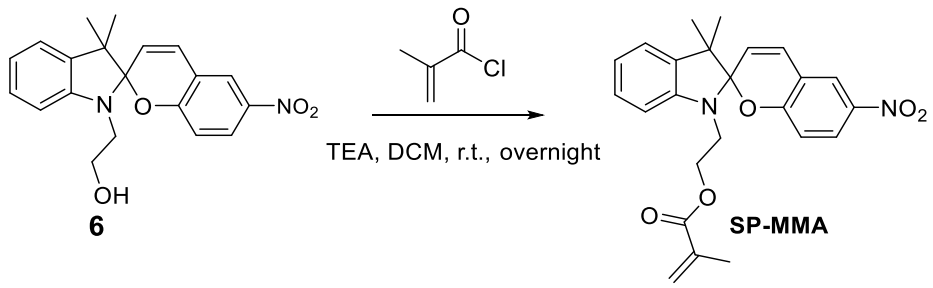

2- (3',3' – dimethyl – 6 – nitrospiro [chromene - 2,2' – indolin]-1'-yl)ethan-1-ol **3** (2 g, 5.6 mmol) was dissolved in dry DCM (20 mL) in a dried flask under nitrogen and triethyl amine (1.4 mL, 6.7 mmol) was added. The reaction mixture was cooled to 0 °C for 10 minutes and then methacryloyl chloride (0.67 mL, 6.7 mmol) was added to the solution dropwise over 30 minutes. The solution was then stirred at room temperature overnight under a nitrogen atmosphere. 50mL DCM was then added to the solution and followed by washing with water (100 mL ×3) and dried with anhydrous Na_2SO_4. The solvent was removed under reduced pressure to give a purple oil that was purified by flash chromatography (2:1, hexanes:EtOAc). Yield: 42%.

^{1}H NMR (400 MHz, Chloroform-*d*) δ 8.01 – 7.87 (m, 2H), 7.17 – 7.10 (m, 1H), 7.02 (dd, *J* = 7.3, 1.3 Hz, 1H), 6.86 – 6.80 (m, 2H), 6.66 (dd, *J* = 19.1, 8.2 Hz, 2H), 6.00 (t, *J* = 1.4 Hz, 1H), 5.80 (d, *J* = 10.3 Hz, 1H), 5.53 – 5.45 (m, 1H), 4.23 (t, *J* = 6.3 Hz, 2H), 3.55 – 3.24 (m, 2H), 1.85 (t, *J* = 1.3 Hz, 3H), 1.21 (s, 3H), 1.09 (s, 3H). ^{13}C NMR (101 MHz, Chloroform-*d*) δ 159.4, 146.7, 136.1, 135.7, 128.3, 127.9, 126.0, 126.0, 122.8, 121.8, 119.9, 118.4, 115.6, 106.8, 106.5, 62.7, 52.8, 42.4, 25.9, 19.8, 18.4. HRMS(MaXis) m/z $[M+H]^+$: 421.1760, calculated 421.1763.

4.5.4 Preparation of Nanogel *via* Micro-emulsion Polymerization

The synthesis of nanogel was followed by the previous paper reported by our group.[52] In a typical procedure, sodium dodecyl sulfate (0.1 g) was firstly dissolved in water (50 mL) under N_2 bubbling at room temperature. Subsequently, the methyl methacrylate (**MMA**, 0.5 g), Ethylene glycol dimethacrylate (**EGDMA** 2.5 mg, cross-linking density: 1%), **DTMMA** and **SPMA** were mixed before being added to the above solution under N_2 protection. The reaction was kept stirring at 800 rpm and a solution of potassium persulfate (10 mg in 1 mL H_2O) was added. Upon being further stirred overnight at 70 °C for 14 h. Then the resulting nanogels were filtered using a 0.45 μm Nylon syringe filter and dialyzed (MWCO 3.5 kDa) against water prior to analysis. The final concentration was determined after freeze-drying and overnight dialysis.

4.5.5 Preparation of Functionalized Nanogels *via* Click Reaction

The azide functionalized nanogel was prepared by a similar method above with minor changes. Briefly, sodium dodecyl sulfate (0.1g) was added to water (50 mL) under N_2 bubbling at room temperature. Subsequently, the MMA, EGDMA (0.125 g, CLD= 50%), DTMMA (1 mg), SPMA (8.4 mg) and azide monomer (3-azidopropyl methacrylate) were mixed before being added to the above solution under N_2 protection. The reaction was kept stirring at 800 rpm and the solution of potassium persulfate (10 mg in 1 mL H_2O) was added. Upon being further stirred overnight at 70 °C for 14 h. The resulting nanogels were filtered using a 0.45 μm Nylon syringe filter and dialysis (MWCO 3.5 kDa) against water prior to analysis.

Triphenylphosphonium (TPP) group functionalized nanogel was prepared *via* the Cu catalyzed click reaction.[83] The (But-3-yn-1-yl) triphenylphosphonium bromide was synthesized followed by the previous report.[82] Firstly, to the 50 mL solution (water/DMSO=1:1) of azide functionalized nanogel (DoF 13%, 2 mg mL^{-1}) was added the sodium dodecyl sulfate (50 mg) under N_2 bubbling at room temperature. Subsequently, the (But-3-yn-1-yl) triphenylphosphonium bromide (50 mg), sodium ascorbate (5 mg) and $CuSO_4 \cdot 5H_2O$ (2.5 mg) were mixed before being added to the above solution under N_2 protection. The reaction was kept stirring at 60 °C for 24 h. The resulting nanogels were filtered using a 0.45 μm Nylon syringe filter and dialysed (MWCO 3.5 kDa) against water for 2 days. The final concentration was determined after freeze-dring and overnight dialysis.

4.5.6 General Procedure of Fluorescence Lifetime Decay Measurement and Analysis

Fluorescence lifetime image (FLIM) was collected using a LSM upgrade kit (PicoQuant) mounted on a FV3000 (Olympus) confocal microscope with a IX-81 inverted base (Olympus) and the 20x and 60x oil lens (Olympus) were used for imaging. FLIM images and spectra were detected by single-photon avalanche diodes using analyzed using the FLIM method implemented in SymPhoTime software (PicoQuant) and ImageJ. All IRF deconvolved exponential fits were performed with the 3 exponents selected for completeness of fit as determined by bootstrap Chi-square analysis in SymPhoTime software (PicoQuant) using the following equations:

Exponential model function:

$$S(t) = \int_0^t E(t')R(t-t')dt' \qquad (S1)$$

S(t): Measured fluorescence decay;

E(t$^{'}$): Measured instrumental response function;

R(t-t$^{'}$): Theoretical sample decay model function;

$$R(t) = A_1 exp\left\{-\frac{t}{\tau_1}\right\} + A_2 exp\left\{-\frac{t}{\tau_2}\right\} + A_3 exp\left\{-\frac{t}{\tau_3}\right\} \qquad (S2)$$

Reduced chi-square:

$$\chi^2 = \sum_k w_k^2 \frac{(F_k - S_k)^2}{n} \qquad (S3)$$

W_k: Weighting factors for the individual data points.

S_k: The measurement data points.

F_k: The data points of the fitted curve.

N: The number of the free parameters which is approximately the number of fitted data points subtracted by the number of lifetime parameters used in the fit.

4.5.7 Simulation Methods

Table 4.5 TD-DFT excitation and emission energies, their corresponding oscillator strengths and the HOMO-LUMO gap of **DTM**, ring-opened and ring-closed **SP** structures at B3LYP-B3DJ/6-311G(d,p) level of theory using the PCM with ε = 2.0165.

	State	Major contribution	λ_{exc}[a]	f_{exc}[b]	Major contribution	λ_{em}[a]	f_{em}[b]	$\Delta\lambda$[a]	Δ_{L-H}[a]
DTMMA	1	H → L (70%)	453 (2.7)	0.100	H → L (70%)	574 (2.2)	0.079	121 (10.2)	369 (3.4)
	2	H-1 → L (62%)	360 (3.4)	0.019					
	3	H-3 → L (59%)	326 (3.8)	0.030					
Ring-opened SPMA	1	H → L (70%)	510 (2.4)	0.825	[c]				455 (2.7)
	2	H-1 → L (69%)	473 (2.6)	0.008					
	3	H-2 → L (70%)	373 (3.3)	0.389					
Ring-Closed SPMA	1	H → L (70%)	401 (3.1)	0.006	H → L (71%)	662 (1.9)	0.004	261 (4.7)	354 (3.5)
	2	H-1 → L (69%)	348 (3.6)	0.178					
	3	H -> L+1 (70%)	332 (3.7)	0.013					

[a] Values in nm and eV (in parenthesis). [b] Values in a.u. [c] The geometry of the first singlet excited state was not possible to converge.

Table 4.6 TD-DFT excitation and emission energies, their corresponding oscillator strengths and the HOMO-LUMO gap of **DTM**, ring-opened and ring-closed **SP** structures at PBE1PBE-B3DJ/6-311G(d,p) level of theory using the PCM with ε = 2.0165.

	State	Major contribution	λ_{exc}[a]	f_{exc}[b]	Major contribution	λ_{em}[a]	f_{em}[b]	$\Delta\lambda$[a]	Δ_{L-H}[a]
DTMMA	1	H → L (70%)	438.2 (2.8)	0.108	H → L (70%)	558.6 (2.2)	0.092	120 (10.3)	335 (3.7)
	2	H-1 → L (60%)	347.9 (3.6)	0.015					
	3	H-3 → L (56%)	313.6 (4.0)	0.037					
Ring-opened SPMA	1	H → L (70%)	494.8 (2.5)	0.872	[c]				410 (3.0)
	2	H-1 → L (69%)	450.6 (2.8)	0.006					
	3	H-2 → L (70%)	356.6 (3.5)	0.372					
Ring-Closed SPMA	1	H → L (70%)	361.2 (3.4)	0.007	H → L (71%)	556.7 (2.2)	0.004	196 (6.3)	313 (4.0)
	2	H-1 → L (69%)	326.3 (3.8)	0.183					
	3	H → L+1 (69%)	313.2 (4.0)	0.015					

[a] Values in nm and eV (in parenthesis). [b] Values in a.u. [c] The geometry of the first singlet excited state was not possible to converge.

Table 4.7 TD-DFT excitation and emission energies, their corresponding oscillator strengths and the HOMO-LUMO gap of **DTM**, ring-opened and ring-closed **SP** structures at CAM-B3LYP-B3DJ/6-311G(d,p) level of theory using the PCM with ε = 2.0165.

	State	Major contribution	λ_{exc}[a]	f_{exc}[b]	Major contribution	λ_{em}[a]	f_{em}[b]	$\Delta\lambda$[a]	Δ_{L-H}[a]
	1	H → L (69%)	390 (3.2)	0.126	H → L (69%)	523 (2.4)	0.110	133 (9.3)	206 (6.0)
DTMMA	2	H-1 → L (52%)	315 (3.9)	0.008					
	3	H-3 → L (48%)	286 (4.3)	0.037					
Ring-	1	H → L (70%)	464 (2.7)	1.053	H → L (69%)	534 (2.3)	0.721	76 (16.2)	250 (5.0)
opened	2	H-2 → L (64%)	383 (3.2)	0.002					
SPMA	3	H-1 → L (65%)	315 (3.9)	0.165					
Ring-	1	H-6 → L (61%)	302 (4.1)	0.001	H-3 → L (71%)	532 (2.3)	0.000	230 (5.4)	199 (6.2)
Closed	2	H-1 → L (68%)	289 (4.3)	0.199					
SPMA	3	H-1 → L+1 (56%)	275 (4.5)	0.042					

[a] Values in nm and eV (in parenthesis). [b] Values in a.u.

Table 4.8 TD-DFT excitation and emission energies, their corresponding oscillator strengths and the HOMO-LUMO gap of **DTM**, ring-opened and ring-closed **SP** structures at M06-2X/6-311G(d,p) level of theory using the PCM with ε = 2.0165.

	State	Major contribution	λ_{exc}[a]	f_{exc}[b]	Major contribution	λ_{em}[a]	f_{em}[b]	$\Delta\lambda$[a]	Δ_{L-H}[a]
	1	H → L (69%)	386 (3.2)	0.120	H → L (69%)	513 (2.4)	0.104	127 (9.7)	5.7
DTMMA	2	H-4 → L (47%)	321 (3.9)	0.007					
	3	H-1 → L (48%)	293 (4.2)	0.029					
Ring-	1	H → L (70%)	471 (2.6)	1.049	H → L (69%)	565 (2.2)	0.678	94 (13.2)	4.5
opened	2	H-2 → L (62%)	378 (3.3)	0.003					
SPMA	3	H-1 → L (68%)	315 (3.9)	0.195					
Ring-	1	H-8 → L (50%)	303 (4.1)	0.000	H → L+4 (66%)	557 (2.2)	0.000	254 (4.9)	6.0
Closed	2	H-1 → L (67%)	283 (4.4)	0.121					
SPMA	3	H-1 → L+1 (54%)	272 (4.6)	0.081					

[a] Values in nm and eV (in parenthesis). [b] Values in a.u. [c] The geometry of the first singlet excited state was not possible to converge.

4.6 References

1. Jin, D.; Xi, P.; Wang, B.; Zhang, L.; Enderlein, J.; van Oijen, A. M., Nanoparticles for super-resolution microscopy and single-molecule tracking. *Nat. Methods* **2018,** *15* (6), 415.

2. Shikha, S.; Salafi, T.; Cheng, J.; Zhang, Y., Versatile design and synthesis of nano-barcodes. *Chem. Soc. Rev.* **2017,** *46* (22), 7054.

3. Yang, M.; Liu, Y.; Jiang, X., Barcoded point-of-care bioassays. *Chem. Soc. Rev.* **2019,** *48* (3), 850.

4. Ren, W.; Lin, G.; Clarke, C.; Zhou, J.; Jin, D., Optical Nanomaterials and Enabling Technologies for High-Security-Level Anticounterfeiting. *Adv. Mater.* **2019**, 1901430.

5. Huang, K.; Idris, N. M.; Zhang, Y., Engineering of Lanthanide-Doped Upconversion Nanoparticles for Optical Encoding. *Small* **2016,** *12* (7), 836.

6. Lin, G.; Baker, M. A. B.; Hong, M.; Jin, D., The Quest for Optical Multiplexing in Bio-discoveries. *Chem* **2018,** *4* (5), 997.

7. Han, M.; Gao, X.; Su, J. Z.; Nie, S., Quantum-dot-tagged microbeads for multiplexed optical coding of biomolecules. *Nat. Biotechnol.* **2001,** *19* (7), 631.

8. Fang, X.; Zheng, Y.; Duan, Y.; Liu, Y.; Zhong, W., Recent Advances in Design of Fluorescence-Based Assays for High-Throughput Screening. *Anal. Chem.* **2019,** *91* (1), 482.

9. Berezin, M. Y.; Achilefu, S., Fluorescence lifetime measurements and biological imaging. *Chem. Rev.* **2010,** *110* (5), 2641.

10. Sarder, P.; Maji, D.; Achilefu, S., Molecular probes for fluorescence lifetime imaging. *Bioconjug. Chem.* **2015,** *26* (6), 963.

11. Wang, L.; Xiao, Y.; Tian, W.; Deng, L., Activatable rotor for quantifying lysosomal viscosity in living cells. *J. Am. Chem. Soc.* **2013,** *135* (8), 2903.

12. Goujon, A.; Colom, A.; Strakova, K.; Mercier, V.; Mahecic, D.; Manley, S.; Sakai, N.; Roux, A.; Matile, S., Mechanosensitive Fluorescent Probes to Image Membrane Tension in Mitochondria, Endoplasmic Reticulum, and Lysosomes. *J. Am. Chem. Soc.* **2019,** *141* (8), 3380.

13. Zhou, S.; Peng, X.; Xu, H.; Qin, Y.; Jiang, D.; Qu, J.; Chen, H. Y., Fluorescence Lifetime-Resolved Ion-Selective Nanospheres for Simultaneous Imaging of Calcium Ion in Mitochondria and Lysosomes. *Anal. Chem.* **2018,** *90* (13), 7982.

14. Damayanti, N. P.; Parker, L. L.; Irudayaraj, J. M., Fluorescence lifetime imaging of biosensor peptide phosphorylation in single live cells. *Angew. Chem. Int. Ed.* **2013,** *52* (14), 3931.

15. Lu, Y.; Lu, J.; Zhao, J.; Cusido, J.; Raymo, F. M.; Yuan, J.; Yang, S.; Leif, R. C.; Huo, Y.; Piper, J. A.; Paul Robinson, J.; Goldys, E. M.; Jin, D., On-the-fly decoding luminescence lifetimes in the microsecond region for lanthanide-encoded suspension arrays. *Nat. Commun.* **2014,** *5*, 3741.

16. Li, X.; Xie, Y.; Song, B.; Zhang, H. L.; Chen, H.; Cai, H.; Liu, W.; Tang, Y., A Stimuli-Responsive Smart Lanthanide Nanocomposite for Multidimensional Optical Recording and Encryption. *Angew Chem Int Ed* **2017,** *56* (10), 2689.

17. Kwiatek, J. M.; Owen, D. M.; Abu-Siniyeh, A.; Yan, P.; Loew, L. M.; Gaus, K., Characterization of a new series of fluorescent probes for imaging membrane order. *PLoS ONE* **2013,** *8* (2), e52960.

18. Chen, C.; Corry, B.; Huang, L.; Hildebrandt, N., FRET-Modulated Multihybrid

Nanoparticles for Brightness-Equalized Single-Wavelength Barcoding. *J. Am. Chem. Soc.* **2019,** *141* (28), 11123.

19. Zhou, L.; Fan, Y.; Wang, R.; Li, X.; Fan, L.; Zhang, F., High-Capacity Upconversion Wavelength and Lifetime Binary Encoding for Multiplexed Biodetection. *Angew. Chem. Int. Ed.* **2018,** *57* (39), 12824.

20. Zhang, H.; Fan, Y.; Pei, P.; Sun, C.; Lu, L.; Zhang, F., Tm(3+) -Sensitized NIR-II Fluorescent Nanocrystals for In Vivo Information Storage and Decoding. *Angew Chem Int Ed* **2019,** *58* (30), 10153.

21. Zhang, D. Y.; Zheng, Y.; Zhang, H.; Sun, J. H.; Tan, C. P.; He, L.; Zhang, W.; Ji, L. N.; Mao, Z. W., Delivery of Phosphorescent Anticancer Iridium(III) Complexes by Polydopamine Nanoparticles for Targeted Combined Photothermal-Chemotherapy and Thermal/Photoacoustic/Lifetime Imaging. *Adv. Sci.* **2018,** *5* (10), 1800581.

22. Baggaley, E.; Botchway, S. W.; Haycock, J. W.; Morris, H.; Sazanovich, I. V.; Williams, J. A. G.; Weinstein, J. A., Long-lived metal complexes open up microsecond lifetime imaging microscopy under multiphoton excitation: from FLIM to PLIM and beyond. *Chem. Sci.* **2014,** *5* (3), 879.

23. Yang, Y.; Liu, H.; Han, M.; Sun, B.; Li, J., Multilayer Microcapsules for FRET Analysis and Two-Photon-Activated Photodynamic Therapy. *Angew. Chem. Int. Ed.* **2016,** *55* (43), 13538.

24. Lei, Z.; Sun, C.; Pei, P.; Wang, S.; Li, D.; Zhang, X.; Zhang, F., Stable, Wavelength-Tunable Fluorescent Dyes in the NIR-II Region for In Vivo High-Contrast Bioimaging and Multiplexed Biosensing. *Angew. Chem. Int. Ed.* **2019,** *58* (24), 8166.

25. Tang, S.; Zhang, Y.; Dhakal, P.; Ravelo, L.; Anderson, C. L.; Collins, K. M.; Raymo,

F. M., Photochemical Barcodes. *J. Am. Chem. Soc.* **2018,** *140* (13), 4485.

26. Li, M.; Zhao, J.; Chu, H.; Mi, Y.; Zhou, Z.; Di, Z.; Zhao, M.; Li, L., Light-Activated Nanoprobes for Biosensing and Imaging. *Adv. Mater.* **2018**, 1804745.

27. Kim, D.; Park, S. Y., Multicolor Fluorescence Photoswitching: Color-Correlated versus Color-Specific Switching. *Adv. Opt. Mater.* **2018,** *6* (20), 1800678.

28. Zhang, Y.; Zhang, K.; Wang, J.; Tian, Z.; Li, A. D., Photoswitchable fluorescent nanoparticles and their emerging applications. *Nanoscale* **2015,** *7* (46), 19342.

29. Stumpel, J. E.; Broer, D. J.; Schenning, A. P., Stimuli-responsive photonic polymer coatings. *Chem. Commun.* **2014,** *50* (100), 15839.

30. Cheng, H.; Yoon, J.; Tian, H., Recent advances in the use of photochromic dyes for photocontrol in biomedicine. *Coord. Chem. Rev.* **2018,** *372*, 66.

31. Klajn, R., Spiropyran-based dynamic materials. *Chem. Soc. Rev.* **2014,** *43* (1), 148.

32. Yao, C.; Wang, P.; Li, X.; Hu, X.; Hou, J.; Wang, L.; Zhang, F., Near-Infrared-Triggered Azobenzene-Liposome/Upconversion Nanoparticle Hybrid Vesicles for Remotely Controlled Drug Delivery to Overcome Cancer Multidrug Resistance. *Adv. Mater.* **2016,** *28* (42), 9341.

33. Li, H.; Vaughan, J. C., Switchable Fluorophores for Single-Molecule Localization Microscopy. *Chem. Rev.* **2018,** *118* (18), 9412.

34. Fu, Y.; Han, H. H.; Zhang, J.; He, X. P.; Feringa, B. L.; Tian, H., Photocontrolled Fluorescence "Double-Check" Bioimaging Enabled by a Glycoprobe-Protein Hybrid. *J. Am. Chem. Soc.* **2018,** *140* (28), 8671.

35. Samanta, D.; Galaktionova, D.; Gemen, J.; Shimon, L. J. W.; Diskin-Posner, Y.; Avram, L.; Kral, P.; Klajn, R., Reversible chromism of spiropyran in the cavity of a flexible

coordination cage. *Nat. Commun.* **2018,** *9* (1), 641.

36. Osaki, H.; Chou, C. M.; Taki, M.; Welke, K.; Yokogawa, D.; Irle, S.; Sato, Y.; Higashiyama, T.; Saito, S.; Fukazawa, A.; Yamaguchi, S., A Macrocyclic Fluorophore Dimer with Flexible Linkers: Bright Excimer Emission with a Long Fluorescence Lifetime. *Angew. Chem. Int. Ed.* **2016,** *55* (25), 7131.

37. Xie, Y.; Husband, J. T.; Torrent-Sucarrat, M.; Yang, H.; Liu, W.; O'Reilly, R. K., Rational design of substituted maleimide dyes with tunable fluorescence and solvafluorochromism. *Chem. Commun.* **2018,** *54* (27), 3339.

38. Mabire, A. B.; Robin, M. P.; Quan, W. D.; Willcock, H.; Stavros, V. G.; O'Reilly, R. K., Aminomaleimide fluorophores: a simple functional group with bright, solvent dependent emission. *Chem. Commun.* **2015,** *51* (47), 9733.

39. Robin, M. P.; Wilson, P.; Mabire, A. B.; Kiviaho, J. K.; Raymond, J. E.; Haddleton, D. M.; O'Reilly, R. K., Conjugation-Induced Fluorescent Labeling of Proteins and Polymers Using Dithiomaleimides. *J. Am. Chem. Soc.* **2013,** *135* (8), 2875.

40. Robin, M. P.; Osborne, S. A. M.; Pikramenou, Z.; Raymond, J. E.; O'Reilly, R. K., Fluorescent Block Copolymer Micelles That Can Self-Report on Their Assembly and Small Molecule Encapsulation. *Macromolecules* **2016,** *49* (2), 653.

41. Robin, M. P.; Mabire, A. B.; Damborsky, J. C.; Thom, E. S.; Winzer-Serhan, U. H.; Raymond, J. E.; O'Reilly, R. K., New Functional Handle for Use as a Self-Reporting Contrast and Delivery Agent in Nanomedicine. *J. Am. Chem. Soc.* **2013,** *135* (25), 9518.

42. Hu, W.; Guo, L.; Bai, L.; Miao, X.; Ni, Y.; Wang, Q.; Zhao, H.; Xie, M.; Li, L.; Lu, X.; Huang, W.; Fan, Q., Maximizing Aggregation of Organic Fluorophores to Prolong Fluorescence Lifetime for Two-Photon Fluorescence Lifetime Imaging. *Adv. Healthc.*

Mater. **2018,** *7* (15), 1800299.

43. Hoffmann, K.; Behnke, T.; Drescher, D.; Kneipp, J.; Resch-Genger, U., Near-infrared-emitting nanoparticles for lifetime-based multiplexed analysis and imaging of living cells. *ACS Nano* **2013,** *7* (8), 6674.

44. Zhang, H.; Jiang, J.; Gao, P.; Yang, T.; Zhang, K. Y.; Chen, Z.; Liu, S.; Huang, W.; Zhao, Q., Dual-Emissive Phosphorescent Polymer Probe for Accurate Temperature Sensing in Living Cells and Zebrafish Using Ratiometric and Phosphorescence Lifetime Imaging Microscopy. *ACS Appl. Mater. Interfaces.* **2018,** *10* (21), 17542.

45. Sapsford, K. E.; Berti, L.; Medintz, I. L., Materials for fluorescence resonance energy transfer analysis: beyond traditional donor-acceptor combinations. . *Angew. Chem. Int. Ed.* **2006,** *45* (28), 4562.

46. Algar, W. R.; Hildebrandt, N.; Vogel, S. S.; Medintz, I. L., FRET as a biomolecular research tool - understanding its potential while avoiding pitfalls. *Nat. Methods* **2019,** *16* (9), 815.

47. Jares-Erijman, E. A.; Jovin, T. M., FRET imaging. *Nat. Biotechnol.* **2003,** *21* (11), 1387.

48. Robin, M. P.; O'Reilly, R. K., Fluorescent and chemico-fluorescent responsive polymers from dithiomaleimide and dibromomaleimide functional monomers. *Chem. Sci.* **2014,** *5* (7), 2717.

49. Yu, M. L.; Zhang, P. S.; Krishnan, B. P.; Wang, H.; Gao, Y.; Chen, S.; Zeng, R. J.; Cui, J. X.; Chen, J., From a Molecular Toolbox to a Toolbox for Photoswitchable Fluorescent Polymeric Nanoparticles. *Adv. Funct. Mater.* **2018,** *28* (46), 1804759.

50. Beyer, C.; Wagenknecht, H. A., Synthesis of spiropyrans as building blocks for

molecular switches and dyads. *J. Org. Chem.* **2010,** *75* (8), 2752.

51. Sakata, T.; Yan, Y.; Marriott, G., Family of Site-Selective Molecular Optical Switches. *J. Org. Chem.* **2005,** *70* (6), 2009.

52. Robin, M. P.; Raymond, J. E.; O'Reilly, R. K., One-pot synthesis of super-bright fluorescent nanogel contrast agents containing a dithiomaleimide fluorophore. *Mater. Horiz.* **2015,** *2* (1), 54.

53. Burghart, A.; Thoresen, L. H.; Chen, J.; Burgess, K.; Bergström, F.; Johansson, L. B. Å., Energy transfer cassettes based on BODIPY® dyes. *Chem Comm* **2000,** (22), 2203.

54. Giordano, L.; Jovin, T. M.; Irie, M.; Jares-Erijman, E. A., Diheteroarylethenes as Thermally Stable Photoswitchable Acceptors in Photochromic Fluorescence Resonance Energy Transfer (pcFRET). *J. Am. Chem. Soc.* **2002,** *124* (25), 7481.

55. Chen, J.; Zhang, P.; Fang, G.; Yi, P.; Yu, X.; Li, X.; Zeng, F.; Wu, S., Synthesis and characterization of novel reversible photoswitchable fluorescent polymeric nanoparticles via one-step miniemulsion polymerization. *J. Phys. Chem. B* **2011,** *115* (13), 3354.

56. Yang, M.; Moroz, P.; Jin, Z.; Budkina, D. S.; Sundrani, N.; Porotnikov, D.; Cassidy, J.; Sugiyama, Y.; Tarnovsky, A. N.; Mattoussi, H.; Zamkov, M., Delayed Photoluminescence in Metal-Conjugated Fluorophores. *J. Am. Chem. Soc.* **2019,** *141* (28), 11286.

57. Jorgensen, W. L.; Tiradorives, J., The OPLS potential functions for proteins - energy minimizations for crytsals of cyclic-peptides and crambin. *J. Am. Chem. Soc.* **1988,** *110* (6), 1657.

58. Jorgensen, W. L.; Maxwell, D. S.; TiradoRives, J., Development and testing of the OPLS all-atom force field on conformational energetics and properties of organic liquids.

J. Am. Chem. Soc. **1996,** *118* (45), 11225.

59. Becke, A. D., Density-functional thermochemistry .3. the role of exact exchange. *J. Chem. Phys.* **1993,** *98* (7), 5648.

60. Stephens, P. J.; Devlin, F. J.; Chabalowski, C. F.; Frisch, M. J., Ab-initio calculation of vibrational absorption and circular-dichroism spectra using density-functional force-fields. *J. Phys. Chem.* **1994,** *98* (45), 11623.

61. Yanai, T.; Tew, D. P.; Handy, N. C., A new hybrid exchange-correlation functional using the Coulomb-attenuating method (CAM-B3LYP). *Chem. Phys. Lett.* **2004,** *393* (1-3), 51.

62. Hehre, W. J.; Ditchfield, R.; Pople, J. A., Self-consistent molecular-orbital methods. 12. Further extensions of gaussian-type basis sets for use in molecular-orbital studies of organic-molecules. *J. Chem. Phys.* **1972,** *56* (5), 2257.

63. Hehre, W. J.; Random, L.; Schleyer, P. v. R.; Pople, J. A., *Ab initio Molecular Orbital Theory*. Wiley: New York, 1986.

64. Zhao, Y.; Truhlar, D. G., The M06 suite of density functionals for main group thermochemistry, thermochemical kinetics, noncovalent interactions, excited states, and transition elements: two new functionals and systematic testing of four M06-class functionals and 12 other functionals. *Theor. Chem. Acc.* **2008,** *120* (1-3), 215.

65. Adamo, C.; Barone, V., Toward reliable density functional methods without adjustable parameters: The PBE0 model. *J. Chem. Phys.* **1999,** *110* (13), 6158.

66. Grimme, S.; Antony, J.; Ehrlich, S.; Krieg, H., A consistent and accurate ab initio parametrization of density functional dispersion correction (DFT-D) for the 94 elements H-Pu. *J. Chem. Phys.* **2010,** *132* (15), 154104.

67. Grimme, S.; Ehrlich, S.; Goerigk, L., Effect of the Damping Function in Dispersion Corrected Density Functional Theory. *J. Comput. Chem.* **2011,** *32* (7), 1456.

68. Johnson, E. R.; Becke, A. D., A post-Hartree-Fock model of intermolecular interactions: Inclusion of higher-order corrections. *J. Chem. Phys.* **2006,** *124* (17).

69. Cossi, M.; Rega, N.; Scalmani, G.; Barone, V., Energies, structures, and electronic properties of molecules in solution with the C-PCM solvation model. *J. Comput. Chem.* **2003,** *24* (6), 669.

70. Tomasi, J.; Mennucci, B.; Cammi, R., Quantum mechanical continuum solvation models. *Chem. Rev.* **2005,** *105* (8), 2999.

71. Adamo, C.; Jacquemin, D., The calculations of excited-state properties with Time-Dependent Density Functional Theory. *Chem. Soc. Rev.* **2013,** *42* (3), 845.

72. Laurent, A. D.; Adamo, C.; Jacquemin, D., Dye chemistry with time-dependent density functional theory. *Phys. Chem. Chem. Phys.* **2014,** *16* (28), 14334.

73. *Macromodel, Schödinger, LLC, New York, NY*, 2019.

74. *Maestro, Schödinger, LLC, New York, NY*, 2019.

75. Frisch, M. J.; Trucks, G. W.; Schlegel, H. B.; Scuseria, G. E.; Robb, M. A.; Cheeseman, J. R.; Scalmani, G.; Barone, V.; Petersson, G. A.; Nakatsuji, H.; Li, X.; Caricato, M.; Marenich, A. V.; Bloino, J.; Janesko, B. G.; Gomperts, R.; Mennucci, B.; Hratchian, H. P.; Ortiz, J. V.; Izmaylov, A. F.; Sonnenberg, J. L.; Williams; Ding, F.; Lipparini, F.; Egidi, F.; Goings, J.; Peng, B.; Petrone, A.; Henderson, T.; Ranasinghe, D.; Zakrzewski, V. G.; Gao, J.; Rega, N.; Zheng, G.; Liang, W.; Hada, M.; Ehara, M.; Toyota, K.; Fukuda, R.; Hasegawa, J.; Ishida, M.; Nakajima, T.; Honda, Y.; Kitao, O.; Nakai, H.; Vreven, T.; Throssell, K.; Montgomery Jr., J. A.; Peralta, J. E.; Ogliaro, F.; Bearpark, M. J.;

Heyd, J. J.; Brothers, E. N.; Kudin, K. N.; Staroverov, V. N.; Keith, T. A.; Kobayashi, R.; Normand, J.; Raghavachari, K.; Rendell, A. P.; Burant, J. C.; Iyengar, S. S.; Tomasi, J.; Cossi, M.; Millam, J. M.; Klene, M.; Adamo, C.; Cammi, R.; Ochterski, J. W.; Martin, R. L.; Morokuma, K.; Farkas, O.; Foresman, J. B.; Fox, D. J. *Gaussian 16 Rev. C.01*, Wallingford, CT, 2016.

76. Zhu, H.; Fan, J.; Du, J.; Peng, X., Fluorescent Probes for Sensing and Imaging within Specific Cellular Organelles. *Acc. Chem. Res.* **2016,** *49* (10), 2115.

77. Zhu, Y. X.; Jia, H. R.; Pan, G. Y.; Ulrich, N. W.; Chen, Z.; Wu, F. G., Development of a Light-Controlled Nanoplatform for Direct Nuclear Delivery of Molecular and Nanoscale Materials. *J. Am. Chem. Soc.* **2018,** *140* (11), 4062.

78. Li, J.; Kwon, N.; Jeong, Y.; Lee, S.; Kim, G.; Yoon, J., Aggregation-Induced Fluorescence Probe for Monitoring Membrane Potential Changes in Mitochondria. *ACS Appl. Mater. Interfaces.* **2018,** *10* (15), 12150.

79. Yang, Y.; Wang, S.; Chen, S.; Shen, Y.; Zhu, M., Switching the subcellular organelle targeting of atomically precise gold nanoclusters by modifying the capping ligand. *Chem. Commun.* **2018,** *54* (66), 9222.

80. Yuan, P.; Mao, X.; Wu, X.; Liew, S. S.; Li, L.; Yao, S. Q., Mitochondria-Targeting, Intracellular Delivery of Native Proteins Using Biodegradable Silica Nanoparticles. *Angew. Chem. Int. Ed.* **2019,** *58* (23), 7657.

81. Sumerlin, B. S.; Tsarevsky, N. V.; Louche, G.; Lee, R. Y.; Matyjaszewski, K., Highly Efficient “Click” Functionalization of Poly(3-azidopropyl methacrylate) Prepared by ATRP. *Macromolecules* **2005,** *38* (18), 7540.

82. Sui, B.; Tang, S.; Woodward, A. W.; Kim, B.; Belfield, K. D., A BODIPY-Based

Water-Soluble Fluorescent Probe for Mitochondria Targeting. *Eur. J. Org. Chem.* **2016,** *16* (16), 2851.

83. Rodionov, V.; Gao, H.; Scroggins, S.; Unruh, D. A.; Avestro, A. J.; Frechet, J. M., Easy access to a family of polymer catalysts from modular star polymers. *J. Am. Chem. Soc.* **2010,** *132* (8), 2570.

Chapter 5 Conclusions and Future Work

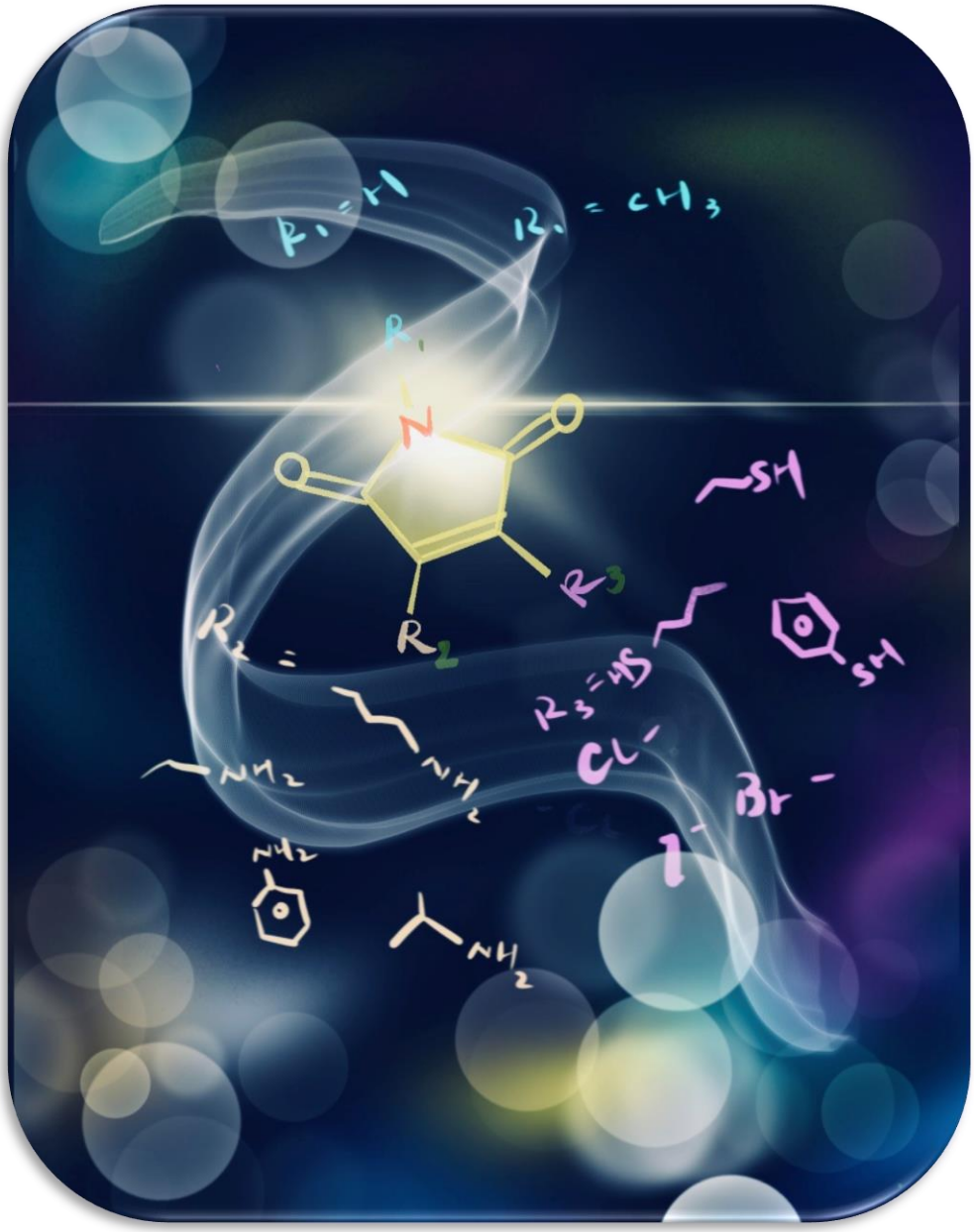

In summary, the fluorescent properties of substituted maleimides have been explored by varying the molecular structures and substitution patterns. In this thesis, we systematically synthesized a series of mono-substituted maleimide fluorophores to investigate the effect between the substitution groups and fluorescent properties. The effect on optical properties when altering the halogen group (Cl, Br and I) and the donor groups (amines and alcohols) have been discussed in chapter 2 which provide evidence of the previously hypothesized push-pull model and confirmed that smaller charge differences on the C=C bond positively affect fluorescence *via* computational results. In chapter 3, we expanded the scope of substitution patterns of mono-substituted maleimides to the unsymmetrical di-substituted maleimides patterns through readily available amino maleimides as building blocks. The two-step substitution reactions allowed for a higher degree of modification within one molecule. More importantly, the unexpected fluorescence in ATM bearing thiophenol groups was explored for the first time by the effect of aggregation state.

Exploring the relationship between the structure of maleimides and their optical properties is critical for a full understanding of the fluorescence mechanism and provides a potential strategy for future prediction of the fluorescent behavior through the design of the molecular structures. Building upon these two chapters, the further optimization of the maleimides structures with maintained fluorescent properties in protic solvent and expanded emission to red or infrared regions are important for applications in biological and chemical sensing applications. Meanwhile, the multiple reaction sites in the maleimides structures allow for bearing up to three functional groups within one molecule, which potentially useful as the fluorescent linker for the construction of the crosslinked structures like nanogel or hydrogel.

The understanding of the fluorescent properties on substituted maleimides leads to the applications in bioimaging and fluorescent related information storage. In chapter 4, the methacrylic monomers contain substituted maleimide group that has been polymerized into the polymeric nanogel a spiropyran photoswitch. A series of nanogels with the same structure and surface chemistries but a broad range of dynamic lifetimes suitable for multiplex system coding and counting was synthesized. By incorporation a mitochondrial tracker, we applied the nanogel in live-cell lifetime barcoding at the subcellular scale *via* remote control.

Owing to the stable microenvironment of the nanogel, the fluorescent lifetime of substitution maleimides provided the reliable and reproducible results in this chapter without being affected by the concentration of the fluorophores or the measurement techniques, which provide the first insight in fluorescent lifetime coding. Based on this chapter, the environment-dependent lifetime of the substituted maleimides potentially generate the interest in manipulating the fluorescent lifetime of maleimides by varying the chemistry of the microenvironment. Meanwhile, the maleimide structure in polymer system allows for real-time reflecting the change of its microenvironment by monitoring the fluorescent lifetime and could be potentially useful for monitoring the responsive properties of the polymer, visualizing the polymer assemble process and investigating the polymer behavior in bioenvironment.